Controls on Dune Dimensions in Rivers

by

Ryan W. Bradley

M.Sc. (Geography), Simon Fraser University, 2012

B.Sc. (Environmental Sciences), University of Guelph, 2010

Thesis Submitted in Partial Fulfillment of the

Requirements for the Degree of

Doctor of Philosophy

in the

Department of Geography

Faculty of Environment

SIMON FRASER UNIVERSITY

Summer 2018

Approval

Name:	**Ryan Bradley**
Degree:	**Doctor of Philosophy**
Title:	**Controls on Dune Dimensions in Rivers**
Examining Committee:	**Chair:** **Kirsten Zickfeld** Associate Professor
	Dr. Jeremy Venditti Senior Supervisor Professor
	Dr. Michael Church Supervisor Professor Emeritus Department of Geography University of British Columbia
	Dr. Shahin Dashtgard Supervisor Professor Department of Earth Sciences
	Dr. Brent Ward Internal Examiner Professor Department of Earth Sciences
	Dr. David Mohrig External Examiner Professor Department of Geological Sciences University of Austin
Date Defended/Approved:	July 3, 2018

Abstract

Dunes are bedforms commonly found in sand-bedded rivers. They are important sources of flow resistance and mechanisms for sediment transport, so there is a practical need to directly predict dune dimensions. Migrating dunes also leave signatures of their presence and evolution as cross-strata in sand deposits, which can be used to indirectly hindcast paleo-flows. The most common method to predict dimensions in modern flows or hindcast paleo-flows is depth-scaling relations, which assume a depth control on dunes. There is substantial scatter about depth-scaling relations, suggesting that other physical processes may control dimensions. This study identifies primary controls on dune dimensions in rivers through a meta-analysis of published dune data, and a series of flume experiments. The data compilation shows approximately two orders of magnitude variation in dune height and length at any given flow depth. Dune heights in shallow flows (< 2.5 m), where asymmetric dunes with high lee angles are common, grow relatively higher in the flow than symmetrical low lee angle dunes in deeper channels (> 2.5 m). The data set is used to provide depth-scaling relations with added statistical uncertainty. Scatter about the scaling relations is attributed to natural variability in dune dimensions and transport stage effects. Flume experiments are used to better identify controls on dune dimensions. Results confirm dune-depth scaling is weak and that transport stage is a fundamental control. The experimental data are used to derive new non-linear scaling relations between equilibrium dune dimensions and transport stage. The relations provide a physically-sound method to guide predictions of dune dimensions in rivers and paleo-reconstructions from estimated dune dimensions in the rock record. A series of experimental observations of dune growth from a flat bed were also made. The results show that growth behaviour also depends on transport stage, and the time to equilibrium dimensions decreases non-linearly with transport stage. The observations are used to propose a series of relations that can predict dune dimensions through time as they respond to an imposed flow.

Keywords: rivers; geomorphology; sedimentology; bedforms; dunes; sediment transport

Dedication

To my brother, Dylan, who may not have had much time for this “book learnin’” but would have been impressed with it nonetheless.

Acknowledgements

Thanks to my supervisor, Jeremy Venditti, for the guidance and encouragement along the way. Jeremy's unwavering support has helped me become a much more confident researcher over the years. I am also grateful for our conversations about science and academia, in general. These talks provided valuable insight into how to be successful in my studies and career, while maintaining my core beliefs.

Mike Church has also played a pivotal role in my career and this work. Not only is Mike's passion for the geosciences inspirational, he always saw potential in me as a researcher and provided constant support. I would also like to thank Ray Kostaschuk for encouraging me when I was a student at Guelph. Ray's enthusiasm and attitude towards science (and low-angle dunes) often provided me with extra motivation.

Thanks to Shahin Dashtgard for coming on-board and providing thoughtful critiques that led to a much stronger dissertation. I am also grateful for Brent Ward and David Mohrig's comments and discussion surrounding this work. Matt Akenhead, Malcolm Little, Martin Lin, Kirsti Fairweather, Kyle Kusack, Moslem Kazemi, and B-Jae Kelly provided support at various stages that contributed to the success of this project.

I am privileged to have met great friends at SFU who enriched this experience in so many ways. I am especially grateful to Megan Hendershot, Maureen Attard, Sheena Spencer, Alex Gitto, Dan Haught, Eva Kwoll, Jonny Cripps, Michael Martin, and Leon Hoffman who were always there to talk school life or utter non-sense. While there are too many many friends outside of SFU to list here, their support and encouragement (in various forms) were constant sources of strength.

I would like to thank my partner, Christy Gunn, who patiently stood with me during the ups and downs of this process. She made the highs so much better, and the lows seem not so bad. Her support has meant the world to me.

Finally, I must thank my family. Each of them has been instrumental in helping me achieve this goal in their own unique way. The one constant from them all has been complete support to pursue my goals. I am incredibly grateful for the foundation they provided me with (and continue to provide). Without that solid foundation, this would have been a heck of a lot tougher.

Table of Contents

List of Tables

List of Figures

List of Notations

a	Parabolic shape coefficient
a_H	Coefficient that describes equilibrium dune height
a_i	Regression intercept
a_L	Coefficient that describes equilibrium dune length
α	Standard error of regression
BCF	Bias Correction Factor
b	Horizontal parabolic position coefficient
b_H	Height growth constant
b_L	Length growth constant
β	Dune shape coefficient
β_H	ratio of a subsample mean height compared to the mean value
β_L	ratio of a subsample mean length compared to the mean value
ε	Scaling coefficient
C	Concentration of suspended sediment at a height above the bed
C_a	Reference suspended sediment concentration
$\bar{C}_h$	Mean depth-averaged suspended sediment concentration
C'	Chezy-coefficient
CV	Coefficient of Variation
c	Vertical parabolic position coefficient
D	Grain size
D_{50}	Median grain size
D_{90}	90% percentile of the grain size
δ	Coefficient describing diffusion between sediment and fluid particles
Fr	Froude number
$\overline{Fr}$	Average Froude number
γ	Growth exponent
g	Gravitational acceleration
H	Dune height
$\overline{H}$	Mean dune height
$\widehat{H}$	Subsample mean dune height

H_e	Equilibrium dune height
H_i	Log-transformed height for which prediction is being made
$H_{interval}$	Dune height prediction interval
$\overline{H_{log}}$	Mean of the log-transformed dune height values
H_p	Averaged bedform height using one profile
H_{pred}	Log-transformed predicted dune height
H_R	Reach-average dune height
H/L	Dune steepness
H/L_R	Reach-average dune steepness
$\overline{H/L}$	Mean dune steepness
h	Flow depth
$\bar{h}$	Mean flow depth
h_i	Log-transformed depth for which prediction is being made
$h_{interval}$	Flow depth prediction interval
$\overline{h_{log}}$	Mean of the log-transformed depth values
h_{pred}	Log-transformed predicted flow depth
h_R	Reach averaged depth
k	von Karman constant
L	Dune length
$\bar{L}$	Mean dune length
$\hat{L}$	Subsample mean dune length
L_e	Equilibrium dune length
$L_{interval}$	Dune length prediction interval
L_p	Averaged bedform length using one profile
L_{pred}	Log-transformed predicted dune length
L_R	Reach-average dune length
m	Regression slope
N	Number of data points
η	Empirical coefficient from the Einstein–Brown formula
p	Probability
ρ_s	Density of sediment
ρ_w	Density of water
Q	Discharge

q_{bl}	Bedload flux
q_s	Suspended flux
q_{ss}	Total bed material flux
R_b	Hydraulic radius
Re_g	Grain Reynolds number
S	Slope
S_{bR}	Reach bed slope
S_{wR}	Reach water surface
SE_H	Standard error for height prediction
SE_L	Standard error for length prediction
SEE_{Hh}	Standard error of estimate for regression between dune height and flow depth
SEE_{hH}	Standard error of estimate for regression between flow depth and dune height
SEE_{hL}	Standard error of estimate for regression between flow depth and dune length
σ_H	Standard deviation of the log-transformed dune height
σ_{HR}	Standard deviation of reach-averaged height data
σ_h	Standard deviation of the log-transformed depth
σ_{LR}	Standard deviation of reach-averaged length data
T	Transport stage parameter
t	Time
t_e	Time required to achieve equilibrium dimension
t_{eH}	Time required to achieve equilibrium dune height
t_{eL}	Time required to achieve equilibrium dune length
$t_\propto$	Two-tailed Student's t-test value
τ	Shear stress
τ_{cr}	Critical shear stress for particle movement
τ_{reach}	Reach-average shear stress
τ_{tot}	Total bed stress
τ_*	Shields number (non-dimensional shear stress)
τ_{*c}	Critical Shields number for sediment entrainment
τ_*/τ_{*c}	Transport stage
τ_*/τ_{*c_R}	Reach-averaged transport stage
$\overline{\tau_*/\tau_{*c}}$	Mean transport stage

U	Mean flow velocity
$\overline{U_h}$	Mean depth-averaged streamwise velocity
U_R	Reach-averaged mean flow velocity
u_*	Shear velocity
u'_*	Grain shear velocity
u_{*c}	Critical grain shear velocity
u_*/w_s	Suspension number
u_*/w_{s_R}	Reach-average suspension number
$(\overline{u_*/w_s})$	Average suspension number
w	Flume width
w_s	Particle settling velocity
z	Height above the bed
z_a	Height of reference suspended sediment concentration above the bed
ζ	Distribution and confidence interval constant

Preface

The research conducted in this thesis was lead by the author, Ryan Bradley, and the work presented in Chapters 1-5 was conducted with contribution from Professor Jeremy G. Venditti. Professor Michael Church provided early reviews of Chapters 1-5 and Professor Shahin Dashtgard provided early reviews of Chapters 1,3-5.

Chapter 2 is a reprinted invited review from Earth-Science Reviews:
Bradley, Ryan W., and Venditti, Jeremy G. (2017). Reevaluating dune scaling relations, Earth-Science Reviews, Volume 165, 2017, Pages 356-376, ISSN 0012-8252.

Chapter 3 will be submitted to the Journal of Geophysical Research: Earth Surface under the title *Transport Stage Scaling of Dunes* with R.W. Bradley and J.G. Venditti as the authors.

Chapter 4 will be submitted to the Journal of Geophysical Research: Earth Surface under the title *Dune Growth from a Flat Bed* with R.W. Bradley and J.G. Venditti as the authors.

Chapter 1. Introduction

Alluvial river channels are the product of complex interactions between water and sediment at the Earth's surface. The complexity of these fluvial and sedimentary processes is compounded by the range of spatial (e.g., grain to landscape) and temporal (e.g., seconds to centuries) scales at which they operate. There has been a long history of research on river dynamics and morphology because rivers are sites of significant socioeconomic development and ecologic importance. Despite over a century of detailed river studies, our ability to understand and predict river processes remains limited because of the inherent complexity.

Low-gradient portions of river networks are typically sand-bedded. The labile bed of these channels typically features sandy bedforms that exist at many different size scales and geometries, and dune bedforms are commonly found at scales smaller than channels. Geomorphologists, sedimentologists, and engineers are particularly interested in dunes because they are important sources of flow resistance and mechanisms for sediment transport. Dunes contribute to flow resistance by adding significant form drag (Einstein & Barbarossa, 1952; Engelund & Hansen, 1967; Van Rijn, 1993) as dune-generated turbulence and flow separation result in the dissipation of mean flow energy (Nelson et al., 1993; Nezu & Nakagawa, 1993; Kwoll et al., 2016). The growth and migration of dunes can also result in significant bedload transport in rivers (Simons & Richardson, 1966; Mohrig & Smith, 1996; McElroy & Mohrig, 2009; Venditti et al., 2016) as dunes translate downstream by stoss erosion and lee slope deposition. Deformation of dunes during migration results in changes to shape, size and spacing that further contributes to sediment transport (McElroy & Mohrig, 2009; Ganti et al., 2013; Venditti et al., 2016). Large volumes of bed material can also be moved via suspension by dune-generated turbulence (*cf.,* Rood & Hickin, 1989; Kostaschuk & Church, 1993; Bradley et al., 2013). Quantitative estimates of flow resistance (e.g., Engelund & Hansen, 1967; Fredsøe, 1982; van Rijn, 1984; Paarlberg et al., 2010), and sediment transport (e.g*.,* Simons et al., 1965; Engel & Lau, 1980; van den Berg, 1987; Mohrig & Smith, 1996) usually require some measure of dune dimensions. Understanding the physical controls on dunes is crucial to strengthening our ability to predict dune characteristics in modern river flows.

Dunes also provide insight into past river flows on Earth or other planetary surfaces. Migrating dunes leave behind characteristic primary sedimentary structures (cross-strata) in sand deposits that provide signatures of their presence and evolution. Cross-stratified units made up of cross-sets preserved between two successive erosional surfaces are formed by ancient dunes (e.g., Allen, 1970; Rubin & Hunter, 1982; Jerolmack & Mohrig, 2005; Ganti et al., 2013) and are common features in sedimentary strata. Cross-set thickness distribution is often linked to formative bedform dimension distributions theoretically (*cf.,* Paola & Borgman, 1991; Bridge & Best, 1997) or empirically (*cf.,* Bridge, 1997; Leclair et al., 1997; Leclair & Bridge, 2001; Leclair, 2002). Estimated dune heights, based on cross-strata, are used to make indirect first order estimates of flow depth in paleo-environmental reconstructions (e.g., Bridge & Tye, 2000; Leclair & Bridge, 2001; Bridge, 2003; Adams & Bhattacharya, 2005; Ponten & Plink-Bjorklund, 2007; Lunt et al., 2013). However, the success of these reconstructions depends critically on our understanding of what controls dune growth and dimensions in modern channels.

This dissertation seeks to identify the controls on dune height and wavelength (herein referred to as length) in rivers and how dunes grow to a statistically steady state (equilibrium). There are physically-based numerical models that predict the evolution of bedforms (e.g., Giri & Shimizu, 2006; Shimizu et al., 2009; Nelson et al., 2011), but these models require testing across a wide range of transport conditions. Therefore, this study employs an empirical approach to understand the fundamental controls on bedform dimensions, which may be used to guide and refine existing theory and models. Before the specific objectives of the work are provided, a brief review of our current understanding of what controls bedform dimensions is presented. The review emphasises flaws and gaps in theories that attempt to describe bedform development in rivers.

1.1. The Bedform Continuum

Bedforms in rivers are traditionally thought of as a continuum in which lower-stage plane beds, ripples, dunes, upper-stage plane beds, antidunes and cyclic steps emerge as a typical sequence as flow velocity is increased over an initially flat bed (Simons & Richardson, 1961; Southard & Boguchwal, 1990; Venditti, 2013; Cartingy et

al., 2014). The continuum is usually separated by the Froude number (Fr), which is a ratio of inertial to gravitational forces expressed as:

$$Fr = \frac{\overline{U}}{\sqrt{gh}} \qquad \text{(Eq 1.1)}$$

where $\overline{U}$ is mean flow velocity, h is flow depth and g is gravitational acceleration. Lower stage plane beds, ripples, and dunes fall under a 'lower flow regime' when flows are subcritical (Fr < 1). As flows approach Fr = 1 and become supercritical (Fr > 1), lower regime bedforms wash out to a plane bed and then form antidunes. These 'upper flow regime' features have relatively higher bed-material discharge and less flow resistance than lower regime bedforms.

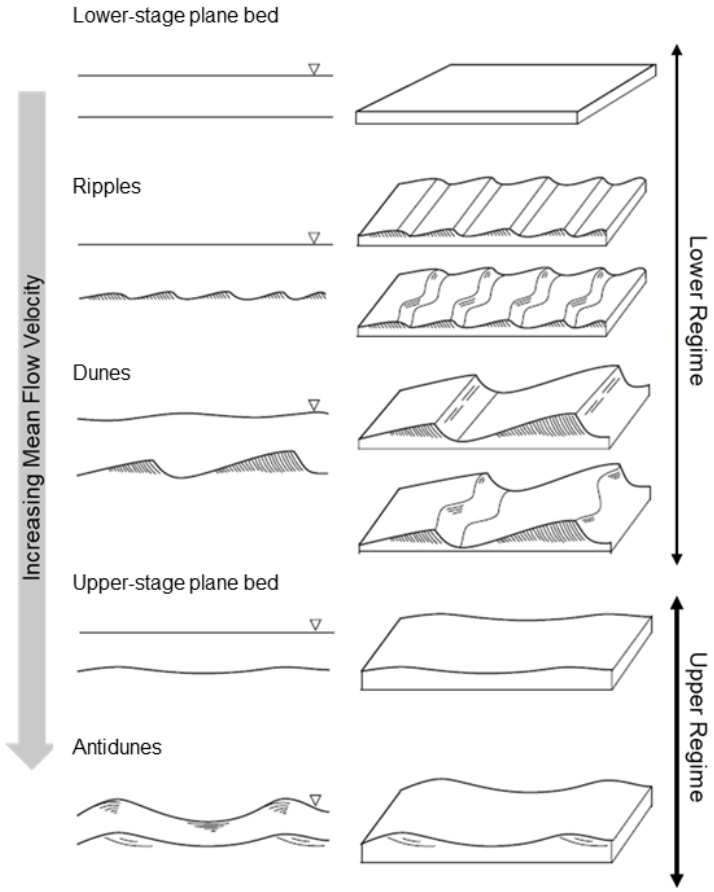

Figure 1.1. The bedform continuum (e.g., Simons & Richardson, 1961; Guy et al., 1966; Southard & Boguchwal, 1990; Cartingy et al., 2014) (figure modified from Venditti 2013).

The bedform continuum concept is a culmination of early efforts to predict bedform behavior (e.g., Simons & Richardson, 1961; Guy et al., 1966; Southard & Boguchwal, 1990), but is too simplistic in concept. Other researchers have developed phase diagrams that apply the continuum concept to predict what type of bedform will appear under certain sets of hydraulic and sedimentary variables. Southard and Boguchwal (1990) provide a series of widely cited phase diagrams that predict general bedform type based on grain size and mean flow velocity. Others have developed phase diagrams using the Froude number and grain size (Vanoni, 1974), dimensionless shear stress and grain size (Allen, 1982; van Rijn, 1993; Southard, 1991; Carling, 1999), or grain settling velocity and the grain Reynolds number (Liu, 1957). Some other phase diagrams use three variables. Rubin and McCulloch (1980) offer three-variable phase diagrams that use grain size, flow, depth, and velocity, and Ohata et al. (2017) use a variety of flow hydraulic and sediment variables in 3-D dimensionless space.

The sheer volume of phase diagrams, employing different hydraulic and sedimentary controls, suggests that the range of controls on bedforms has not been fully identified. Furthermore, even the most well defined and widely applied phase diagrams show overlap in existence fields. Most phase diagrams have been derived using observations entirely from controlled flume experiments where h < 1 m. Attempts to extrapolate to field conditions, especially in deeper sand-bedded rivers, have shown that these phase diagrams cannot predict bedform types in all environments (Kostaschuk & Villard, 1996; van den Berg et al., 1998). These caveats are concerning since sedimentologists often apply phase diagrams to interpret flows that formed sedimentary structures, and engineers use them in natural channel design and river engineering problems.

1.2. Dune Typology

A variety of different metrics and terms have been used to distinguish lower flow-regime bedforms, but there is some commonly accepted terminology for dunes used throughout this dissertation. Dunes are large-scale, flow-transverse bed features that commonly form in sediments ranging from fine sand to gravel (grain diameters: 0.125 mm to 64 mm). They have dimensions that range anywhere from a few centimetres to several metres in height and can be up to 1000 m in length. Dunes are often considered to be distinct from smaller scale ripples, even though they can display similar geometric shapes. Ripple dimensions scale with grain size (Yalin, 1964; 1985; Baas, 1994) and only form in sediment < ~ 0.6 mm (Allen, 1982). Ripples form in hydraulically smooth conditions when the grain Reynolds number ($Re_g = u_* D/\nu$, where u_* is shear velocity, D is grain size, and ν is kinematic viscosity of water) is < 5, while dunes can be found in transitional (5 < Re_g < 70) and hydraulically rough flows (Re_g >70). Dunes are also larger features that can affect the water surface and are widely thought to scale with flow depth (Bridge, 2003; Garcia, 2008; Venditti, 2013), a fallacy addressed below.

Dunes are usually described in terms of their planform and geometry. Their planimetric morphology can be divided into two-dimensional (2D) and three-dimensional (3D) bed features. Two-dimensional dunes have relatively regular spacing and straight crestlines transverse to the mean flow. Most natural dune fields are inherently 3D (e.g., Parsons et al., 2005; Hendershot et al., 2018), exhibiting irregular spacing, heights and

lengths, and complex cross-stream variations in crest lines with irregular scour pits within troughs. Some authors (e.g., Baas et al., 1993; Baas, 1994; Venditti et al., 2005) have suggested that all 2D bedform fields will inevitably develop into 3D morphologies, given a constant flow and enough time, because crestline defects emerge and remain in the field. These defects emerge as bedforms split due to superimposition of bedforms (Allen, 1973; Gabel, 1993), bedform spurs (Allen, 1969; Swanson et al., 2017) and crestline bifurcations (Hendershot et al., 2018).

Dune geometry can appear as angle-of-repose asymmetric or low-angle symmetric (Figure 1.2; Best, 2005; Venditti, 2013). Asymmetric dunes have long, gently sloping (2 to 6°) stoss sides and short, steep (~30°) lee sides. These bedforms are easily produced in flumes and smaller natural channels (h < 1 m), and as a result, have been studied extensively. However, field observations from rivers much larger than flumes show more symmetrical dunes with similar stoss and lee lengths and much lower lee-side angles (<< 30°) (*cf.,* Smith & McLean, 1977; Kostaschuk & Villard, 1996; Hendershot et al., 2016; Hu et al., 2018; Galeazzi et al., 2018). While persistent flow separation is a characteristic feature of flow over asymmetric dunes (e.g., Nelson et al., 1993; McLean et al., 1994; Bennett & Best, 1995; Venditti & Bennett, 2000; Venditti, 2007), it has not been observed over low-angle dunes in the field (e.g., Smith and McLean, 1977; Kostaschuk & Villard, 1996; Bradley et al., 2013). Detailed measurements over experimental low-angle dunes suggest that a decelerated flow region develops in the lee with a small zone of intermittent flow reversal (Best & Kostaschuk, 2002; Kwoll et al., 2016). Even though permanent flow separation is absent, turbulence generated by low-angle dunes is still capable of moving large volumes bed material through suspension (Kostaschuk & Church, 1993; Kostaschuk & Villard, 1999; Bradley et al., 2013).

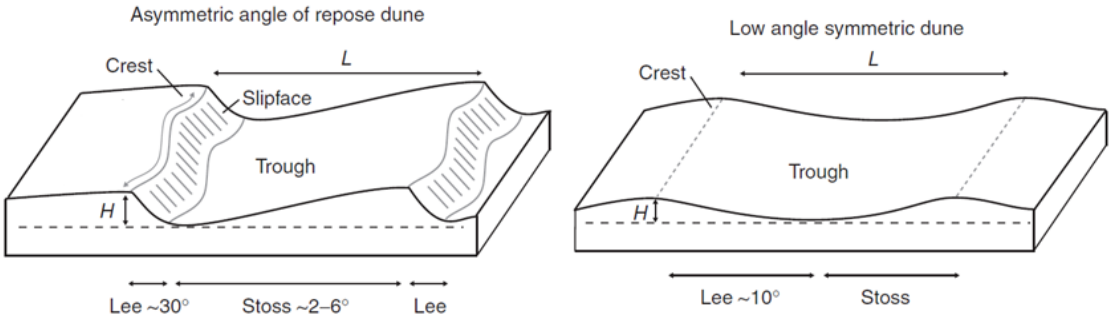

Figure 1.2. Schematics of angle of repose and low angle symmetric dune morphologies (e.g., Smith and McLean, 1977; Kostaschuk & Villard, 1996; Bradley et al., 2013; Hendershot et al., 2016). *L* is dune length, and *H* is dune height. Flow is from left to right (figure from Venditti (2013))

It remains unknown why different dune morphologies occur, mostly because low-angle dunes have never been produced under experimental conditions and it is difficult to make detailed observations in deep rivers. Low-angle dunes have been observed with superimposed high-angle bedforms (e.g., Carling et al., 2000; Sukhodolov et al., 2006) but superimposed bedforms are not found on all low-angle dunes (e.g., Nittrouer et al., 2008; Hendershot et al., 2016). It seems likely that flow depth is somehow important, but high-angle dunes can be present in deep rivers (*cf.*, Hendershot et al., 2016; Galeazzi et al., 2018) and marine environments (*cf.*, Ashley, 1990; Franzetti et al., 2013), so depth may not be the sole control.

The relative importance of bedload versus suspended load is often cited as a control on lee angle. Steep angles are maintained by a constant bedload supply to the crest (Bridge, 2003; Kostaschuk, 2006), and low-angle dunes are commonly found where large volumes of bed material are moved through suspension (e.g., Kostaschuk & Church, 1993; Kostaschuk & Villard, 1996; Bradley et al., 2013). Bed material moving in suspension may bypass the crest and deposit in lower leeside and tough positions, starving the upper lee of a constant sediment supply needed to maintain steep crest avalanching (Kostaschuk & Villard, 1996; Kostaschuk et al., 2009). Hendershot et al. (2016) showed systematic decline in lee slope angle with increased bed-material suspension. However, dunes in shallow channels under conditions of high bed-material suspension, still display a high-angle slip face even though they are longer and flatter (Venditti et al., 2016). Recently, Hendershot et al. (2016) suggested that increased volumes of bed material supplied to crests of large dunes in deep rivers promote

liquefaction on the lee side and generate sand flows or avalanches that can occur on the lower lee angle slope, but this idea requires critical testing.

1.3. Scaling of Dunes

Even though different dune morphologies exist in deep and shallow channels, it is widely accepted that a definable characteristic of dunes is that their dimensions scale with flow depth (Bridge, 2003; Garcia, 2008; Venditti, 2013). Dunes are thought to have heights (H) and lengths (L) that scale with flow depth (h) as:

$$H = \frac{h}{6} \quad \text{(Eq. 1.2)}$$

$$L = 5h \quad \text{(Eq. 1.3)}$$

Dunes not following the above scaling relations are sometimes argued to be non-equilibrium features, adjusting to a change in flow. Equations 1.2 and 1.3 are often applied to predict dimensions in flow resistance calculations and estimates of scour depth (e.g., Engelund & Hansen, 1967; Fredsøe, 1982; van Rijn, 1984; Paarlberg et al., 2010) and some sediment transport equations (e.g., Simons et al., 1965; Engel & Lau, 1980; van den Berg, 1987; Mohrig & Smith, 1996). They also appear in methods to derive first order estimates of flow depth in paleo-environmental reconstructions (e.g., Bridge & Tye, 2000; Leclair & Bridge, 2001; Bridge, 2003; Adams & Bhattacharya, 2005; Poten & Plink-Bjorklund, 2007; Lunt et al., 2013).

The depth-scaling relations in Equations 1.2 and 1.3 are usually attributed to Yalin (1964); however, he originally proposed them as an "average of experimental points" and noted that $h/6$ represents an "average maximum" height. This suggests that his relations have been misused as a definition of equilibrium features. Allen (1984) further showed that field dunes may increase in size with the scale of the system, but the scatter about Equations 1.2 and 1.3 is tremendous (Figure 1.3). The scatter produces scaling relations for H that range between $h/2.5$ and $h/20$ (Figure 1.3a), while L scaling ranges between h and $16h$ (Figure 1.3b). Some of this scatter can be attributed to flow unsteadiness, but that does not solely explain the wide variation in scaling between systems. The lack of constant scaling with flow depth is further supported by empirical data from laboratory flumes (e.g., Venditti et al., 2005; Venditti et al., 2016). Dune

growth data from Venditti et al. (2005) showed that different equilibrium H and L occurred in runs with different flow strengths but with the same flow depth. Individual dunes showed much scatter about the equilibrium H and L, but none of the mean equilibrium heights conformed to the $h/6$ scaling.

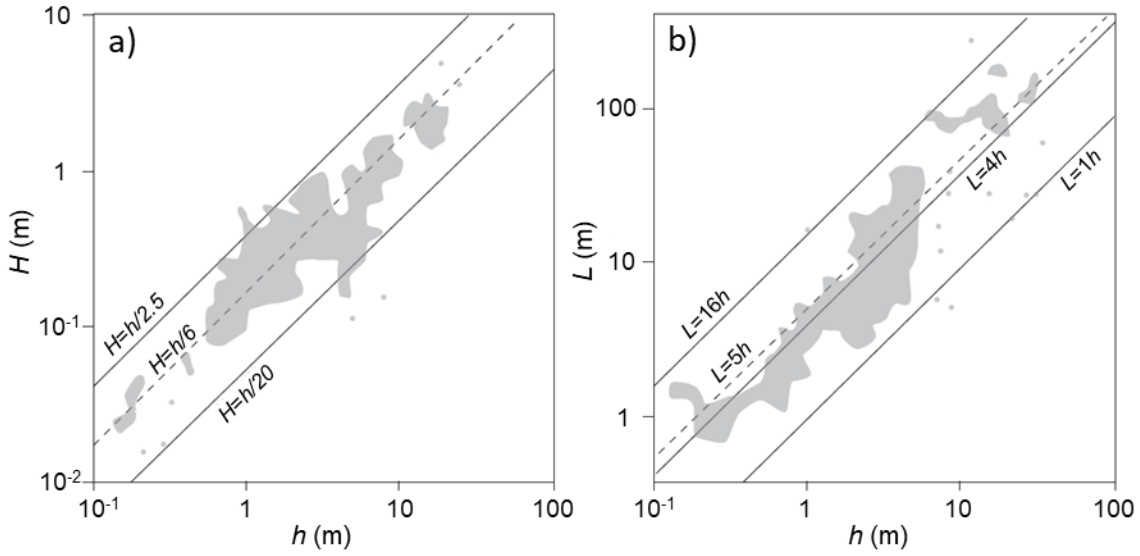

Figure 1.3. (a) Dune Height (*H*) and (b) Length (*L*) against depth (*h*) using data from Allen (1982). The grey areas cover the plot position of the data in Allen's (1982) complilation (figure from Venditti, 2013).

Flow depth must exert some constraint on H since dunes generally increase in size with the scale of the system and cannot grow above the water surface. However, variability about depth-scaling relations indicates that something else controls dune dimensions. Yalin's (1964) original work noted that transport stage, defined as the ratio of bed shear stress (τ) to its critical value for particle movement (τ_{cr}), affects dune dimensions. Transport stage is more commonly defined non-dimensionally using the ratio of the Shields number to the critical Shields number for sediment entrainment (τ_*/τ_{*c}). The Shields number is defined as:

$$\tau_* = \frac{\tau}{(\rho_s - \rho_w)gD} \qquad \text{(Eq. 1.4)}$$

where ρ_s is sediment density, ρ_w is the density of water and D is the representative grain size of the sediment, usually taken as the median grain size, D_{50}. Values of τ_{*c} vary with grain size (e.g., Shields, 1936; Brownlie, 1981). While transport stage as a control has been largely ignored in favor of depth scaling, subsequent data compilations have

confirmed that dune aspect ratio (H/L) changes with τ_*/τ_{*c} (Figure 1.4) (e.g., Yalin, 1972; Yalin & Karahan 1979; Allen 1982; Lin & Venditti, 2013). As τ_*/τ_{*c} increases, dunes steepen until a point where further increases to τ_*/τ_{*c} result in dune flattening until they wash out to an upper-stage plane bed. A series of observations from Venditti et al. (2016) showed that the pattern in Figure 1.4 emerges because H increases and then decreases with τ_*/τ_{*c} while L continually increases. It is therefore of concern that the role of transport stage has been ignored in dune scaling, given that early work by Yalin (Yalin, 1964; Yalin & Karahan, 1979) and Allen (1982) also highlighted the importance of τ_*/τ_{*c}.

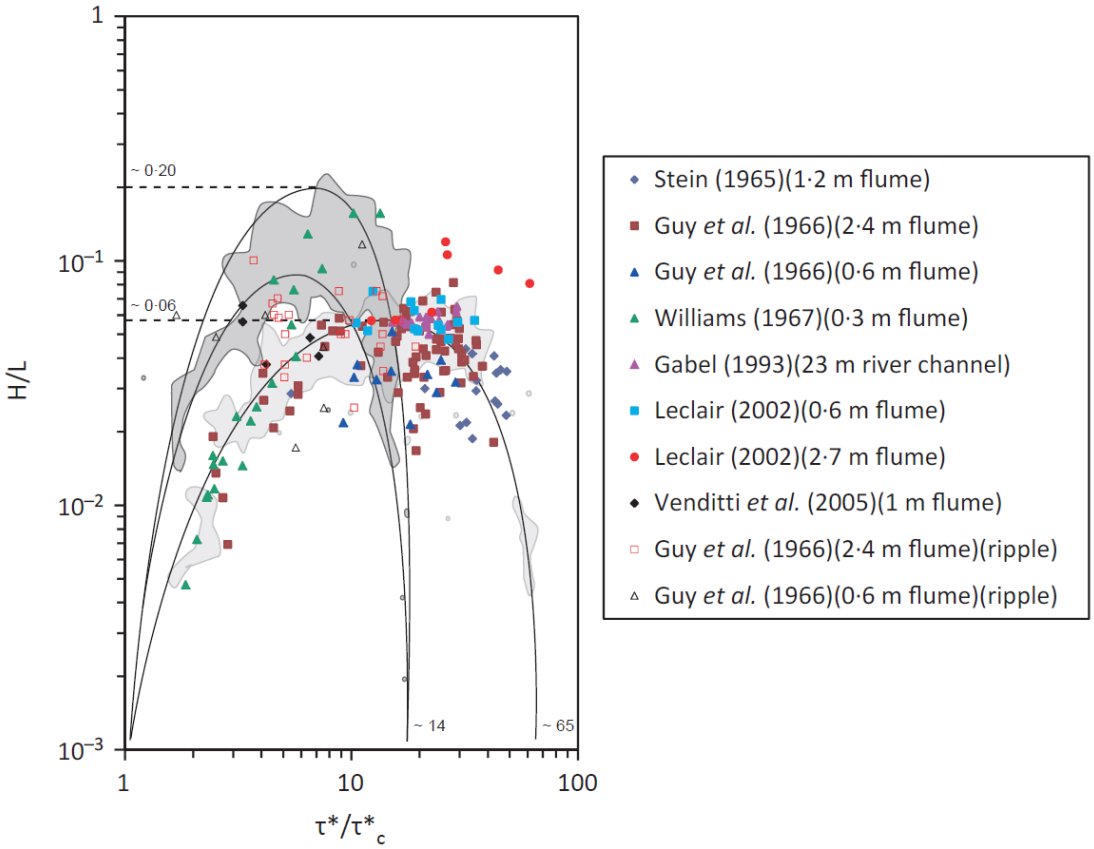

Figure 1.4. The aspect ratio (*H*/*L*) of equilibrium ripples and dunes plotted as a function of the transport stage (τ_*/τ_{*c}). The dark and light shaded areas (drawn in by Lin and Venditti (2013), based on data from Yalin (1972)) represent data clouds for ripples and dunes, respectively (figure from Lin and Venditti, 2013).

1.4. Physical Controls on Dune Size and Growth

Depth-scaling relations imply that dune growth is controlled by flow depth but the physical mechanism for this control has never been fully elucidated. Most geomorphologists and sedimentologists indicate dune size is controlled by boundary layer thickness. This notion appears to date back to Jackson (1975), who linked the thickness of the boundary layer to flow depth but offered no mechanistic reasoning. A boundary layer control is difficult to accept since a classically-defined boundary layer limit, where turbulence shifts from anisotropic to isotropic, seldom exists in rivers. Rivers are too shallow for a boundary layer to fully form, since macroturbulence produced from bed roughness leads to anisotropy throughout the water column (Nowell & Church, 1979).

The Froude number is also often cited as a potential control on dune dimensions. Bennett and Best (1996) proposed that all dunes grow up into the flow until the crest is planed off. They reasoned that growth stops because high Fr conditions at the crest prevent further deposition of sediment. This theory indirectly invokes a depth control since there is some critical height in the flow that a dune must reach to topographically force the flow over the crest such that it accelerates to critical conditions. There is little evidence in the literature to support this theory, especially considering dunes in deep channels. Froude numbers are commonly 0.1 to 0.3 in larger natural rivers, so dunes would have to grow extremely large relative to the flow depth to create critical flow at the crest. Furthermore, dunes exist in eolian and deep-sea environments where the *Fr* number is negligible. Dunes may be able to grow to heights that promote planing of the crest in shallow channels, but this cannot be the universal explanation for what controls the height of dunes.

Individual dune height has also been linked to how shear stress is distributed over a dune. Smith (1970) reasoned that the position of the maximum bedload sediment flux (q_{max}) relative to the topographic maximum over a dune controlled whether it would grow, be stable or erode. Dunes will maintain their height if the position of q_{max} is at the topographic maximum since erosion of the stoss is in balance with deposition on the lee (Figure 1.5a). If q_{max} is upstream of the crest (Figure 1.5b), more sediment is eroded along the stoss and supplied to the crest where deposition at the lee promotes growth. Dune height is lowered when q_{max} is downstream of the crest as bed material is eroded

from the topographic maximum (Figure 1.5c). The position of q_{max} over a dune depends on how the shear stress is distributed, suggesting shear stress as a potential control on dimensions. This supports the idea that transport stage (τ_*/τ_{*c}) controls dune dimensions because τ is included in the calculation of τ_*/τ_{*c} (Equation 1.4).

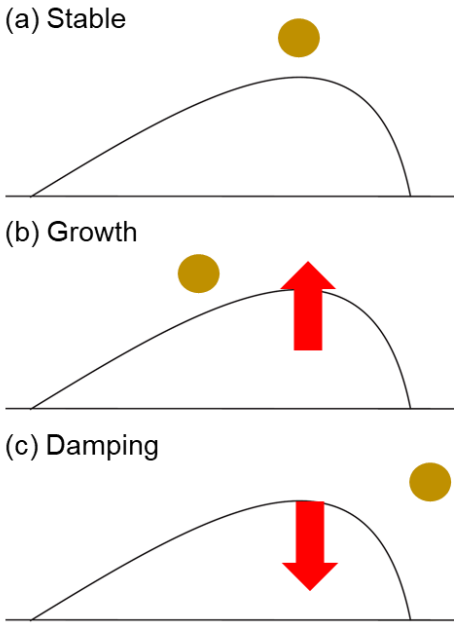

Figure 1.5. Dune response ((a) Stable, (b) Growth, (c) Damping) to position of the maximum sediment flux (circle).

Bed material suspension has also been connected to dune dimensions. Amsler & Schreider (1999) and Damen et al. (2018) observed a decrease in H in natural dune fields when suspension relative to bedload increased. It has been suggested that bed material moving in suspension bypasses the dune crest and deposits further downstream (Figure 1.6) (Naqshband et al., 2014; Hendershot et al., 2016). Less sediment supplied as bedload to the crest and avalanching slip face causes a decrease in H (Fredsoe, 1979; 1982). The propensity for suspension in rivers is defined by the ratio of the shear velocity ($u_* = \sqrt{\tau/\rho_w}$) to the settling velocity of particles (w_s), which also supports a shear stress control on dune dimensions. Furthermore, u_*/w_s is directly proportional to τ_*/τ_{*c} for a given grain-size, reinforcing early suggestions that transport stage may exert a fundamental control over dunes (*cf.,* Yalin, 1964; Yalin & Karahan, 1979; Allen, 1982).

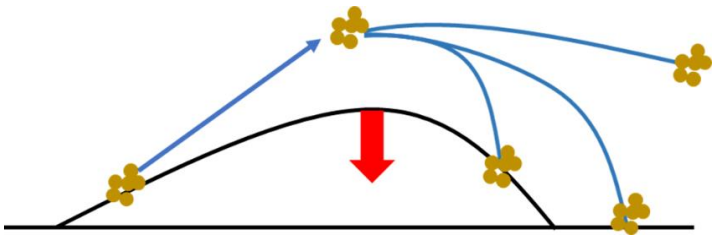

Figure 1.6. Cartoon demonstrating how sediment eroded along the stoss may bypass the crest and be deposited further downstream. This starves the crest of sediment, causing the dune to decrease in height.

1.5. Scope and Objectives

There is a practical need to directly predict dune dimensions in rivers for calculations of flow resistance and sediment transport, and to indirectly use dunes preserved in the rock record to hindcast paleo-flows. The most common way to predict dimensions is through depth-scaling relations that link H and L to h. These relations have the benefit of only requiring one easily measurable variable, but the variability about the relations limits their usefulness. Furthermore, it is likely that there are other processes controlling dune dimensions.

The central research question of this dissertation is: What controls dune dimensions and growth in rivers? This problem is approached through a meta-analysis of the largest collection of published dune dimension data compiled, and through a series of flume experiments in the River Dynamics Laboratory at Simon Fraser University. The specific objectives of the work are to:

1. Evaluate the predictive power of dune scaling relations and quantify the variability about them;

2. Determine the role of depth and transport stage on dune dimensions and variability;

3. Develop new scaling relations based in theory that offer measures of uncertainty;

4. Determine how dunes grow from a flat bed under different flow depths and transport stages and;

5. Develop a method for predicting bedform dimensions during growth.

In Chapter 2, the predictive ability of published scaling relations using depth and other variables is examined using a range of previously reported dune dimension data. The data are used to develop new scaling relations that account for the difference in morphology observed in shallow and deep channels. The data are also used to derive ranges about the scaling relations to provide uncertainty in predictions. Hypotheses are proposed that help explain the apparent scaling of dune dimensions with flow depth.

A series of flume experiments is presented in Chapters 3 and 4 where observations are made of dune development from a flat sand bed. Chapter 3 systematically examines the role of depth and transport stage on setting equilibrium dune dimensions. Measurements consist of dune dimensions and morphologies from a 10-hour equilibrium period when dune fields were in a statistical steady state. These data are used to propose new scaling relations between dune dimensions and transport stage, with the depth effect removed. The relations provide a physically-sound method to guide predictions of dune dimensions in rivers and paleo-reconstructions from estimated dune dimensions in the rock record.

Chapter 4 focuses on observations from the flume experiments when the bed initially evolved from a flatten state towards an equilibrium bedform field. The influence of flow depth and transport stage on bedform dimensions, morphodynamics, and growth curves is examined as the beds evolved through time. New predictive growth relations are proposed to empirically predict dune dimensions as they respond to imposed flows.

Chapter 5 summarizes results of Chapters 2 to 4 in context of the research objectives detailed above.

Chapter 2. Reevaluating Dune Scaling Relations

Abstract

In sand-bedded rivers, dunes dominate sediment transport and flow resistance. Dunes are also commonly preserved in fluvial deposits as cross-stratified units that record their size, shape and migration rates. Prediction of dune dimensions is therefore important for forecasting modern river channel dynamics as well as reconstructing past fluvial environments on Earth and other planets. Predictions are often made by assuming that the formative flow depth (h) sets dune dimensions with height scaling as 1/6h and length as 5h. Yet, there is a suite of other scaling relations that link dune dimensions to other variables like grain size, transport stage and Froude number. Here we present a new compilation of flow and dune dimension data to evaluate scaling relations. The data reveal approximately two orders of magnitude variation in dune height and length at any given flow depth. Dune heights in shallow flows (< 2.5 m), where strongly asymmetric dunes with high lee angles are common, are generally larger than 1/6h. Dunes in deeper channels (> 2.5 m) are often more symmetric, have lower lee angles, are relatively shorter in height than 1/6h and have a wider range of observed heights for a given depth. None of the scaling relations predict the observations exceptionally well, likely because of natural variability in dune dimensions and because they do not explicitly account for the apparent scaling break that occurs at 2.5 m. We propose new simple depth-scaling relations with added statistical uncertainty for the prediction of dune height and length from flow depth, as well as flow depth from dune height. We conclude that shallow and deep flow dunes exhibit different scaling due to a change in the dominant process controls as dunes get larger.

2.1. Introduction

Bedforms are common features in sediment-transporting flows at the Earth's surface. In sand-bedded alluvial channels, deformation of the labile bed through erosion and deposition produces bedforms that display specific geometric properties. These smaller than channel-scale features appear as a continuum where lower-stage plane beds, ripples, dunes, upper-stage plane beds, antidunes and cyclic steps emerge as a typical sequence of bedforms as flow is increased (Simons & Richardson, 1961;

Southard & Boguchwal, 1990; Venditti, 2013; Cartingy et al., 2014). Numerous phase diagrams have been developed that link bedform type to a variety of hydraulic and sedimentary variables such as depth, sediment size and dimensionless shear stress (e.g., Allen, 1982; van Rijn, 1984; Southard & Boguchwal, 1990; Carling, 1999; Cartingy et al., 2014; Baas et al., 2016). However, our ability to predict bedform size, morphology and dynamics is limited due to complex interactions at the fluid–sediment interface.

Dunes are of particular interest to geomorphologists, sedimentologists, and hydraulic engineers because they are common features in modern sand-bedded rivers and significantly affect channel dynamics. Dunes add form drag within a channel and thus can be an important source of flow resistance. The form drag occurs because turbulence and flow separation generated by dunes dissipate the mean flow energy of a river channel (Nelson et al., 1993; Nezu & Nakagawa, 1993; Hutoff, 2012; Kwoll et al., 2016). The growth and migration of dunes also provide an important mechanism for sediment movement via bedload (*cf.*, Simons & Richardson, 1966; van den Berg, 1987; Mohrig & Smith, 1996; Venditti et al., 2005a; McElroy & Mohrig, 2009; Naqshband et al., 2014a, Venditti et al., 2016). Dunes translate downstream by dune stoss erosion and lee slope deposition. As translation occurs, deformation of the dune form due to changes in shape, size and spacing also contributes sediment transport (McElroy & Mohrig 2009, Ganti et al., 2013, Venditti et al., 2016). In addition to bedload, large volumes of suspended sediment can be generated over dunes via large-scale turbulence (*cf.*, Rood & Hickin, 1989; Kostaschuk & Church, 1993; Venditti & Bennett, 2000; Kostaschuk et al., 2009; Bradley et al., 2013) and sediment entrained into suspension on the stoss slope may bypass the crest and move further down the channel (Mohrig & Smith, 1996).

Knowledge of bedform dynamics is important in order to understand modern channel processes but it can also provide information about channels no longer present at Earth and other planetary surfaces. The migration of dunes leaves behind characteristic primary sedimentary structures (cross-strata) in sand deposits. Cross-stratified units made up of cross-sets preserved between two successive erosional surfaces are formed by ancient dunes (e.g., Allen, 1970; Rubin & Hunter, 1982; Jerolmack & Mohrig, 2005; Ganti et al., 2013) and are common features in sedimentary strata. Cross-set thickness distribution is often linked to formative bedform dimension distributions theoretically (*cf.* Paola & Borgman, 1991; Bridge & Best, 1997) or

empirically (*cf.* Bridge, 1997; Leclair et al., 1997; Leclair & Bridge, 2001; Leclair, 2002; Leclair, 2011). Interpretation of these deposits requires a physically based understanding of modern dune processes.

Both the direct problem of predicting dune characteristics from observed flow characteristics and the inverse problem of reconstructing flow conditions from dunes preserved in the rock record rely on relations between flow characteristics and dune dimensions. Dune dimensions predicted through the direct problem are used as a quantitative measure of roughness height in flow resistance calculations and estimates of scour depth (e.g., Engelund & Hansen, 1967; Fredsøe, 1982; van Rijn, 1984; Paarlberg et al., 2010). Furthermore, many sediment transport equations include dune dimensions (*cf.*, Simons et al., 1965; Engel & Lau, 1980; van den Berg, 1987; Mohrig & Smith, 1996). In the inverse problem, estimated dune heights based on cross-strata are used to make first order estimates of flow depth in paleo-environmental reconstructions (e.g., Bridge & Tye, 2000; Leclair & Bridge, 2001; Bridge, 2003; Adams & Bhattacharya, 2005; Poten & Plink-Bjorklund, 2007; Lunt et al., 2013). However, the success of these reconstructions depends critically on the relation that links dune dimensions to flow characteristics.

The importance of dunes for understanding modern river channel dynamics, as well as reconstructing past flows, has resulted in a long history of relations between various flow parameters and dune height and length. These relations are commonly referred to as ‘scaling relations’, even though not all are power laws that express a scale factor (coefficient) and a scale distortion factor (exponent), conditions normally required to establish a formal scaling (Barenblatt, 2003). While some of the relations between flow and dune geometry are formal scaling relations (e.g., Van Rijn, 1984; Julien & Klaassen, 1995; Karim, 1999), many are not (e.g., Yalin, 1964; Gill, 1971; Allen, 1978; Karim, 1995) so we use the term scaling relations in a more informal sense to refer to all relations linking flow and dune dimensions.

The most commonly used scaling relations link dune dimensions to boundary layer thickness, usually assumed to be flow depth in rivers (*cf.* Yalin, 1964). Fully developed dunes, when dimensions are not adjusting to a change in flow strength, are widely thought to have heights 1/6 flow depth (h) and lengths of $5h$ (Yalin, 1964). Dunes not conforming to these simple relations have been argued to be non-equilibrium

features (e.g., Carling et al., 2000; Bridge, 2003; Holmes & Garcia, 2008). In addition to simple depth-scaling relations, there are also more complex relations that link dune dimensions to other hydraulic and sedimentary characteristics (*cf.*, Allen, 1978; van Rijn, 1984; Karim, 1995). The wide array of scaling relations proposed in the literature reflects a lack of consensus on the mechanisms controlling dune dimensions, leading geomorphologists, sedimentologists, and hydraulic engineers alike, to often rely on the Yalin (1964) relations. However, individual dunes in large alluvial dune fields can have a wide range of height and lengths at the same flow depth. For example, dune fields in the lower Fraser River have many sizes of dunes, despite all existing at similar flow depths (Figure 2.1a). Observations of dune heights (H) and lengths (L) in other large alluvial channels (Mississippi, Columbia and Parana Rivers), also show that H and L vary substantially within a dune field (Figure 2.1b,c). Given that so much natural variability exists even within bedform fields, it is surprising that scaling relations do not have some measure to characterize this variability.

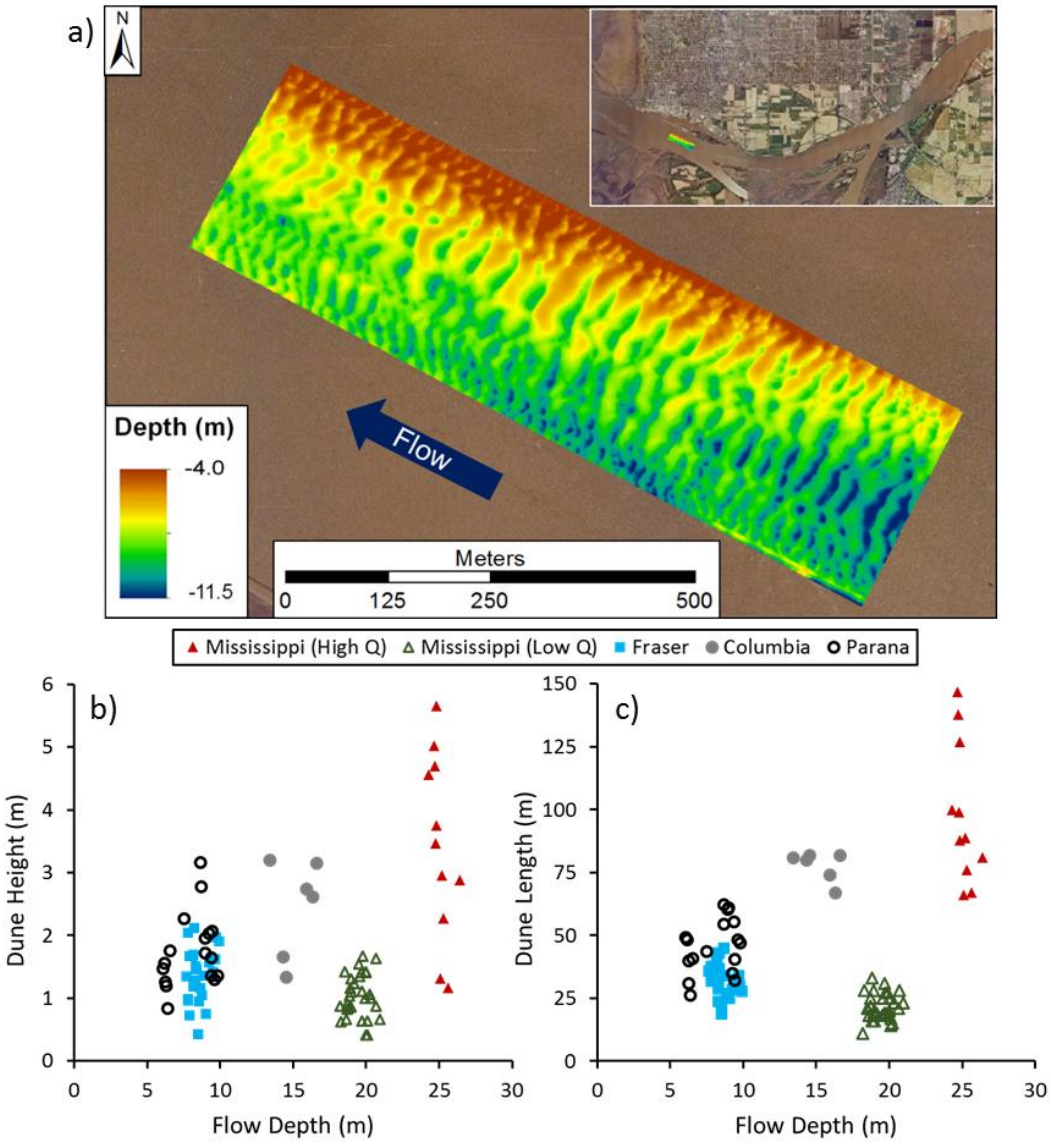

Figure 2.1. **(a) Bathymetric map of the Main Arm of the Fraser River off Steveston, British Columbia Canada (from Hendershot et al., 2016). Individual dune (b) height and (c) length plotted as a function of flow depth. Data from the Mississippi River provided by Jeffery Nittrouer (unpublished) and from the Parana River provided by Dan Parsons (unpublished). Columbia River data are from Smith & McLean (1977) and the Fraser River data are from the centerline of panel a.**

This review examines our current understanding of the controls on dune dimensions in rivers through a meta-analysis of dune scaling relations. A review of published scaling relations is presented, and relations are tested against a newly compiled set of previously published and some unpublished observations of dune dimensions from unidirectional flows in flumes and rivers. This new data set includes high spatial resolution observations derived from multibeam echo-sounding that provide

the complete dune field topography, rather than relying solely on single beam echo-sounders that may poorly characterize dune dimensions when transects are misaligned with the dune field. The data set is used to develop new scaling relations that account for natural dune variability using prediction intervals. The specific objectives of this review are: 1) to evaluate dune scaling relations; 2) to develop new scaling relations that can be used to predict dune dimensions in modern channels, as well as reconstruct past flows from dunes preserved in the rock record; 3) to incorporate variability in appropriate scaling relations; and 4) to determine the controls on dimensions of dunes in rivers.

2.2. Dune Scaling Relations

Dune-dimension scaling relations can broadly be classified as those that are based on: (1) depth (Yalin, 1964); (2) depth and grain size (Julien & Klaassen, 1995); (3) transport stage (Allen, 1978; Karim, 1995; van Rijn, 1984); and (4) transport stage and Froude number (Gill, 1971; Karim, 1999). Transport stage is defined broadly here as any metric that is composed of a ratio of the shear stress to a grain-size. This includes the Shields number and the ratio of shear velocity to particle settling velocity or more exotic metrics in the same form (e.g., van Rijn, 1984). It also includes the ratio of the shear stress to the critical shear stress, the latter of which is indexed to a specific grain size. In our assessment of scaling relations, we have not included relations that mathematically or numerically link dune dimensions to characteristics of the flow because they require explicit coupling of equations for fluid motion and sediment transport (*cf*., Ranga Raju-Soni, 1976; Fredsøe, 1982; Tjerry & Fredsøe, 2005). The resultant numerical and/or analytical solutions are not generally applicable in either the direct or inverse problems at present. We focused on the well-defined empirical relations that are most often applied by geomorphologists, sedimentologists and engineers.

2.2.1. Yalin (1964)

Yalin (1964) provides the most widely used dune scaling relations to link bedform dimensions to flow depth. Using dimensional analysis and previously unpublished and published flume observations (Barton & Lin, 1955; Singh, 1960; Shinohara & Tsubaki,

1959; Vanoni & Brooks, 1957), as well as some field data (Shinohara & Tsubaki, 1959; Lane & Eden, 1940), Yalin proposed the following scaling relation for dune height (*H*):

$$\frac{H}{h} = \frac{1}{6}\left(1 - \frac{\tau_c}{\tau}\right) \quad \text{(Eq. 2.1)}$$

where h is flow depth, τ_c is critical shear stress for the median bed material size from the Shields curve and τ is 'an average value of shear stress acting on the bed', which implies it is the total shear stress (not corrected for form drag). Yalin (1964) attributed any variability about this relation to experimental error, particularly in how authors recorded and reported the dune height. The behavior of Equation 2.1 is shown in Figure 2.2a with varying values of τ_c/τ that correspond to bedload dominated, mixed load and suspension dominated conditions. Church (2006) established ranges for the inverse of τ_c/τ, that suggest bedload dominated (BLD) conditions occur when $1 < \tau/\tau_c < 3.3$, mixed-load dominated (MXD) conditions occur when $3.3 < \tau/\tau_c < 33$ and suspended-load dominated (SSD) conditions occur when $\tau/\tau_c > 33$. The conditions were defined using the thresholds for motion and suspension, established empirically for reach scales. The behavior of these relations is shown in Figure 2.2a for a threshold condition, and the approximate logarithmic mean for BLD, MXD, and SSD. The logarithmic mean for the SSD was determined using an upper limit of $\tau/\tau_c = 65$ which was found by Yalin (1972) to be the upper limit for when dunes form in channels.

In our calculations, the ratio τ/τ_c is calculated from the ratio of the critical Shields number for entrainment (τ_{*c}) to the Shields number calculated as:

$$\tau_* = \frac{\tau}{(\rho_s - \rho_w) g D_{50}} \quad \text{(Eq. 2.2)}$$

where D_{50} is the median diameter of the material, ρ_s is the sediment density (assumed ρ_s = 2650g/m^3), ρ_w is the density of water and τ is bed shear stress given as:

$$\tau = \rho_w g h S \quad \text{(Eq. 2.3)}$$

where g is gravitational acceleration and S is the slope. Values of τ_{*c} vary with properties of the flow and sediment and can be obtained from the Shields diagram. As the bed shear stress increases beyond the critical shear stress required for bed movement, dunes grow towards 1/6h as suggested by the Yalin (1964) relation (Equation 2.1). As shear stress increases at a given flow depth, dunes grow larger (Figure 2.2a). At τ/τ_c =

10, H is within 10% of 1/6h and τ/τ_c has little effect on the relation. Equation 2.1 was subsequently simplified (*cf*. Allen, 1976) as:

$$H = \frac{h}{6} \qquad \text{(Eq. 2.4)}$$

to describe equilibrium dune height, ignoring the effect of shear stress. This assumption is now the conventional definition of dune equilibrium even though Yalin (1964) originally proposed it as an upper limit of growth. Fitting a line to his data set, Yalin (1964) proposed an empirical scaling relation for dune length (L) as:

$$L = 5h \qquad \text{(Eq. 2.5)}$$

which has also been widely accepted as an equilibrium length.

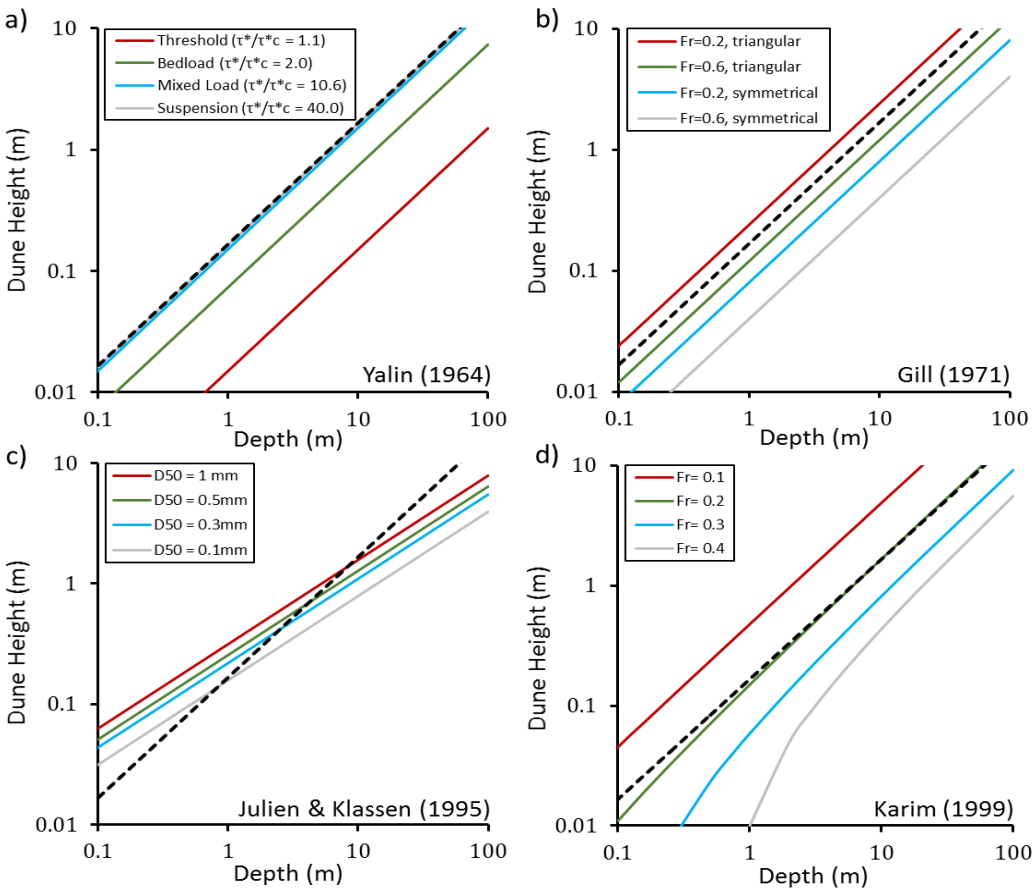

Figure 2.2. Dune height plotted as a function of depth using the scaling relations of (a) Yalin (1964) with different transport stages, (b) Gill (1971) with triangular dunes and symmetrical dunes at Froude numbers of 0.2 and 0.6 under mixed load conditions, (c) Julien and Klaassen (1995) with varying median grain sizes and (d) Karim (1999) with different lower regime Fr numbers. The black dashed line in each panel is the Yalin (1964) simplified equation $H = h/6$.

2.2.2. Gill (1971)

Citing experimental observations from Simons and Richardson (1962) where dunes grew larger in the flow than predicted by $h/6$, Gill (1971) argued that Yalin's (1964) relation was not always valid. Gill (1971) added a modified Brown–Einstein bed load equation from Gill (1968) and the Froude number to derive the following scaling relation:

$$\frac{H}{h} = \frac{1-Fr^2}{2\eta\beta}\left(1 - \frac{\tau_c}{\tau}\right) \qquad \text{(Eq. 2.6)}$$

where Ƞ is an empirical coefficient from the Einstein–Brown formula, β is a shape coefficient that varies with dune geometry (for triangular dunes β = ½, symmetrical dunes β = 2/π) and Fr is the Froude Number:

$$Fr = \frac{\bar{U}}{\sqrt{gh}} \qquad \text{(Eq. 2.7)}$$

where $\bar{U}$ is the mean flow velocity. Gill (1971) did not test Equation 2.6 with any empirical data so it is unclear how well it predicts dune height. Gill also acknowledged that the value for Ƞ could be a significant source of error, stating that it could lie somewhere between 3/2 and 3, but the author did not suggest an appropriate value. The scaling relation using triangular dunes and symmetrical dunes with *Fr* equal to 0.2 and 0.6 is shown in Figure 2.2b using Ƞ = 3. Figure 2.2b is plotted using mixed load conditions (τ/τ_c= 10) to highlight the effect of *Fr* and β on the relation, but varying the τ/τ_c has a similar response to Figure 2.2a where dunes grow larger in the flow towards a maximum height with increasing shear stress above the critical value. The Froude number controls how large dunes will grow in the channel, as lower Froude numbers predict larger dunes, while the shape coefficient predicts that triangular dunes will grow relatively larger than the sinusoidal dunes (Figure 2.2b).

2.2.3. Allen (1978)

Allen (1978) argued that dunes grow larger in a flow with increasing transport stage up to a point when the increasing flow strength leads to smaller dunes as they begin washing out to an upper stage plane bed. Allen (1978) showed this behavior using data from flume experiments of Stein (1965) to which he fit a fourth-order polynomial that included the Shields number (Equation 2.2) to give:

$$\frac{H}{h} = 0.08 + 2.24\left(\frac{\tau_*}{3}\right) - 18.13\left(\frac{\tau_*}{3}\right)^2 + 70.9\left(\frac{\tau_*}{3}\right)^3 - 88.33\left(\frac{\tau_*}{3}\right)^4 \qquad \text{(Eq. 2.8)}$$

The relation is limited to flows where 0.25 < τ_* < 1.5 as this was the range observed in the experiments. This relation shows that dunes grow larger as τ_* initially increases reaching a maximum *H* when τ_*= 1.20. Dunes then get smaller in height until they wash out at τ_*= 1.5 (Figure 2.3a). For most of the Shields number range, dunes plot higher than predicted by the *h*/6 relation (Figure 2.3a).

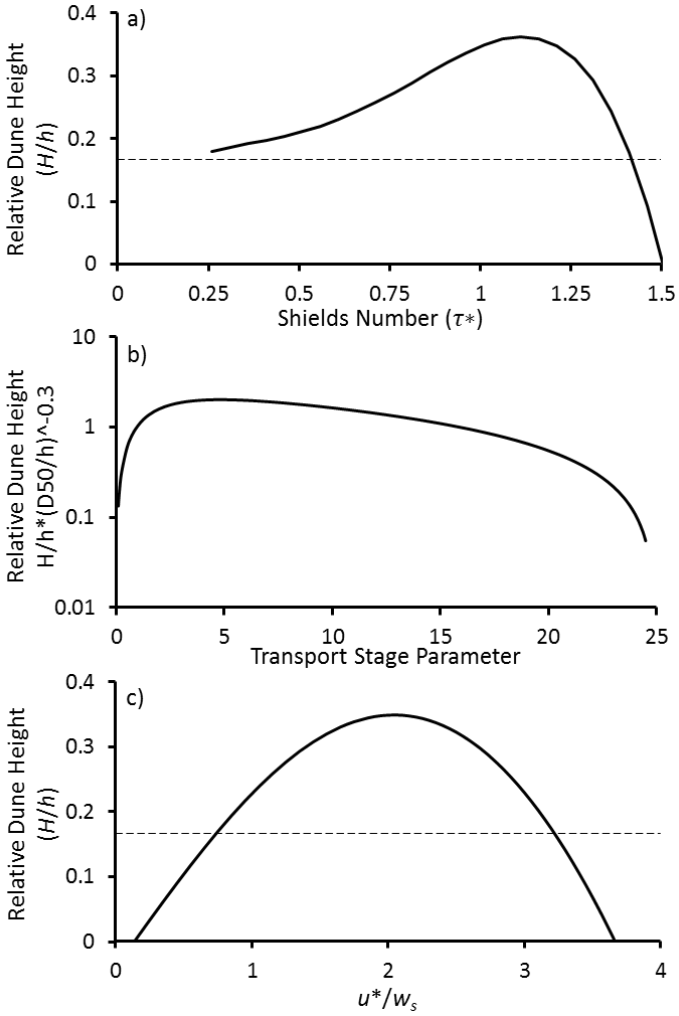

Figure 2.3. (a) Relative dune height plotted against Shields number using Allen (1978). (b) Relative dune height defined as $\frac{H}{h} * \left(\frac{D_{50}}{h}\right)^{-0.3}$ plotted against the van Rijn (1984) transport stage parameter. (c) Relative dune height as a function of a suspension criteria defined as the ratio of shear velocity (u_*) to settling velocity (w_s) using Karim (1995). The black dashed line is the simplified version of Yalin (1964).

2.2.4. van Rijn (1984)

van Rijn (1984) also acknowledged the influence of transport stage. Using data from 84 flume experiments (Guy et al., 1966; Stein, 1965; Delft Hydraulics, 1979; Williams, 1970; Znamenskaya, 1963) and 22 field observations (Lane & Eden, 1940;

Stuckrath, 1969; Tsubaki et al., 1953; van Urk & Klaassen,1982), van Rijn (1984) suggested that:

$$\frac{H}{h} = 0.11\left(\frac{D_{50}}{h}\right)^{0.3}(1 - e^{-0.5T})(25 - T) \quad \text{(Eq. 2.9)}$$

where T is a transport stage parameter defined as

$$T = \frac{(u\prime_*)^2 - (u_{*c})^2}{(u_{*c})^2} \quad \text{(Eq. 2.10)}$$

where u_{*c} is the critical grain shear velocity obtained from the Shields diagram and grain shear velocity u'_* is

$$u'_* = \overline{U}\sqrt{g/C'}. \quad \text{(Eq. 2.11)}$$

The Chezy-coefficient related to grain roughness is

$$C' = 18\log{*}\,12R_b/3D_{90} \quad \text{(Eq. 2.12)}$$

where R_b is the hydraulic radius, and D_{90} is the 90% percentile of the grain size of the bed material. Using alternative formulations of Equations 2.10-2.12 does affect how well Equation 2.9 fits the data and should therefore be avoided. Equation 2.9 imposes an upper limit for dunes since no predictions can be made where T > 25. The scaling relation suggests that dune height increases at an initially steep slope with T until around T = 3 when it begins to decrease with transport stage until the dunes wash out (Figure 2.3b).

van Rijn (1984) also provided an equation for dune steepness:

$$\frac{H}{L} = 0.015\left(\frac{D_{50}}{h}\right)^{0.3}(1 - e^{-0.5T})(25 - T) \quad \text{(Eq. 2.13)}$$

and equated Eq. 2.13 to Eq. 2.9 to provide a depth-scaling relation for dune length:

$$L = 7.3h \quad \text{(Eq. 2.14)}$$

This implies that dune length is only related to mean flow depth while height is controlled by transport stage. It also further suggests that bedform height will increase and then decrease with flow strength at a constant flow depth until dunes flatten and wash out.

2.2.5. Julien and Klaassen (1995)

Julien and Klaassen (1995) showed that the relations of van Rijn (1984) did not accurately predict dune dimensions in deep rivers because the relations were empirical fits to primarily flume data. They also provided evidence that dunes in deep rivers can exist when $T > 25$. Adding some previously unpublished data to published data sets (Julien, 1992; Wijbenga, 1991; Shen et al., 1978; Peters, 1978; Adrianse, 1986; Brillhuis, 1998; Kamphuis, 1990), Julien and Klaassen (1995) proposed that dune height scales with depth as:

$$H = \varepsilon h \left(\frac{D_{50}}{h} \right)^{0.3} \quad \text{(Eq. 2.15)}$$

where $0.8 < \varepsilon < 8$ with a mean ε of 2.5, whereas dune length scales as

$$L = 6.25h. \quad \text{(Eq. 2.16)}$$

No guide is provided by the authors as to what values should be used for the empirical coefficient ε, except that higher values were observed during floods. They furthered argued that dune height does not decrease with increasing shear stress, but rather the height remains relatively constant. The height scaling relation behavior is shown in Figure 2.2c with ε = 2.5 and various sand sizes. Dune height increases with depth at a lower rate than the Yalin (1964) relation, and larger grain sizes predict larger dunes.

2.2.6. Karim (1995)

Building on Allen (1978) and van Rijn (1984), Karim (1995) further acknowledged that dune height is a parabolic function of transport stage and developed a relation between *H*/*h* and a suspension criterion in the form u_*/w_s (u_* is bed shear velocity as $\sqrt{ghs}$, and w_s is the particle fall velocity). The suspension criterion has the same basic form as the Shields number (a metric of the shear stress divided by a grain size metric) and $\tau^* \propto \sqrt{u_*/w_s}$ (see Venditti et al., 2016). Using the data set of Allen (1978), adding some observations from (Guy et al., 1966) and previously unpublished field data, Karim (1995) fit a 4th order polynomial to the observations giving:

$$\frac{H}{h} = -0.04 + 0.294 \left(\frac{u_*}{w_s}\right) + 0.00316 \left(\frac{u_*}{w_s}\right)^2 - 0.0319 \left(\frac{u_*}{w_s}\right)^3 + 0.00272 \left(\frac{u_*}{w_s}\right)^4 \quad \text{(Eq. 2.17)}$$

Dune height increases with u_*/w_s until a maximum value is reached at u_*/w_s = 2.0 where it begins to decrease (Figure 2.3c). Karim (1995) argued that suspended sediment transport becomes more important in controlling bedform height than bed load transport when u_*/w_s = 2.0. In this scaling relation, the presence of dunes is limited to 0.15 < u_*/w_s < 3.64.

2.2.7. Karim (1999)

Karim (1999) argued that energy loss produced by form drag from bedforms could be estimated from the head loss across a sudden expansion in open channel flows. Using this energy loss concept, a scaling relation was derived as:

$$\frac{H}{h} = \left[\frac{\left(S - 0.0168\left(\frac{D_{50}}{h}\right)^{0.33} * Fr^2\right)\left(\frac{L}{h}\right)^{1.20}}{0.47Fr^2}\right]^{0.73} \quad \text{(Eq. 2.18)}$$

In addition to dunes, this relation was proposed for ripples and transitional features when dunes wash out to plane bed. Karim (1999) suggested that the Julien and Klaassen (1995) length scaling relation (Eq. 2.14) should be used in Equation 2.18 when predicting the height of dunes. Equation 2.18 is plotted in Figure 2.2d assuming a grain size of 300 μm and a slope of 0.0002 with varying Froude numbers. Dunes grow higher in the flow with decreasing Froude number.

2.3. Data Compilation

In order to evaluate the dune scaling relations, we compiled a data set of dune dimensions and flow characteristics from both laboratory flume experiments and field observations from all published and unpublished sources known and accessible to the authors. Data were selected from this set for further analysis based on three criteria. First, primary dune dimensions and depth needed to be reported as reach-averaged values of dune fields or such that they could be calculated. Smaller dunes superimposed on larger dunes were excluded because these features more likely scale with local flow conditions over the larger feature (Jackson, 1975). The use of reach-averaged data is also necessary to reduce the variability associated with individual dunes that can be found within a dune field (Figure 2.1). The second criterion was that all dunes were fully adjusted to flow conditions, meaning they were not systematically growing or shrinking in

response to sharp rising or falling hydrographs. Hysteresis effects can result in dunes requiring days to weeks to readjust to flow conditions depending on the flow magnitude change and dune size (Pretious & Blanch, 1951; Allen, 1974; Villard & Church, 2003), so we have eliminated data when authors acknowledged hysteresis effects. The final criterion was that the reported bedforms dimensions were consistent with dune terminology. Bed features that scale with channel width (bars; see Jackson, 1975; Bridge, 2003) or grain size (ripples; see Allen, 1982; Bartholdy et al., 2015) have not been included in this data set. For example, Shen et al. (1978) reported 'dune' features with lengths and heights that are consistent with channel bars, so these data were not included. In total, 664 reach-averaged height observations were recovered from 22 flume experiments (282 observations; Table 2.1) and 24 field studies (382 observations; Table 2.2). Fewer data were available for dune lengths and flow depth, with a total of 498 observations coming from 21 flume experiments (256 observations; Table 2.1) and 20 field studies (242 observations; Table 2.2).

Table 2.1. Flume data used to test the scaling relations. See Appendix A for complete references and Appendix B for detailed data set.

Data Source	# of Points	# of Length Points	# of Transport Stage Points	Flow Depth Range (m)	Dune Height Range (m)	Dune Length Range (m)	Transport Stage Range
Bishop (1977)	22	22	22	0.10-0.19	0.02-0.08	0.80-1.60	1.79-9.63
Blom et al. (2005)	8	8	8	0.15-0.39	0.02-0.12	0.6-1.79	4.83-21.36
Bridge & Best (1988)	2	2	2	0.1	0.02-0.03	0.75-0.76	29.96-33.29
Coleman & Melville (1994)	2	-	2	0.13	0.02-0.02	-	5.50-7.37
Coleman et al. (2005)	13	13	13	0.10-0.17	0.01-0.04	0.11-0.72	1.77-22.68
Guala et al. (2014)	3	3	3	0.19-0.22	0.02-0.03	0.29-0.48	2.94-4.57
Guy et al. (1966)	65	65	65	0.13-0.34	0.01-0.2	0.31-5.40	2.21-46.53
Iseya (1984)	6	6	6	0.17-0.48	0.02-0.18	0.79-3.42	5.24-41.84
Kuhnle & Wren (2009)	2	2	2	0.22	0.06	1.13-1.42	13.99-20.27
Leclair (2002)	26	23	24	0.15-0.90	0.04-0.14	0.71-1.50	7.31-99.42
Naqshband et al. (2014a)	2	2	2	0.25	0.07-0.08	2.25-4.35	7.99-22.27
Nordin (1971)	4	4	4	0.16-0.85	0.04-0.08	0.88-1.47	12.29-27.98
Schindler & Robert (2005)	4	4	4	0.15-0.17	0.03-0.03	0.46-0.84	35.06-41.25
Simons et al. (1961)	10	10	10	0.12-0.30	0.05-0.16	0.39-0.70	3.16-33.74
Simons et al. (1963)	41	40	41	0.16-0.41	0.02-0.13	1.01-2.50	2.33-44.23
Stein (1965)	37	17	37	0.12-0.37	0.03-0.13	1.37-3.41	2.90-50.22
Tuijinder et al. (2009)	3	3	3	0.15-0.20	0.07-0.08	1.37-1.44	7.99-14.73
Venditti et al. (2005)	5	5	5	0.15	0.02-0.05	0.30-1.17	1.87-5.11
Venditti et al. (2016)	3	3	3	0.13-0.15	0.04-0.07	0.91-2.06	5.52-34.92
Wijbenga & Klaassen (1983)	7	7	7	0.20-0.41	0.07-0.10	1.20-1.59	9.05-20.94
Williams (1967)	9	9	9	0.15-0.16	0.01-0.05	0.55-1.59	2.83-13.09
Wren et al. (2007)	8	8	8	0.19-0.21	0.06-0.07	1.35-1.71	4.94-10.38

Table 2.2. Field data used to test the scaling relations. See Appendix A for complete references and Appendix B for detailed data set.

Data Source	River	# of Points	# of Length Points	# of Transport Points	Flow Depth Range (m)	Dune Height Range (m)	Dune Length Range (m)	Transport Stage Range
Adel-Fattah et al. (2004)	Nile	4	4	4	3.51-5.17	0.70-1.60	22.00-44.00	5.85-10.85
Amsler (2003)	Parana	58	-	-	6.80-24.50	0.27-4.62	-	-
	Amazon	1	-	-	35.50	6.13	-	-
	Uruguay (FICH 2002)	8	-	-	7.10-9.50	0.70-1.65	-	-
	Araguaia	4	-	-	2.10-3.80	0.40-0.61	-	-
Culbertson et al. (1972)	Rio Grande	3	3	3	4.27-4.56	0.79-1.28	9.14-13.41	219.36-255.59
Gabel (1993)	Calamus	15	15	10	0.34-0.06	0.10-0.20	2.00-4.05	45.40-61.07
Holmes & Garcia (2008)	Missouri	3	3	3	4.84-6.46	0.32-1.25	5.70-140.00	53.7-67.43
Jordan (1962)	Mississippi	6	6	-	8.53-27.43	1.52-5.49	73.15-228.60	
Julien (1992)	Zaire (Peters 1978)	21	21	21	9.50-17.00	1.20-1.90	90.00-450.00	20.42-60.27
	Jamuna	33	33	33	8.2-19.5	0.80-5.10	15.00-251.00	33.87-104.46
	Parana	13	13	15	22.00-26.00	3.00-7.50	100.00-450.00	61.69-74.65
Korchoka (1968)	Polomet	56	-	-	0.16-2.43	0.02-0.35	-	-
Kostaschuk (unpub)	Ob (2010)	1	1	-	6.00	0.53	20.30	-
	Parana (2004)	3	3	-	7.00-12.90	1.53-3.93	51.10-157.50	-
Mason (unpub)	Trinity (2014)	15	15	-	1.86-4.60	0.15-0.41	6.22-9.16	-
Neill (1969)	Red Deer	29	29	-	0.91-3.66	0.15-0.91	2.44-21.34	-
Nittrouer (unpub)	Mississippi	2	2	-	20.00-25.00	1.04-3.43	21.00-97.00	-
Nordin (1971)	Atrisco Lateral	3	3	3	0.67-0.70	0.11-0.12	1.61-1.87	18.02-20.35
Parsons (unpub)	Parana	1	1	-	6.79	1.48	53.92	-
Ramirez & Allison (2013)	Mississippi	8	8	-	19.33-20.67	0.15-0.39	4.07-10.87	-
Shinohara & Tsubaki (1959)	Hii	8	-	-	0.59-1.03	0.09-0.25	-	-
Strasser et al. (2002)	Amazon	7	7	7	16.82-60.36	1.74-7.44	81.61-312.94	15.96-78.47
Sukhodolov et al. (2006)	Embarras	1	1	1	0.35	0.13	2.00	4.45
Szupiany et al. (2012)	Parana	2	2	-	10.27-10.88	1.59-1.70	68.09-72.47	-
Toniolo (2013)	Tanana	4	4	-	5.14-5.90	0.60-1.20	41.30-66.70	-
Van der Mark et al. (2008)	North Loup	2	-	-	7.30-9.10	0.25	-	-
	Rhine	1	-	-	8.00	0.31	-	-
Venditti (unpub)	Fraser	1	1	-	14.46	0.65	10.05	-
Vendtiti & Bauer (2005)	Green	1	1	1	1.50	0.30	4.50	43.46
Wilbers (2004)	Rhine	68	66	-	3.28-10.73	0.14-1.19	3.91-46.70	-

The data compilation shows that dune height and length follow a power law:

$$H = 0.0513L^{0.7744} \quad \text{(Eq. 2.19)}$$

with a R^2 value of 0.89 (Figure 2.4). Equation 2.19 is similar to the relation of Flemming (1988):

$$H = 0.0677L^{0.8098} \quad \text{(Eq. 2.20)}$$

which was based on 1491 deep sea, tidal and river bedforms. This suggests that the dunes presented here are consistent with previous observations and implies similarity between the sub-aqueous environments.

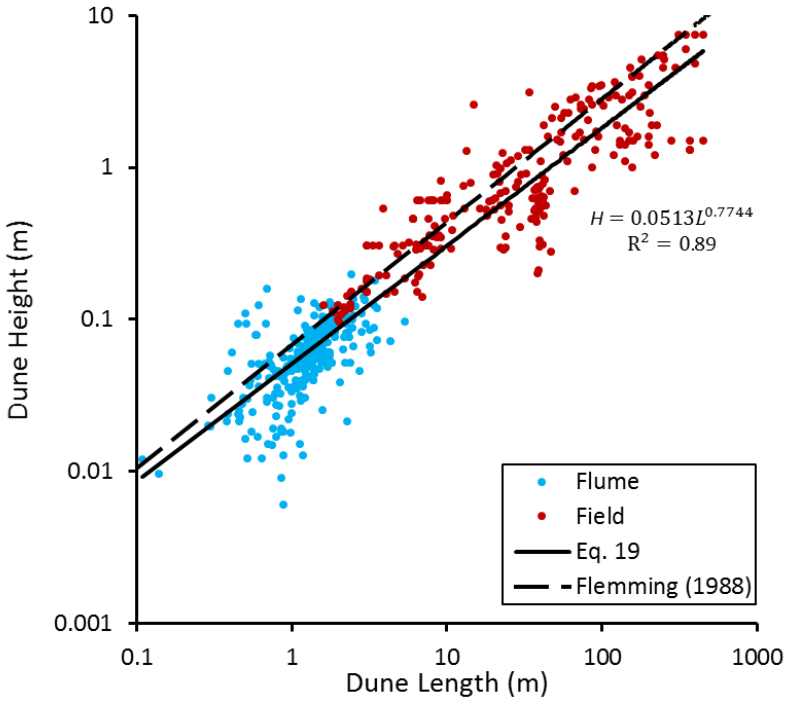

Figure 2.4. Dune height plotted as a function of length.

Dune heights (Figure 2.5a) and lengths (Figure 2.5b) increase with flow depth, supporting the long-held belief that flow depth influences dune dimensions (e.g., Yalin, 1964; Allen, 1982). This is expected since depth must exert some control on how large dunes can grow because dunes cannot emerge out of the water. The limits observed here are similar to those reported by Allen (1982) in his data compilation (Figure 2.5). Almost no data plot above $H = h/2.5$, indicating that this may represent the upper limit of dune growth in rivers, contrary to Yalin's suggestion that $H = h/6$ is the limit of dune

growth. A lower limit for height is more poorly defined. However, recent work with multi-beam echo sounders has shown that individual dunes in a larger dune field can have heights much smaller than h/H = 20 in the Mississippi River (Nittrouer et al., 2011) (Figure 2.1b) and under sediment supply limited conditions in the Fraser River, dunes can be as small as h/H= 100 (Figure 2.6a). These observations from the Mississippi and Fraser River cast doubt on the idea that depth is the fundamental control on dune dimensions. Our data compilation suggests that any size dune is possible below ~$h/2$. The $h/6$ Yalin relation (Equation 2.3) roughly runs through the middle of the data set, but does not adequately characterize the variability.

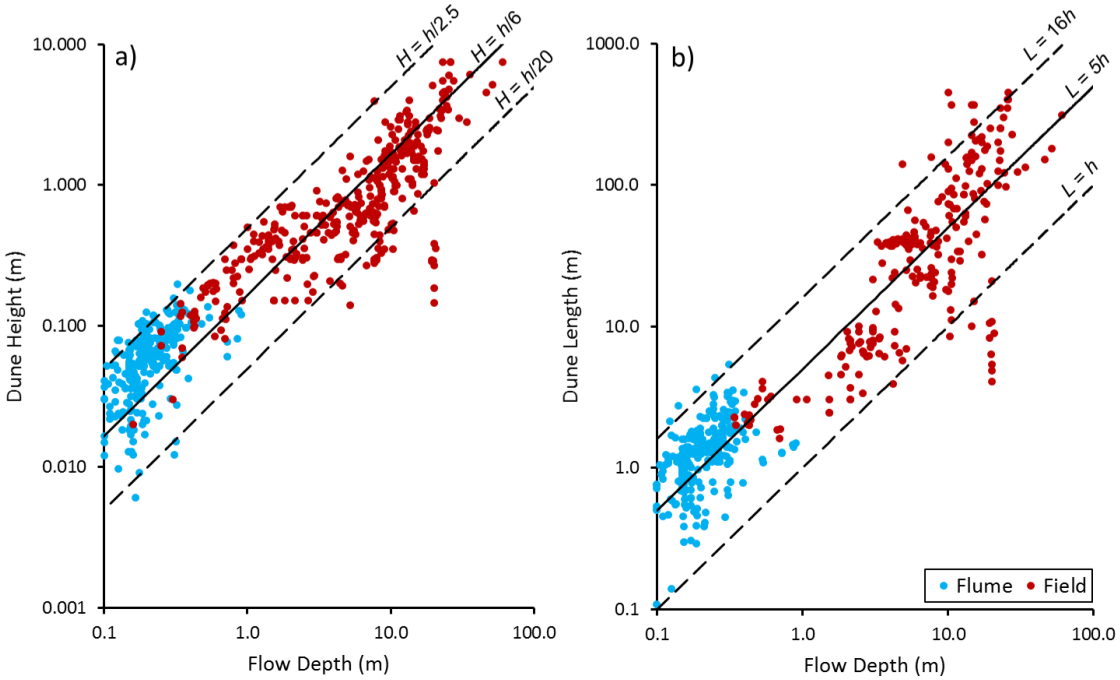

Figure 2.5. (a) Dune height plotted against flow depth. (b) Dune length plotted against flow depth. The dashed black lines are limits reported by Allen (1982) and the solid black lines are the simplified $H = h/6$ and $L = 5h$ scaling relations of Yalin (1964).

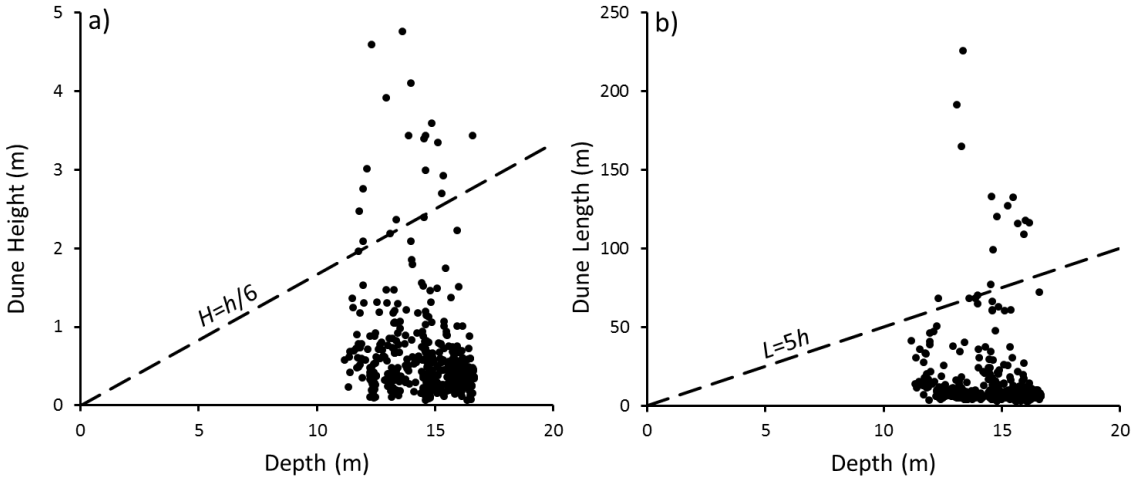

Figure 2.6. Individual (a) dune height and (b) length plotted against depth immediately downstream of the gravel sand transition in the Fraser River.

The *L*=5*h* relation from Yalin similarly plots through the center of the data but with even more scatter about it (Figure 2.5b). The data roughly follow the range of Allen (1982) where they were limited to *L*/*h* = 16 and *L*/*h* = 1. However, well-defined limits are more difficult to define. Mississippi dunes have been observed with lengths smaller than *L*/*h* = 1 (Nittrouer et al., 2011) (Figure 2.1b) and sediment-supply-limited dunes in the Fraser River have *L*/*h* < 1 (Figure 2.6b). It appears that for a given flow depth, a range of dune heights and lengths is possible. Moreover, there is approximately two orders of magnitude difference for dune heights and lengths for a given flow depth.

Probability histograms of *h*/*H* as well as the mean and median *h*/*H* values are given in Figure 2.7. For all the data, the most probable value of *h*/*H* falls between 4 and 5, with a long tail in the distribution. This suggests a wide range of *h*/*H* values with decreasing probability (Figure 2.7a). The *L*/*h* distribution for all the data (Figure 2.7b) also displays a long tail but the distribution is less skewed. Probability peaks in the range of *L*/*h*= 6 to 7 but the absolute probability of this peak is low. When the *h*/*H* data are separated by flume and field observations (Figure 2.7c), the distribution for flume data peaks between *h*/*H* = 2 to 4. The field data similarly peak at *h*/*H* = 3 to 4 with a second peak at 7 to 8 but the absolute probability of these peaks is low. The mean and median *h*/*H* for the flume data are lower than the field data. The *L*/*h* distribution for the flume data peaks around 6 to 8 and is less skewed than the field data which peaks

around 3 to 5. The mean *L/h* is similar for the flume and the field data but the median is lower for field data.

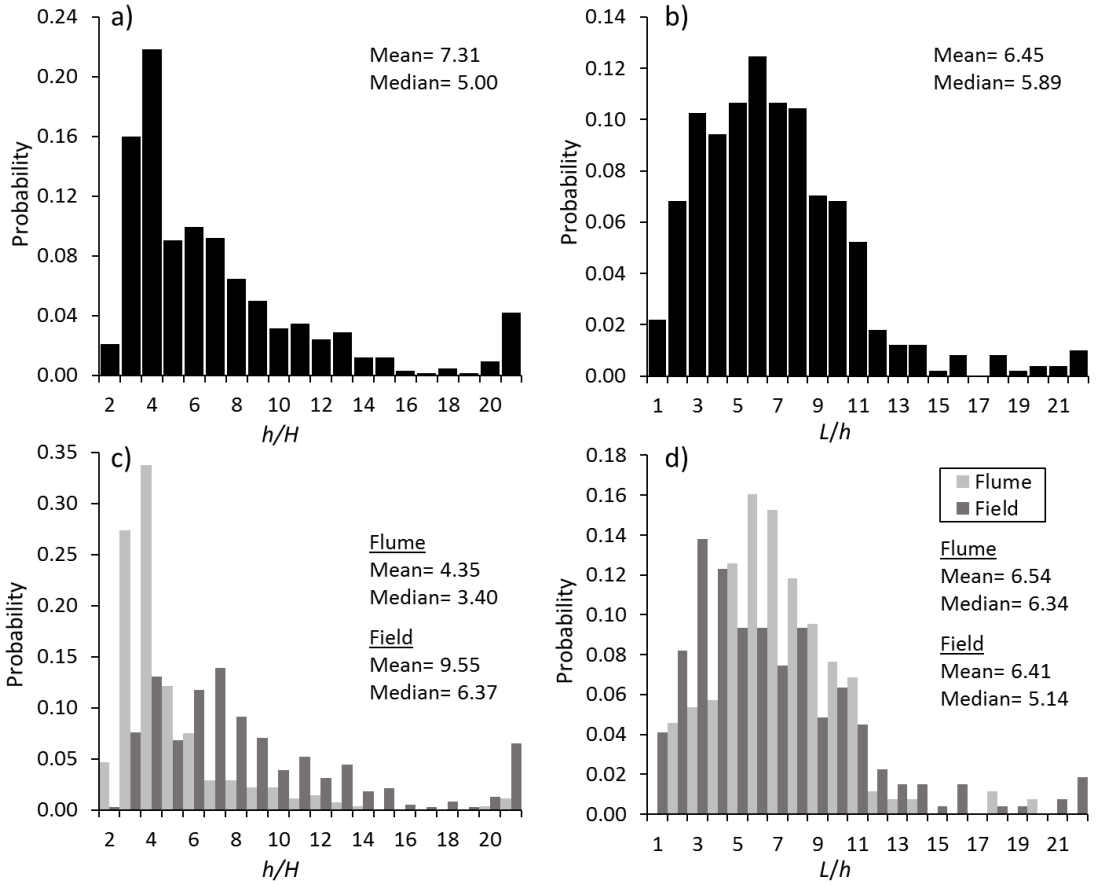

Figure 2.7. Probability histograms of (a) dune height (*H*) and (b) dune length (*L*) relative to depth (*h*) using all data. In (c) and (d) data are separated into flume and field observations. Relative dune height is presented as *h*/*H* (rather than *H*/*h*) to quote ratios as integers.

2.4. Assessment of the Relations

Previous assessments have tested the predictive ability of only a few select scaling relations with limited data sets (e.g., Allen, 1982; van Rijn, 1984; Karim, 1999). The wide range of geometries and flow conditions in this newly compiled data set, provides a unique opportunity to re-evaluate scaling relations. Simple height scaling relations (e.g., Yalin, 1964) can be tested with the entire data set but others that require more detailed inputs (e.g., van Rijn, 1984; Karim, 1999) have less data to test against (Table 2.3) because the necessary information was not reported in the original sources listed in Tables 2.1 and 2.2. For example, since the Yalin (1964) simplified relation

(Equation 2.4) only requires *h* to predict *H*, all of the data (664 observations) can be used. However, the van Rijn (1984) relation (Equation 2.13), requires mean velocity and grain size so only 368 observations can be used since these values were less frequently reported in the literature. Some height relations (e.g., Allen, 1978; Karim ,1995) are limited to a certain range of observations, and thus cannot be used outside their limits. Of the 368 observations that can be used to test the van Rijn (1984) relation, 6 are outside the range of the relation and predict no dunes will be present in the channel. The total useable observations that can be used for each height relation and the number of predictions that can be made within the limits of the relation are provided in Table 2.3. The length relations only rely on depth to make a prediction so all the length observations (498) can be used to test them (Table 2.4).

Table 2.3. Performance statistics for prediction of observed variables using the dune height scaling relations.

Source	Equation	# of useable observations	# of predictions	% within a factor of 1.5	% within a factor of 3.5
Yalin (1964)	$\frac{H}{h} = \frac{1}{6}\left(1 - \frac{\tau_c}{\tau}\right)$	394	394	29.2%	96.7%
Yalin (1964) (simplified)	$H = \frac{h}{6}$	664	664	39.5%	95.0%
Gill (1971) (triangular)	$\frac{H}{h} = \frac{1 - Fr^2}{2\eta\alpha}\left(1 - \frac{\tau_c}{\tau}\right)$	394	394	52.3%	95.2%
Gill (1971) (symmetrical)		394	394	38.8%	97.7%
Allen (1978)	$\frac{H}{h} = 0.08 + 2.24\left(\frac{\tau_*}{3}\right) - 18.13\left(\frac{\tau_*}{3}\right)^2 + 70.9\left(\frac{\tau_*}{3}\right)^3 - 88.33\left(\frac{\tau_*}{3}\right)^4$	394	319	51.1%	98.1%
Van Rijn (1984)	$\frac{H}{h} = 0.11\left(\frac{D_{50}}{h}\right)^{.3}(1 - e^{-.5T})(25 - T)$	368	362	47.5%	88.1%
Julien & Klaassen (1995)	$H = \varepsilon h\left(\frac{d_{50}}{h}\right)^{.3}$	588	588	55.6%	91.0%
Karim (1995)	$\frac{H}{h} = -0.04 + 0.294\left(\frac{u_*}{w_s}\right) + 0.00316\left(\frac{u_*}{w_s}\right)^2 - 0.0319\left(\frac{u_*}{w_s}\right)^3 + 0.00272\left(\frac{u_*}{w_s}\right)^4$	374	337	49.9%	92.3%
Karim (1999)	$\frac{H}{h} = \left[\frac{\left(S - 0.0168\left(\frac{D_{50}}{h}\right)^{.33} * F^2\right)\left(\frac{L}{h}\right)^{1.20}}{0.47F^2}\right]^{0.73}$	363	363	52.9%	96.4%

Table 2.4. Performance statistics for prediction of observed variables using the dune length scaling relations.

Source	Equation	# of useable observations	% within a factor of 1.5	% within a factor of 3.5
Yalin (1964)	$L = 5h$	498	44.8%	93.4%
Van Rijn (1984)	$L = 7.3h$	498	53.6%	89.4%
Julien & Klaassen (1995)	$L = 6.25h$	498	53.2%	91.8%

In order to examine the predictive ability of these scaling relations in a systematic way, adjustments and some assumptions needed to be made to some data sets. We calculated the shear stress for all the data using Equation 2.3 and applied the sidewall correction to flume data using the Williams (1970) method:

$$\tau_{corrected} = \frac{\tau}{(1+0.18h/w^2)} \quad \text{(Eq. 2.21)}$$

where *w* is the width of the flume. In Coleman et al. (2005) and Strasser et al. (2002) the data necessary to use Equation 2.3 were not reported, so we adopted their reported values of shear. The Yalin (1964), Gill (1971) and van Rijn (1984) relations require τ_{*c} (or $u_{*c} = \sqrt{\tau_{*c}/\rho}$), which varies with grain size according to the Shields diagram. τ_{*c} was calculated for each grain size using the Brownlie (1981) fit to the Shields diagram:

$$\tau_{*c} = 0.22{Re_g}^{*-.06} + 0.06 * 10^{(-7.7{Re_g}^{-0.6})} \quad \text{(Eq. 2.22)}$$

where Re_g is the grain Reynolds number as:

$$Re_g = \frac{u^* D_{50}}{\nu} \quad \text{(Eq. 2.23)}$$

and ν is the kinematic viscosity of water. Gill's (1971) relation further requires a decision about the empirical sediment transport exponent ŋ. Gill (1971) suggested it could lie somewhere between 3/2 and 3, and stated that most authors suggest a value of 3 is appropriate so we follow that here. Particle settling velocity (w_s) in Karim (1995) was calculated using Dietrich (1982). Temperatures were seldom reported by the original authors, so we assumed a ν value of 1.307 x 10^{-6} m^2/s and a ρ_w of 999.7 kg/m^3 for 10°C water because we suspect this is a reasonable approximation of the temperature when the observations occurred. We explored the sensitivity of our results to temperature and

found varying temperature by 10°C caused < 1 mm changes in our predicted H for laboratory flows and < 1 cm scale changes in predicted H for field scale flows. The bias is less than the resolution of the observations.

van Rijn (1984) requires an estimate of D_{90}, but we do not have the grain size distribution for these data, so we assume that $D_{90} = D_{50}$. We explored the sensitivity of predicted dune heights to this assumption. For very well sorted sands, D_{90} can be approximated as ~$1.2D_{50}$ and for poorly sorted sediment, ~$3D_{50}$ (Folk, 1980). For $D_{90} = 1.2D_{50}$, predicted H values are ~2% larger than for $D_{90} = D_{50}$ and for $D_{90} = 3D_{50}$, predicted H values are ~16% higher, assuming no scale distortion. Most of our observations are for uniform sand in flume experiments or well sorted sands in the field, so we conclude that the variability induced by our assumption of $D_{90} = D_{50}$ is relatively small. We also think this is the safest assumption in the absence of grain size distributions.

All of the relations predict 90% of the dune height data within a factor of 3.5 (Figure 2.8, Table 2.3) but this represents a substantial amount of variability. Most of the relations are only able to predict the observations within a factor of 1.5 about 50% of the time (Figure 2.8, Table 2.3). The relations with the fewest predictions within a factor of 1.5 are from Yalin (1964), and Gill (1971) using the symmetrical dune coefficient, whereas the most predictions that fall within a factor of 1.5 occur with Julien and Klaassen (1995). The length scaling relations all have similar predictive capabilities but van Rijn (1984) and Julien & Klaassen (1995) better predict L, with 53.6% and 53.2% of predictions falling within a factor of 1.5, respectively while Yalin (1964) has 44.8% (Figure 2.9, Table 2.4).

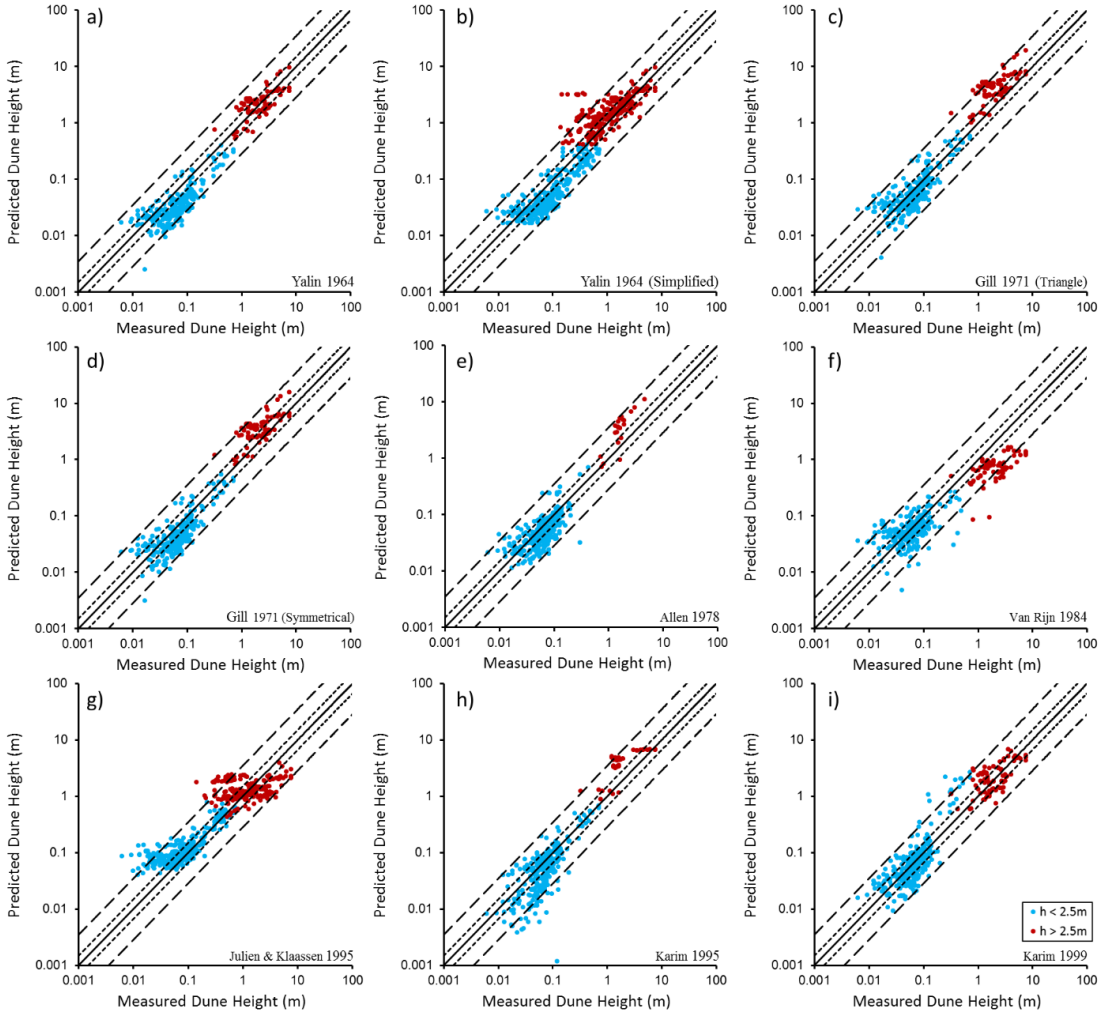

Figure 2.8. **Comparison of observed and predicted dune heights. Predictions are made using (a) Yalin (1964), (b) simplified Yalin (1964), (c) Gill (1971) with triangular coefficient (β = ½), (d) Gill (1971) with symmetrical coefficient ($\beta = 2/\pi$), (e) Allen (1978), (f) van Rijn (1984), (g) Julie and Klaassen (1995), (h) Karim (1995), and (i) Karim (1999). The 1:1 (perfect prediction) is indicated by the solid black line, the dotted line is for a factor of 1.5 and the dashed line is for a factor of 3.5.**

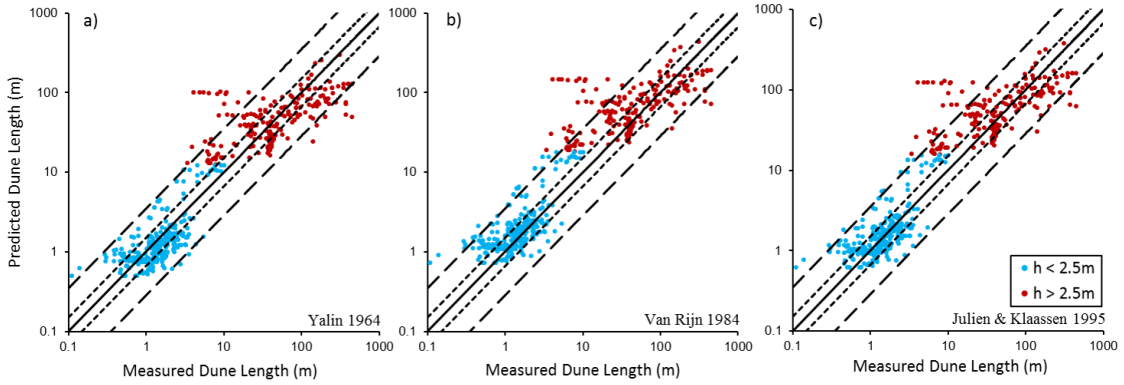

Figure 2.9. Comparison of observed and predicted dune length. Predictions are made using (a) Yalin (1964), (b) van Rijn (1984) and (c) Julie and Klaassen (1995). The solid black line indicates perfect prediction, the dotted line is for a factor of 1.5 and the dashed line is for a factor of 3.5.

The reason for the poor predictive power of the scaling relations is not immediately evident. It is conventional to attribute any variability about these relations to dunes adjusting to variable flow conditions (e.g., Holmes & Garcia, 2008). Yet, dunes in flumes exhibit the same order of magnitude variability in H or L for a given h where flow conditions are steady and dunes are fully formed. We might expect that dunes would plot above predicted values when they formed and fully adjusted to a flood flow prior to a drop in flow intensity. Conversely, we might expect dunes to form during short duration flood flows, but not reach their maximum height for the flow because the flood flow was too short. By removing unsteady flow data from this analysis, we have substantially reduced the possibility of either effect. Clearly, there is some source of variability not captured by these scaling relations.

2.5. Reevaluation of the Data Set

A more critical examination of the data set provides some insight into why the scaling relations do not predict dune dimensions well. There is evidence that dunes in smaller channels conform to a different height scaling than dunes in larger channels, which implies a different process control rather than a continuum of processes as depth increases. If we reexamine the data as one complete set, we find a more logical division can be made between rivers deeper and shallower than 2.5 m. When probability distributions in Figure 2.7 are separated at 2.5 m, the shallower channels maintain a distinct peak in h/H between 3 and 5, whereas deeper flows have one defined peak at

h/*H* = 7 to 8 (Figure 2.10a). For *h* < 2.5 m, 83% of the data plot above the *H* = *h*/6 line (Figure 2.5a), the mean relation is *H* = *h*/4.4 and the median is *H* = *h*/3.5. In deeper channels (> 2.5 m), 76% of the data plot below the *H* = *h*/6 line (Figure 2.5a), the mean relation is *H* = *h*/11.5, and the median is *H* = *h*/7.7. The difference between the mean and median arises because the distribution is skewed towards large values of *h*/*H* (dunes much smaller than the flow depth).

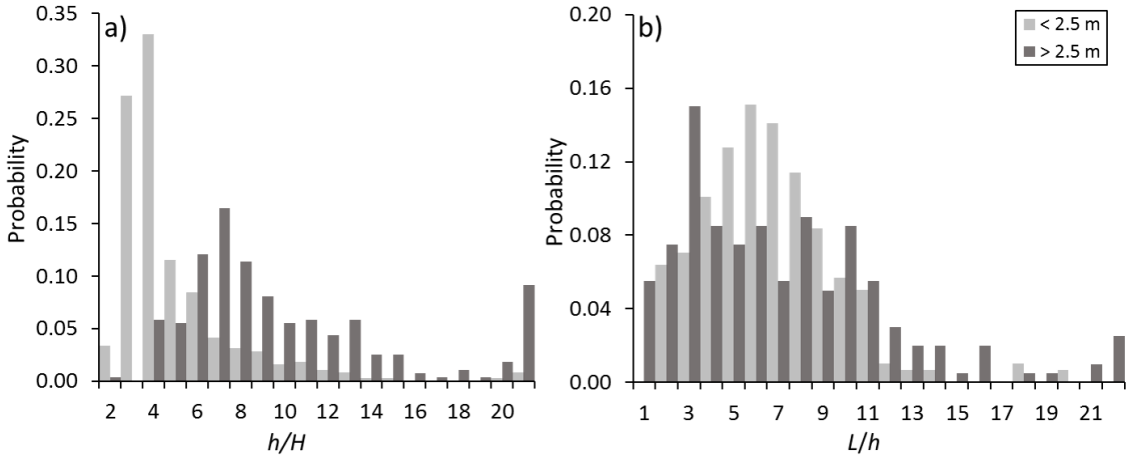

Figure 2.10. Probability histograms of dune (a) height (*H*) and (b) length (*L*) relative to depth (*h*), separated by flows < 2.5 m and > 2.5 m deep.

There is less evidence for a scaling break in the length data, because the shallow and deep flow distributions overlap and have lower absolute probabilities than the *h*/*H* data (Figure 2.10b). For flows less than 2.5 m deep, *L*/*h* peaks between 6 and 8 with a mean of 6.2 and a median of 5.9. The shallow flow data peak at *L*/*h* = 4, but dune length can reasonably scale anywhere from *L*/*h* = 1 to 11 as the distribution has a long tail. The mean of 6.9 and median of 5.7 of *L*/*h* for deep flows are similar to those in the shallow flows. These results suggest that a scaling break is either not present, or at the very least is not obvious, for the length data. However, there is a noticeable lack of length observations in the literature from flows 0.8 to 3.0 m deep. The gap in data is concerning since it may prove to be an important depth range for dune morphology.

The apparent scaling break in dune height between deep and shallow flows has not been formally documented. However, we know that dunes in bed-load dominant shallow channels are commonly asymmetric and angle-of-repose in morphology, while dunes in suspension-dominant deep rivers typically have lee angles < 30°, and are more rounded and symmetrical (Figure 2.11a) (Smith & Mclean, 1977; Kostaschuk & Villard,

1996; Bradley et al., 2013; Hendershot et al., 2016). Our proposed scaling break depth agrees well with observations of lee angle and channel depth since dunes with lee angles > 27° are found in flows less than 2.5 m while dunes in deeper flows exhibit lower lee angles (Figure 2.11b).

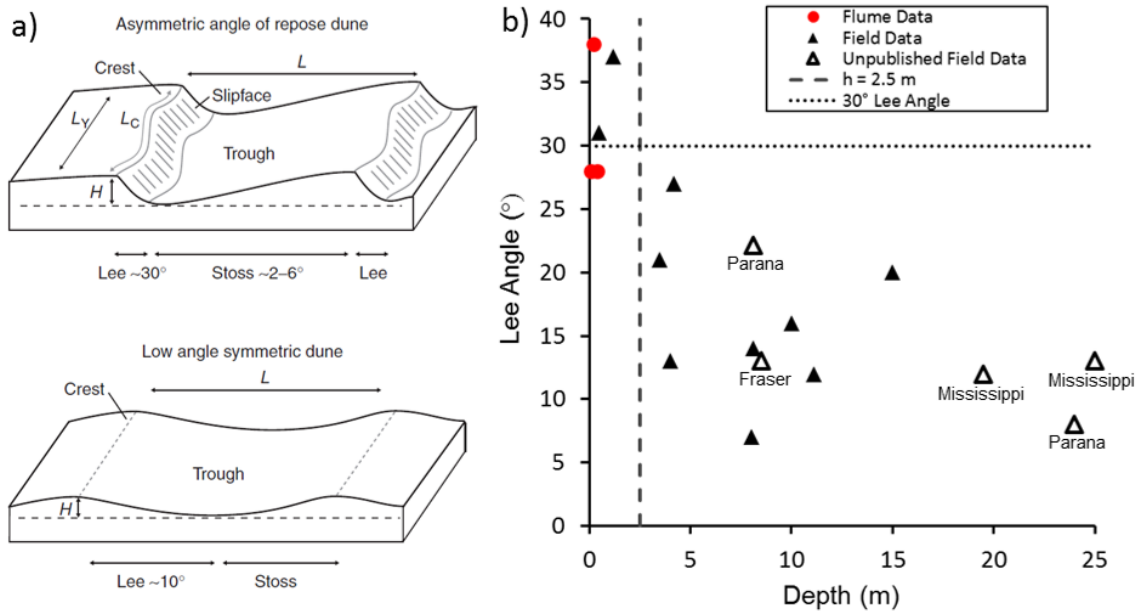

Figure 2.11. a) High angle asymmetric dune (HAD) planform compared to low angle symmetric dune (LAD) shape (from Venditti 2013). b) Reach-averaged lee angle plotted as a function of reach-averaged depth. Flume data are from Robert and Uhlman (2001), Tujinder et al. (2009) and Blom et al. (2003). Field data are from Gabel (1993), Venditti and Bauer (2005), Prent and Hickin (2001), Carling et al. (2000), Wilbers (2004), Kostaschuk and Ilersich (1995), Bradley et al. (2013), and Roden (1998). Also plotted are unpublished data (open triangles) from the Fraser River, the Parana River (provided by Dan Parsons and Ray Kostaschuk), and the Mississippi River (provided by Jeffery Nittrouer).

The reason for the different morphology between high-angle dunes (HADs) and low-angle dunes (LADs) is not clear, although several hypotheses have been proposed. Some researchers (e.g., Carling et al., 2000; Sukhodolov et al., 2006) have observed LADs where superposition and amalgamation of bedforms leads to the interception of bed-load that would normally avalanche down the lee to maintain a steep face. However, this is unlikely a universal control since LADs are frequently observed in predominately suspended sediment environments in the absence of superposition (Figure 2.1a; Kostaschuk and Villard, 1996; Bradley et al., 2013; Hendershot et al., 2016). Best (2005), on the basis of observations by Wan (1982) and Wan and Wang

(1994), reasoned that turbulence suppression due to high suspended sediment concentrations produces lower amplitude dunes, although it is unclear how turbulence damping feedbacks to the LAD morphology. The most commonly cited hypothesis is that suspended sediment bypasses the dune lee and deposits in the trough promoting a more rounded morphology since less sediment is available at the crest to maintain a steep avalanching lee-side slope for LADs (Smith & McLean, 1977; Kostaschuk & Villard, 1996; Kostaschuk et al., 2009; Hendershot et al., 2016). Recently, Hendershot et al. (2016) suggested that the dynamics of sand flows generated by lee side avalanching may also play a role in maintaining LAD morphology. They hypothesize that as subaqueous dunes get larger, the thickness of leeside grain flows becomes larger. This generates higher excess pore pressures in the grains flows, allowing leeside grain flows to occur on lower slopes. Loosely structured deposits formed by suspension deposition just past the dune crest may promote the formation of leeside grain flows with high excess pore pressures. Ultimately, all of these hypotheses require critical tests to identify why HADs and LADs emerge as distinct morphologies in shallow and deep rivers.

Regardless of the physical processes controlling HADs and LADs, our data suggest that different scaling relations are necessary for shallow and deep rivers, with a change in height scaling at $h \approx 2.5$ m. Existing scaling relations do not explicitly account for this scaling break, which contributes to their poor performance. Yalin's (1964) $H = h/6$ scaling relation predicts the dimensions of deep-flow dunes better than the shallow-flow dunes (Figure 2.8b), whereas Julien & Klaassen (1995) predict shallow-flow dunes better than deep flow dunes (Figure 2.8g). The triangular shape coefficient for the Gill (1971) equation performs better in flows less than 2.5 m than in the deeper flows, while the sinusoidal coefficient outperforms the triangular coefficient in deep flows (Figure 8c,d), which might reasonably be expected given the change in morphology observed (Figure 11a).

2.6. Dune-Depth Scaling Revisited

The generally poor performance of the scaling relations led us to re-examine depth-scaling relations in order to recover a useful methodology for use in the direct problem of predicting dune heights and lengths from flow depth, as well as for the inverse problem of predicting flow depth from dune heights reconstructed from fossilized

dunes. Simple dune depth-scaling relations are appealing because they require only one known input to recreate a flow depth or a dune height. Furthermore, adding more complex variables to the relations does not seem to substantially improve their predictive power. Given the two orders of magnitude variability about the mean relations between *h* and *H* and in *h* and *L*, metrics of uncertainty ought to be incorporated into scaling relations. We propose application of prediction intervals and a probability-based approach to carry the inherent variability in the data forward in predictions. The prediction intervals indicate the likelihood (probability) of a future observation falling within a range defined by a sample of a population. They differ from confidence intervals, which assign a probability that the true linear regression line of the population will lie within the confidence interval of the regression line calculated from a sample of the population. Confidence intervals do not incorporate a metric of the data's variability that can be carried forward in predictions. Prediction intervals indicate whether a new observation will fall within a range defined by our data. Our interest here lies in prediction and carrying the variability of the sample forward as an uncertainty, so we use prediction intervals.

2.6.1. Regression analysis and prediction intervals

To address the direct prediction problem, regression analysis was applied to both flows < 2.5 m deep and > 2.5 m deep to predict *H* from *h* (Figure 2.12a). The analysis was also performed to predict *L* from *h* but the data set was not separated since a clear scaling break with *h* is less obvious in the *L* data because of the scarcity of observations between *h* = 0.8 and 3 m (Figure 2.13a). The analysis reveals power relations, or proper scaling relations, that have the form:

$$H = BCF \cdot a_i h^m \quad \text{(Eq. 2.25)}$$

$$L = BCF \cdot a_i h^m \quad \text{(Eq. 2.26)}$$

where a_i is the intercept, m is the slope and BCF is the bias correction factor, which accounts for the conversion of log-transformed variables back into the original units and has the form:

$$BCF = e^{\alpha^2/2} \quad \text{(Eq. 2.27)}$$

where α is the standard error of the regression (Miller, 1984). The resulting power law relations are summarized in Table 2.5. The BCFs for the regressions are low (< 5%) due to high correlations and the relations are all significant at the 99% confidence level (Table 2.5). For the prediction of dune height from flow depth, the proportion of the variance explained by *h* is larger for the < 2.5 m data (74%) than for the > 2.5 m data (49%). The lower R^2 value for the deeper flow is due to the larger range of dune sizes that can be found in these flows. The proportion of the variance in *L* explained by *h* is 86%. The error in the regression slopes (Table 2.5) is small at < 5% of *m* at the 90% confidence interval for most of the relations. The error is higher (~10%) for the dune height relation in flows deeper than 2.5 m, because the underlying data are more variable. The forward prediction using the range of possible slopes would fall within the prediction interval range for all relations.

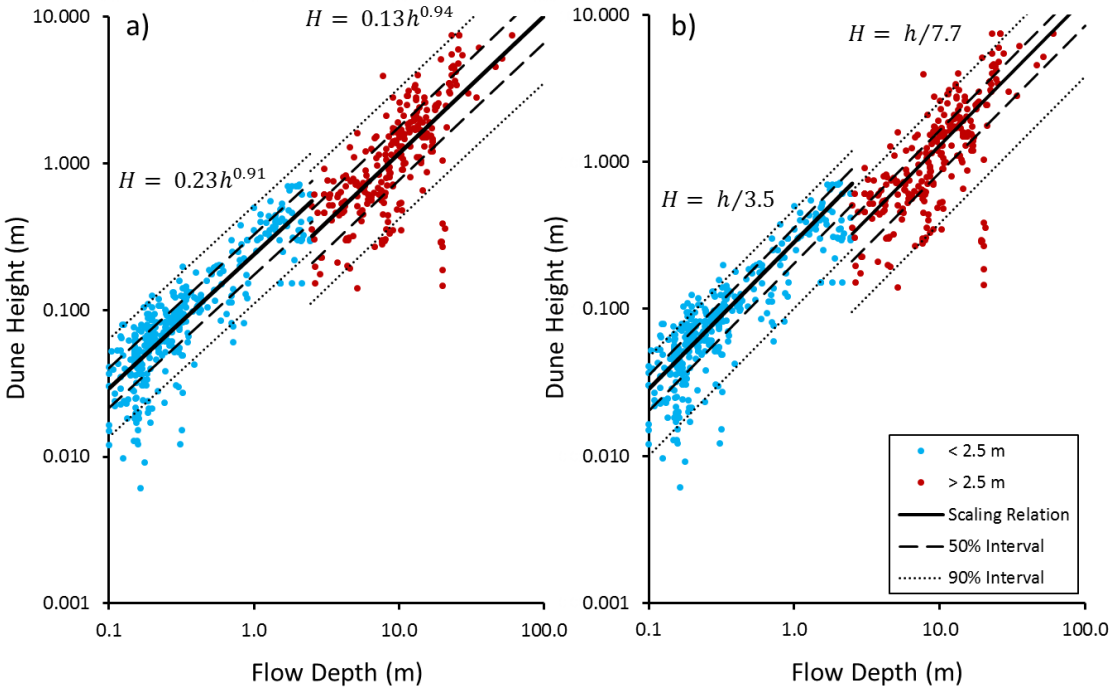

Figure 2.12. Relations and prediction intervals with *BCF* applied between flow depth and dune height derived from (a) regression analysis and (b) calculation of the median relations (see Section 2.6.2).

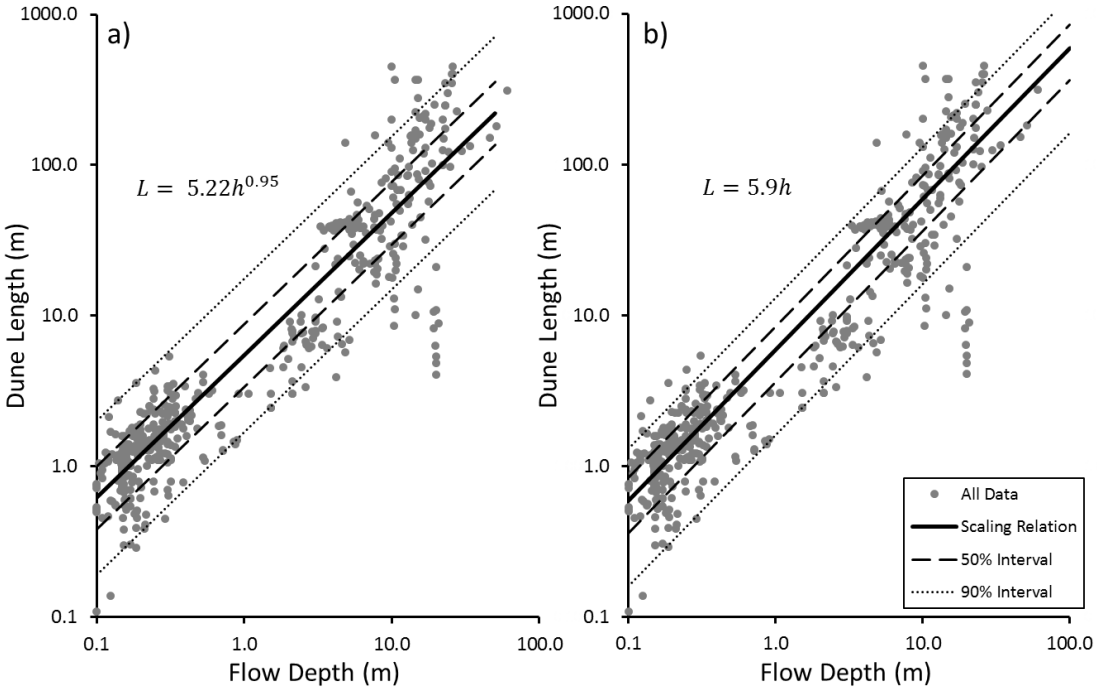

Figure 2.13. Relations and prediction intervals with *BCF* applied between flow depth and dune length derived from (a) regression analysis and (b) calculation of the median relation (see Section 2.6.2). The entire data set is presented here without any separation by flow depth.

Table 2.5. The scaling relations and summary statistics from the linear regression analysis.

	Scaling Relation	Bias Correction Factor (BCF)	Slope Range at 90% Confidence Interval	R^2	p-value	Approximate Prediction Interval Intercept (a_i) 50%	80%	90%	95%
Height Prediction (Fig. 2.12)									
< 2.5 m	$H = 0.23h^{0.91}$	1.02	0.87-0.96	0.74	< 0.001	0.17-0.32	0.13-0.43	0.11-0.51	0.09-0.64
> 2.5 m	$H = 0.13h^{0.94}$	1.04	0.84-1.03	0.49	< 0.001	0.08-0.20	0.06-0.31	0.05-0.38	0.04-0.46
Length Prediction (Fig. 2.13)									
All Data	$L = 5.22h^{0.95}$	1.05	0.92-0.97	0.86	< 0.001	3.43-8.40	2.10-12.99	1.62-16.83	1.30-21.07
Flow Prediction (Fig. 2.14)									
Field	$h = 6.96H^{0.95}$	1.04	0.89-1.00	0.69	< 0.001	4.44-10.90	2.96-16.35	2.32-20.84	1.87-25.95

Regression analysis allows us to assign prediction intervals to the relations using a parametric approach that indicates the probability of a future observation falling within

the range. The regression prediction intervals are calculated using log-transformed height and depth data that are then transformed back to linear units. The dune height ($H_{interval}$) and length ($L_{interval}$) prediction intervals can be calculated as:

$$H_{interval} = H_{pred} \pm t_{\propto} SE_H \quad \text{(Eq. 2.28)}$$

$$L_{interval} = L_{pred} \pm t_{\propto} SE_L \quad \text{(Eq. 2.29)}$$

where H_{pred} and L_{pred} are the log-transformed predicted dune height and length, respectively, using the scaling relations in Table 2.5, $t_{\propto}$ is the two-tailed Student's t-test value for a given prediction interval and number of degrees of freedom, and SE_H and SE_L are the standard error for height and length prediction. Standard error for height and length prediction are determined as:

$$SE_H = SEE_{hH}\sqrt{1 + \frac{1}{N} + \frac{(h_i - \overline{h_{log}})^2}{(N-1)\sigma_h}} \quad \text{(Eq. 2.30)}$$

$$SE_L = SEE_{hL}\sqrt{1 + \frac{1}{N} + \frac{(h_i - \overline{h_{log}})^2}{(N-1)\sigma_h}} \quad \text{(Eq 2.31)}$$

where SEE_{hH} is the standard error of estimate for the regression between *h* and *H*, SEE_{hL} is the standard error of estimate for the regression between *h* and *L*, *N* is the number of data of points, $\overline{h_{log}}$ is the mean of the log-transformed depth values, h_i is the log-transformed depth for which the prediction is being made, and σ_h is the standard deviation of the log-transformed depth. A prediction interval must be determined for a selected probability using Equations 2.28-2.31 and the data provided in Table 2.6. However, prediction intervals are nearly linear, so they have a slope that is approximately equal to the derived scaling relations. We have provided approximate prediction interval intercepts for a given level of probability in Table 2.5 by setting h_i = 0 in Equations 2.30 & 2.31. For a given level of probability, the prediction interval can be estimated using the scaling relation slope and these approximate intercepts.

Table 2.6. Variables needed to calculate a prediction interval.

Scaling Relation	Number of Data Points N	Degrees of Freedom	Mean of Log-transformed Depth $\overline{h}$ or Height $\overline{H}$ (m)	Standard Error of Estimate SEE	Standard Deviation σ
Dune height from flow depth < 2.5 m	391	389	-0.4958	0.2026	0.3689
Dune height from flow depth > 2.5 m	273	271	1.0261	0.2689	0.2372
Dune length from flow depth	498	496	0.7431	0.3078	0.8279
Flow depth from dune height	382	380	-0.1610	0.2886	0.4556

It is common practice to simply use the inverse of the forward relations to reconstruct past flow depths from dune heights extracted from the rock record, however, this is not appropriate when using regressions. Regression analysis assumes all the error lies in the independent variable, so they cannot be inverted without introducing a bias. So we derive a relation using *H* as the independent variable and *h* as the dependent variable for use in the inverse problem (Figure 2.14a). We do not derive a relation for *L* because *H* is more practically estimated from cross-strata (e.g., Paola & Borgman, 1991; Bridge & Best, 1997; Leclair & Bridge, 2001; Jerolmack & Mohrig, 2005). We have also only included field data because the large number of flume experiments creates a substantial bias as most of the flume data plot above the *h*/6 scaling relation. Dunes in natural channels are responsible for the features preserved in the rock record and the inclusion of data from idealized flume experiments may not be appropriate. We do not separate the data based on shallow and deep flows since this information would not be known a priori in a paleo-environmental reconstruction. Furthermore, we cannot separate the data into small dunes and large dunes, since there is no evidence for a scaling break when *H* is used as the independent variable (Figure 2.14).

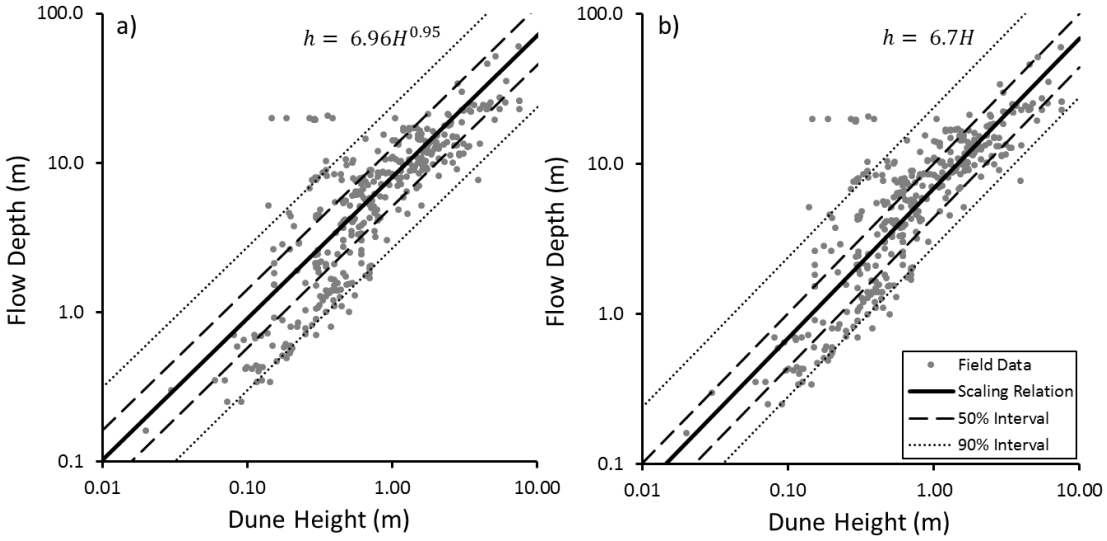

Figure 2.14. Relations and prediction intervals with BCF applied between dune height and flow depth derived from (a) regression analysis and (b) calculation of the median relations using field data only.

The power relation for inverse prediction has the form:

$$h = BCF \cdot a_i H^m \quad \text{(Eq. 2.32)}$$

The resulting power law relation and statistics are summarized in Table 2.5 and the relation is plotted in Figure 2.14a. The proportion of the variance in *h* explained by *H* is 69%. The flow depth prediction interval ($h_{interval}$) is:

$$h_{interval} = h_{pred} \pm t_{\propto} SE_h \quad \text{(Eq. 2.33)}$$

where h_{pred} is the log-transformed predicted flow depth using the scaling relation in Table 2.5, and SE_h is the standard error for depth prediction as:

$$SE_h = SEE_{Hh} \sqrt{1 + \frac{1}{N} + \frac{(H_i - \overline{H_{log}})^2}{(N-1)\sigma_H}} \quad \text{(Eq. 2.34)}$$

where SEE_{Hh} is the standard error of the estimate for the regression between *H* and *h*, *N* is the number of data of points, $\overline{H_{log}}$ is the mean of the log-transformed dune heights, H_i is the log-transformed dune height for which the prediction is being made, and σ_H is the standard deviation of the log-transformed dune height. As with the direct approach, any prediction interval level can be calculated using the data in Table 2.6 and Equation 2.34

or estimated using the scaling relation slope and the approximate prediction interval intercepts provided in Table 2.5.

2.6.2. Non-parametric approach

While adding prediction intervals to the regressions is appealing, a Shapiro–Wilk test reveals that the *h*/*H*, *L*/*h* and *H*/*h* data are not normally or log-normally distributed. The regression prediction intervals do not properly represent the long tails of the distributions. An alternative to the parametric approach is to use the cumulative distributions derived from the probability histograms (e.g., Figures 2.7 & 2.10) to characterize the scaling relations and their inherited uncertainty. Ranges of uncertainty can be added as percentages of the total distribution around the median that reveal the likelihood of an observation falling within the range defined by the bounds.

Cumulative probability plots (Figure 2.15) were used to add uncertainly ranges about the median relation for dune height predictions from flows less and greater than 2.5 m deep, predictions of length from flow depth and predictions of flow depth from dune height. The level of uncertainty is set by the probability (*p*) of a value falling within a range of values. The median was found on the cumulative probability curve and becomes the new scaling relation. A range was determined as ± *p*/2 about the median as in Figure 2.16. For example, for a 50% probability the *h*/*H* value at 0.75 provided the upper limit, while the relation at 0.25 provided the lower limit. The range is symmetric about the median for a normal distribution but asymmetric for non-normal distributions.

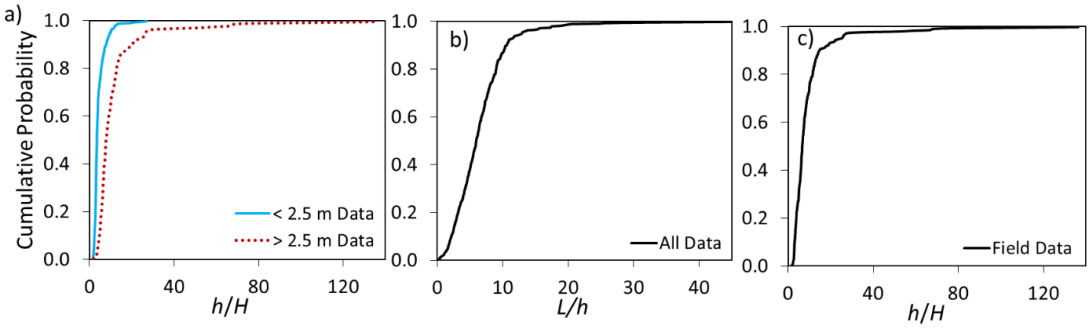

Figure 2.15. Cumulative probability plots of (a) *h*/*H* with data separated at depths < 2.5 m and depths > 2.5 m, (b) *L*/*h* using the entire data set and (c) *h*/*H* for field data only.

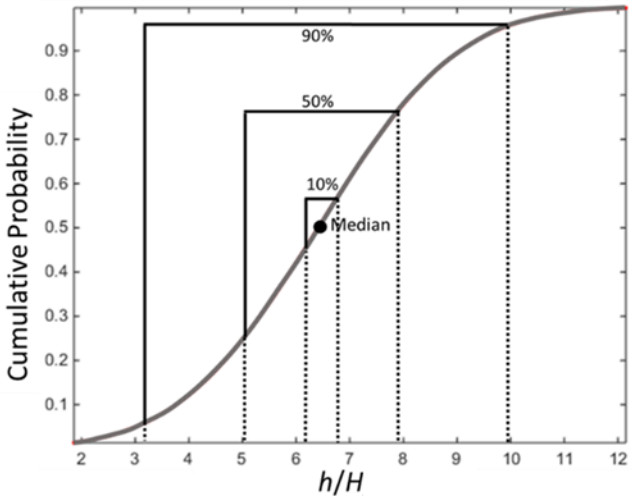

Figure 2.16. Idealized cumulative probability plots that demonstrate how the prediction intervals about the median were determined.

The median relations run through the center of the data (Figures 2.12b, 2.13b, 2.14b) while the ranges about them captures the variability (Table 2.7). Conventional uncertainly intervals such as 90% or 95% produce ranges that are too wide to be useful for any prediction. For example, a 1 m high dune could be could be formed by flows ranging from 2.8 to 23.9 m at the 90% prediction interval. A more reasonable range occurs with a lower probability, although the likelihood of a correct prediction is decreased. There is a 50% chance that a 1 m high dune is formed by a flow that is 4.4 to 10.1 metres deep.

Table 2.7. Median scaling relations and their associated uncertainty range bounds.

	Scaling Relation	Scaling coefficient (ε)	Range of ε for various levels of uncertainty 50%	80%	90%	95%
Height Prediction (Figure 2.12)						
< 2.5 m	$H = h/\varepsilon$	3.5	2.8-4.9	2.3-7.8	2.1-9.9	1.9-11.8
> 2.5 m	$H = h/\varepsilon$	7.7	6.1-11.8	4.6-19.4	3.9-26.3	3.4-57.9
Length Prediction (Figure 2.13)						
All Data	$L = \varepsilon h$	5.9	3.6-8.4	2.1-10.6	1.6-13.0	1.0-17.3
Flow Prediction (Figure 2.14)						
Field	$h = \varepsilon H$	6.7	4.4-10.1	3.1-14.6	2.8-23.9	2.7-29.5

The parametric and non-parametric approaches provide new scaling relations. While there is significant variability about them, it is comparable to that observed when using both the simple (e.g., Yalin, 1964; Julien & Klaassen, 1995) and more complex (e.g., Gill, 1971; Allen, 1978; Karim, 1995; van Rijn, 1984; Karim, 1999) scaling relations in the literature. The relations presented here improve on those by requiring only one simple input, but also by allowing a variability metric. The method provides a tool to assign an error estimate to prediction of modern dune dimensions from flow depth, as well as in paleo-environmental reconstructions of flow from preserved dunes.

2.7. Synthesis

Scaling relations generally predict dune dimensions poorly. The simplified depth scaling attributed to Yalin (1964) is the worst at predicting the observations, partially due to natural variability of dunes but it also does not acknowledge the scaling break at 2.5 m depths. Adding grain size to depth-scaling relations (Julien & Klaassen, 1995) improves accuracy modestly, but it could hardly be considered a physically based data collapse. Using more complex variables (Shields number, Froude number, suspension criteria) may more faithfully reflect the actual dynamics of dunes as they grow from lower stage plane beds, then washout to upper stage plane beds. However, these more complex relations do not substantially improve predictive power (Table 2.3; Table 2.4). Our revised H to h scaling relations that include uncertainty estimates are an improvement over the existing simple scaling relations because they recognize the scaling break between dunes in deep and shallow rivers and because they are fit to a more extensive data set than all previous relations. The percent of H observations within a factor of 1.5 is 67% and 63% for our shallow water regression and median relations, respectively, and 59% and 57% for our deep water relations. This is comparable to the accuracy obtained with the depth and grain-size scaling relations (e.g., Julien & Klaassen, 1995), which performed best in our testing. Yet the magnitude of the variability about all scaling relations, including our own, suggests that we still do not understand the fundamental controls on dune dimension scaling. Several critical questions emerge: Are dunes depth controlled? What are the fundamental controls on dune dimensions? Why do dunes appear to scale with depth?

2.7.1. Are dunes depth-controlled?

At some level, depth must exert some limitation on how large dunes can get. Dunes cannot grow out of the water surface. Furthermore, it is intuitive that there is some maximum height a dune can reach before streamline compression causes sufficient flow acceleration over the dune crest to prevent further deposition on the crest and dune growth. Our data set suggests that the highest dunes observed are ~40% of the flow depth ($H = h/2.5$), but dunes very rarely reach this hypothetical maximum height. Most dunes exist in equilibrium with the flow at heights much less than $h/2.5$ (Figure 2.5a). So we examine the arguments that have been put forward to support a depth control on dunes.

Dune dimensions have traditionally been linked to 'boundary layer thickness', under the belief that boundary layer thickness somehow prevents dunes from getting larger (e.g., Jackson, 1975). The physical mechanism for this control has never been fully elucidated, but the idea that dunes scale with boundary layer thickness in rivers is so pervasive, that it has led aeolian geomorphologists, sedimentologists and physicists to propose scaling of giant desert dunes with atmospheric boundary layer depth (*cf.*, Andreotti et al., 2009) and oceanographers to seek boundary layer depth controls on continental shelf dunes for decades without much success (see recent review in Franzetti et al. (2013) and references therein to earlier work).

A boundary layer thickness control on dune height seems unlikely because boundary layers do not fully form in rivers, at least in the classical sense. Flow in rivers is depth-limited insofar as turbulence is anisotropic through the full flow depth due to bed roughness effects (Nowell & Church, 1979). By contrast, there is an atmospheric boundary layer limit defined where turbulence is isotropic and no longer affected by the Earth's surface (Oke, 1978). Rivers are too shallow for a similar boundary layer to fully develop since mean flow fields are dominated by large-scale, macroturbulent coherent flow structures that form at the bed and upwell through the water column where they may emerge at the surface as boils (Jackson, 1976; Kostaschuk & Church, 1993; Bradley et al., 2013). Because boundary layers do not ever fully form, boundary layer thickness is solely controlled by flow depth, which as noted above, does not appear to be the fundamental control on fully developed dune dimensions.

It has been speculated that dunes grow until the area above the crest is planed off because flow conditions are similar to those over an upper-stage plane bed (*cf.,* Bennett & Best, 1996). The theory would suggest that given enough time, all dunes would grow to the height required to accelerate the flow over the dune crest towards critical Froude number conditions that produce upper-stage plane beds. Yet, there is little evidence in the literature to support the idea. Critical Froude number conditions are rare in rivers in general and certainly do not exist in large rivers where the Froude number is commonly 0.1 to 0.3 (e.g., Julien, 1992; Kostaschuk &Villard, 1996; Holmes & Garcia, 2008). For example, Bradley et al. (2013) reports dune heights of 1.5 m in flow 11 m deep and moving at 2.2 m/s. The Froude number for the flow is 0.21 and Fr = 0.22 over the crest. In order to produce critical flow conditions over the Bradley et al. (2013) dune crest, the dune would have to be ~7 m high, reducing the flow depth to ~4 m, a condition obviously impossible. In deep rivers where lower Froude number flows are common, dunes are relatively smaller in height which cannot be due to erosion at the crest. While we cannot exclude the possibility that critical Froude number conditions can occur over a dune crest in shallow flows, this cannot be the universal explanation for what controls the height of dunes.

The idea that flow depth is the fundamental control on dune heights is further flawed because it ignores the role of flow strength in controlling dune height. Experimental work by Venditti et al. (2005b) showed that dunes formed at constant flow depths, but with different flow strengths, vary in size when fully adjusted to the flow. Bedform growth curves (Figure 2.17) reveal that the fully developed equilibrium dune size decreases with decreasing flow strength at a constant flow depth. This suggests that the fundamental control on dune dimensions is something other than flow depth.

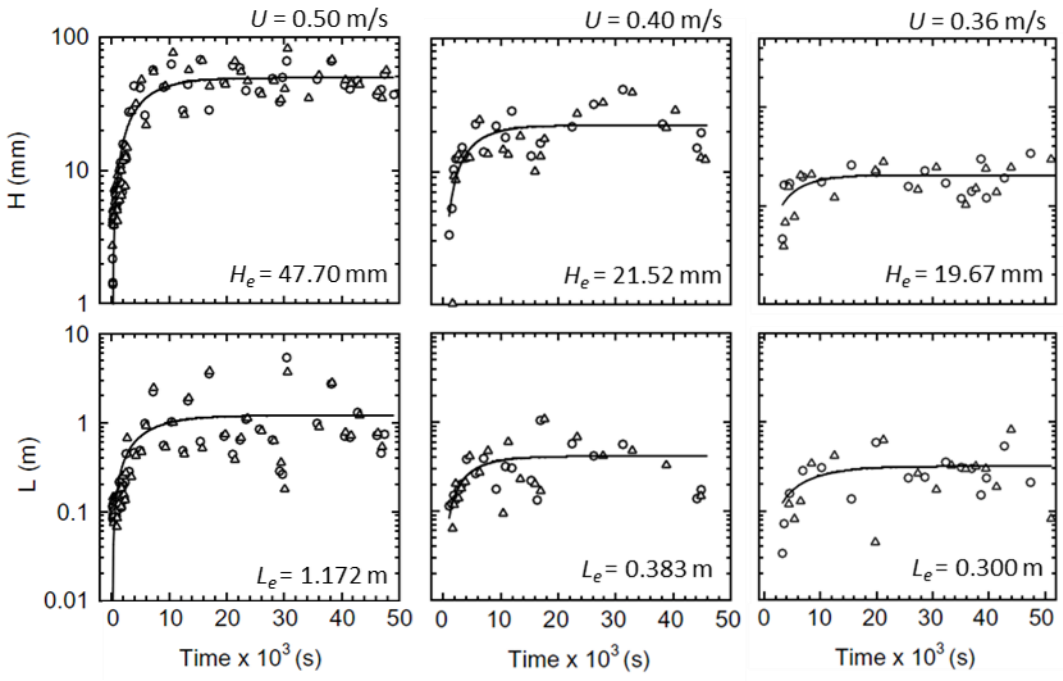

Figure 2.17. Dune growth curves for height (*H*) and length (*L*) from experiments by Venditti et al. (2005b). For each flow, the average depth was held constant at 0.15 m but the mean flow velocity was different. H_e and L_e are average equilibrium heights and lengths, respectively.

2.7.2. What are the fundamental controls on dune dimensions?

The work of Yalin and collaborators (Yalin, 1972; Yalin & Karahan, 1979) and Allen (1982) showed that dune steepness (*H/L)* varies with the transport stage. They showed that *H/L* increases from BLD to MXD conditions and declines to SSD conditions as the dunes wash out to an upper stage plane bed. A similar pattern can be observed in our data compilation overlain onto the data cloud from Yalin (1972), which roughly reveals the hyperbolic relation between transport stage and *H*/*L* (Figure 2.18a). The hyperbolic behavior of dune steepness with transport stage also emerges when the ratio of shear velocity u_* to settling velocity w_s is examined rather than transport stage (Figure 2.18b). Dune steepness increases with the suspension criteria (u_*/w_s) until around a value of 1, where substantial suspension begins (Bagnold, 1966). There is also a group of field data that shows a decrease in steepness at higher values of u_*/w_s than the flume data. Nashband et al. (2014) argued that in high Froude number flume experiments, dunes wash out to USPB at smaller values of u_*/w_s than in deeper flows where Froude numbers are typically smaller (e.g., Julien, 1992; Kostaschuk &Villard, 1996; Holmes & Garcia, 2008). This suggests that transport stage (or mode) and the free surface

interaction with the bed are two important controlling factors in determining dune dimensions as previously recognized in scaling relations.

It is difficult to discern what is happening to the height and length separately as τ_*/τ_{*c} or u_*/w_s increase because both dimensions could be covarying to give the variation in *H*/*L*. However, recent work by Venditti et al. (2016), showed that the pattern emerges because *H* increases then decreases as more sediment goes into suspension, against a background of continuously increasing *L* (Figure 2.19). At higher transport stages, *L* continues to grow while *H* decreases as dunes wash out to upper stage plane beds. Similar observations were made by Nashband et al. (2014), who shows that length continually increased with u_*/w_s.

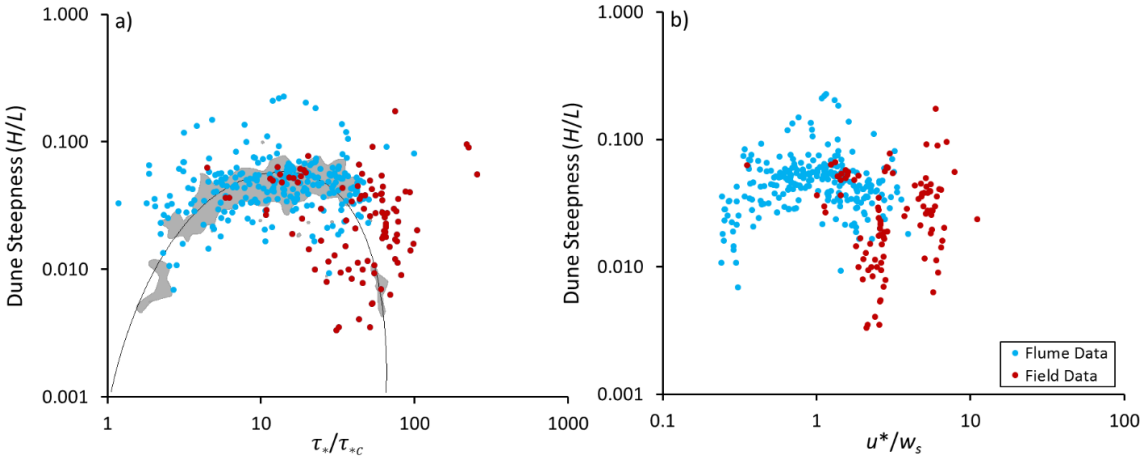

Figure 2.18. The aspect ratio (*H*/*L*) of the dune in the data compilation plotted as a function of (a) transport stage (τ_*/τ_{*c}) and (b) suspension criterion (u_*/w_s). The shaded area (drawn by Venditti, 2013) in (a) represents the data cloud from Yalin (1972) for dunes. Data included here are 254 points from flume experiments and 99 from field observations.

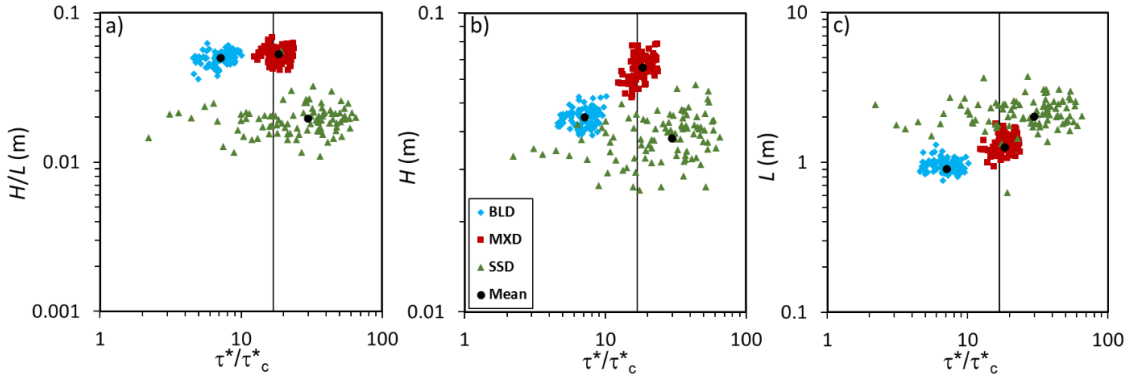

Figure 2.19. Results of flume experiments by Venditti et al. (2016) showing (a) dune aspect ratio, (b) dune height, and (c) dune length plotted as a function of transport stage (τ_*/τ_{*c}). Blue diamonds, red squares and green triangles are reach averaged values from individual runs under bedload (BLD), mixed load (MXD), and suspended sediment (SSD) conditions, respectively. The black circles represent the averages of all the runs for each condition.

The observations of Venditti et al. (2016) highlight an issue with defining the controlling conditions for dune dimensions. The data that underlie their results (Figure 2.19) are observations obtained over 16-hour flume runs, after fully developed dunes formed. While the mean of the observations at any one transport stage reveal underlying relations, the individual observations, all taken under the same hydraulic conditions, vary substantially. This exposes a potential problem with defining dune scaling relations from individual observations in that inadequate averaging through time may result in substantial variability at constant hydraulic conditions.

In spite of this caveat, it is clear that metrics of shear stress, transport stage and mode, surface and bed topography interaction, and the scale of the flow are important for what ultimately controls dune dimensions. It is also clear that further meta-analysis is unlikely to clarify the controlling mechanisms because there may be substantial variability introduced to the empirical data simply from inadequate averaging. Yet there are practical reasons to recover some mechanistic reasoning for why depth scaling is acceptable.

2.7.3. Why do dunes appear to scale with depth?

While there is evidence to suggest that depth is not the fundamental control on dune dimensions, we cannot ignore that dune dimensions have been long observed to

increase with the scale of the system. There are physically-based reasons why dunes may appear to scale with depth. Smith (1970) reasoned that the distribution of shear stress and bedload sediment flux over a dune controlled whether it would grow, be stable or erode. If the maximum flux (q_{max}) is upstream of the crest, deposition is occurring in the lee of the crest and the dune is growing. Conversely, if q_{max} is downstream of the crest, the crest is eroding and the dune height is lowering. Only when the topographic maximum and q_{max} coincide is the dune fully adjusted to the imposed shear stress causing downstream migration of a dune with a constant height through an equal balance of erosion of the stoss and deposition in the lee. Building on Smith (1970), Nelson et al. (1993) further proposed that increased flow acceleration related to a growing dune moves the maximum sediment flux towards the crest. The increased acceleration also damps the turbulence field, decreasing the turbulence intensity, and further promoting the sediment flux maximum to move towards the crest because the local mean flow properties have greater correlation with local sediment flux than fluctuating components. This would suggest that dune height should scale with the shear stress, insofar as the stress distribution is controlled by the total applied shear stress (τ), which itself is dependent on the flow depth because $\tau = \rho g h S$. Flow depth may not be a fundamental control on dune dimensions but it certainly is involved with the dynamics of the shear stress distribution.

We may have also recovered an indirect correlation between flow depth and the appearance of HAD and LAD morphologies in rivers (Figure 2.11). This change in dune morphology and the scaling break coincide with a greater propensity for suspension in deeper rivers, which causes particles to escape the dune crest and deposit in the trough, thus lowering the dune height (e.g., Hendershot et al., 2016). Flemming and collaborators (Flemming, 2000; Bartholdy et al., 2005; Bartholdy et al., 2010) have proposed that grain size is important in setting the height of deep sea dunes since shear velocity at a dune crest determines whether a dune will be dominated by bedload or suspension. The scaling break can be linked to flow depth, insofar as the threshold for suspension is controlled by the ratio of the shear velocity $u_* = \sqrt{ghS}$ to the settling velocity of particles.

Ultimately, our development of dune-depth scaling relations is born of a need to link dune dimensions to some flow variable. The physical controls on the height of dunes are not yet clear even though there has been a long history of scaling relations that have

attempted to identify flow variables that are important to dune dimensions. Reconstruction of paleo-depth is not fully limited by our ability to interpret dune heights from the rock record and our ability to predict flow depths is not limited by how we measure topography. Forecasting of formative flows or prediction of dune heights is hindered by our knowledge of how flows in rivers shape dune geometry, indicating that we require a better understanding of the mechanisms that control dune height. The apparent scaling of dunes with flow depth may be an indirect correlation and arise because the shear stress and shear velocity are dependent on depth.

2.8. Application

The application of our new depth-scaling relations to engineering, geomorphological or sedimentological problems involves four steps. For the direct approach, we suggest the following procedure:

(1) Determine reach-averaged flow depth;
(2) Use the median relation (Figure 2.12b; Table 2.7), selecting the relation for flows < 2.5 m or > 2.5 m deep to predict a dune height;
(3) Use the median relation for dune length (Figure 2.13b; Table 2.7) if desired;
(4) The potential range of dune heights and lengths at a depth should then be estimated for a desired uncertainty level using the non-parametric approach (Figure 2.12b; Figure 2.13b; Table 2.7).

We recommend the application of non-parametric scaling relations over the derived regression relations because the data are not normally or log-normally distributed. The regressions are formal scaling relations and provide information about the scale factor and scale distortion, which may be useful for further research. But, the non-parametric relations and the uncertainty ranges about them better represent the variability in the data set. The amount of uncertainly applied in Step 4 depends on the specific problem. Using a smaller uncertainly range, provides a more reasonable spectrum of possible dune heights, but there is a lower probability of a predicted dune falling within the range. When larger uncertainly bounds are applied, there is a much higher probability that the observed dune will appear in that range, but the range of possibilities is so large that it may not be useful. For example, for roughness estimates from dune heights, a lower uncertainty range could be applied in order to constrain the possible estimates.

However, for higher risk engineering purposes where the depth of scour related to dunes is required, such as at pipeline, tunnel or bridge crossings, a larger uncertainty range is recommended in order to capture all the possible dune sizes. Ultimately, it is up to the user to evaluate what is an appropriate level of uncertainly for the problem at hand.

For the inverse problem we recommend the following procedure:

(1) Estimate dune heights from exposed dunes or from preservations in cross strata using either a theoretical (Paola & Borgman, 1991; Bridge & Best, 1997) or empirical (*cf*. Bridge, 1997; Leclair et al., 1997; Leclair & Bridge, 2001; Leclair, 2002; Leclair, 2011) model;
(2) Use the median relation for predicting flow depth that was derived from the field data (Figure 2.14b; Table 2.7);
(3) Apply a reasonable level of uncertainty using the non-parametric approach (Figure 2.14b; Table 2.7).

As in the direct approach we recommend using the non-parametric median relation because it better represents the data and makes no assumptions about the data distribution. We do not provide a dune length-depth relation because there is limited use for this in paleo-environmental reconstructions since length is not easily recovered from cross-strata. We have made no distinction between dunes in shallow (< 2.5 m) and deep (> 2.5 m) flows because there is no way to determine whether the flow was deep or shallow from cross-strata. Ultimately, the recommended relation (Figure 2.14b; Table 2.7) is derived from field observations solely, because inclusion of laboratory observations, all of which are made in shallow flows, would bias the relation intended to predict flows at field scale.

There is clear advantage to using our ranges of uncertainty rather than relying on seemingly arbitrary ranges of H/h derived from other data compilations. Our ranges are based on the largest data set ever compiled and the ranges are objectively determined using probability theory. When applying our relations and the associated uncertainty, predicted flow depth ranges will be smaller when a 50% probability is applied, but the chance of the flow being outside of the range is greater than if a higher probability range is used. However, selecting the appropriate level of uncertainty for the inverse problem is more complex than this. Application of our non-parametric uncertainty estimates assumes that dune heights can be accurately reproduced from the rock record but

bedforms are rarely entirely preserved. Cross-sets more often represent the erosional remains of bedforms so only a fraction of bedform heights are preserved. The uncertainty associated with the theoretical and empirical models for reconstructing dune heights needs to be combined with the uncertainty derived from our relations. If the uncertainty derived from a cross-set thickness to dune height model is high, adding uncertainty from our flow depth-dune height relation would, at best, be a conservative estimate of uncertainty. If the prediction of dune height from cross-strata can be better constrained (based on many observations of well-preserved cross-strata), then some uncertainty of that prediction can be developed which should then be combined with the uncertainty from our relations.

2.9. Conclusions

We compiled all known observations of dune dimensions and flow characteristics from both laboratory flume experiments and field observations in order to assess dune scaling relations available in the literature. So far as we are aware, this is the most extensive data set compiled to date. Our assessment of previously proposed dune scaling relations reveals that none of them predict dune dimensions particularly well. Only about 50% of the predicted dune dimensions are within a factor of 1.5 of the actual dune height and length. Approximately 90% of the predictions are within a factor of 3.5 of the observed dune dimensions. The dataset reveals that the reason for the poor predictive power is the order of magnitude variability in dune dimensions for any particular flow condition, regardless of how the flow is parameterized. Furthermore, there is evidence that dunes in smaller channels conform to a different height scaling than dunes in larger channels. This scaling break in dune height between deep and shallow flows has not been formally documented. However, the emergence of the scaling break reflects a change in dune morphology from strongly asymmetric dunes with high lee angles in flows < 2.5 m deep to more symmetric, lower lee angles dunes in flows > 2.5 m deep.

In order to recover scaling relations for application in paleo environmental reconstructions and prediction for dune dimensions in modern flows, we develop a series of simple relations between dune dimensions and flow depth that include uncertainty bounds derived from our dataset. These simple depth-scaling relations remain useful because they require only one observable quantity to predict bed

roughness from flow depths, or only one estimate (dune height) from cross-strata to reconstruct paleoflows. By providing separate relations for dunes in flow depths greater and less than 2.5 m, the relations recognize that high angle dunes grow relatively higher in shallow flows than low angle dunes in deeper flows. Our proposed depth-scaling relations further improve on previous relations by including uncertainty that allows first-order estimates of the variability to be carried forward in predictions.

There remains no clear mechanistic explanation for how flow depth could be responsible for setting the equilibrium dimensions of dunes, despite the observation that dunes clearly increase in size with the scale of the river system. We have proposed that the apparent scaling of dunes with flow depth may be indirect and emerge because shear stress and shear velocity, which are both dependent on depth, are important physical controls on dune morphology. Until critical tests of the hypotheses for what controls the height and length of dunes can be made, our newly developed relations better represent the available data for both forward prediction of dune height from flow depth and inverse prediction of flow depth from dune height.

Acknowledgements

This work was supported by a National Sciences and Engineering Research Council of Canada (NSERC) Discovery grant to JV and Postgraduate Scholarship to RB.

Chapter 3. The Transport Scaling of Dunes

Abstract

Dune dimensions in sand-bedded rivers are often thought to scale with flow depth (*h*), with height (*H*) scaling as 1/6*h* and length (*L*) as 5*h*, even though substantial scatter about the relations has been observed. Transport stage has been shown to affect bedform geometry, but this control is usually ignored in favor of depth-scaling relations. Here, we use a series of flume experiments to systematically test controls on dune dimensions and variability. Experiments involved three sets of runs under five constant transport stages, ranging threshold to washout conditions, at three different flow depths. The mobile bed was repeatedly scanned during a 10-hour equilibrium period to derive mean values and quantify the variability. The results show that dune-depth scaling is not consistent because of a transport stage effect. Dune height increases with transport stage until a point when *H* decreases. Length remains nearly constant with transport stage until further increases in transport stage leads to lengthening. In general, dunes grow higher when significant bedload transport occurs, but become flatter and longer in the presence of substantial suspension. Ultimately, dunes scale with transport stage, which is a function of slope, grain size and *h*. The results are used to derive transport stage relations to guide predictions of dune dimensions in rivers and reconstructions of paleoflows based on dimensions estimated from cross-strata. The relations incorporate the non-linear response of dune dimensions with transport stage and provide metrics of uncertainty to include in predictions.

3.1. Introduction

The interaction between water and sediment at the Earth's surface creates bedforms in sand-bedded channels that range in size, scale and morphology. Dunes are bedforms that typically range anywhere from a few centimetres to several metres in height and can be up to 1000 m in wavelength/spacing (herein referred to as length). Dunes in small channels and flumes display an asymmetric shape with a stoss slope ranging from 2-6° and a high lee slope at the angle of repose (~30°). Dunes in rivers with depths > 2.5 m display a symmetrical shape with low lee side slopes, often < 10° (Venditti, 2013; Bradley & Venditti, 2017; Chapter 2). Modern river managers are

interested in the prediction of dune dimensions because they are important mechanism of bed material transport and are major sources of flow resistance. Dunes are also preserved in the rock record as cross-strata, so there is interest in using extracted dimensions from preserved features to hindcast their formative flows.

The ability to accurately predict dune dimensions and hindcast flows is limited by a poor understanding of what controls their size and shape in rivers. Yalin (1964) first linked dune dimensions to flow depth (*h*) and suggested that dune heights (*H*) scale as *h*/6 and lengths (*L*) scale as 5*h*. These simple conventions have become so pervasive that many authors argue dunes not following the scaling are out of equilibrium with the flow (e.g., Carling et al., 2000; Bridge, 2003; Holmes & Garcia, 2008). However, Bradley & Venditti (2017; Chapter 2) recently complied all available published dune dimensions from a range of rivers and showed that *H* and *L* were poorly predicted by the Yalin relations. Dune size does increase with flow depth, but *H* and *L* vary by up to two orders of magnitude for a given *h,* even when data are filtered to ensure dunes were fully adjusted to the flow. The substantial scatter indicates that depth is not the fundamental control on dune dimensions and, despite decades of research, we still do not understand what sets dune size.

A depth control has also been invoked, albeit less directly, in discussion surrounding the Froude number ($Fr = \overline{U}/\sqrt{gh}$, where $\overline{U}$ is the mean flow velocity and *g* is gravitational acceleration). Decades of experimental work (e.g., Simons & Richardson, 1966; Southard & Boguchwal, 1990; Cartigny et al., 2014; Naqshband et al., 2017a) and theory (e.g., Englund, 1970; Fredsøe, 1974; Colombini & Stocchino, 2008) have shown that *Fr* is important in controlling whether a dune field will transition to an upper stage plane bed, but the physical mechanism that links dune dimensions to *Fr* is tenuous. It has been proposed that dunes grow up into the flow until the area above the crest is planed off because the flow conditions are similar to an upper staged plane bed (Bennett & Best, 1996). However, dunes in deep rivers, where *Fr* is consistency sub-critical (< 0.3), do not grow as relatively high in the flow as dunes in shallower channels (Naqshband et al., 2014; Bradley & Venditti, 2017; Chapter 2). Instead, they adopt a low-angle symmetrical morphology (e.g., Smith & McLean, 1977; Kostaschuk & Villard, 1996; Hendershot et al., 2016; Hu et al., 2018) during high flows without any obvious relation to the *Fr*. Critical *Fr* conditions may limit growth in shallow channels, where flow

interaction with the water surface promotes planing of dune crests, but dunes do not necessarily grow to a constant fraction of flow depth (Venditti et al., 2016). Thus, the *Fr* control is not universal since it does not explain why dunes can adopt different heights at different flow strengths in shallow flows or why dunes in deep channels generally do not grow as high as in shallower flows.

The evidence that multiple dune dimensions can emerge for a given *h*, and that all dunes are not limited by the Froude number, suggests that something else acts as a control on dune dimensions. Early work (e.g., Yalin, 1972; Yalin & Karahan, 1979; Allen, 1982; Fredsøe, 1982) showed that transport stage can control the shape of a dune. Transport stage can be quantified as the ratio of the non-dimensional Shields stress (τ_*) to the critical Shields number for sediment entrainment (τ_{*c}). Shields stress is defined as

$$\tau_* = \frac{\tau}{(\rho_s - \rho_w) g D} \qquad \text{(Eq. 3.1)}$$

where τ is the shear stress at the bed, ρ_s and ρ_w are the sediment and water densities, respectively, and D is the representative grain size of the sediment, usually taken as the median grain size D_{50}. Values of τ_{*c} vary with grain size (e.g., Shields, 1936; Brownlie, 1981).

Transport stage can alternatively be quantified using a suspension threshold as the ratio of the shear velocity (u_*) to settling velocity of the sediment (w_s), which is a variant of the Rouse Number. Although u_*/w_s is directly proportional to τ_*/τ_{*c} for a given grain size, the former provides a boundary for when suspension occurs. It has been shown that particles can be entrained into the flow at u_*/w_s values as low as 0.4 (Van Rijn, 1984; Nino et al., 2003), but a vertical concentration profile of suspended sediment starts to develop at u_*/w_s = 1 (Bagnold, 1966).

Dune steepness (*H*/*L*) generally increases with transport stage from dominantly bedload to mixed load conditions. As transport stage further increases and more sediment moves in suspension, dunes become less steep (Yalin & Karahan, 1979; Allen, 1982; Naqshband et al., 2014; Bradley & Venditti, 2017; Chapter 2). Using a single flow depth and a range of transport stages, Venditti et al. (2016) showed a similar pattern in

H/*L* at a constant flow depth but as τ_*/τ_{*c} increases, *H* increases then decreases, while *L* continues to increase asymptotically until dunes wash out to a flat bed.

Natural variability further complicates our understanding of what controls bedform dimensions. Observations from flume experiments (e.g., Nordin, 1971; Venditti et al., 2016) and field studies (e.g., Hendershot et al., 2016; Ma et al., 2017) show tremendous natural variability in dune dimensions within and between reaches, but it is not entirely clear what drives this variability. At the dune scale, variability has been linked to merging and splitting causing dunes to increase or decrease in size (e.g., Gabel, 1993; Swanson et al., 2017; Hendershot et al., 2018). Others have related variability to the formation of lobe- and saddle-shaped crestlines (Venditti et al., 2005) and locally-controlled dune trough scour depth (*cf.,* LeClair, 2002). Ultimately, it is variation in sediment flux that drives local changes to dune morphology, with some treating this variability as a stochastic process (e.g., Paola & Borgman, 1991; Leclair & Bridge, 2001; Jerolmack & Mohrig, 2005; McElroy & Mohrig, 2009).

How dune variability within dune fields responds to bulk flow changes is also not well known. van der Mark et al. (2008) suggested that in deep natural channels, overall variability is constant between dune fields regardless of flow conditions, and variability is only reduced in small narrow channels such as flumes. However, Venditti et al. (2016) showed that variability in bedform dimensions is inherently linked to transport stage with considerably more variability occurring at higher τ_*/τ_{*c}. Improved prediction of dune dimensions will require a deeper understanding of what sets bedform variability.

The scaling of dune dimensions with flow depth is generally accepted despite both weak evidence to support the scaling and observations that show different equilibrium dune dimensions for a given flow depth at different transport stages. However, evidence of a transport control on dimensions has been limited to *H/L* (e.g., Yalin & Karahan, 1979; Allen, 1982; Bradley & Venditti, 2017) or to a single flow depth at a few different transport stages (Venditti et al., 2005; Venditti et. al., 2016). Bradley and Venditti (2017) recently tested a series of scaling relations that indicate potential controls, including transport stage, grain size, and *Fr*, but found that the relations poorly predicted dimensions. This highlights our limited understanding of the governing controls on dimensions and may also indicate that theoretical and empirical predictive relations should account for inherent variability.

Here, bedform dimensions and morphologies were examined under different transport conditions at different flow depths. Our experiments involved 3 sets of runs. Each set of runs had a different initial flow depth. In each run, a constant flow was applied over a flattened bed until the emergent bedforms remained in equilibrium for 10-hours. For runs within a set, a different constant flow was applied to achieve observations ranging from just above the threshold for sediment motion to a near complete washout of dunes. The bed was scanned repeatedly in each run to derive mean values, remove uncertainty and quantify the variability about them. We set out to explore the role of depth on dune dimensions, how dune dimensions and morphology are affected by transport stage and what controls variability in dune dimensions. Our overarching goal is to answer the question: What sets dune dimensions in rivers?

3.2. Methods

Laboratory experiments were conducted in the River Dynamics Laboratory (RDL) at Simon Fraser University, Canada. The 15 m long, 1 m wide and 0.6 m deep RDL flume has a slope that can be adjusted from -0.5 to 2% and recirculates both sediment and water. Well-sorted sand that had a D_{50} = 550 um was used in the experiments (Figure 3.1). The sand was 99.9% quartz with trace amounts of sillimanite, garnet, sphalerite, muscovite and gold.

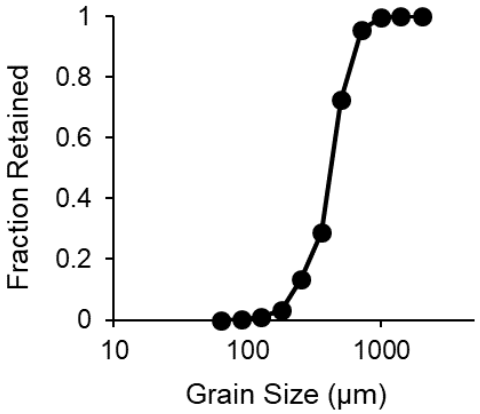

Figure 3.1. Grain-size distribution of sediment used in experiments

3.2.1. Experimental Design

The experiments involved three sets of runs and each set had a different initial flow depth of 15 cm, 20 cm, and 25 cm (Table 3.1). Each set included individual runs at different transport stages that were achieved by increasing the pump discharge. The recirculating flume was first filled to the designed depth then the pump was started to induce flow. The bed was flattened before each run and constant flow was then applied for 10-25 hours. This allowed the bed to reach a stable configuration with no apparent increase or decrease in the characteristic bedform dimensions, although later analysis showed that this was not entirely true for some of the lowest transport stage runs. For the 15 cm and 20 cm sets, observations were made at five different transport stages, ranging from just above the threshold for sediment motion to a near the washout of the bedforms. The runs are named Threshold (THLD), Bedload (BDLD), Lower Mixed (LMIX), Upper Mixed (UMIX), and Suspension (SPSN) based on visual observations of sediment transport. Only THLD and BDLD conditions were possible for the 25 cm depth because higher discharges were outside of the capacity the flume pumps. The initial flow depth for each run is identified in the run name herein (e.g., 15-THLD, 20-THLD, 25-THLD). The initial flume slope for each run was set so that it matched the water surface slope over the flat bed when the pumps were initially turned on. As the bed evolved through time, the water surface and bed slope changed, and they became emergent properties that responded to the imposed flow conditions.

Table 3.1. Initial experimental conditions.

Condition	Depth (m)	Discharge (m^3s^{-1})	Initial Flume Slope	Water Temp (°C)	No. of Scans
15-THLD	0.15	0.060	0	14	59
15-BDLD	0.15	0.075	0.00047	18	53
15-LMIX	0.15	0.090	0.00084	22	60
15-UMIX	0.15	0.110	0.00149	25	57
15-SPSN	0.15	0.130	0.00199	25	59
20-THLD	0.20	0.086	0	14	59
20-BDLD	0.20	0.100	0.00045	25	57
20-LMIX	0.20	0.120	0.00081	27	57
20-UMIX	0.20	0.140	0.00113	27	59
20-SPSN	0.20	0.167	0.00194	27	55
25-THLD	0.25	0.100	0	25	59
25-BDLD	0.25	0.125	0.00081	27	57

3.2.2. Measurements

Measurements of water surface and bed topography profiles were made using a Swath Mapping System (described in Venditti et al. (2016)). A stepper motor on the system allows the cart to run along rails mounted on top of the flume tank. The cart is equipped with a 32- transducer Seatek Instruments echo-sounding system mounted in a Plexiglas beam oriented across the channel. Each transducer is spaced 2.5 cm apart and a mechanical stepper motor moves the sensors vertically to ensure they could be positioned immediately below the water surface. Three MassaSonic ultrasonic sensors are also mounted on the cart to measure water surface elevations at positions of 20.6 cm, 49.9 cm and 80.5 cm across the channel from the right-hand flume wall looking downstream. An onboard computer records the Seatek and Massa sensor signals and positions.

Measurements were made in the along stream direction from 4.5 to 10 m to ensure no entrance or exit effects. The speed of the cart was set to maximize the number of scans that could be performed while providing high density measurements in the downstream direction. The downstream spacing of the Seatek measurements were 1.29 cm and the Massa measurements were 12.4 cm. The Seatek sensors were placed a few mm below the water surface so that they did not have any interaction with the labile bed. Individual scans were made approximately every 10 minutes. Data presented herein for each run are from a 10-hour period, consisting of 53 to 60 scans, after the bed had fully adjusted to the flow (Table 3.1).

3.2.3. Sediment Transport Measurements

A syphon system with an L-shaped copper tube, a nylon tube and a variable speed pump were used to isokinetically collect suspended sediment samples over the bed. The system was mounted to a point gauge positioned in the center of the channel and samples were collected 4 cm above dune crests to ensure a consistent sample location between measurements. Because downstream velocity profiles have a logarithmic form at the crest (e.g., Nelson et al., 1993), measurements can be converted to provide the least biased flux values. Flow velocity at 4 cm above the bed was estimated assuming a logarithmic velocity profile which was then used to set the siphon

pump speed to ensure isokinetic samples. Samples were filtered using glass microfiber filters with a pore size of 1.6 μm and weighed to derive sediment concentrations.

Measured 'at-a-point' sediment concentrations were converted to depth integrated total fluxes using the Rouse equation (Rouse, 1939):

$$\frac{C}{C_a} = \left(\frac{h-z}{z}\,\frac{z_a}{h-z}\right)^{\frac{w_s}{\delta k u_*}} \qquad \text{(Eq. 3.2)}$$

where *C* is the concentration of suspended sediment at height *z* above the bed, C_a is the reference concentration measured at elevation z_a = 4 cm above the bed, δ is a coefficient that describes the difference in diffusion between a sediment particle and a fluid particle (assumed to be 1), and k is the von Karman constant (0.41). Suspended sediment flux (q_{ss}) is then estimated per unit width as:

$$q_{ss} = \overline{U_h} \cdot \bar{C}_h h \qquad \text{(Eq. 3.3)}$$

where $\overline{U_h}$ and $\bar{C}_h$ are the mean depth-averaged streamwise velocity and concentration of suspended sediment, respectively.

Even though narrowly graded sand was used, the bed material contained much less than 1% of fine silt sediment (Figure 3.1). The fine sediment remained in suspension and did not interact with the bed. A correction for this washload component was performed to remove it from the calculated bed material suspended sediment flux. Washload was quantified using the siphon samples from the THLD condition where no bed material was in suspension (Venditti et al., 2016). Three washload concentrations were calculated from the 15 cm, 20 cm and 25 cm THLD conditions and subtracted from the measured suspended sediment concentrations from the other runs at the same flow depths.

Miniaturized Helley-Smith samplers scaled down to a 20 mm square mouth (Dietrich & Smith, 1984; Mohrig & Smith, 1996; Venditti et al., 2016) with a 75 μm meshbag were used to measure bedload flux. Bedload samples were collected by setting the samplers on the bed at dune crests. Three samples were collected at positions ¼, ½, and ¾ the channel width, but some sample sets contain only two samples because the measurement dunes migrated too quickly to identify the crest for the third sample. Bedload flux q_{bl} was calculated for each set of samples by adding the

weight of the three samples and dividing by the total collection time, and then multiplying by 50 to provide a per unit width value. Sediment carried in intermittent suspension in the near bed region (< 20 mm above the bed) was also collected in the Helley-Smith samplers, introducing a bias in the bedload measurements. A correction was applied to separate suspended load from the bedload when sediment was transported above the saltation layer. To split the loads, the Van Rijn (1984) saltation model was used to calculate saltation height, and a linear vertical concentration profile was assumed from the bed to z = 20 mm. The contribution to the suspended sediment collected in the Helley-Smith samplers was removed from the bedload component and added to the suspended bed material flux calculated with Equation 3.3. The total measured flux is not affected by the correction.

3.2.4. Filtering method

A filtering method was required to remove noise from the Seatek data (e.g., Figure 3.2a), especially at higher transport stages when large volumes of bed material were in transport. Most noise appeared as positive excursions above the bed, induced by sediment moving in suspension (e.g., Figure 3.2a,c). A simple smoothing filter such as a moving average, polynomial or spline could not be used because, while they did remove some of the noise, they ultimately smoothed out troughs. Given the extra noise at high transport stages, and difficulties recovering troughs, noise was removed using (1) an along stream profile filter, (2) a cross stream filter and (3) a smoothing moving window. A detailed step-by-step explanation of the method is available in Appendix 3 but the general steps are:

1. A data point (i) in an along stream profile was removed if the difference in vertical elevation (z) between the upstream point (i+1) and downstream point (i-1) was greater than 1 cm or less than -1 cm. A 9-point moving average (i-4:i+4) was then run through the profile and i was removed if it was -0.5 > z < 0.5 cm from the calculated average.
2. At high flow conditions (UMIX and SSPN), up to 5 sensors failed to return a useable signal (Sensors #9, 18, 23, 26, 31) because they had higher sensitivity to suspended sediment concentrations than the other transducers. Transducer sensitivity could only be adjusted for all sensors rather than individually, so these profiles were ultimately removed. Each point on the removed profile was

replaced with the mean value of the data points from the two nearest sensors in the cross-stream direction. A cross stream filter then removed any remaining noise by removing data points that had $z > 1.2$ cm from the mean value of two adjacent data points in the cross stream. A removed data point was replaced with the mean value of the two adjacent points.

3. A moving average with a 5-point window was calculated and run through the downstream profiles. Any data that were had $z > 0.50$ cm from the average of the window were replaced with the average value.

Figure 3.2b shows an example of the bed after the filter has been applied and Figure 3.2c provides a comparison between a noisy raw profile and a profile after the filtering method is applied. Despite the noise due to the increased sediment in suspension during this high transport stage (Figure 3.2a), profiles and bed structures are recovered.

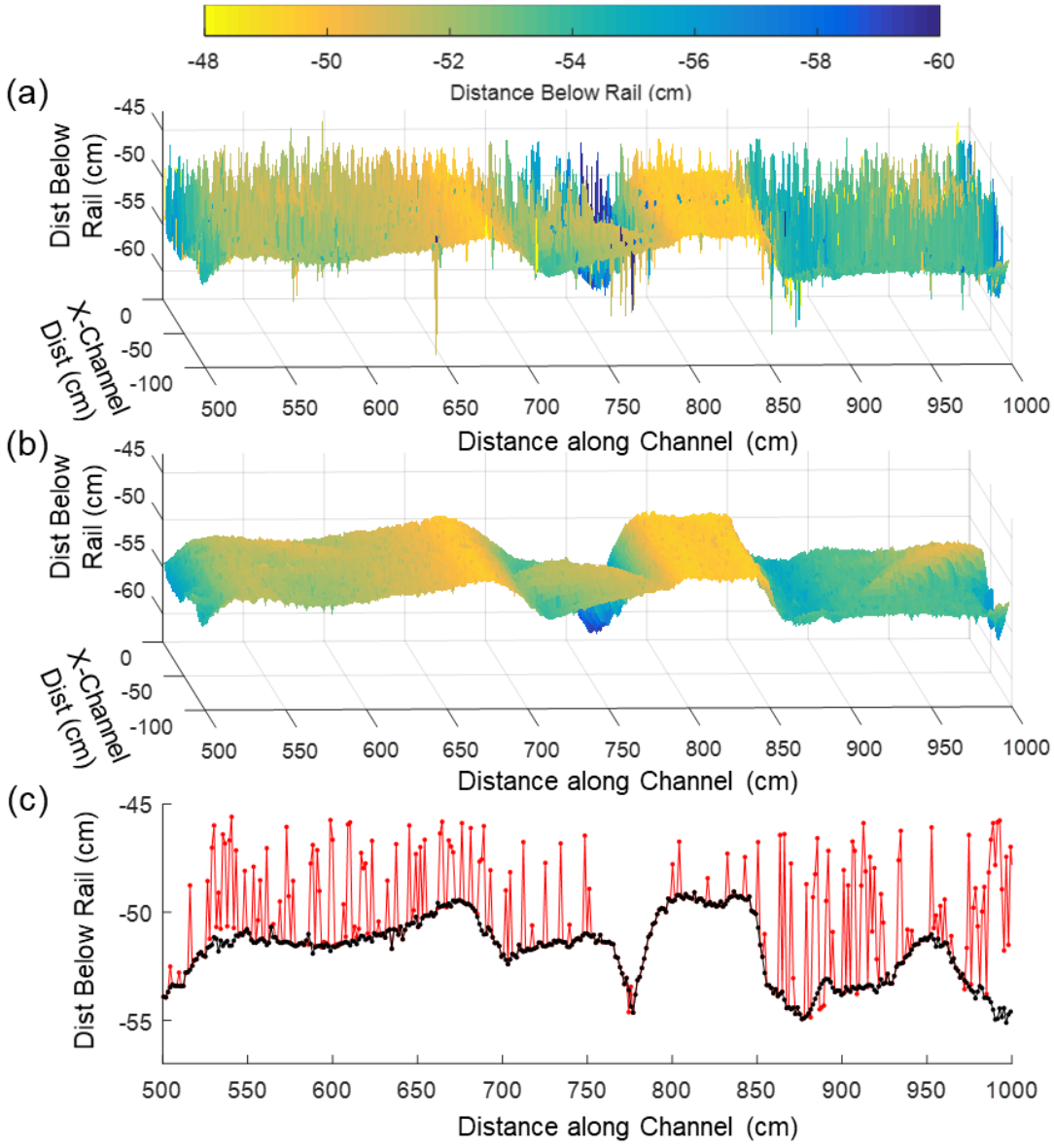

Figure 3.2. **(a) Example of a contour map generated from Seatek raw data and (b) a contour map using the same data after the filter has been applied. (c) Unfiltered (red) and filtered (black) data from the center Seatek sensor. Data are from a Run 15-UMIX, when increased sediment in suspension added extra noise in the raw data.**

3.2.5. Data Analysis

Depth was calculated for three profiles as the difference between the water surface profile and the bed profile (Seatek Sensors #7, 17, 24) located directly below the Massa sensors. This required data points from each profile to have identical along channel spacing so data from the water surface profiles were linearly interpolated to the

same spatial position as the data points in the bed profile. An average depth was calculated for each profile and the average of the three was used to derive a reach averaged depth (h_R) for each scan. Seatek Sensors #7, 17, 24 were also used to calculate the bed slope of each profile which were then averaged to derive a reach bed slope (S_{bR}). The slope for each Massa profile was calculated as the sum of the slope of the flume and the water surface slope, and a reach water surface slope (S_{wR}) was calculated as the average from the three profiles. In the UMIX and SPSN conditions, where Fr > 0.60, disturbances to the water surface, larger dunes in the channel affected the water surface profile. For example, a large dune near the end of the measurement range interacted with the flow such that the water surface was drawn down as it accelerated over the dune (Figure 3.3). To capture slopes that better characterized the shear stress, we manually selected a section of the center profile that was unaffected by large water surface disturbance (Figure 3.3). The S_{wR} and S_{bR} values for the UMIX and SPSN runs are limited to the center profile since it was too labor intensive to visually inspect all three profiles.

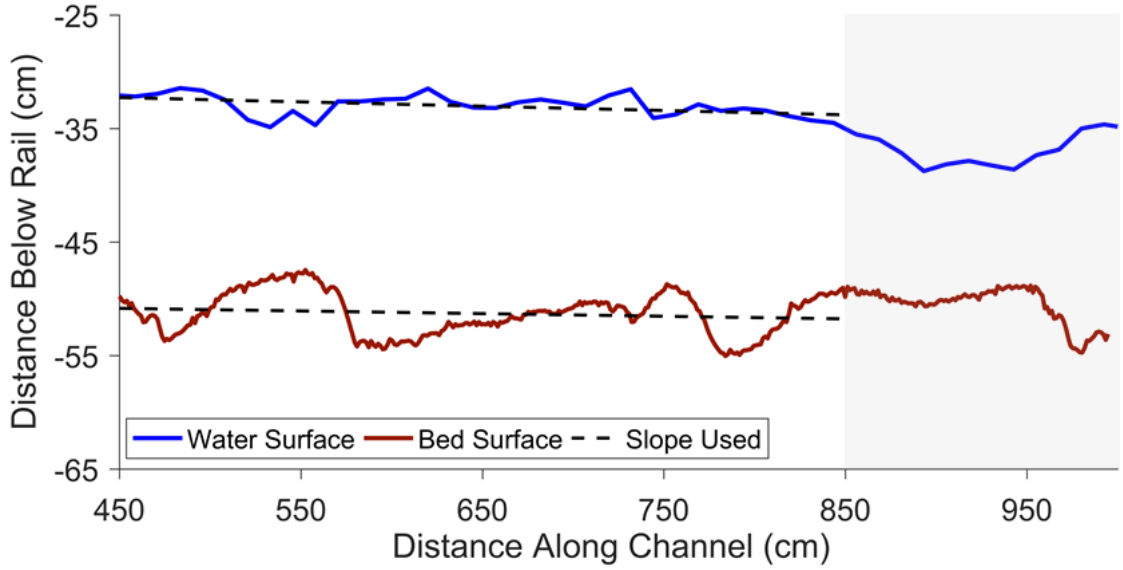

Figure 3.3. Example of a center profile from a 20-UMIX scan. Data in the shaded box have been excluded from the slope calculation to remove the effect of the water surface being drawn down over the large dune.

In most scans, S_{bW} and S_{bR} were well within +/- 0.005 of each other but some scans had slopes that deviated +/-0.008, even though the mean dune dimensions were not systematically increasing or decreasing. To account for this convective acceleration, we used the 1-D shallow-water momentum equation to calculate the total bed stress that

includes a convective acceleration term as (for full derivation see Le Bouteiller & Venditti (2014)):

$$\tau_{tot} = \rho_w g h_R S_{wR} + \rho {U_R}^2 (S_{bR} - S_{wR}) \quad \text{(Eq. 3.4)}$$

where U_R is the reach-averaged mean flow velocity. Sidewall correction was made using the Williams (1970) method:

$$\tau_{reach} = \frac{\tau_{tot}}{(1+0.18 h_R/w^2)} \quad \text{(Eq. 3.5)}$$

where w is the width of the flume. The reach-averaged shear stress, τ_R, was used to quantify transport stage τ_*/τ_{*cR} where τ_* is defined by Equation 3.1 and a value of τ_{*c} = 0.03 was approximated using the Shields curve. The suspension number (u_*/w_{s_R}) was also calculated where u_* is the reach bed shear velocity defined as:

$$u_* = \sqrt{\frac{\tau_R}{\rho}} \quad \text{(Eq. 3.6)}$$

and w_s was calculated using Dietrich (1982).

3.2.6. Automated bedform dimension method

Bedform dimensions were calculated using an automated method developed by McElroy (2009) (see Venditti et al. (2016) for a review of the method). This allowed spatially-averaged bedform height and lengths to be estimated from each of the 32 profiles. The method requires evenly spaced measurements along profiles, so the profiles were detrended and linearly interpolated to the approximate spacing of the measurements. Venditti et al. (2016) noted a consistent bias when they compared manually measured bedforms to those estimated with the automated method. To test for a bias in our data, bedform dimensions were manually measured for the center profile using the detrended center profiles to allow comparison with the automated method. In the manual method, dune heights were measured from trough to peak in the lee side and length from the lowest point in the upstream and downstream trough. A spatially averaged value from the manual method was determined by dividing the dimensions by the number of bedforms in the profile. Reach-averaged dune height (H_R)

and length (L_R) are reported as the mean values of the 32 spatially averaged dimensions for a scan.

3.2.7. Equilibrium Test

Observations were made as bedforms emerged from a flat bed until they grew into a stable bed configuration when the bedforms were not systematically increasing or decreasing in size. Equilibrium conditions were required to ensure that a mean height ($\bar{H}$) and mean length ($\bar{L}$) value derived from H_R and L_R of individual scans were representative of the transport stage being observed. At least ten hours of data were collected for each run during this equilibrium phase based on visual assessment, however, we applied a Nonstationary Mean Value (NSMV) technique (Bendat & Piersol, 1966) to ensure the bedform fields were not systematically growing or getting smaller during this period. The ratio of a subsample mean height $\hat{H}$ or length $\hat{L}$ is compared to the mean value of all scans during the observation period by calculating:

$$\beta_H = \frac{\bar{H}}{\hat{H}} \quad \text{(Eq. 3.6)}$$

$$\beta_L = \frac{\bar{L}}{\hat{L}} \quad \text{(Eq. 3.7)}$$

$\hat{H}$ and $\hat{L}$ are incrementally calculated using an additional scan until β_H or β_L enters and remains within a given confidence interval. The 95% confidence intervals for height (CI_H) and length (CI_L) are calculated for the observation time using

$$CI_{H_{(N)}} = \left(1 \pm \zeta \left[\frac{\sigma_{HR}}{\sqrt{N}H}\right]\right)^{-1} \quad \text{(Eq. 3.8)}$$

$$CI_{L_{(N)}} = \left(1 \pm \zeta \left[\frac{\sigma_{LR}}{\sqrt{N}L}\right]\right)^{-1} \quad \text{(Eq. 3.9)}$$

where σ_{HR} and σ_{LR} are the standard deviation of the H_R and L_R data, respectively, N is the number of scans included and ζ is a constant that changes with distribution and confidence interval (here set to 2 for a normal distribution at a 95% interval). As N increases the confidence interval bounds decrease, and the mean value will move to a stable saturation level within the confidence intervals if the mean is stationary and the bedforms are in equilibrium. The scan number at which β_H or β_L enters and remains

within the confidence interval indicates the number of scans needed to achieve a stable mean value that is representative of the long-term mean. We used this NSMV technique on the 10-hour window that ended on the last scan in the time series for each run.

3.3. Observations

3.3.1. Automated Method Comparison

Figure 3.4 shows the comparison between the manual and McElroy (2009) automated method for measuring averaged bedform height (H_p) and length (L_p) using profiles from the center Seatek (#16). The average bias associated with the method for most runs is less than 10% for H_p and L_p so no correction is required. However, our SPSN runs showed that the average bias in H_p and L_p ranged from approximately 10 to 20% because the automated method underestimates the reach-averaged dimensions. The automated method assumes the measured bedforms have the classical asymmetric triangular planform shape. However, bedforms from the SPSN transport condition had much lower H/L values than the method was designed for, so the increased error during this condition is not surprising. Therefore, we present the manually measured H_p and L_p for the centerline, as values for H_R and L_R for the SPSN condition. Only the center line is presented since it was too laborious to manually measure the dimensions for all 32 profiles in the runs. Occasionally measurements from the automated method substantially deviated from manual measurements in the UMIX runs, because some of the profiles showed bedforms with H/L values too low for the automated method. To remove these false extreme values from the reach-averaged values, we calculated the mean value from the 32 profiles, then removed the values that exceeded two standard deviations to provide the most accurate H_R and L_R.

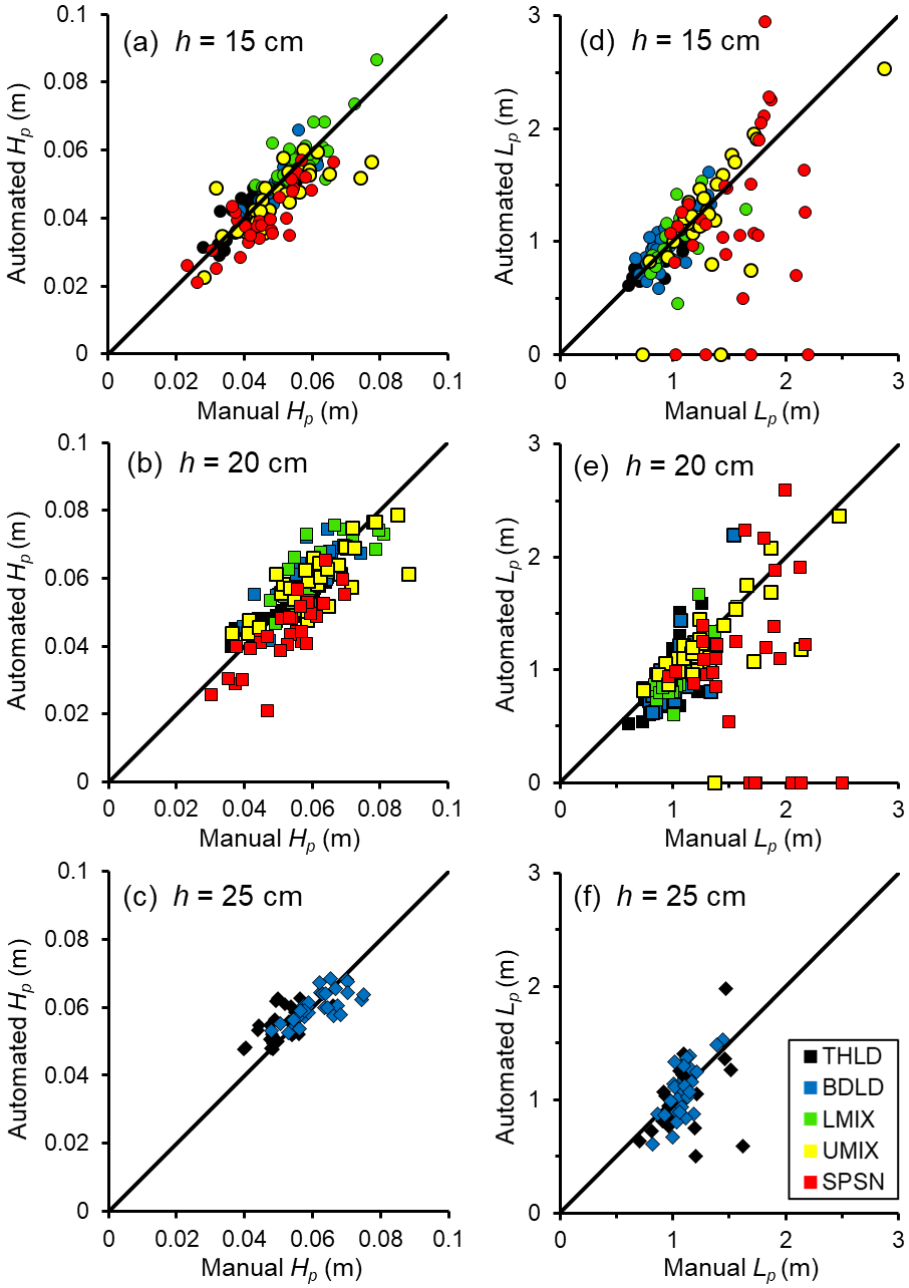

Figure 3.4 **Comparison between H_p at (a) 15 cm, (b) 20 cm, (c) 25 cm initial flow depths and L_p at (d) 15 cm, (e) 20 cm, (f) 25 cm initial flow depths for the manual method and the McElroy (2009) automated method.**

3.3.2. Equilibrium Identification

The NSMV analysis was applied to time series of bedform H_R and L_R to determine if the time series was statistically stationary within the 10-hour measurement period. Statistically stable $\overline{H}$ and $\overline{L}$ values were achieved < 25 scans in almost all runs, suggesting stability in the mean values after ~ 4 hours (Appendix D). One exception to

this was the THLD conditions when a few larger- or smaller-than-average dunes in the channel could have a lasting impact on the mean values because they require more time to migrate through the measurement window than at higher flows. Despite this caveat, the 10-hr periods (50-60 scans) achieved statistically stable $\overline{H}$ and $\overline{L}$ values.

3.3.3. Mean flow conditions

Mean flow conditions derived from the reach-averaged values from each scan are given in Table 3.2. Mean depth ($\overline{h}$) for the 10-hour observation period was ~10% less than the initially imposed depth as the bed adjusted to the flows. Runs with the highest mean flow velocity $\overline{U}$ had lower $\overline{h}$ values because dunes were smaller in height and had smaller flow recirculation cells that would extract less momentum from the mean flow. Average Froude number ($\overline{Fr}$) increased with discharge from 0.30 to 0.85, providing observations from the subcritical to near critical conditions. Mean shear stress $\bar{\tau}$ also increased with discharge creating mean suspension threshold ($\overline{u_*/w_s}$) and transport stage ($\overline{\tau_*/\tau_{*c}}$) values from 0.50 to 1.22 and 4.36 to 25.61, respectively, which represents a range from mostly bedload transport to beyond significant suspension transport conditions (e.g., Bagnold, 1966; Van Rijn, 1984; Nino et al., 2003).

Table 3.2. Mean flow conditions and bedform dimensions for the 10-hour statistically stationary observation period.

Condition	$\overline{h}$ (m)	$\overline{U}$ (m^2s^{-1})	$\overline{Fr}$	$\bar{\tau}$ (Nm^{-2})	$\overline{u_*/w_s}$	$\overline{\tau_*/\tau_{*c}}$	$\overline{H}$ (m)	$\overline{L}$ (m)	$\overline{H}/\overline{L}$
15-THLD	0.139	0.443	0.38	1.17	0.511	4.392	0.038	1.01	0.039
15-BDLD	0.141	0.547	0.47	3.54	0.882	13.26	0.063	0.945	0.064
15-LMIX	0.139	0.660	0.57	4.16	0.948	15.85	0.065	1.11	0.058
15-UMIX	0.129	0.854	0.76	4.98	1.04	19.03	0.051	1.22	0.041
15-SPSN	0.135	0.965	0.84	6.15	1.15	23.51	0.050	1.67	0.032
20-THLD	0.182	0.474	0.35	1.42	0.553	5.494	0.045	0.897	0.041
20-BDLD	0.176	0.575	0.44	2.86	0.779	10.69	0.070	1.07	0.066
20-LMIX	0.179	0.673	0.51	3.97	0.935	15.69	0.069	1.15	0.062
20-UMIX	0.174	0.805	0.62	5.55	1.10	21.22	0.065	1.38	0.049
20-SPSN	0.158	1.06	0.85	7.07	1.21	26.45	0.058	1.79	0.034
25-THLD	0.227	0.444	0.30	2.41	0.721	8.992	0.062	1.21	0.049
25-BDLD	0.221	0.569	0.39	3.62	0.891	13.51	0.066	1.19	0.059

The time series for the 10-hr observation period show that reach-averaged flow characteristics are marked by substantial variability, that increases with transport

condition (Figures 3.5 & 3.6). At lower transport stages, h_R varied < 1 cm between scans but at the higher transport stage runs, h_R varied up to 2 cm between scans (Figure 3.5a). Since Q is held constant over the run period, this pattern in variability is reflected in the reach averaged mean velocity U_R (Figure 3.5b) as h_R and U_R covary. More variability is present in the $u_*/\ w_{s_R}$ (Figures 3.6a-c) and τ_*/τ_{*c_R} time series (Figures 7d-f), because the variability in S_{wR}, S_{bR}, and U_R are incorporated into the calculation of τ_{tot} (Equation 3.4). Almost all scans in the THLD and BDLD conditions have $u_*/\ w_{s_R}$ < 1 while the LMIX, UMIX and SPSN conditions frequently often have $u_*/\ w_{s_R}$ > 1 (Figures 3.7a-c).

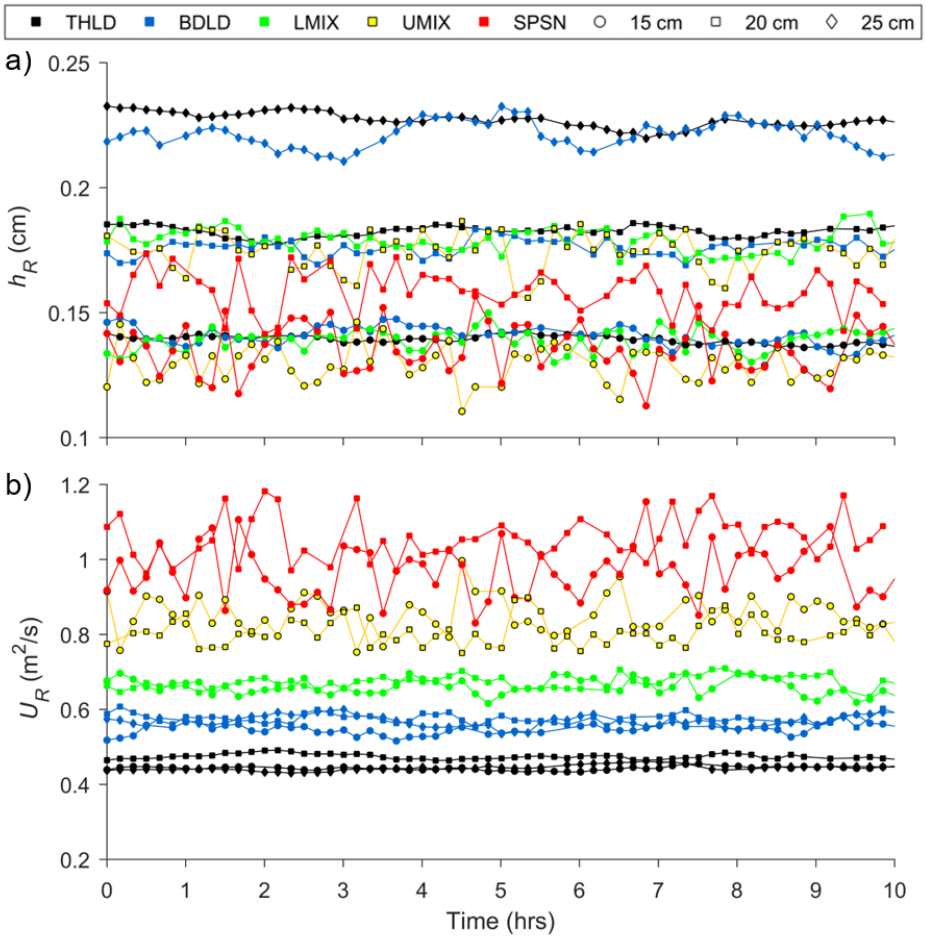

Figure 3.5. Time series of (a) reach averaged flow depth (h_R) and (b) reach averaged mean velocity (U_R) for all conditions.

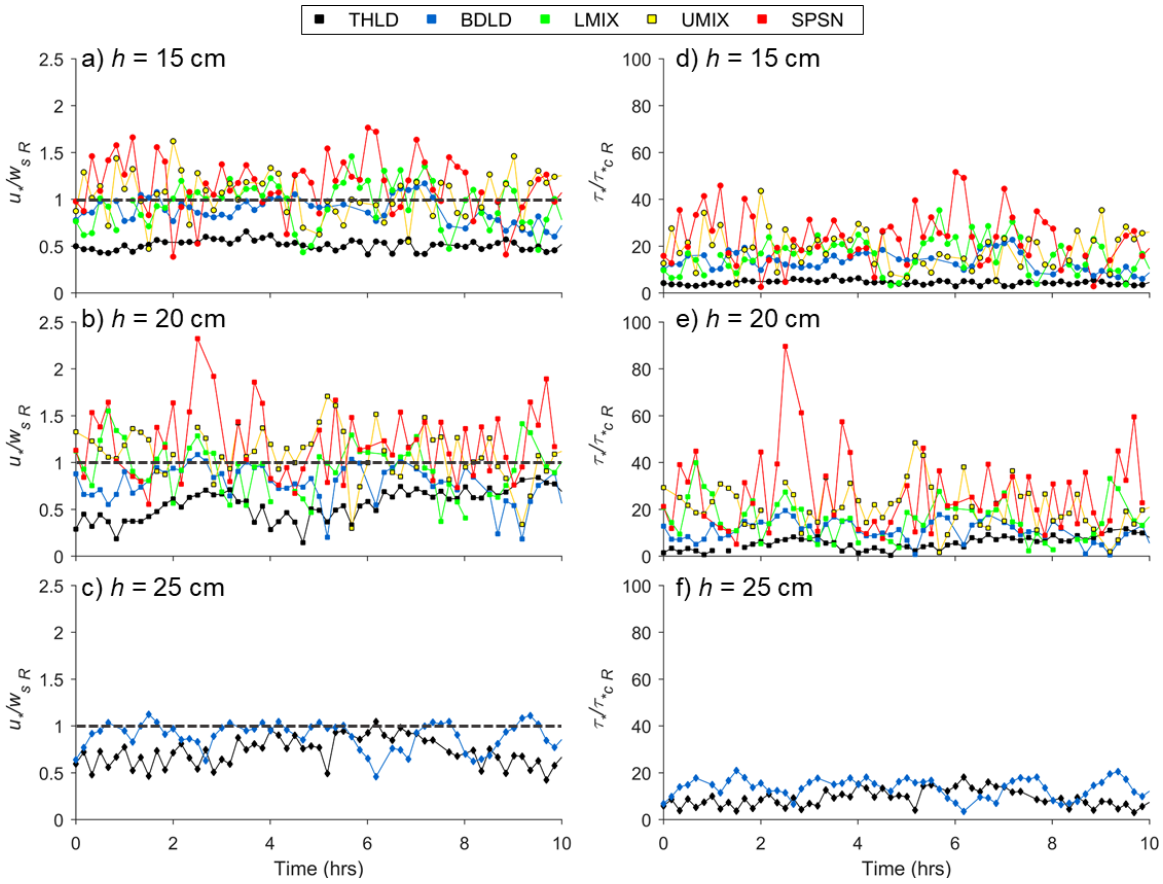

Figure 3.6. Time series of u_*/w_{s_R} separated by initial depths of (a) 15 cm, (b) 20 cm and (c) 25 cm and τ_*/τ_{*cR} for (d) 15 cm, (e) 20 cm and (f) 25 cm. The dashed line indicates the suspension threshold u_*/w_s = 1.

3.3.4. Sediment Transport

The calculated bedload (q_{bl}), suspended (q_{ss}), and total bed material flux as q_s = q_{bl} + q_{ss} corrected for the saltation layer shown in Figure 3.7 (data available in Appendix E; Supplementary Table E1). Bedload flux q_{bl} increases with transport stage (Figure 3.7a,f) and generally follows the Fernandez-Luque and van Beek (1976) bedload relation where $q_{bl} = 5.7(\tau_* - 0.037)^{1.5}$. No q_{ss} was observed at the THLD and BLD stage but q_{ss} increased with transport stage at beginning LMIX u_*/w_s > ~0.9 and τ_*/τ_{*C} > ~15 (Figure 3.7b,g). Nino et al. (2003) showed that suspension can occur at u_*/w_s = 0.4 but measurable suspension did not occur until u_*/w_s > ~0.9 in our experiment, likely due to the presence of well-developed bedforms and narrowly graded sand. They also observed significant volumes of sediment transported in suspension u_*/w_s =1 which is entirely consistent with our observations. Total load flux q_s increases with transport

stage and substantial increases in flux occurred when u_*/w_s > ~0.9 and τ_*/τ_{*C} > ~15 due to the large volume of bed material moving in suspension (Figures 3.7c,h). Our measurements show that q_{ss}/q_s (Figures 3.7d,e) and q_s/q_{bl} (Figures 3.7i,j) decreased with transport stage (Figures 3.7i,j).

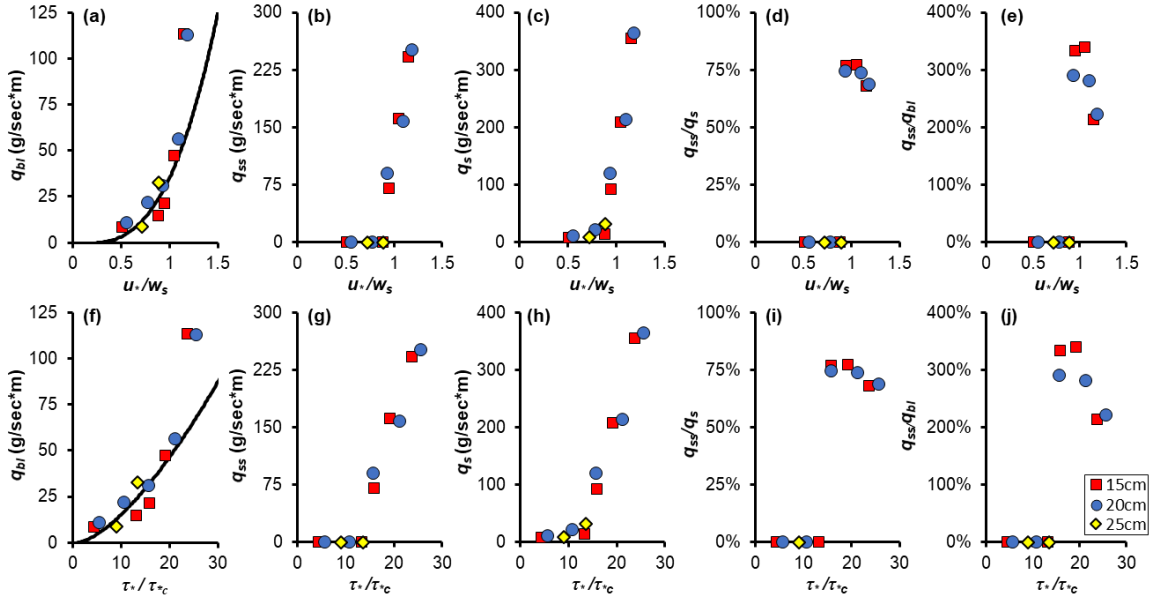

Figure 3.7. (a) Bedload q_{bl}, (b) suspended load q_{ss}, (c) total load flux q_s, (d) q_{ss}/q_s and (e) q_s/q_{bl} versus u_*/w_s. (f) Bedload q_{bl}, (g) suspended load q_{ss}, (h) total load flux q_s (i) q_{ss}/q_s and (j) q_s/q_{bl} versus τ_*/τ_{*C}. The black line in (a) and (f) is the Fernandez-Luque and van Beek (1976) bedload relation.

3.3.5. Bedform Morphology and Dimensions

All bedforms displayed angle of repose lee sides, but the general morphology and bed patterns were distinct for the different transport stages, regardless of initial depth. Characteristic examples of bed morphology are provided in Figure 3.8, while bed maps for all individual scans from each run can be found in Appendix F (Supplementary Videos F1-F12). Bedforms at the THLD stage (Figure 3.8a) had relatively shallow troughs and did not grow as high in the flow as at higher transport stages. Smaller secondary bedforms that were < 10% of the height of primary bedforms commonly migrated on the back of the larger dunes. At the BDLD transport stage, dunes clearly displayed angle-of-repose geometry with fewer individual secondary dunes migrating over larger dunes (Figure 3.8b). At the LMIX stage, when some sediment was moving in suspension, bedforms were higher in the flow and had deeper trough scour than at lower

transport stages. During the UMIX stage, bedforms were longer and crests were planed off, however, stoss and lee slopes, as well as troughs, were still well defined (Figure 3.8d). At the highest transport stage, when the bed was close to washing out to a plane bed, avalanching lee faces and shallow troughs were still evident on the bed (Figure 3.8e). The low-angle dunes observed in deep rivers were not observed. These morphological characteristics are reflected in the mean dimensions (Table 3.3). In each of the initial depth set of runs (e.g., 15 cm, 20 cm, 25 cm), $\overline{H}$ increases for each transport stage condition, up until the LMIX runs when $\overline{H}$ decreases. From the THLD to LMIX condition, $\overline{L}$ remained constant for each run during the THLD to LMIX condition but was larger during the UMIX than the SPSN runs.

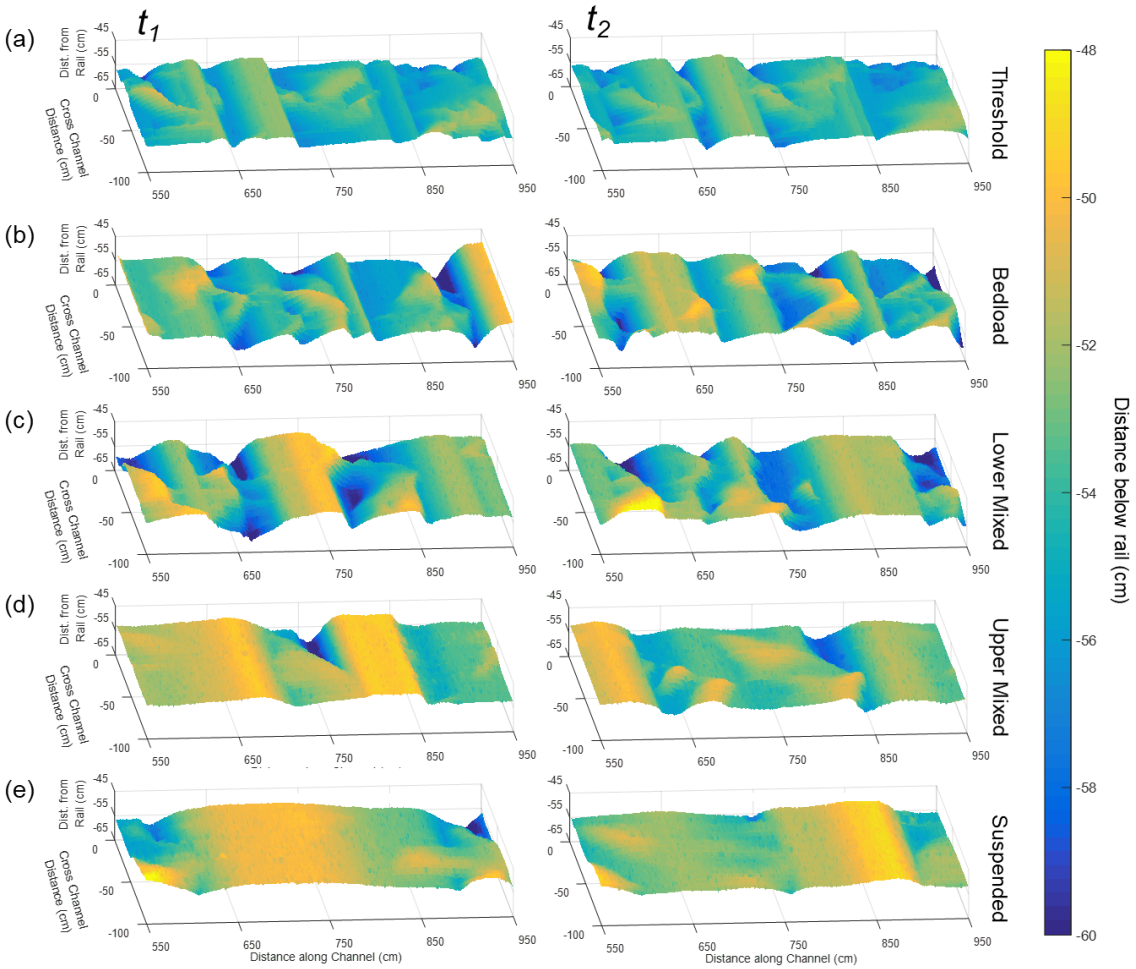

Figure 3.8. **Examples from the time series of bed configurations between two scans (0.3 hrs) from (a) 15-THLD (Appendix F; Supplementary Video F1), (b) 15-BLD (Appendix F; Supplementary Video F2), (c) 15-LMIX (Appendix F; Supplementary Video F3), (d) 15-UMIX (Appendix F; Supplementary Video F4), and (e) 15-SPSN (Appendix F; Supplementary Video F5).**

Table 3.3. Mean bedform characteristics and Coefficient of Variation (CV).

	Height			Length			
Condition	$\bar{H}$ (m)	CV	$\overline{h/H}$	$\bar{L}$ (m)	CV	$\overline{L/h}$	$\overline{H/L}$
15-THLD	0.036	0.074	3.73	1.01	0.209	7.34	0.039
15-BDLD	0.063	0.096	2.28	0.96	0.186	7.11	0.064
15-LMIX	0.065	0.104	2.17	1.11	0.174	8.28	0.058
15-UMIX	0.050	0.156	2.61	1.22	0.254	9.95	0.041
15-SPSN	0.049	0.239	2.85	1.38	0.280	12.53	0.032
20-THLD	0.046	0.118	4.12	1.06	0.319	6.10	0.041
20-BDLD	0.070	0.120	2.55	1.07	0.223	6.21	0.066
20-LMIX	0.071	0.128	2.61	1.15	0.222	6.47	0.062
20-UMIX	0.065	0.208	2.73	1.38	0.416	8.03	0.049
20-SPSN	0.053	0.229	2.90	1.46	0.320	11.26	0.034
25-THLD	0.063	0.123	3.72	1.13	0.216	5.70	0.049
25-BDLD	0.065	0.134	3.39	1.13	0.304	5.16	0.059

Time series visually confirm that the bedform fields were in an equilibrium state as dimensions were not systematically changing over the 10-hour averaging window (Figure 3.9). A striking contrast between the THLD and SPSN runs was observed as values of H_R and L_R during the SPSN runs were much different between scans because the rapid evolution of the bed results in a new bedform configuration between scans (Figure 8e). There is no autocorrelation in the time series. However, during THLD runs, bedforms had a lower migration rate leading to more subtle changes in the bed between scans (e.g., Figure 3.8a). For example, in the 25-THLD condition (Figure 3.5c), from 4-10 hours H_R is relatively stable, but this is preceded by a 3-hour period with smaller than average dunes. Despite this observation, NSMV analysis confirmed that a stable mean value was achieved within the 10 hours of observations.

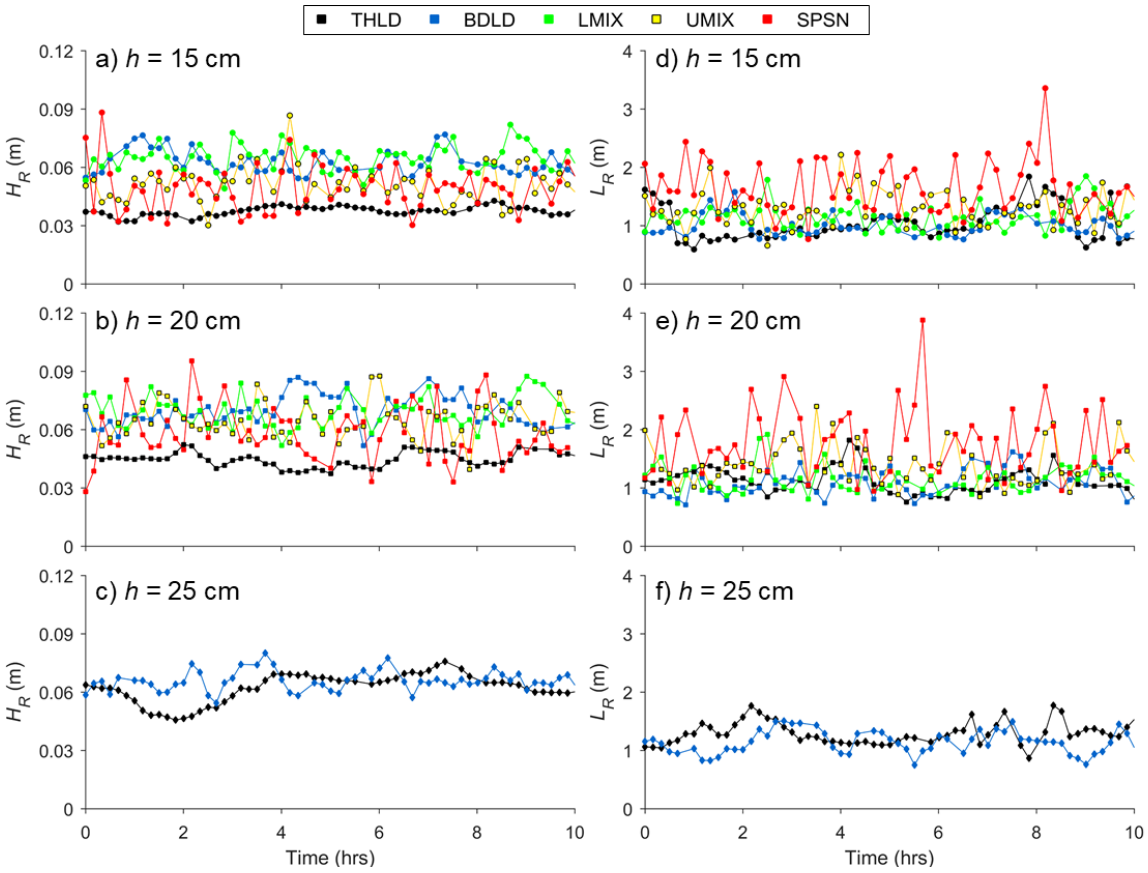

Figure 3.9. Time series of H_R at initial depth of (a) 15 cm, (b) 20 cm, (c) 25 cm, and L_R at (d) 15 cm, (e) 20 cm, (f) 25 cm.

3.3.6. Variability in Dimensions

The time series of dune dimensions are marked by tremendous variability between scans, especially at the higher transport stage (Figure 3.9). This is reflected in the coefficient of variability for $\overline{H}$, which systematically increases in runs with larger transport stage and depth (Table 3.3). The pattern in median bedform height from the 10-hr equilibrium periods (Figure 3.10a) follows that of $\overline{H}$ (Table 3.3), but the 25th and 75th percentile and the 5th and 95th percentile ranges are systematically larger for the runs at higher transport stages (Figure 3.10a). Variability increases because the distributions are narrower at lower transport stage runs than higher transport stages within the same initial flow depth (Figures 3.10b-d). The range of H_R values is so wide in the SPSN runs that it encompasses values observed in all conditions (Figures 3.10b,c). Flow depth also appears to influence the variability as the H_R distributions for the 15 cm initial flow depth (Figure 3.10b) are generally narrower and have higher peaks in the

normalized frequency when comparing the 20 cm and 25 cm runs (Figure 3.10c,d). There is a less clearly defined pattern to the coefficient of variability for L_R (Table 3.3) but the 25th and 75th percentile and the 5th and 95th percentile ranges about the median length increase with runs at higher transport stages (Figure 3.10e). There is less evidence for a depth effect on the L_R variability but overall L_R distributions are narrower and have higher peaks in the normalized frequency for the 15 cm initial flow depth (Figure 10f) than for deeper flows (Figures 3.10g,h).

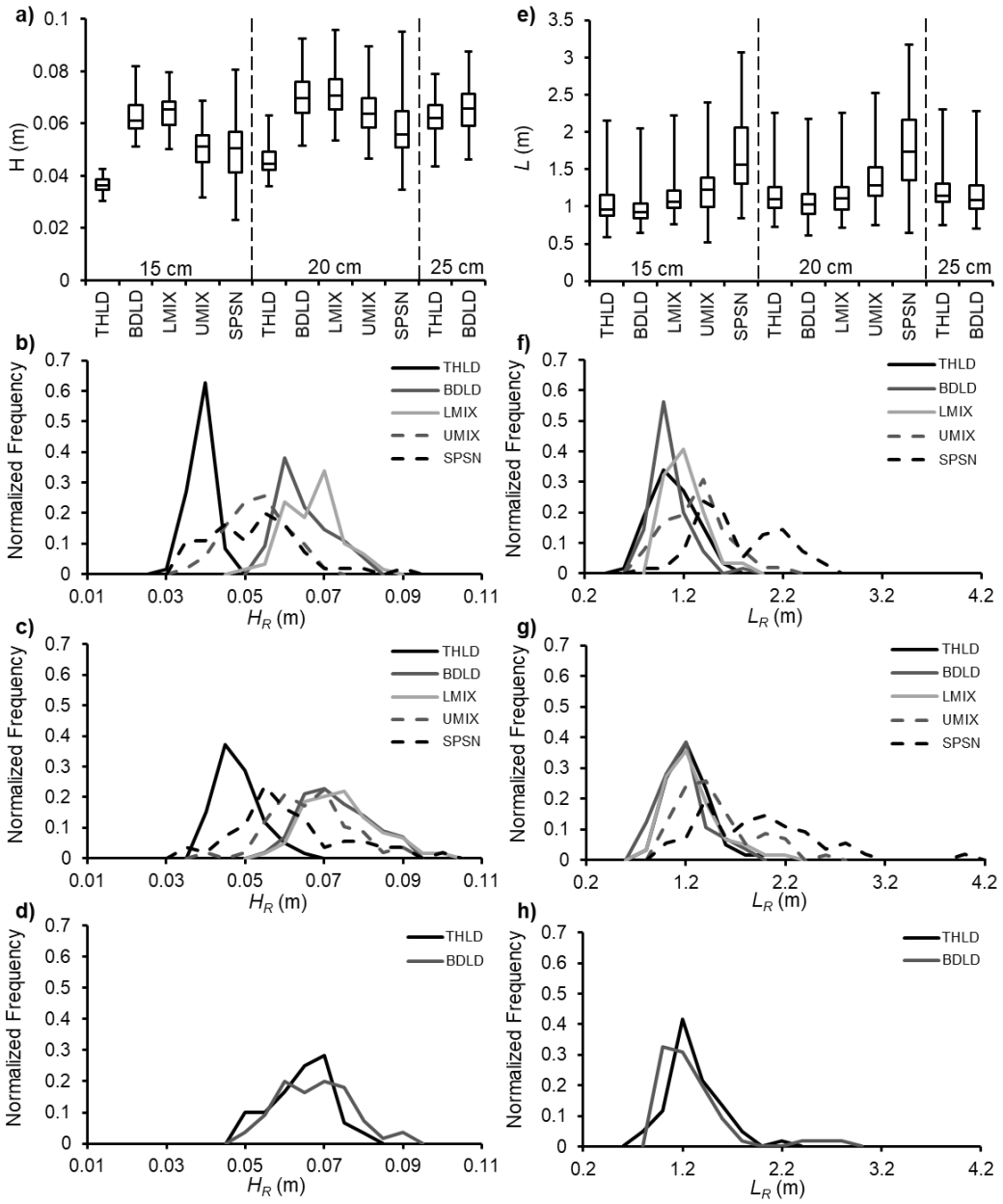

Figure 3.10. (a) Box and whisker plots showing median *H*, 25th and 75th percentile, and the 5th and 95th percentile. Normalized frequency plots of H_R for the (b) 15 cm (c) 20 cm and (d) 25 cm runs. (e) Box and whisker plots showing median *L*, 25th and 75th percentile, and the 5th and 95th percentile. Normalized frequency plots of L_R for the (b) 15 cm (c) 20 cm and (d) 25 cm runs.

3.3.7. Bedform Response to Flow

A wide range of H_R and L_R values are possible for a given h_R (Figures 3.11a,b). For example, where h_R = 0.13 m, bedforms could have H_R anywhere from 0.03 to 0.10

m. The average dune height, $\overline{H}$, for each transport stage condition was different even though they shared similar flow depths (Figure 3.11a; Table 3.3). However, $\overline{H}$ from same transport stage increases at a deeper initial flow depth (Figure 3.11a) because there is simply more room in the water column for the bedforms to grow. A wide range of L_R values is also possible for a given h_R (Figure 3.11b), although L_R values from the THLD, BDLD, and LMIX stage are often similar within the same initial depth range, with more scatter appearing during the UMIX and SPSN stages for larger $\overline{L}$ values. Bedform steepness is largely unaffected by the depth (Figure 3.11c).

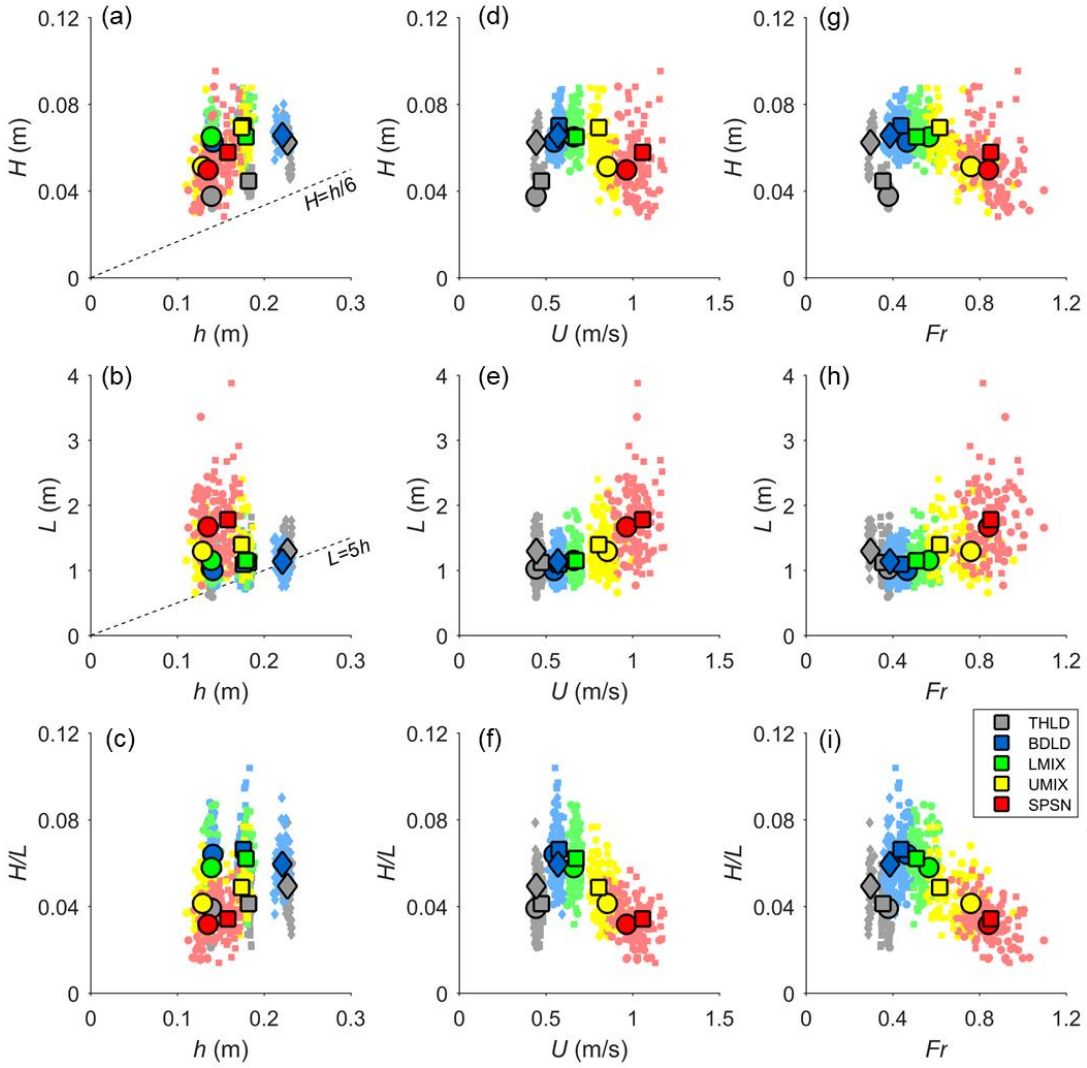

Figure 3.11. Relations between (a-c) dune height (*H*), (d-f) length (*L*) and (g-i) steepness (*H/L*) and flow characteristics, including depth (*h*), mean velocity (*U*) and Froude number (*Fr*). Circles, Squares and diamonds are from runs with the initial depths of 15 cm, 20 cm, and 25 cm, respectively. Smaller symbols are reach-averaged values and larger symbols are mean values for a run.

The effect of flow velocity (Figure 3.11e-f) and the Froude number (Figures 3.11g-i) on dune dimensions in these experiments are similar because, while different initial depths are used, a wider *h* range would be required to observe substantial variation in the Froude number. Dune height increases and then decreases from runs at lower $\overline{U}$ and *Fr* to runs at higher $\overline{U}$ and *Fr* (Figures 3.11d,g). Runs with $\overline{U}$ ~ 0.45 to ~ 0.55 ms^{-1} and *Fr* ~ 0.30 to 0.40 have dunes that increase in height from 0.035 to 0.063 m. Dune height remains stable until runs when $\overline{U}$ > 0.80 ms^{-1} (*Fr* > 0.60) where $\overline{H}$

decreases at a gentler slope than the initial increase in $\overline{H}$ (Figure 3.11d,g). Mean dune length is consistent in runs with $\overline{U}$ < 0.80 m/*s* and *Fr* < 0.75, but runs beyond these values have longer dunes (Figure 3.11e,h). These patterns in $\overline{H}$ and $\overline{L}$, lead to $\overline{H/L}$ in runs that increase with mean velocity until ~0.80 m/s (*Fr* = 0.50) where $\overline{H/L}$begins to decrease (Figures 3.11f,i).

Dune dimensions are affected by both u_*/w_s (Figure 3.12a-c) and τ_*/τ_{*C} (Figure 3.12d-f). Individual scans show tremendous scatter in reach averaged values, particularly where u_*/w_s > 1 and τ_*/τ_{*C} > 10. However, mean values for each condition show that $\overline{H}$ increases until u_*/w_s ~ 0.8 or τ_*/τ_{*C}~10 and remains at a steady $\overline{H}$ until u_*/w_s = 1 or τ_*/τ_{*C}~ 17, where $\overline{H}$ decreases (Figure 3.12a,d). Mean bedform length remains constant with u_*/w_s until u_*/w_s = 1 or τ_*/τ_{*C}~ 15, when $\overline{L}$ increases with increasing transport stage (Figure 3.13b,e). These patterns create a parabolic trend in $\overline{H/L}$ as $\overline{H/L}$ increases until $u_*/w_s \approx 0.9$ and $\tau_*/\tau_{*C} \approx 16$, when it then begins to decrease (Figure 3.12c,f).

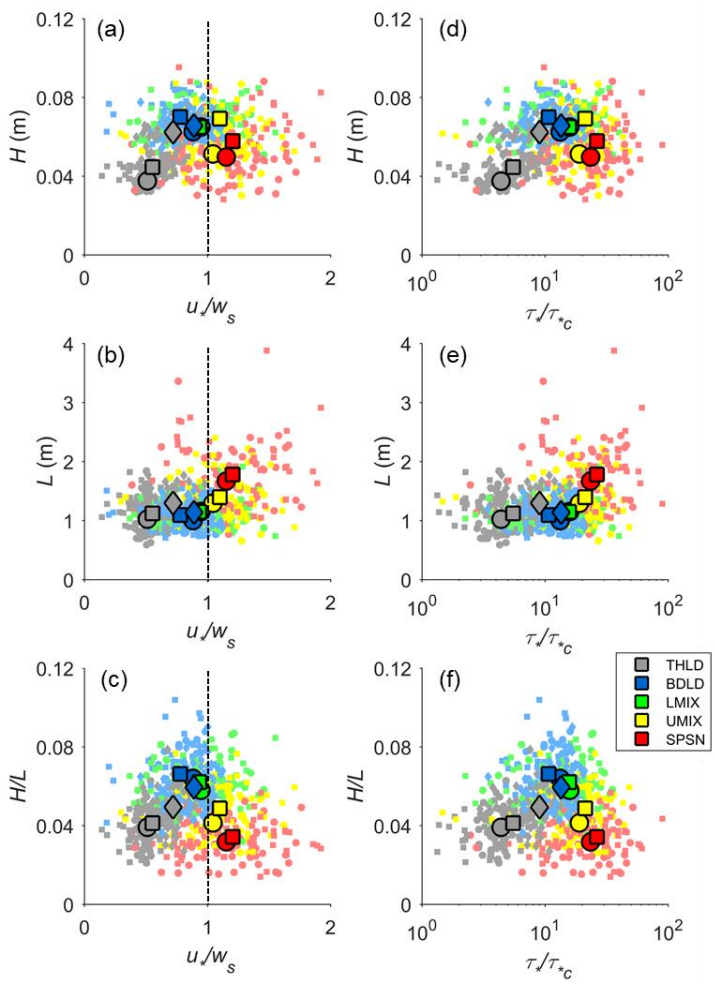

Figure 3.12. Relation between (a-b) dune height (*H*), (b-c) length (*L*) and (c-d) steepness (*H/L*) and transport stage defined as u_*/w_s and τ_*/τ_{*c}. Circles, Squares and diamonds are from runs with the initial *h* of 15 cm, 20 cm, and 25 cm, respectively. Smaller symbols are reach-averaged values and larger symbols are mean values for a run.

3.4. Dune-scaling

3.4.1. Depth-scaling

The $\overline{H}$ and $\overline{L}$ values are close approximations of the true mean dimensions and not samples of a larger population. Additional samples would have a negligible effect on $\overline{H}$ and $\overline{L}$ values or the level of variability observed. The true mean values allow for an assessment of dune scaling relations. Dunes in these experiments did not follow the depth-scaling relations commonly attributed to Yalin (1964) since all dunes grew larger than $H=h/6$ and most were longer than $L=5h$ (Figure 3.11a,b). This phenomenon was

documented previously by Bradley and Venditti (2017) for dunes developed in small channels. For flow where h < 2.5 m, they proposed $H=h/3.5$ and $L=5.9h$ as better fits to observations of reach-averaged dune dimensions and flow depth. Some H_R and L_R data from these experiments are predicted using the Bradley and Venditti (2017) relations, but substantial deviation from the relations occurred due to the applied transport stage (Figure 3.13). The THLD runs are within ~10% of $H=h/3.5$ but, with the exception of 25-BDLD, deviation is much larger (~50%) for the BDLD and LMIX runs. Deviation from the $H=h/3.5$ relations declines for the higher UMIX (~30%) and SUSP (~20%) (Figure 3.13). Deviation from $L=5.9h$ is low for the THLD and BDLD (< 20%) and increases up to ~65% for the runs with substantial suspended sediment flux. This suggests that the empirical depth-scaling relations of Bradley and Venditti (2017) best represent lower transport stages. The dune dimensions for runs at higher transport stages, particularly where substantial suspended sediment flux was observed, are underpredicted.

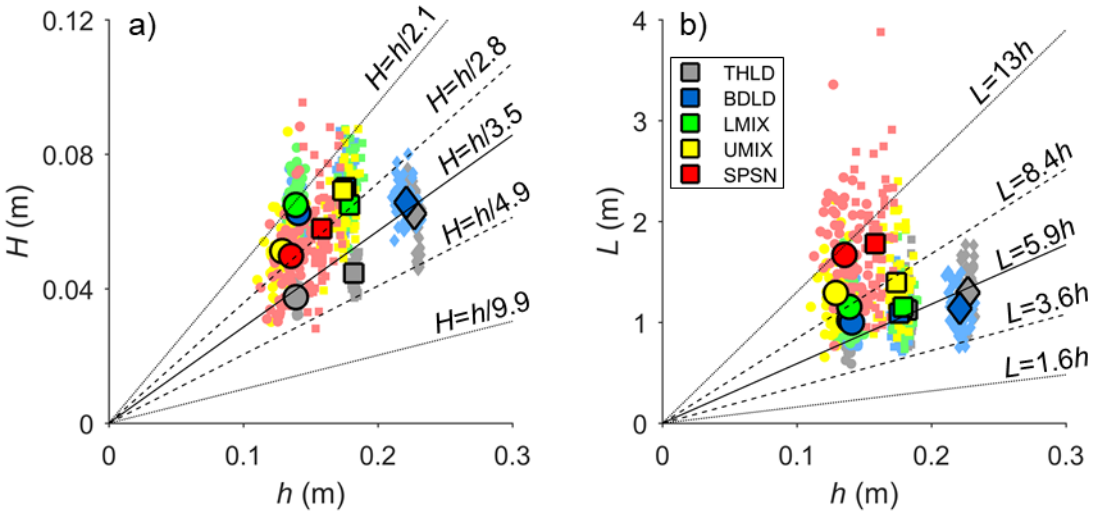

Figure 3.13. (a) Dune height and (b) length plotted against depth for each scan. Circles, Squares and diamonds are from runs with the initial *h* of 15 cm, 20 cm, and 25 cm, respectively. The solid lines are Bradley and Venditti's (2017) depth-scaling relations for flows < 2.5 m deep. Dashed and Dotted lines are their 50% and 95% uncertainty bounds, respectively.

Bradley and Venditti (2017) also note substantial variability about the proposed relations that they attributed to natural variability in bedforms and a transport stage effect. They suggest uncertainty ranges to capture variability so that simple depth-scaling relations could be used in paleo-environmental reconstructions and flow roughness predictions. The uncertainty ranges were derived by setting bounds about the

median relations such that 50% of the data (25th and 75th percentile) and 90% (5th and 95th percentile) were captured within the ranges. Figure 3.13 shows the 50% and 90% uncertainty intervals from Bradley and Venditti (2017) overlaid on the true mean height ($\bar{H}$) and length ($\bar{L}$) values and the natural variation about the true means represented by the reach-averaged height (H_R) and length (L_R) values from individual scans. The H_R data more often plot above $H=h/3.5$ than below, yet ~50% of the data fall within the Bradley and Venditti (2017) 50% uncertainty bounds and nearly all the scans are within the 90% intervals (Figure 3.13a). Many individual observations of L_R for the dune fields plot above $L=5.9h$, although 68.5% of those data lie within the 50% uncertainty bounds and almost all the scans are within the 90% intervals (Figure 3.13a).

3.4.2. Transport stage scaling

Following his early work (Yalin, 1964), Yalin argued that ripple and dune aspect ratios (*H/L*) are controlled by transport stage, an idea that has been supported by various data compilations (Yalin, 1972; Yalin & Karahan, 1979; Bradley & Venditti, 2017). Others have used data compilations to also propose that *H* is a non-linear function of transport stage (*cf.*, Allen, 1982; van Rijn, 1984; Karim, 1995; Naqshband et al., 2014). Venditti et al. (2016) suggest *H/L* increases and then decreases with transport stage because *H* increases, then decreases with increasing transport stage and *L* constantly increases until the bed washes out to an upper-stage plane bed.

We have derived the true mean values of the bedform dimensions in our experiments, allowing identification of the underlying relation between transport stage, and *H*, *L* and *H/L*. The mean values remove the inherent natural variability in dune fields and remove differences in measurement techniques or inadequate sampling of the dune fields that limit data compilation exercises. While the scaling of dunes by depth has poor predictive power (Figure 3.13), there is a depth effect on dunes; they get larger with the scale of the flow. To remove the depth effect, we scale dune dimensions by flow depth as *H/h* and *L/h*. This has the added benefit of producing relations that may be applicable outside the range of observations in our small-scale experiments.

The underlying relation between *H/L*, *H/h* and *L/h* and transport stage is a parabolic function (Figure 3.14). Regression analysis yields relations that have the following form:

$$\frac{H}{L} = a_{H/L} * \left(x - b_{H/L}\right)^2 + c_{H/L} \quad \text{(Eq. 3.10a)}$$

$$\frac{H}{h} = a_{H/h} * \left(x - b_{H/h}\right)^2 + c_{H/h} \quad \text{(Eq. 3.10b)}$$

$$\frac{L}{h} = a_{L/h} * \left(x - b_{L/h}\right)^2 + c_{L/h} \quad \text{(Eq. 3.10c)}$$

where *x* is transport stage (u_*/w_s or τ_*/τ_{*C}), the coefficient a is the shape of the parabolic function, and *b* and *c* are the horizontal and vertical position of the curve inflection point, respectively. The results of the regressions are presented in Table 3.4. Values from the 25-BDLD were omitted from the *H/h* regressions (Figures 3.14b,e) because it was a conspicuous outlier in the data set (see Figure 3.13). The R^2 values for the regression range from 0.70-0.81 (Table 3.4) suggesting that a substantial proportion of the variance amongst the mean dimensions is predicted by transport stage. The relations capture the observation that bedforms grow higher in the flow at moderate transport stages and that length remains relatively constant until the higher transport stages produce longer bedforms (Figure 3.12).

Using u_*/w_s as a measure of transport stage collapses the data over a narrow range of u_*/w_s (Figures 3.14a-c) when compared to regression using τ_*/τ_{*c} (Figures 3.14d-f). The value of the inflection point, b, in Equations 3.10a, 3.10b, and 3.10c represents an important change in the scaling of dunes. The transport stage at *b* in Equation 3.10b indicates when *H* begins to decrease, rather than increase, with transport stage (Figures 3.14b,e). The value of *b* in Equation 3.10c shows the transport stage when *L* begins to increase with transport stage (Figures 3.14c,f). Dune height relative to depth increases until u_*/w_s = 0.96 (τ_*/τ_{*c} = 18), suggesting the point when *H* begins to decrease is coincident with the threshold for substantial suspension. Length scaling decreases slightly or remains constant until u_*/w_s = 0.72 (τ_*/τ_{*c} = 9).

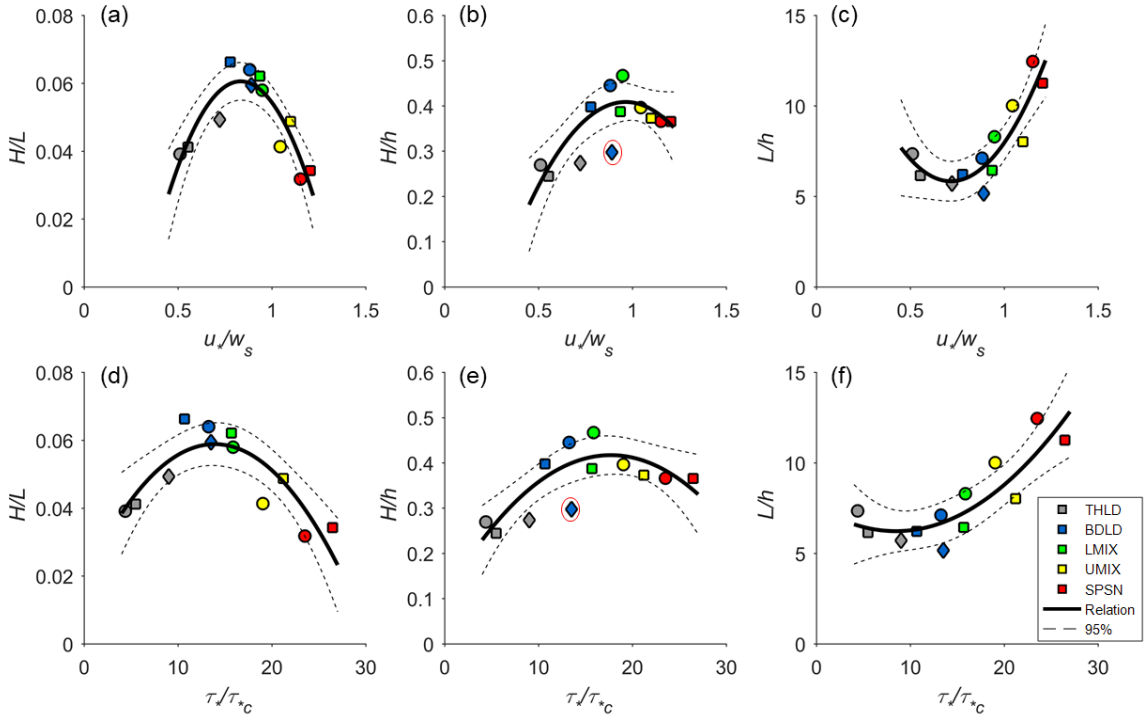

Figure 3.14. Relations between mean dune dimensions and mean flow variables: (a) $\overline{H/L}$ (b) $\overline{H/h}$, (c) and $\overline{L/h}$ versus $\overline{u_*/w_s}$ and (d) $\overline{H/L}$, (e) $\overline{H/h}$, (f) and $\overline{L/h}$ versus $\overline{\tau_*/\tau_{*c}}$. The red circle in (b) and (e) indicate the outlier $\overline{H/h}$ value from the 25-BDLD stage that was omitted from the regression. Circles, Squares and diamonds are from runs with the initial h of 15 cm, 20 cm, and 25 cm, respectively. The dotted lines represent the 95% confidence limits of the regression relations.

Table 3.4. Results of regression analysis using mean values and Equation 3.10.

Figure	y	x	a	b	c	R^2
3.14a	$\frac{H}{L}$	$\frac{u_*}{w_s}$	-0.2257	0.8338	0.0606	0.81
3.14b	$\frac{H}{h}$	$\frac{u_*}{w_s}$	-0.8595	0.9640	0.4085	0.70
3.14c	$\frac{L}{h}$	$\frac{u_*}{w_s}$	26.27	0.7159	5.837	0.79
3.14d	$\frac{H}{L}$	$\frac{\tau_*}{\tau_{*c}}$	-0.0208 x 10^{-2}	13.91	0.0588	0.73
3.14e	$\frac{H}{h}$	$\frac{\tau_*}{\tau_{*c}}$	-0.0010	17.69	0.4169	0.71
3.14f	$\frac{L}{h}$	$\frac{\tau_*}{\tau_{*c}}$	0.0192	8.459	6.226	0.75

The regression analysis using mean values (Figure 3.14, Table 3.4) demonstrates the underlying relations between transport stage and dune scaling. However, there is no representation of the variability about the mean relations. The intervals in Figure 3.14 indicate 95% confidence that the underlying relation lies between them; they do not explicitly provide a measure of the variability observed in the reached averaged dimensions from individual scans (Figure 3.12). The inherent variability can be important in circumstances where only single transects of a dune field or individual observations of cross-strata in the rock record are made. Since variability changes with transport stage and the functions are nonlinear, it is not possible to rigorously assign uncertainty ranges using the regression method in Figure 3.14 and Table 3.4. As an alternative, we do the following: 1) calculate the median *H/L*, *H/h*, *L/h*, u_*/w_s and τ_*/τ_{*c} ; 2) calculate the 25th and 75th and 5th and 95th percentiles about the median values, and then 3) estimate the relations for the median values and the lines bounding the percentile ranges (Figure 3.15). The resulting relations have the same form as the underlying true mean relations (Equations 3.10a-c) and the median relations are nearly identical (Appendix E; Table E2). The estimated fits to the percentile ranges have no statistical predictive power, however they do provide continuous functions (Appendix E; Table E2) that envelope an estimated range of variability about the median relations. In this sense, they are analogous to the non-parametric uncertainty ranges generated by Bradley and Venditti (2017) for depth-scaling relations. They provide a range of values between which approximately 50% and 90% of the data will lie about the median relations.

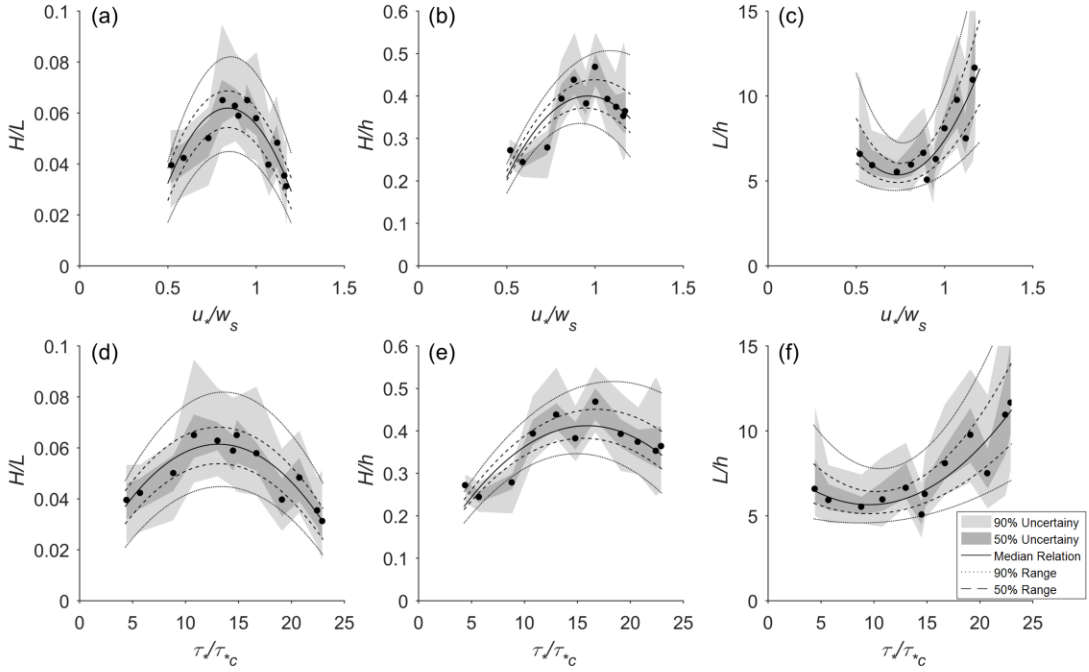

Figure 3.15. Relations between the median dune dimensions and median flow variables: (a) H/L_{med}, (b) h/H_{med}, (c) and L/h_{med} versus $u_*/w_{s_{med}}$ and (d) H/L_{med}, (e) h/H_{med}, (f) and L/h_{med} versus $\tau_*/\tau_{*C_{med}}$.

3.5. Discussion

3.5.1. Depth-Scaling Revisited

The notion that *H* scales as *h*/6 and *L* scales as 5*h* as originally proposed by Yalin (1964) has become so widely accepted that these depth-scaling relations are commonly listed in sedimentology and engineering textbooks as the definitive equilibrium dune size (e.g., Bridge, 2003; Garcia, 2008). While depth scaling is traditionally linked to some boundary layer thickness (e.g., Jackson, 1975), the boundary layer process that limits dune dimensions has never been fully elucidated (see discussion in Bradley & Venditti, 2017). It is concerning that depth-scaling relations are so widely applied given the substantial scatter about the relations in the original Yalin (1964) work and subsequent data compilations (e.g., Yalin, 1972; Yalin & Karahan, 1979; Allen, 1982; Bradley & Venditti, 2017). Furthermore, bedforms in shallow flows with depths < 2.5 m generally grow higher in the flow while dunes in flows > 2.5 m are relatively lower in the flow, indicating that *h*/6 cannot describe all dunes (Bradley & Venditti, 2017).

Some experimental work has shown that different equilibrium dune sizes can emerge at the same flow depth (Venditti et al, 2005; Venditti et al., 2016). Venditti et al. (2016) used three sets of experiments at the same initial depth but with different transport stages to show that each transport stage had a different $\overline{H}$ and $\overline{L}$. Our results expand on these observations by providing a systematic evaluation of dune-depth scaling through an examination of equilibrium bedform dimensions under three different initial flow depths and multiple transport stages. Dunes in deeper flows, under the same transport condition, are generally larger than observed in the shallower flows (Table 3.3, Figure 3.13), indicating that depth plays some role in setting the absolute values of dune dimensions. For example, dune dimensions at the 15-UMIX transport stage are $\overline{H}$ = 0.050 m and $\overline{L}$ = 1.11 m while increasing to an initial flow depth of 0.20 m produces larger dunes of $\overline{H}$ = 0.065 m and $\overline{L}$ = 1.31 m. It may be expected that *H* would be influenced by *h* since there is more volume in the flow for a dune to grow vertically. Dunes also do not grow above the water surface, so this defines an upper limit of dune growth based on depth. However, dune-depth scaling suggests that bedforms from the same flow depth, regardless of transport stage, should all have similar dimensions. In our experiments, different characteristic depth-scaling relations emerge for runs with the same depth. This variation indicates that it is not appropriate to use one depth-scaling relation to predict bedform dimensions.

3.5.2. The Role of Transport Stage on Bedform Dimensions

While depth has been the traditional focus of dune scaling, transport stage has been shown to have an influence on dune shape. Yalin (1972), Yalin & Karahan, (1979), and Allen (1982) all showed that dune steepness (*H*/*L*) increased with transport stage (τ_*/τ_{*C}) up to a point when further increases in τ_*/τ_{*C} led to dune flattening. This pattern of steepness occurs in our data as well (Figure 3.12c,f) as the steepness changes with the non-dimensional values of transport stage. Regression analysis shows that steepness increases with transport stage until a maximum where u_*/w_s ~ 0.85 and τ_*/τ_{*C} ~14 (Figure 3.14a,d) after which further increases to the transport stage lead to a decrease in *H/L* as the bed transitions to an upper stage plane bed.

It had never been fully elucidated how *H* and *L* change with transport stage since both dimensions covary in the steepness term. Venditti et al. (2016) showed that the

increasing then decreasing pattern in *H/L* with transport stage occurs because height increases then decreases while *L* continually increases. However, the experiments were limited to a single flow depth and three transport stages so the threshold when dunes change from increasing to decreasing in size could not be identified. Our results confirm that height increases then decreases with transport stage (Figure 3.13a) but further show that this transition occurs when u_*/w_s ~ 0.96 and τ_*/τ_{*C} ~ 18 (Figure 3.15b,e; Table 3.6). These transport stages are near values that have been shown to promote substantial transport bed material through suspension (Bagnold, 1966; Van Rijn, 1984; Nino et al., 2003).

Decreases in dune height have been linked to increased sediment in suspension. Using stability analysis, Fredsoe (1979, 1982) argued that as large volumes of bed material are transported through suspension, less sediment is supplied to the crest and the avalanching slip face, causing a decrease in *H*. Amsler & Schreider (1999) and Damen et al. (2018) observed a decrease in *H* in natural bedform fields when suspension relative to bedload increased and Naqshband et al. (2014a) showed experimentally that a significant amount of sediment can bypass a dune crest, resulting in decrease in height. Our experiments confirm that as more sediment is moved through suspension, *H* is decreased.

It less clear why dunes under the lowest transport stage (THLD; when u_*/w_s < 0.7) do not grow as high in the flow as moderate transport stages (BDLD, LMIX). During the THLD stage we observe no suspension, so sediment bypassing the crest cannot explain the lower heights. Bedforms during the THLD stage have shallower troughs (Figure 8a) than those developed in the BDLD stage (Figure 3.8b), likely due to decreased turbulence associated with lower mean flow velocity. Dunes may have had a lower *H* at the low transport stages because a strong recirculation cell, necessary for deep trough scour, did not development. This hypothesis requires require detailed measurements of the flow and sediment transport which were beyond the scope of this study.

Length does not vary much with transport stage until when u_*/w_s ~ 0.72 and τ_*/τ_{*C} ~ 8.5 is surpassed and significant lengthening occurs. The pattern of dune length remaining nearly constant through TLHD and LMIX conditions until UMIX has not been previously observed and is difficult to explain. Much less attention has been focused on

the controls of *L* compared to *H*. Venditti et al. (2016) showed a linear increase in length with transport stage but they did not capture the transport range that we used in the present experiments. Our results suggest that length scaling is nearly unaffected by transport stage until sediment begins to be moved through suspension. It may be possible that particles are fully bypassing individual dunes and depositing downstream when $u_*/w_s > 1$. Dune length may then scale with particle excursion length when excursion length exceeds dune length. Some recent progress has been made in defining particle excursion lengths (Naqshband et al. 2017b) but these are poorly defined over bedforms and it is unknown how these could affect dune dimensions.

3.5.3. Controls of Bedform Dimension Variability

Natural variability is a characteristic of bedforms (e.g., Nordin, 1971; Gabel, 1993; Leclair, 2002; Jerolmack & Mohrig, 2005) and is inherently built into methods to reconstruct dunes from the rock record (Paola & Borgman, 1991; Leclair & Bridge, 2001), but what sets the scale of the variability is not known. van der Mark et al. (2008) argue that variability in dune dimensions is nearly constant in large rivers, and only decreases in smaller narrow channels. They propose a positively skewed distribution with one constant coefficient of variation to quantify variability in bedform field geometry. Our experiments show that variability is affected by flow depth since larger ranges of *H* and *L* are possible in deeper flows (Figure 3.11). The increased variability with depth can be attributed to increased flow volume of the flow providing more space for the bedforms to grow and decrease in size. While our observations are confined to a relatively small flow-depth range, it seems likely that dune dimension variability would increase in even deeper flows compared to shallower channels.

Venditti et al. (2016) showed that, under the same flow depth, variability increased with transport stage, suggesting that a single coefficient of variation is not appropriate to describe all bedform variability. Our results also show that variability in bedform height and length increases with transport stage (Figure 3.10; Table 3.3), suggesting that it is another source of variability in addition to depth. The scatter about our mean values is so substantial, especially at higher transport stages, that individual dunes could be formed at virtually any transport stage. We were only able to uncover the underlying trends in bedform scaling with transport stage because of the number of scans (~55) that were made to derive a mean value. It is important to recognize

variability in bedform data, especially when only limited measurements of a bedform field can be made or when only a few bedforms are used in a paleo-reconstruction. Uncertainty must be included in prediction when temporally and spatially resolved measurements cannot be made to derive true means.

3.5.4. A physically realistic method for predicting bedform dimensions in rivers

We propose that scaling relations using transport stage should guide future prediction of bedform dimensions. Some authors have attempted to include measures of transport stage in scaling relations (e.g., van Rijn, 1984) but these poorly predict dune dimensions and do not include uncertainty to guide prediction (Bradley & Venditti, 2017). Regression analysis using mean dimensions (Figure 3.14; Table 3.4) allows for the best estimate of the mean relations, but they cannot be used to add uncertainty to predictions. Our relations based on the median transport stage and dimensions (Figure 3.15; Appendix E (Supplementary Table E2)) are the best method to calculate dune dimensions in rivers or flow depth from the rock record because the relations provide a metric of uncertainty.

For the direct prediction of dimension in modern rivers, Equation 3.10 requires that flow depth, water surface slope, and grain size be measured or calculated. These values allow a transport stage calculation using $\tau_* = \frac{\rho_w g h S}{(\rho_s - \rho_w) g D}$ and τ_{*c} from Shields-type curves (e.g., Yalin, 1972; Brownlie, 1981; Garcia, 2008). Alternatively, the suspension threshold can used by calculating $u_* = \sqrt{ghS}$ and w_s using Dietrich (1982) or the simplified method of Ferguson and Church (2004). The indirect approach of reconstructing a flow depth from dune dimensions in the rock record is similar, but involves the following steps: (1) measure cross set thickness and estimate dune height using methods that statistically link cross-set thickness to dune height (e.g., Paola & Borgman, 1991, Leclair & Bridge, 2001); (2) measure channel slope in outcrop or reconstruct slope using methods such as that described by Lynds et al (2014); and (3) measure grain size. Because *h* exists on both the right- and left-hand side in Equation 3.10, it must be solved iteratively. A measure of uncertainty can be added by applying the 50% or 90% uncertainty ranges provided in Appendix E (Supplementary Table E2) for a particular transport stage.

The application of the relations defined herein requires some caution since they require testing with more extensive data from flumes and rivers. While numerous flume data sets exist in the literature, our results suggest that care must be exercised when measuring and reporting experimental data. A single measurement from an equilibrium dune field does not capture equilibrium dimensions as many measurements are required to establish true mean dimension values for a particular transport stage. Dunes in rivers with depths > 2.5 m still represent an unknown since they adopt low-lee angles and do not grow as high in the flow (Bradley & Venditti, 2014). In these experiments, depth and transport stage affect the level of variability in dune dimensions, but it is unclear whether this is true in deep rivers. The range of variability could be affected in large rivers since there are substantial volumes of bed material that can be moved during hydrologic events.

3.6. Conclusions

We systematically examined the response of bedform dimensions to different flow depths and transport stages. We used three sets of runs, each with a different initial flow depth of 15 cm, 20 cm and 25 cm. Each set had five different runs and each run had a different discharge applied and held constant until the bed remained in a statistically steady state for 10 hours. Each run had a larger discharge applied than the previous to achieve conditions ranging from just above the threshold for motion to substantial bed material in suspension. Fifty-three to sixty scans of the bed were made during the 10-hour period to reveal the true underlying mean relations and to quantify the variability about them. The results indicate that:

1. A wide range of dune heights and lengths are possible for a given flow depth. Mean dune heights at moderate transport stages are larger than predicted by depth-scaling relations and mean lengths are longer at the higher transport stages than predicted by depth-scaling relations.

2. Dunes grow larger with flow depth, but dune scaling with depth is not consistent because of a transport stage effect.

3. Dune steepness increases and then decreases with transport stage. This pattern occurs because dune height increases until u_*/w_s ~ 0.96 and τ_*/τ_{*C} ~ 18 when it

begins to decrease while length remains relatively constant until u_*/w_s ~ 0.72 and τ_*/τ_{*C} ~ 8.5 when they start to become longer.

4. Variability in dune dimensions increases with transport stage and depth. Care should be taken when measuring and reporting dune dimensions since many samples are required to determine true underlying relations.

5. Dune scaling relations with uncertainty included can be estimated using transport stage relations based on the median values and the variability about them. The relations developed here should be used to guide predictions of dune dimensions in rivers and reconstruction of past flows based on dune heights estimated from cross-strata. The relations require further testing using data from flumes and especially large rivers.

Chapter 4. Dune Growth from a Flat Bed

Abstract

Dune response to variable flow has been well documented, but there is no universal model to predict dune dimensions as they respond to imposed flows. Here, we use a series of flume experiments to explore dune growth in response to constant flow to better understand the form of dune growth curves. Observations of dune growth from a flat sand bed were made at three flow depths, under five different constant transport stages in a laboratory flume. The transport stages ranged from the sediment entrainment threshold to suspension conditions. The bed was flattened before each run and topography was continually mapped, providing observations of dune growth and morphology at each distinct transport stage condition. The results show that dune growth curves exhibited three different behaviors: 1) exponential growth, 2) punctuated growth, when a period of initially linear growth was abruptly interrupted by exponential growth and 3) instantaneous growth, when bed evolution happened so quickly that we were unable to take measurements of the phenomenon. Growth behaviour is dependent on the applied transport stage and the time for a growing dune field to reach equilibrium decreases non-linearly with transport stage. Observations of evolving dunes and the time required to achieve an equilibrium bed state are used to propose a series of relations that can predict dune dimensions through time.

4.1. Introduction

The bottom boundary of sand-bedded alluvial channels is often characterized by bedforms that display a range of geometries at scales smaller than bar forms. Dune bedforms are important sources of flow resistance and sediment transport in rivers and, as such, their dynamics are important in river engineering and management problems. The migration of dunes also leaves characteristic signatures in the rock record; however, our ability to interpret cross strata and reconstruct past flows is limited by our understanding of how these features respond to flows. Previous observations have shown that dunes grow and shrink in response to changes in flow induced by tides, synoptic-scale storm events and seasonal hydrographs (e.g., Allen, 1974; Terwindt & Brouwer, 1986; Julien et al., 2002; Hendershot et al., 2016). Dune response to changes

in flow is not instantaneous because substantial volumes of sediment need to be moved as bedform fields adjust. There is presently no universal method to predict dune response to changes in flow. To address this problem, we will explore how dunes grow in response to a constant flow to better understand the time required to reach a statistical steady state (referred to as equilibrium) and the form of bedform growth curves.

Dune growth towards equilibrium from a flat sand bed has been examined previously. Bedform initiation from a flat bed has been linked to small bed defects that cause flow separation, allowing the defects to grow into a bedform field by downstream propagation (e.g., Grass, 1970; Gyr & Schmidt, 1989; Best, 1992). Others (e.g., Lui, 1957; Venditti et al., 2006) have argued that an instability at the water-sediment interface causes bedforms to instantaneously initiate everywhere on the bed. At the scale of individual bedforms, growth has been linked to the position of the sediment flux maximum relative to the topographic maximum (e.g., Smith, 1970; Fredsoe, 1982; Venditti, 2013; Naqshband et al., 2017). Dunes grow when the maximum sediment flux is upstream of the crest, leading to deposition on the stoss and crest. At a broader spatial scale, bedform field growth has been attributed to the coalescence of smaller, faster-migrating bedforms to form larger, slower-migrating dunes (Raudivi & Witte, 1990; Coleman & Melville, 1994) and slow downstream stretching of bedform fields (Venditti et al., 2005a). Coalescence appears to dominate in experimental investigations with flumes that have relatively small widths that may mask or suppress spatial adjustments and accelerations. Furthermore, bedform growth does not always occur when smaller sand waves are present in bedform fields (Ditchfield & Best, 1990; Venditti et al., 2005a). Bedform fields likely grow through a combination of coalescence and stretching processes, but the relative importance of each is unknown.

Some experimental work has focused on dune growth in response to incremental increases in flow. Leeder (1983) originally proposed that when flow velocity is increased over a stable ripple field, a ‘rogue ripple’ will appear and coalesce with smaller ripples to form larger bedforms. Once a rogue ripple gets large enough, growth is enhanced, as greater height enhances leeside turbulence and trough scour. Later work suggested that rogue ripple emergence may be associated with small, local fluctuations in sediment transport caused by flow separation dynamics (Bennett & Best, 1996) and a transition from two-dimensional (2D) to three-dimensional (3D) planform (Schindler & Robert,

2005). Whether this form of punctuated growth occurs in a constant flow has not been explored.

Predicting bedform dimensions during growth requires knowledge of: 1) equilibrium dimensions for a given flow, 2) the form of the underlying growth relation, and 3) the time required to reach equilibrium. Bradley and Venditti (2017; Chapter 3) provide a series of empirical functions that can be used to predict bedform dimensions from either flow depth or transport stage. Transport stage is defined using the ratio of shear velocity to particle settling velocity, or the ratio of the Shields number (non-dimensional shear stress) to the critical value for particle entrainment (τ_{*c}). The Shields number is defined as

$$\tau_* = \frac{\tau}{(\rho_s - \rho_w) g D_{50}} \quad \text{(Eq. 4.1)}$$

where τ is the shear stress at the bed, ρ_s and ρ_w are the sediment and water densities, respectively, and *g* is the gravitational acceleration. Values of τ_{*C} vary with grain size (e.g., Shields, 1936; Brownlie, 1981).

Nikora and Hicks (1997) proposed that the growth of bedform fields follows a power function:

$$\frac{H}{H_e} = \left(\frac{t}{t_{eH}}\right)^{\gamma} \quad \text{(Eq. 4.2a)}$$

$$\frac{L}{L_e} = \left(\frac{t}{t_{eL}}\right)^{\gamma} \quad \text{(Eq. 4.2b)}$$

where t is time, H and L are the bedform height and length, respectively, at t, H_e and L_e are the equilibrium bedform height and length respectively, t_{eH} and t_{eL} are the times to achieve H_e and L_e, and γ is the growth exponent. These power relations were fit to data from five experiments reported in Iseya (1984). Coleman et al. (2005) used a larger data set from flume experiments to quantify the growth exponents and found different exponents for height (γ_H) and length (γ_L) of 0.37 and 0.32, respectively. While Equations 4.2a & 4.2b allow prediction of growth from a flat bed, they do not saturate at equilibrium dimensions. Instead, these equations are only applicable from initiation to t_e, which is defined when equilibrium dune size is first reached.

The application of Equations 4.2a and 4.2b requires separate functions for the equilibrium and growth phase. Defining t_e is relatively straightforward for experiments in narrow flumes where temporal variability is low. In the Iseya (1984) data set, equilibrium times were defined using mean length time series derived from infrequent measurements of the number of dunes in the flume divided by the flume length. This approach masks the variability in dune fields and does not necessarily reflect when the bed has reached a statistical steady H (Figure 4.1a,b; Appendix G (Supplementary Figure G1)). Determining when the power growth phase ends can be challenging given natural variability observed within bedform fields (Venditti et al., 2005a; Venditti et al., 2016; Chapter 3). For example, there is no objective way to define when the growth phase ends using measurements of individual dunes migrating past a particular point (e.g., Figure 4.1c,d; Appendix G (Supplementary Figure G2)), without defining equilibrium dimensions as a statistically steady state. Furthermore, power relations (Equations 4.2a,b) generally under predict dimensions in the Iseya data (Figure 4.1a,b; Appendix G (Supplementary Figure G1)) and indicate much faster initial growth from a flat bed where high temporal resolution data are available (Figure 1c,d; Appendix G (Supplementary Figure G2)).

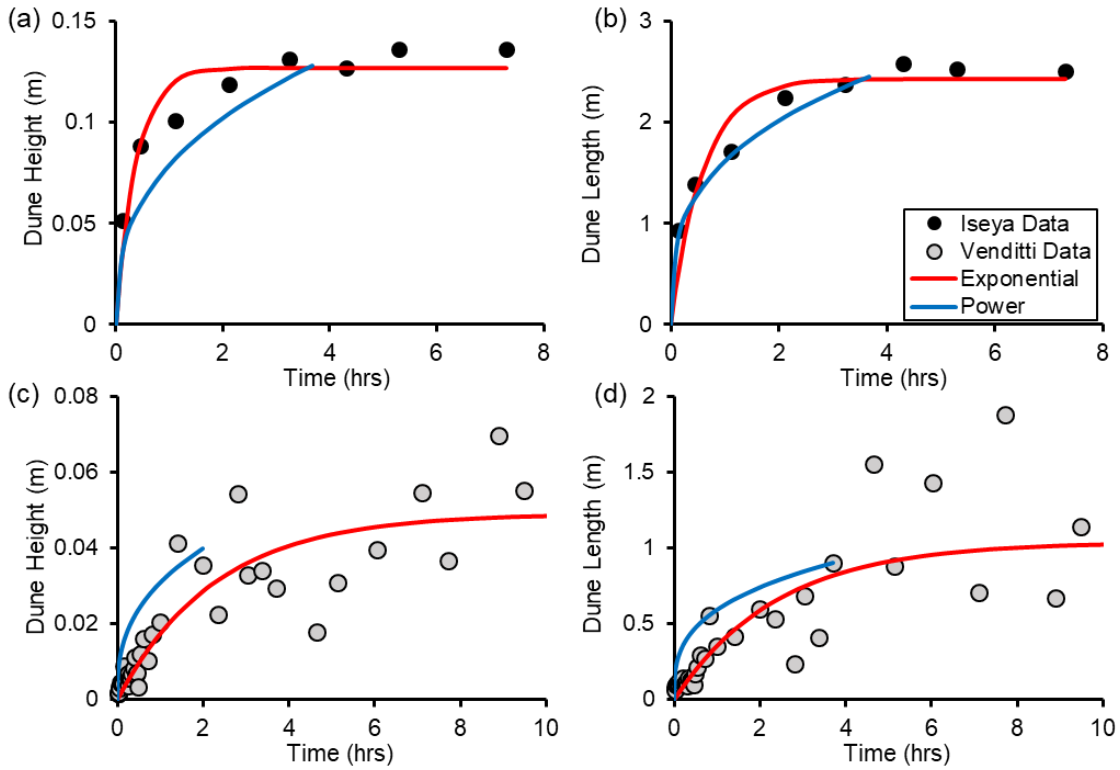

Figure 4.1. Examples of bedform (a) height and (b) length growth time series data from Iseya (1984; Run 3) and (c) height and (d) length growth time series data from Venditti et al. (2005a; Flow B). The power relations are defined by Equations 4.2a and 4.2b, and the exponential relations are Equations 4.3a, and 4.3b.

Recognizing these limitations, others have suggested that bedform growth is an exponential function (Baas, 1999; Venditti et al., 2005a). Venditti et al. (2005a) expressed growth as:

$$H = a_H\left(1 - e^{-b_H * t}\right) \quad \text{(Eq. 4.3a)}$$

$$L = a_L\left(1 - e^{-b_L * t}\right) \quad \text{(Eq. 4.3b)}$$

where a_H and a_L, are asymptotes that describe the equilibrium height and length, respectively, and b_H and b_L are growth constants. The exponential relations better capture growth phases than power functions and saturate at equilibrium dimensions (Figure 4.1; Appendix G (Supplementary Figures G1 & G2)), eliminating the need for a piece-wise solution and subjective determination of t_e. However, the relations need to be fit to data and cannot be used to predict evolving dune dimensions with respect to

equilibrium dimensions. In order to predict bedform growth, Equations 4.3a & 4.3b must be recast in the form of Equations 4.2a and 4.2b as:

$$\frac{H}{H_e} = 1 - e^{\left(-b_H * \frac{t}{t_{eH}}\right)} \quad \text{(Eq. 4.4a)}$$

$$\frac{L}{L_e} = 1 - e^{\left(-b_L * \frac{t}{t_{eL}}\right)}. \quad \text{(Eq 4.4b)}$$

The application of Equations 4.4a and 4.4b requires an objective determination of t_{eH} or t_{eL}. Coleman et al. (2005) proposed that:

$$t_e \frac{u_*}{D_{50}} = f\left(\frac{D_{50}}{h}, \frac{\tau_*}{\tau_{*C}}\right) \quad \text{(Eq. 4.5)}$$

where u_* is shear velocity ($u_* = \sqrt{\tau/\rho_w}$), D_{50} is the median grain size and τ_*/τ_{*C} is the transport stage. Coleman et al. (2005) used some empirical data to define the relation as:

$$t_e \frac{u_*}{D_{50}} = \alpha \left(\frac{D_{50}}{h}\right)^{-3.5} \left(\frac{\tau_*}{\tau_{*C}}\right)^{-1.12} \quad \text{(Eq. 4.6)}$$

where α = 0.00205. The t_e values used by Coleman et al. (2005) in the derivation of Equation 4.6 were defined when the equilibrium dune size was first reached, rather than when a statistical steady state was achieved. It is unclear how widely Equation 4.6 can be applied since much of the data used to define it was mostly limited to a few, low transport stages when sediment transport occurred mostly as bedload.

Here we examine bedform growth from a flat sand bed at three flow depths, under five different constant transport stages in a laboratory flume. The transport stages range from the threshold for sediment motion to suspension conditions, when dunes begin to wash out to an upper-stage plane bed. The bed was screed flat before each run and topography was repeatedly mapped, providing measurements of bedform growth and morphology at each distinct transport stage condition. Our fundamental questions are: 1) How do bedform morphodynamics and dimensions change as they grow under different transport conditions? and 2) Can dimensions and time to equilibrium be predicted during dune growth using Equations 4.4 and 4.6?

4.2. Methods

Experiments were performed in the River Dynamics Laboratory (RDL) at Simon Fraser University, Canada. The 15 m long, 1 m wide and 0.6 m deep RDL flume recirculates sediment and water, and has a slope that can be adjusted from -0.5 to 2%. Well sorted quartz sand, (D_{50} = 550 μm) with trance amounts of sillimanite, garnet, sphalerite, muscovite and gold, was used in the experiment. The experimental design, setup and conditions follow that of Chapter 3 which examined the fundamental underlying relations between equilibrium dune dimensions, flow depth and metrics of transport stage. Chapter 3 focused on a 10-hr equilibrium period and specifically excluded observations in which the bedform field was systematically growing from the flat bed. Here, we focus on observations during the growth phase. Our methodology is briefly outlined below; see Chapter 3 for more specific details.

4.2.1. Experimental Design

The experiments involved three sets of runs with each set having initial flow depths of 15, 20, and 25 cm (Table 4.1). Before each run, the flume was filled with water and the bed was screed flat using an aluminum angle attached to a beam on a cart that runs on rails above the flume. The cart was moved up and down the length of the flume until the uncompacted bed was completely flat. The flow depth was then set to the desired initial condition. For each run, a pump discharge was applied and held constant for 25 hours, allowing the bed to reach a statistically stable equilibrium condition in which bedform dimensions were not systematically changing. During the equilibrium period, any changes in bedform dimensions were due to internal dynamics of the bedform field. The initial flume slope for each run (Table 4.1) was set so that it matched the water surface slope immediately after the pumps were turned on. This allowed the water surface and bed slope to coevolve through time, so they became emergent features during each run.

Table 4.1. Initial experimental and equilibrium conditions (see Chapter 3 for details).

	Initial Conditions				Equilibrium Conditions						
	Depth (m)	Discharge ($m^3 s^{-1}$)	Flume Slope	Water Temp (°C)	Depth (m)	Mean Velocity ($m s^{-1}$)	Froude	τ_*/τ_{*c}	Bedload Flux ($g s^{-1} m^{-1}$)	Suspended Flux ($g s^{-1} m^{-1}$)	Total Flux ($g s^{-1} m^{-1}$)
15-THLD	0.15	0.060	0	14	0.139	0.443	0.38	4.39	8.43	0	8.43
15-BDLD	0.15	0.075	0.00047	18	0.141	0.547	0.47	13.3	14.8	0	14.8
15-LMIX	0.15	0.090	0.00084	22	0.139	0.660	0.57	15.9	21.3	70.8	92.1
15-UMIX	0.15	0.110	0.0015	25	0.129	0.854	0.76	19.0	59.6	161	220
15-SPSN	0.15	0.130	0.0020	25	0.135	0.965	0.84	23.5	113	242	355
20-THLD	0.20	0.086	0	14	0.182	0.474	0.35	5.50	11.1	0	11.1
20-BDLD	0.20	0.100	0.00045	25	0.176	0.575	0.44	10.7	21.9	0	33.6
20-LMIX	0.20	0.120	0.00081	27	0.179	0.673	0.51	15.9	30.9	89.9	121
20-UMIX	0.20	0.140	0.0011	27	0.174	0.805	0.62	21.2	56.3	158	214
20-SPSN	0.20	0.167	0.0019	27	0.158	1.06	0.85	26.5	113	251	364
25-THLD	0.25	0.100	0	25	0.227	0.444	0.30	9.00	8.94	0	8.94
25-BDLD	0.25	0.125	0.00081	27	0.221	0.569	0.39	13.5	35.5	0	35.5

Five different transport stages, ranging from just above the threshold for sediment motion to a near washout of bedforms, were achieved for the 15 and 20 cm runs. The runs are qualitatively named Threshold (THLD), Bedload (BDLD), Lower Mixed (LMIX), Upper Mixed (UMIX), and Suspension (SPSN) in order of increasing τ_*/τ_{*C} based on visual observations of the characteristic sediment transport mechanisms. Only THLD and BDLD stages were possible for the 25 cm depth because higher discharges were beyond the capacity of the flume pumps. The initial flow depth for each run is identified in the run name herein (e.g., 15-THLD, 20-THLD, 25-THLD). Average flow and sediment flux conditions from a 10-hour equilibrium period are reported in Table 4.1. All flows were subcritical and final equilibrium depths were less than the initial flow depths after the bed adjusted to the imposed flows. No suspended sediment flux was observed during the THLD and BDLD stages during equilibrium.

4.2.2. Measurements

The RDL Swath Mapping System was used to record bed topography profiles (Venditti et al., 2016; Chapter 3). The system includes a cart powered by a stepper motor that runs on rails mounted on top of the flume side walls. A Plexiglas beam oriented across the channel is attached to the cart, and contains thirty-two Seatek Instruments echo-sounding transducers spaced 2.5 cm apart in the across stream

direction. The beam is attached to a mechanical motor that allows it to move vertically such that the sensors can be placed immediately below the water surface. This allows measurements that have minimal disturbance to the flow and does not affect the mobile bed. Signals and positions from the Seatek Instruments were recorded by an onboard computer. Noise in the Seatek data were filtered using the method described in Chapter 3.

Measurements were made in the along stream direction from 4.5 to 10 m from the flume headbox to avoid entrance or exit effects on the observations. However, later analysis showed defects propagated from the headbox during the 25-THLD and 25-BDLD runs and affected the evolution of the bed. The speed of the cart was set to maximize the number of scans that could be performed while ensuring high density measurements in the downstream direction. The cart speed resulted in scans of 32 along stream profiles with observations every 1.29 cm. A scan of the bed was made before the pumps were turned on and then approximately every 10 minutes after the flow was applied. Data presented herein are from the initial evolution of the flat bed for up to 10 hours. If an equilibrium bedform field was not achieved in a 10-hour window, we provide a longer series of observations until equilibrium was achieved.

During the LMIX, UMIX and SPSN runs, intense erosion in dune troughs after the first few scans produced a thick sediment transport layer that prevented the Seatek sensors from locating the solid bed. In order to fill in these gaps in the LMIX and UMIX time series, additional, redundant runs were undertaken with changes to the sensitivity of the Seatek sensors. During redundant runs, the cart speed was increased, and scans were made from 7.65-9.50 m from the headbox approximately every 1.5 minutes until bedform lengths exceeded the measurement window. This created a downstream spacing in individual measurements of 1.9 cm, but allowed for quicker scans, providing observations of the more rapid bed evolution. Evolution of the bed during the SPSN runs made additional measurements during redundant runs impossible.

4.2.3. Data Analysis

Bedform dimensions from each Seatek profile were calculated using an automated method developed by McElroy (2009), which has been verified using manual measurements of bedform dimensions (Venditti et al., 2016; Chapter 3). The automated

method estimates spatially-averaged bedform height and lengths for each of the 32 profiles in a scan. Reach-averaged bedform heights (*H*) and lengths (*L*) are reported as the mean values of the 32 spatially-averaged heights and lengths for each scan. Chapter 3 showed that the automated method was not appropriate for the long and relatively flat bedforms of SPSN runs. For the SPSN runs, the dimensions of individual dunes were manually measured along the centerline. Dune heights were measured from trough to peak in the lee side and length between the lowest points in the upstream and downstream troughs. Reach-averaged bedform heights (*H*) and lengths (*L*) were determined by adding the heights and lengths of individual bedforms and diving by the number of bedforms in the profile. The automated method could also not be applied to the redundant LMIX and UMIX runs because the along stream distance of the profiles was too short. For these scans, we present manually measured bedforms along the center profile to characterize H and L.

4.3. Results

4.3.1. Dimensions through Time

Figure 4.2 shows reach-averaged bedform height and length through time. Thirteen hours of data for 20-THLD and 23 hours for 25-THLD are shown since this observation period was required for the bed to reach a stable configuration (Figure 4.2a & 4.2f). In general, the duration of the bedform growth phase decreased with higher transport stages. Equilibrium bedform dimensions did not scale with depth (e.g., Yalin, 1964; Bradley & Venditti, 2017) but, rather, they scaled with transport stage (Chapter 3). Bedforms grew higher in the flow with transport stage until the LMIX condition, at which *H* began to decrease. Length remained about the same in each transport stage until the UMIX runs, at which *L* began to increase (Chapter 3). Variability between scans increased with transport stage with a nearly different bed configuration appearing between scans in the SPSN runs (Chapter 3). The initial flat bed evolved rapidly during the LMIX and UMIX stage due to intense scour of the bed, so shorter and more frequent scans were required to capture the evolution.

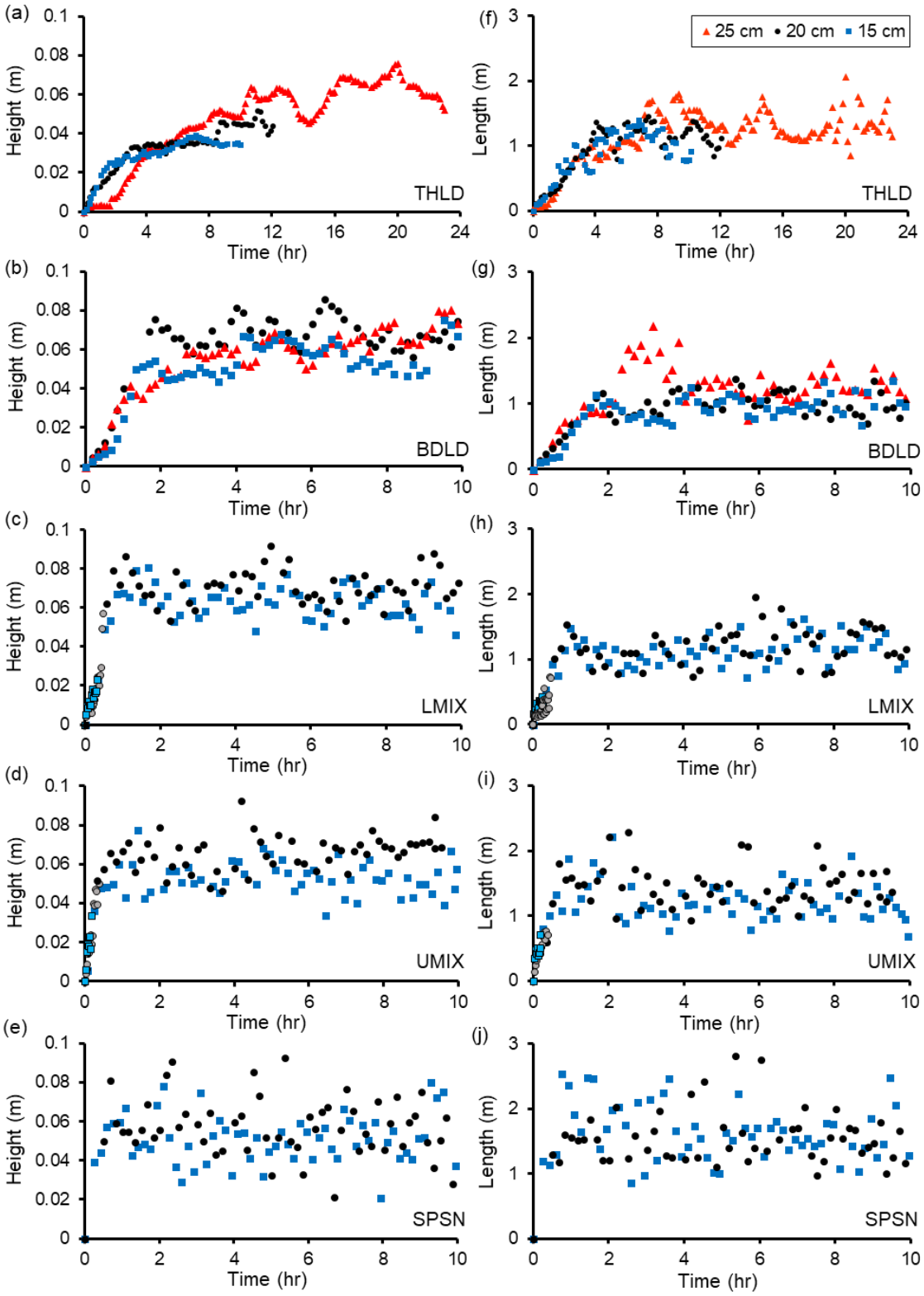

Figure 4.2. **Bedform height (a-e) and length (f-i) through time for the different transport stage conditions. The lighter blue and grey symbols are from the redundant scans for the 15 and 20 cm runs, respectively.**

4.3.2. Phenomenology of Bedform Growth

Videos that detail the topography for each bed scan in Figure 4.2 are available in Appendix H (Supplementary Videos H1-H12). Here, we present examples of distinct stages of bed evolution for the observed transport conditions under the initial flow depth of 15 cm. The examples in Figures 4.3-4.8 are from different time intervals because the bed evolution occurred faster with increasing transport stage, so distinct growth phases appeared at separate times between runs at different transport stages. The patterns of bed evolution are similar for the 20 cm initial flow depth, with some subtle differences in when distinct patterns occur in the time series. The 25 cm initial flow depth runs are distinct from the 15 and 20 cm runs because they were influenced by a defect that formed at the headbox. The defect growth process observed in 25-THLD and 25-BDLD is discussed further below.

Growth from the flat bed was relatively slow during the 15-THLD run. After 0.17 hrs, bedforms with $H < 1$ cm and $L < 10$ cm began to emerge from the plane bed (Figure 4.3a). The appearance of bedforms was widespread over the bed and appeared to follow the instantaneous initiation mechanism described by Venditti et al. (2006). This instantaneous initiation process was consistent for all runs except for 25-THLD and 25-BDLD. After initiation, the bedforms grew steadily through time, becoming 3D with $H \sim 2$ cm and $L \sim 30$ cm (Figure 4.3b) at $t = 1.00$ hr. The bed underwent a relatively rapid transition between $t = 1.25$ and 1.42 hrs when some of the 3D features organized into larger 2D features (Figure 4.3c). These 2D features remained characteristic of the field and grew longer through time (Figure 4.3d). During the final growth stage, smaller 3D features passed through the dune field as crestline defects and spurs (Swanson et al., 2017). Small-scale bedforms ($H < 1$ cm) were also observed to be superimposed on the stoss of larger features.

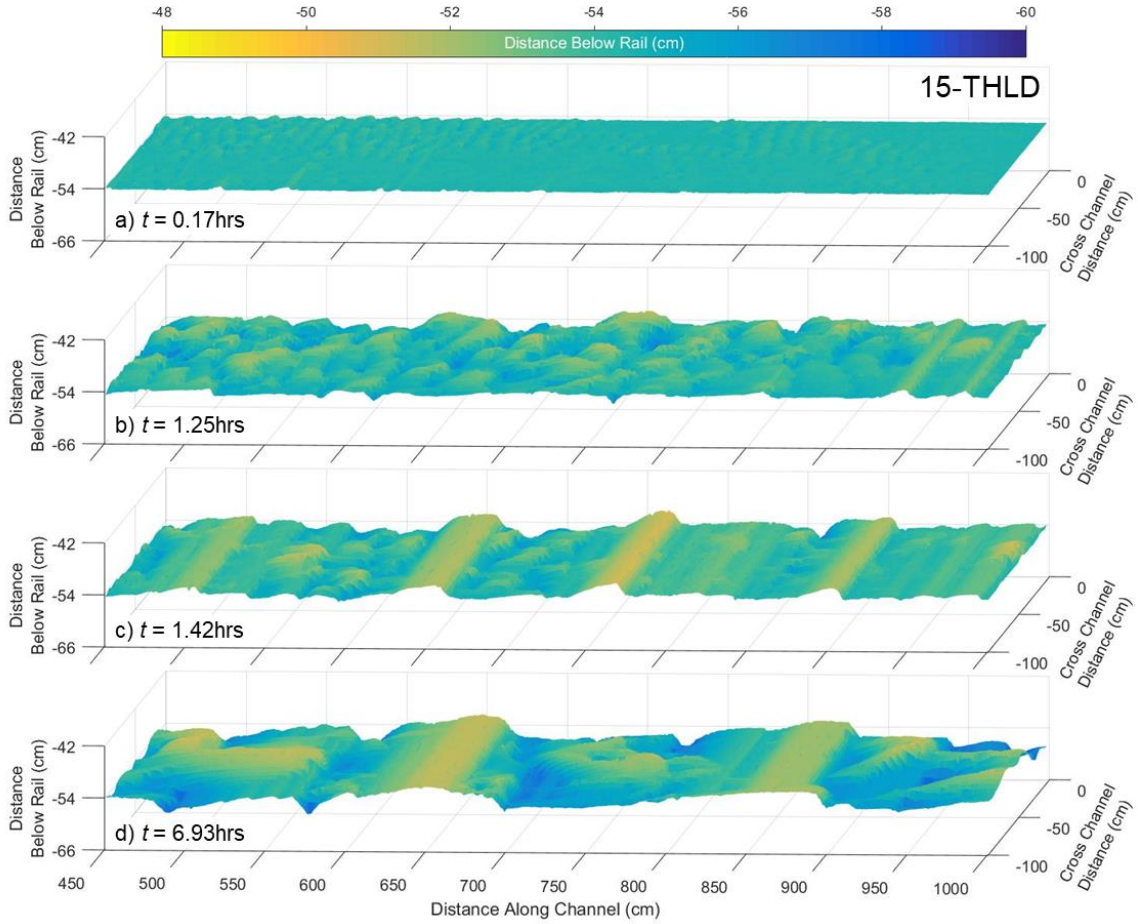

Figure 4.3. Bed topography for the Threshold Stage at an initial depth of 15 cm (15-THLD) at (a) 0.17, (b) 1.25, (c) 1.42 and (d) 6.93 hrs. (Appendix H, Supplementary Video H1).

During the initial scans of the 15-BDLD stage, the bed organized into small, 2D, channel-spanning features (H < 1 cm, L < 10 cm) (Figure 4.4a). As the bedforms increased in size, they became more 3D (Figure 4.4b) and a period of rapid growth occurred from t = 0.5 to t = 1.17 hrs (Figure 4.4c). This phase was marked by intense scour of dune troughs and produced larger 2D bedforms with smaller 3D features passing through the field. Growth of the bedforms then continued via scouring of the bedform troughs (Figure 4.4d).

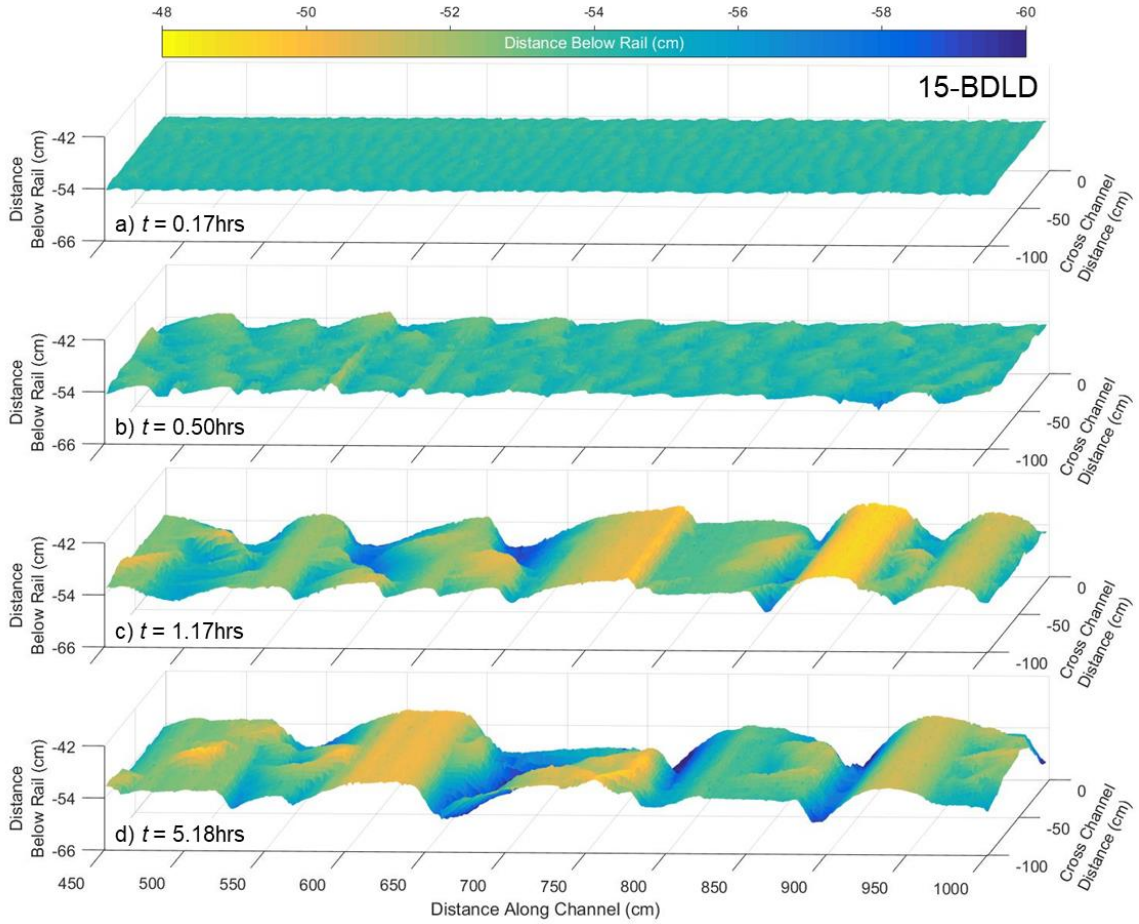

Figure 4.4. Bed topography for the Bedload Stage at an initial depth of 15 cm (15-BDLD) at (a) 0.17, (b) 0.50, (c) 1.17 and (d) 5.18 hrs (Appendix H, Supplementary Video H2).

The 15-LMIX (Figure 4.5) and 15-UMIX (Figure 4.6) beds underwent similar processes, although the bedform field developed more slowly during the LMIX run. Small bedforms (H < 1 cm, L < 10 cm) with 2D planforms appeared immediately after flow was applied (Figures 4.5a & 4.6a). As the bedforms reached H > 1 cm and L > 10 cm, they transitioned to a more 3D shape (Figures 4.5b & 4.6b) and began to grow rapidly (Figure 4.5c). The equilibrium bed state for the LMIX stage had dunes with deep troughs that grew relatively high into the flow, sometimes with flattened crests (Figure 4.5d). Bedforms in the UMIX stage more rapidly transitioned from small features (Figure 4.6b) to dunes that had smaller equilibrium heights and longer equilibrium lengths than observed during the LMIX stage (Figure 4.6c). Growth from the flat bed happened so quickly during the 15-SPSN run (Figure 4.7) that we were unable to capture the growth phenomenon. However, the equilibrium bed state was characterized by longer and flatter bedforms (Figure 4.7b).

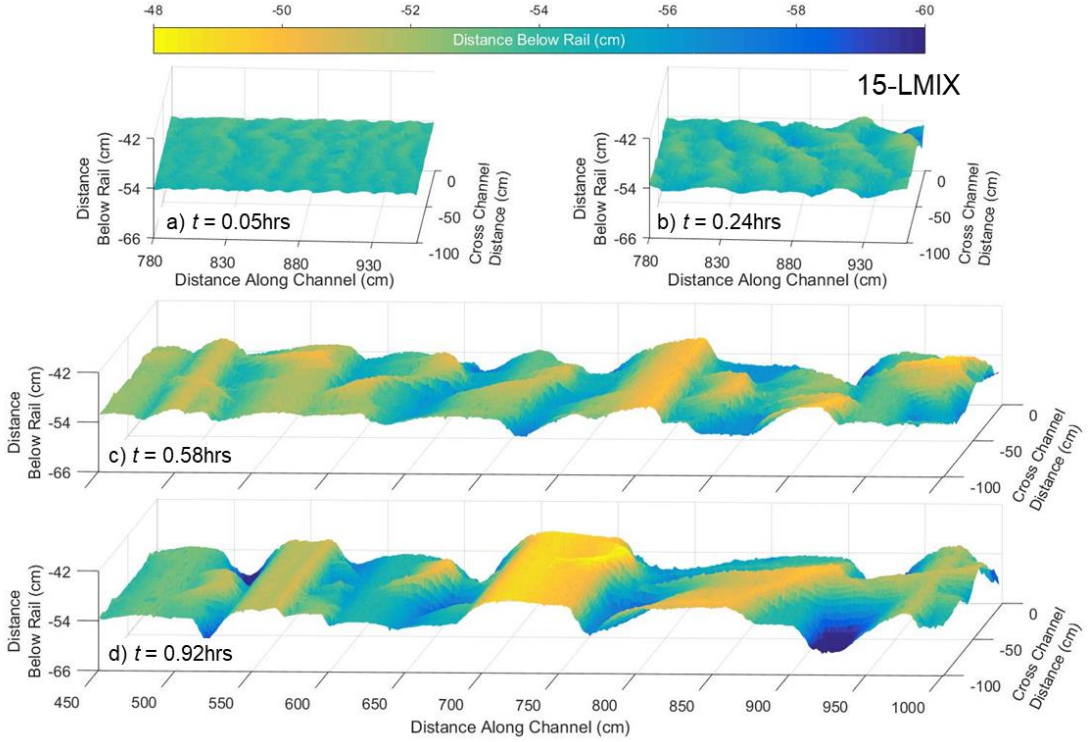

Figure 4.5. Bed topography for the Lower Mixed Stage at an initial depth of 15 cm (15-LMIX) at (a) 0.05, (b) 0.24, (c) 0.58 and (d) 0.92 hrs (Appendix H, Supplementary Video H3,H3b).

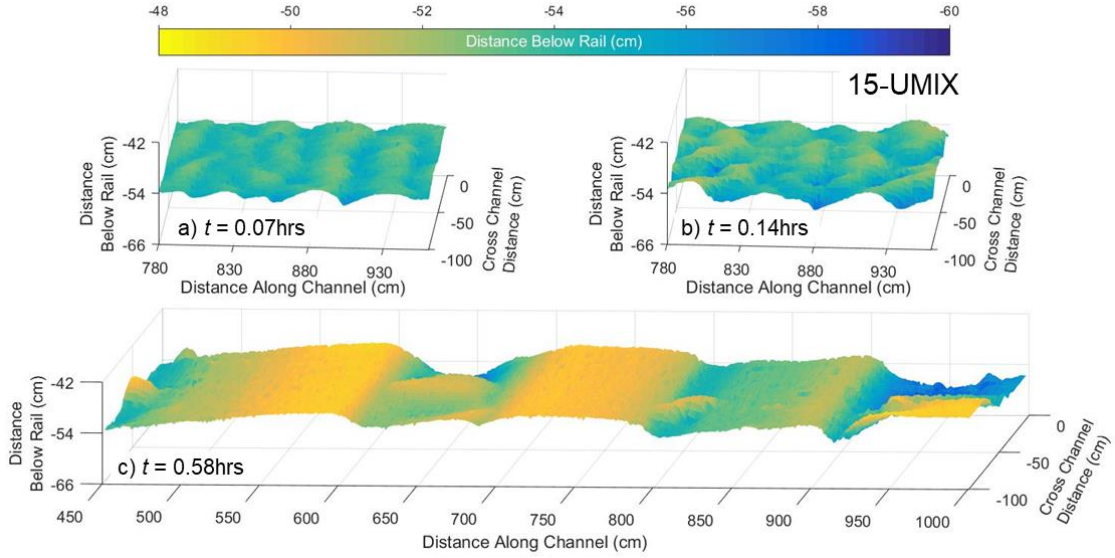

Figure 4.6. Bed topography for the Upper Mixed Stage at an initial depth of 15 cm (15-UMIX) at (a) 0.03, (b) 0.2, and (c) 0.58 hrs. (Appendix H, Supplementary Video H4, H4b).

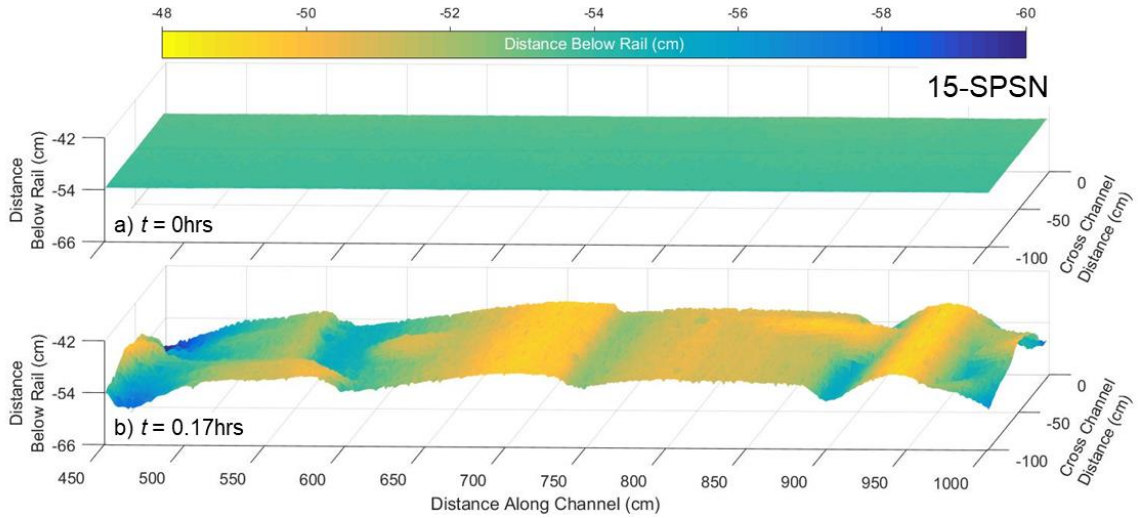

Figure 4.7. Bed topography for the SPSN at an initial depth of 15 cm (15-SPSN) at (a) 0 and (b) 0.17 hrs (Appendix H, Supplementary Video H5).

The patterns of bedform growth were consistent for similar transport stage conditions, except during the 25 cm initial flow depth runs (25-THLD and 25-BDLD) when defects that initiated at the headbox propagated through the bedform field and influenced growth. The defects propagated downstream through flow separation processes promoting bedform field growth (e.g., Grass, 1970; Gyr & Schmidt, 1989; Best, 1992) rather than through the instantaneous initiation observed during the other runs. During the 25-THLD runs, there was a period of ~2 hrs when only small sand waves appeared on the bed (Figure 4.8a), suggesting the applied flow conditions were below the threshold for dune development. After this period, sand that built near the head box, began to migrate through the observation range as larger-than-average bedforms (Figure 4.8b) and the bedforms continued to grow in *H* and *L* as they traveled the length of the flume (Figure 4.8c). The initial defect bedforms exited the channel after ~11 hrs (Figure 4.8d), but the bedforms that followed persisted and grew (Appendix H (Supplementary Video H11)). The initial defects in the 25-BDLD run passed through more quickly (~1 hr), leaving a developed bedform field that continued to grow to equilibrium dimensions (Appendix H (Supplementary Video H12)).

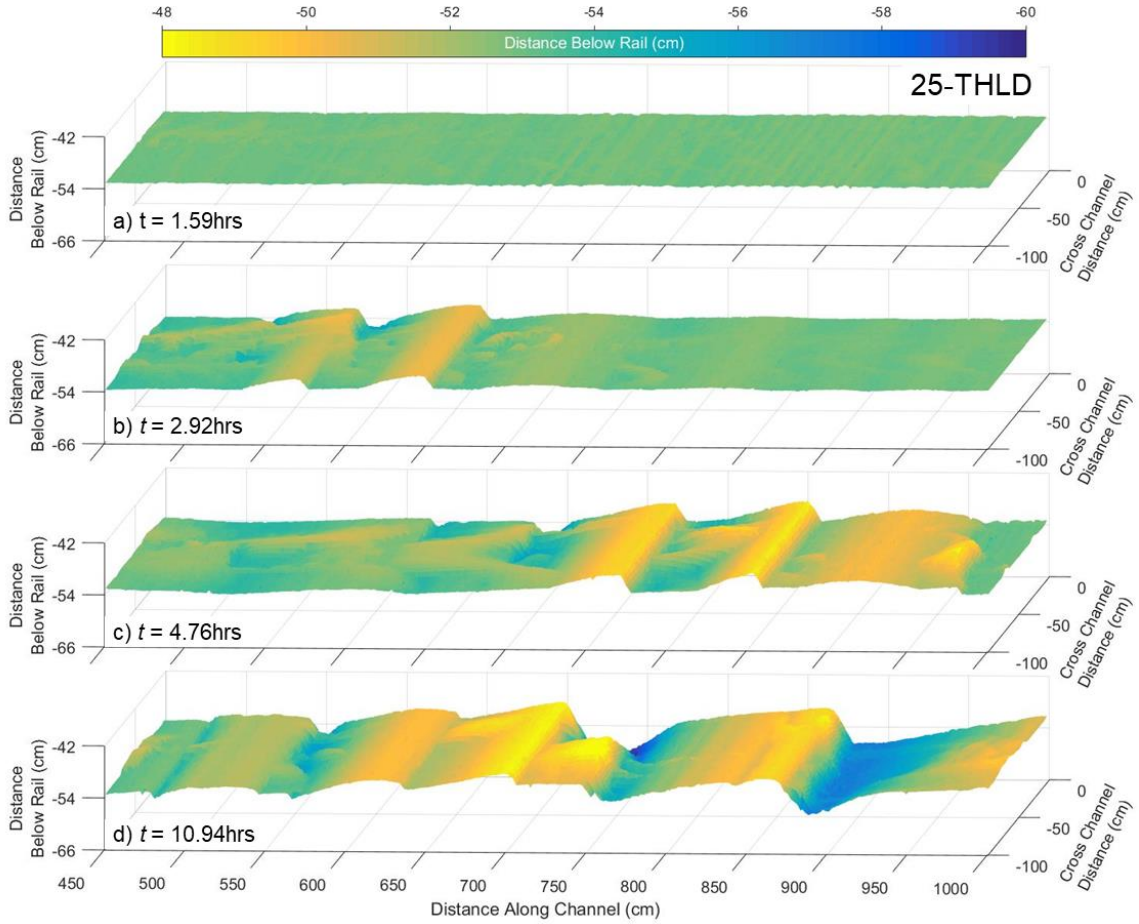

Figure 4.8. Bed topography for the Threshold Stage at an initial depth of 25 cm at (a) 1.59, (b) 2.92, (c) 4.76 and (d) 10.94 hrs (Appendix H11, Supplementary Video H11).

4.3.3. Shape of Growth Curves

Growth curves exhibited three different behaviors (Figure 4.9): 1) exponential growth, 2) punctuated growth, when a period of initially linear growth was abruptly interrupted by exponential growth and 3) instantaneous growth, when bed evolution happened so quickly that we were unable to take measurements of the phenomenon. Exponential functions (Equations 4.3a & 4.3b) were fit to the data in Figure 4.2 except for the SPSN runs, in which the bed instantaneously achieved equilibrium. In the cases of punctuated growth, the exponential function was fit to the curve beginning at the time when growth became nonlinear. Table 4.2 gives the distinct types of growth observed and the associated exponential model fits. Figure 4.10 shows how the models fit the data for the 15 cm runs (fits for the 20 and 25 cm deep flows are in Appendix G (Supplementary Figures G4.3 & G4.4).

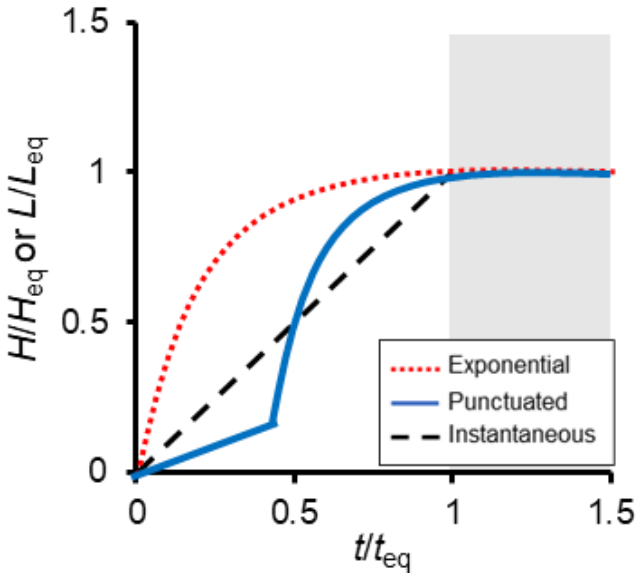

Figure 4.9. Example growth curves of H/H_e of L/L_e plotted with t/t_e.

Table 4.2. Model fitting results.

Height	Growth Type	a (m)	b	Initial *H* at exp growth (m)	*t* when exp growth begins (hr)	99% Sat (hr)	H_e (m)	t_e (hr)
15-THLD	Exponential	0.035	0.610				0.035	7.55
20-THLD	Exponential	0.043	0.368				0.043	12.5
25-THLD	Defect/Exp	0.058	0.194	0.007	1.75	23.74	0.066	25.5
15-BDLD	Punctuated	0.050	1.36	0.009	0.668	3.39	0.058	4.06
20-BDLD	Punctuated	0.056	1.69	0.013	0.501	2.73	0.069	3.23
25-BDLD	Exponential	0.068	0.558				0.068	8.25
15-LMIX	Punctuated	0.046	5.44	0.017	0.284	0.847	0.063	1.13
20-LMIX	Punctuated	0.052	7.32	0.020	0.356	0.639	0.072	0.985
15-UMIX	Exponential	0.053	4.10				0.053	1.12
20-UMIX	Exponential	0.067	3.18				0.067	1.45
15-SPSN	Instantaneous						0.051	0.251
20-SPSN	Instantaneous						0.059	0.501
Length	Growth Type	a (m)	b	Initial *L* at exp growth (m)	*t* when exp growth begins (hr)	99% Sat (hr)	L_e (m)	t_e (hr)
15-THLD	Exponential	1.14	0.468				1.14	9.84
20-THLD	Punctuated	0.922	0.698	0.306	1.34	6.60	1.23	7.94
25-THLD	Defect/Exp	1.17	0.391	0.190	1.09	11.78	1.36	12.9
15-BDLD	Punctuated	0.763	2.52	0.200	0.668	1.83	0.96	2.50
20-BDLD	Exponential	1.03	1.03				1.03	4.49
25-BDLD	Exponential	1.35	1.06				1.35	4.36
15-LMIX	Punctuated	0.788	4.83	0.359	0.284	0.95	1.15	1.24
20-LMIX	Punctuated	0.827	8.90	0.387	0.402	0.52	1.21	0.920
15-UMIX	Exponential	1.22	4.66				1.22	1.00
20-UMIX	Exponential	1.47	2.30				1.47	2.00
15-SPSN	Instantaneous	1.70	4.83				1.70	0.251
20-SPSN	Instantaneous	1.72	2.30				1.72	0.501

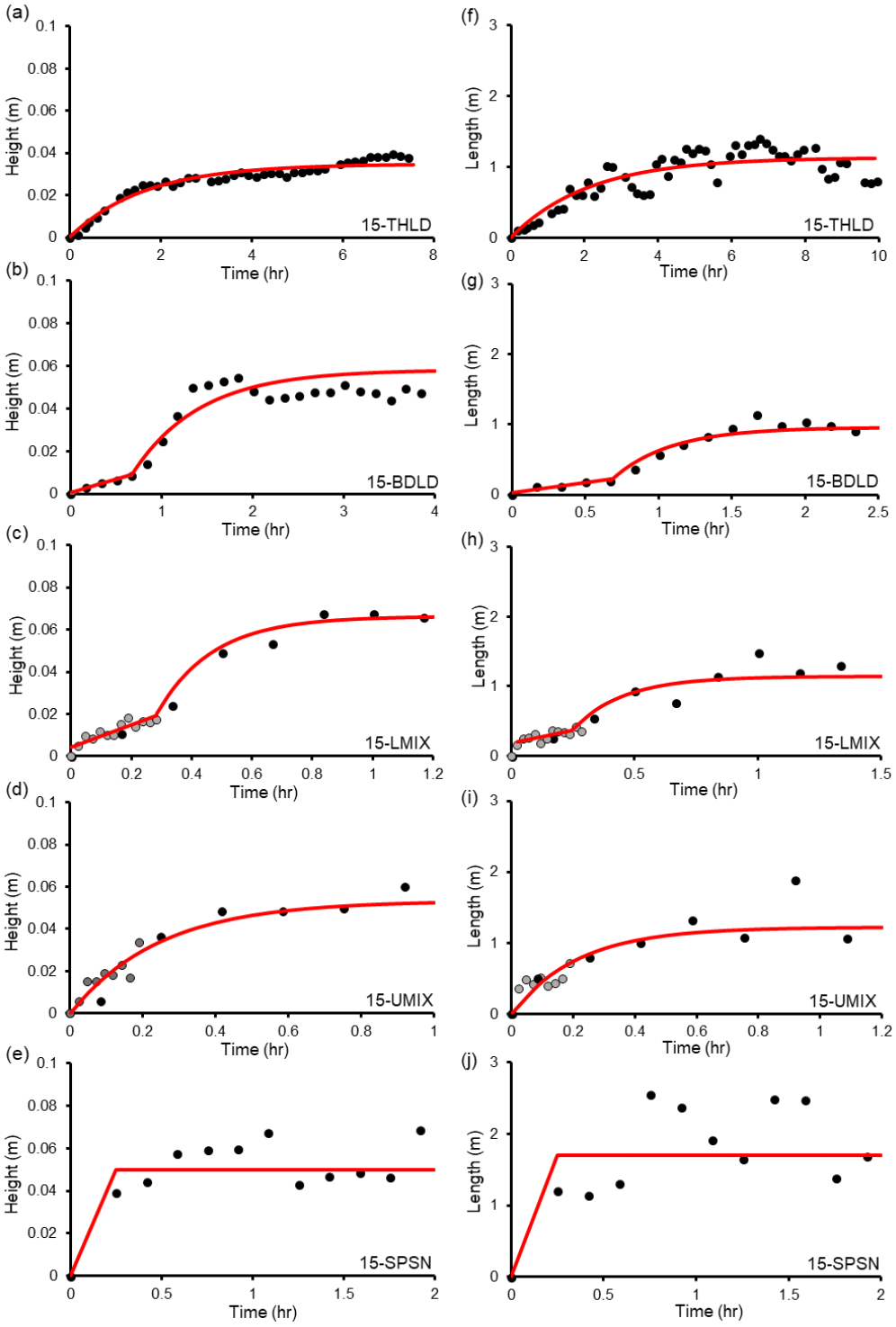

Figure 4.10. Curve fits to the height (a-e) and length (f-j) time series data until equilibrium is achieved in the runs with 15 cm initial flow depths. Two hours of data are shown for the SPSN time series (e,j) since equilibrium was instantaneously achieved. The grey circles are from the short scans and the black are from the long scans.

The type of growth curve was mostly consistent for the same transport stage regardless of depth. The THLD height data followed an exponential curve (Figure 4.10a) while the BDLD and LMIX data displayed a period of linear growth until H was ~ 0.01 to 0.02 m, when growth became exponential (Figure 4.10b,c). It is more challenging to characterize the UMIX height curve (Figure 4.10d). There is some evidence for punctuated growth but a distinct transition from linear to exponential growth is difficult to define since the bed evolved quickly. We applied an exponential curve starting from the beginning of the run, but there was a short linear growth phase. In the 25-THLD and 25-BDLD stage, growth was exponential despite the presence of a defect that passed through the field from the headbox (Appendix G (Supplementary Figures G4a & G4b)). The general shapes of the L curves were consistent with the shape of the H curves with some exceptions. The 20-THLD length curve (Appendix G (Supplementary Figure G4f)) showed some evidence of punctuated growth while the 15-THLD was exponential (Figure 4.10f). The 20-BDLD length curve exhibited no punctuated growth (Appendix G (Supplementary Figure G4g)), but the 15-BDLD length showed a period of linear growth before an exponential phase (Figure 4.10g).

4.3.4. Time to Equilibrium

Bedforms are usually considered to be in equilibrium when there is no systematic change in dimensions through time. Coleman et al. (2005) suggested that the time to equilibrium (t_{eq}) is defined when bedform dimensions become constant. This definition is subjective because dimensions can only become constant in a statistical sense. A single point on a growth curve where dimensions are statistically constant is hard to define due to substantial variation in bedform dimensions through time (Chapter 3). Following Baas (1994) and Venditti et al. (2005a), t_{eq} was defined as the time required for the exponential growth curve to reach 99% of the asymptote. This definition provides an objective method to quantify t_{eq} that is entirely consistent between growth curves. In the case of punctuated growth, t_{eq} is the time required for the exponential growth period to reach 99% of the asymptote, plus the time of the linear growth phase. The SPSN runs likely reached equilibrium sometime before our first measurements but, we do not have these data so t_{eq} is defined by our first measurement. In almost all runs, t_{eq} was achieved well within the observation range except for the 25-THLD height data in which the 99% value of the asymptote lies outside our measurement period of 23 hrs. We

omitted the 25 cm runs from further analysis of t_{eq} because they followed a defect growth process.

Time to equilibrium for both *H* (t_{eH}) and *L* (t_{eL}) decreased nonlinearly with equilibrium transport stage (τ_*/τ_{*C}) in our experiments (Figure 4.11). The observation of a nonlinear decrease in t_{eH} and t_{eL} with τ_*/τ_{*C} agrees well with the data from Iseya (1984) and Venditti et al. (2005a) (Figure 4.11). Including these data, the relation between t_{eH} and τ_*/τ_{*C} is a power function:

$$t_{eH} = 106\frac{\tau_*}{\tau_{*c}}^{-1.39} \qquad \text{(Eq. 4.7a)}$$

with an R^2 value of 0.53. The relation between t_{eL} and L_e is also a power function:

$$t_{eL} = 69.5\frac{\tau_*}{\tau_{*c}}^{-1.22} \qquad \text{(Eq. 4.7b)}$$

with an R^2 value of 0.42. While Equations 4.7a & 4.7b fit the data reasonably well, there is some evidence that variability about the relations could be related to a depth effect. Many, but not all, deeper flow runs had longer t_{eq} values compared to runs at shallower flow depths under similar τ_*/τ_{*C} values. The longer t_{eq} can be attributed to the larger volume of bed material that must be transported to form the larger features.

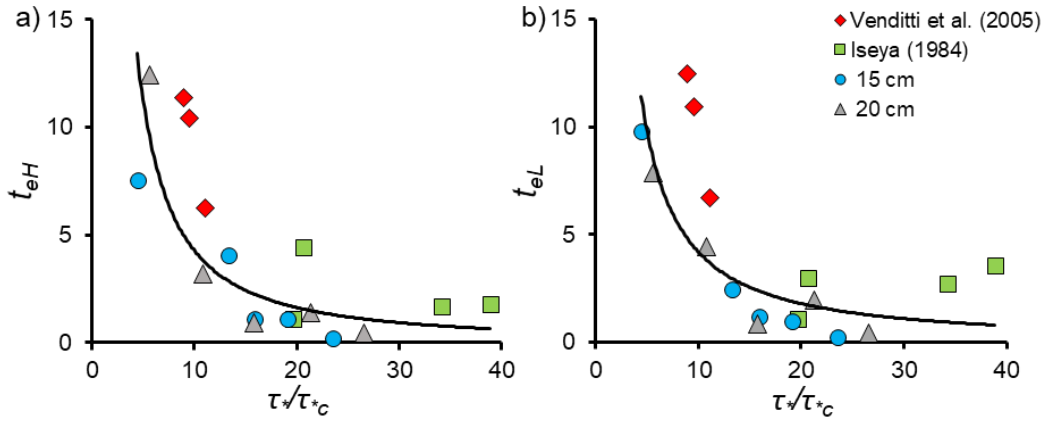

Figure 4.11. Equilibrium transport stage against t_e for (a) height and (b) length using data from the experiments presented here plus data of Iseya (1984) and Venditti (2005a).

4.3.5. Bedform Growth Constant

Exponential growth was observed for nearly all transport stages, which allows for robust estimates of the growth constants, b_H and b_L, in Equation 4.4. There is remarkably little variation in b, with an average value of 4.57 for b_H (Equation 4.4a) and 4.60 for b_L (Equation 4.4b) (Table 4.3), when Equation 4 was fit to our data (Appendix G (Supplementary Figure G4-G7)). The average b_H and b_L differ by < 1%, suggesting that the growth constant b may be universal, with a value of 4.59, calculated as the grand average of all b_H and b_L values. Equation 4 plotted with b = 4.59 (Figure 4.12) visually represents the Iseya (1984) and Venditti et al. (2005a) data better than the regressions in Figure 4.1.

Table 4.3. Height and length growth constants from Equations 4.4.

	Height growth constant, b_H	Length growth constant, b_L
15-THLD	4.56	4.57
20-THLD	4.59	4.69
25-THLD	4.77	4.66
15-BDLD	4.30	4.74
20-BDLD	4.59	4.55
25-BDLD	4.50	4.55
15-LMIX	4.58	3.67
20-LMIX	4.66	4.62
15-UMIX	4.60	4.65
20-UMIX	4.55	5.29
Average	4.57	4.60

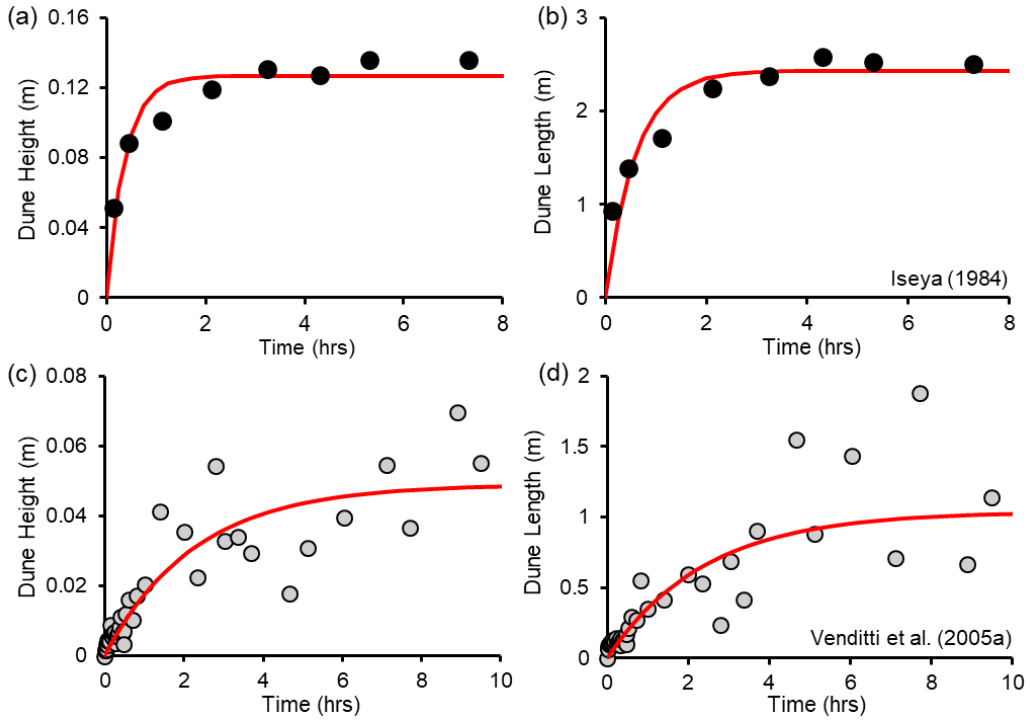

Figure 4.12. Examples of exponential fits using Equations 4.4 with b = 4.59 to bedform (a) height and (b) length growth time series data from Iseya (1984; Run 3) and (c) height and (d) length growth time series data from Venditti et al. (2005a; Flow B).

4.4. Discussion

4.4.1. Morphodynamics of bedforms growth

Bedform growth from a flat bed has been attributed to the coalescence of smaller features (Raudkivi & White, 1990; Coleman & Melville, 1994) while others have argued for growth by bedform field stretching through subtle downstream acceleration of bedforms (Venditti et al., 2005a). Coalescence has been invoked to explain power-law growth (Coleman & Melville, 1994), while bedform field stretching has been observed for exponential growth (Venditti et al., 2005a). Our results show that growth processes and the functional form of growth curves are more complex than these explanations and are dependent on transport stage.

Our observations indicate that there are three distinct types of growth patterns: 1) Exponential, 2) Punctuated and 3) Instantaneous. Exponential growth occurs at low transport stages due to a combination of bedform field stretching and individual bedform

coalescence. Bedforms appear as small 2D features in the initial stages of bed development but relatively quickly change to 3D as they grow and pass defects through crestlines. Three dimensional bedforms coalesce and form 2D features with crestlines that span the entire width of the flume within $t < 10$ mins. The larger 2D features grow more slowly through the downstream stretching process. In later growth stages, coalescence is limited to 2D sand sheets supplied to the crest (e.g., Venditti et al., 2005b).

Punctuated growth is characterized by relatively slow linear growth of bedforms, followed by a period of exponential growth. The initial growth is characterized by an organization of small 2D features, that gradually transitions to 3D features. The presence of initial linear growth opens the possibility of linear growth to equilibrium dimensions, but this does not occur in our experiments. Once bedforms reached heights of 1 to 2 cm, large volumes of bed material began to move as a thick layer of bedload and suspension as troughs were scoured, leading to an exponential growth phase. In many respects, this is similar to the 'rogue ripple' process (Leeder, 1983; Bennett & Best, 1996) that has been used to explain the transition from ripples to dunes as velocity increases. Indeed, Schindler and Robert (2005) noted a similar process where 2D ripples transitioned into 3D ripples when flow velocity was increased, leading to the generation of a rogue ripple. Our observation of increased trough scour when H reaches 1 to 2 cm, suggests that this may represent a critical height at which the separation zone in the lee is large enough to enhance turbulence at the bed, promoting exponential bedform growth by trough deepening. The process occurs simultaneously over the entire bed rather than through one single 'rogue ripple'.

It remains unclear what occurs in the initial stages of evolution when there is substantial suspension. In the UMIX runs, the linear growth phase appeared to happen but was sufficiently short that it was difficult to characterize. Bedforms emerged at their equilibrium H and L so quickly in the SPSN runs that it was perceived as instantaneous.

4.4.2. Towards a method for predicting bedform growth in rivers

The exponential relations in Equations 4.4a and 4.4b are powerful tools for predicting bedform response to an imposed flow. Dune height and length can be predicted as a function of time if H_e, L_e, t_e and b are known. The growth exponent b is

4.59 for our experiments, and comparison with data from Iseya (1984) and Venditti et al. (2005a) indicates that it is universal. Traditionally, H_e and L_e are predicted with simple depth-scaling relations (e.g., Yalin, 1964), but these have been shown to have tremendous variability about them (Bradley & Venditti, 2017). Chapter 3 showed that H_e and L_e scale with transport stage as:

$$\frac{H_e}{h} = a_{H/h} * \left(\frac{\tau_*}{\tau_{*c}} - b_{H/h}\right)^2 + c_{H/h} \quad \text{(Eq. 4.8a)}$$

$$\frac{L_e}{h} = a_{L/h} * \left(\frac{\tau_*}{\tau_{*c}} - b_{L/h}\right)^2 + c_{L/h}. \quad \text{(Eq. 4.8b)}$$

where $a_{H/h}$ = -0.0014, $b_{H/h}$ = 16, $c_{H/h}$ = 0.42, $a_{L/h}$ = 0.031, $b_{L/h}$ = 9.6, and $c_{L/h}$ = 5.7, representing coefficients derived from individual data sets of median values. The coefficients vary slightly depending on whether the mean or the median values are used to derive the relation. The median relations are convenient because they can include metrics of variability in forward predictions (Chapter 3). The scaling relations in Equations 4.8a and 4.8b require some further testing in larger channels, which may result in some refinement of the coefficients. However, the parabolic form of Equations 4.8a and 4.8b is consistent with the largest data compilation of dune data assembled to data (Bradley & Venditti, 2017). It is likely that Equations 4.8a and 4.8b, with the coefficients presented here, can be applied in other small channels since the underlying data are from flume experiments.

The more difficult variable to predict in Equations 4.4a and 4.4b is t_e. We have shown that t_e decreases non-linearly with transport stage in our experiments (Figure 4.11) and the underlying functions are power laws described by Equations 4.7a and 4.7b. Coleman et al. (2005) used dimensional analysis to show that t_e was a function of depth, grain size and transport stage, resulting in Equation 4.6. However, Equation 4.6 underpredicts t_e from our experiments and those of Venditti et al. (2005a), and overpredicts t_e in Iseya (1984) (Figure 4.13). The poor fit of Equation 4.6 to these data either confirms our opening critique that t_e was defined subjectively by Nikora and Hicks (1997) and Coleman et al (2005), or suggests that the equation is not appropriate. We regard the former explanation for the poor fit as more likely because Coleman et al. (2005) achieve an impressive data collapse, even if it is not reproducible with our data

sets. Equation 4.6 also assumes the same t_e for bedform height and length, which we have shown is not generally the case.

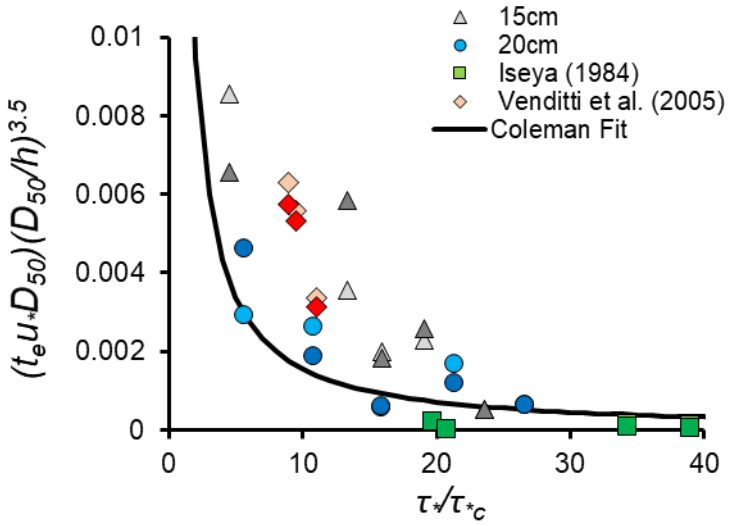

Figure 4.13. Time to equilibrium plotted against transport stage using the same non-dimensional variables presented in Coleman et al. (2005). The lighter and darker shades are height and length data, respectively.

Nevertheless, the Coleman et al. (2005) relation correctly identifies a scale dependence of t_e. Larger scale dunes take longer to achieve equilibrium dimensions than smaller scale dunes simply because more bed material must be mobilized to alter their size. It is not clear why grain size is in the dimensionless groupings of Equation 4.6 but it appears to be included to define universal relations for t_e that are separate for ripples and dunes. There is no evidence that grain size affects dune dimensions, but ripple dimensions are thought to scale with grain size (Yalin, 1985; Baas, 1994). Assuming that grain size affects only transport stage, and not dune dimensions, the Coleman et al. (2005) relation may be recast to remove scale effects as either $t_e \frac{u_*}{h} = f\left(\frac{\tau_*}{\tau_{*c}}\right)$ or $t_e \frac{\overline{U}}{h} = f\left(\frac{\tau_*}{\tau_{*c}}\right)$, where $\overline{U}$ is the mean velocity.

The non-dimensional time to equilibrium dimensions decreases nonlinearly with transport stage, regardless of whether $t_e \frac{u_*}{h}$ (Figure 4.14a, b) or $t_e \frac{\overline{U}}{h}$ (Figure 4.14c, d) is used. The difference between the two functions for all our data set is minimal, because our observations are for shallow flows and ~0.5 mm sand, including those from Iseya (1984) and Venditti et al. (2005a). We suspect that $t_e \frac{\overline{U}}{h} = f\left(\frac{\tau_*}{\tau_{*c}}\right)$ is the more appropriate

relation because $\overline{U}$ and *h* are fundamental scales of flow and the use of u_* to make t_e non-dimensional results in metrics of shear stress on both sides of the relation. The relation for the time to equilibrium made non-dimensional with mean velocity for dune height is a power law that has the form:

$$t_{eH}\left(\frac{\overline{U}}{h}\right) = 283\frac{\tau_*}{\tau_{*c}}^{-1.34} \quad \text{(Eq. 4.9a)}$$

and the relation for length is:

$$t_{eL}\left(\frac{\overline{U}}{h}\right) = 185\frac{\tau_*}{\tau_{*c}}^{-1.15} \quad \text{(Eq. 4.9b)}$$

with R^2 values of 0.71 and 0.54 for t_{eH} and t_{eL}, respectively. Using u_* to make t_e non-dimensional produces similar R^2 values (Figure 4.14a,b). While the Equations 4.9a and 4.9b fit the data reasonably well, the exponents are close to 1, suggesting that a linear relation may also be appropriate. However, more data are required to fully test the relation.

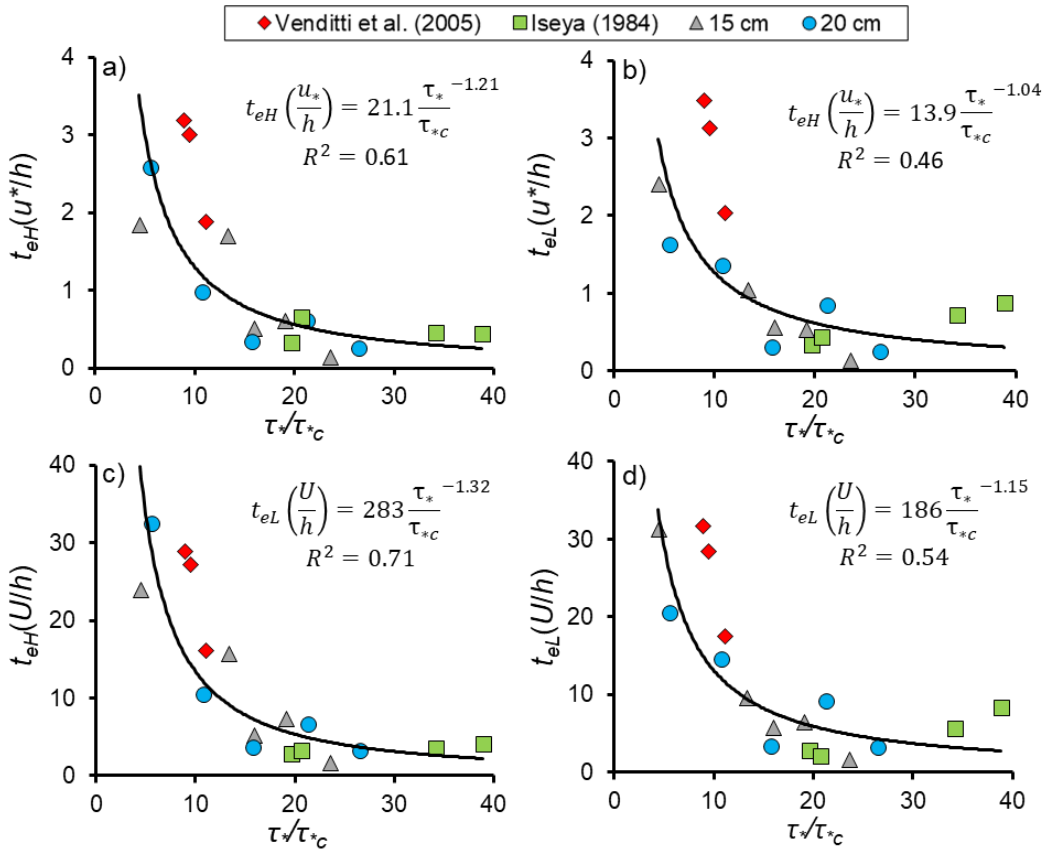

Figure 4.14. Equilibrium transport stage against the non-dimensional time to equilibrium for (a) $t_{eH}\left(\frac{u_*}{h}\right)$, (b) $t_{eL}\left(\frac{u_*}{h}\right)$, (c) $t_{eH}\left(\frac{\bar{U}}{h}\right)$ and (d) $t_{eL}\left(\frac{\bar{U}}{h}\right)$ using data from the experiments presented here, Iseya (1984) and Venditti (2005a).

The series of relations formed by Equations 4.4, 4.8 and either 4.7 (dimensional version) or 4.9 (non-dimensional version) constitute powerful tools for predicting the response of dunes to imposed flows. They allow for the prediction of dune dimensions given the magnitude and duration of flows. The relations are especially useful because, in many circumstances, dunes may not reach equilibrium dimensions during a flood flow. The exponential form of the growth curves in our experiments does not appear to be affected by whether growth occurs from a flat bed or a field composed of smaller bedforms. It is, therefore, likely that the series of relations presented here can be applied to field situations. However, the series of relations is based on observations made in a small channel with a constant grain size (~0.5 mm), so they require testing against field observations, particularly for deep rivers. We suspect that the relations can be applied in all channels, but that the coefficients will need to be adjusted for deep rivers. There is a pressing need for spatially-resolved observations of dune

development during flood flows that will provide the data necessary to test these empirical relations.

4.5. Conclusions

We have systematically examined the response of bedform dimensions and morphodynamics as bedform fields evolved from a flat bed under different flow depths and transport stages. We used three sets of runs, each with a different initial flow depth of 15, 20 and 25 cm. The 15 and 20 cm sets had five different discharges applied over a flat bed and the bed was continually mapped as it evolved towards an equilibrium state. Each run had a larger discharge applied to achieve transport stages ranging from just above the threshold for sediment mobility to conditions in which substantial volumes of bed material moved in suspension. Only two of the lower transport stages could be achieved for the 25 cm depth. The results indicate that:

1. At low transport stages, growth curves are exponential. The bed initially evolved through coalescence of smaller features and then grew through a slow stretching process.
2. At higher transport stages, when punctuated growth curves were observed, small bed features appeared on the bed and grew linearly until heights were > 2 cm. At this height, a thick transport layer developed due to intense trough erosion, and growth became exponential.
3. Instantaneous growth was observed at the highest transport stage, as the bed rapidly evolved.
4. The time for a growing bedform field to reach equilibrium decreases non-linearly with transport stage.
5. The dimensions of evolving dunes through time can be predicted with the proposed series of relations. It is likely that the relations can be applied in all channels, but they will need to be tested with field data, particularly in large rivers, to refine the coefficients**.**

Chapter 5. Synthesis and Conclusions

This dissertation sought to identify what controls dune height (H) and length (L) in rivers through a meta-analysis of published dune dimension data and a series of flume experiments in the River Dynamics Laboratory at Simon Fraser University. An empirical approach was used to improve the current understanding of the fundamental controls on dune dimensions, and the results help guide and refine existing theory. The overarching research question of 'What controls dune dimensions and growth in rivers?' was addressed through a series of objectives introduced in Chapter 1. In this Chapter, the findings of the dissertation are synthesised in the context of the proposed objectives.

5.1. Predictive power of dune scaling relations

Simple depth-scaling relations are often used to predict both dune dimensions in rivers and paleoflows using cross-stratification thicknesses measured in the rock record. Depth-scaling relations imply that flow depth (h) is the control on H and L. The implication of a depth control was examined in Chapter 2 through an analysis of previously published dune and flow characteristics data. The compiled data set is the most extensive of its kind, allowing for a critical re-evaluation of the widely used $H = h/6$ and $L = 5h$ relations attributed to Yalin (1964). Ultimately, these relations proved to be poor predictors of dune dimensions. The substantial scatter about the relations may not be surprising given that the mechanistic, physical reasoning for a depth control has never been fully elucidated.

Even though depth may not be the fundamental control on dunes, size does increase with the scale of rivers. This makes depth-scaling relations attractive because only one easily measured variable is required to predict dimensions. The data set in Chapter 2 showed that dunes in deep channels do not grow as high relative to water depth as they do in shallow channels. The data revealed that H in channels where $h <$ 2.5 m scale as

$$H = h/3.5 \qquad \text{(Eq. 5.1)}$$

while dunes where $h >$ 2.5 m follow:

$$H = h/7.7 \quad \text{(Eq. 5.2)}$$

These relations are much better fits to the underlying data than $H = h/6$. They also separate dunes in shallow and deep channels, which often display distinct morphologies. Dunes in shallow channels are always asymmetric and have angle-of-repose lee sides, while dunes in deep channels commonly have low lee angles, with a more symmetrical morphology. The rounder, less steep morphology is reflected in the $h/7.7$ scaling. There was no clear evidence to support a scaling break in the dune length data, so *L* scales as:

$$L = 5.9h \quad \text{(Eq. 5.3)}$$

for all flow depths. Equation 5.3 is similar to the Yalin (1964) length relation but is refined with more underlying data. For the prediction of flow depth from an estimated dune height in the rock record, the relation is:

$$h = 6.7H. \quad \text{(Eq. 5.4)}$$

Equation 5.4 was fit only to field data to remove bias associated with idealized flume experiments since dunes in natural channels are responsible for features preserved in the rock record. Furthermore, whether a dune in the rock record was formed in a shallow or deep flow is not necessarily known *a priori* in a paleo-environmental reconstruction.

There are physically-based reasons that can be invoked to explain why dunes appear to scale with flow depth. The shear stress distribution over dunes has been linked to dune growth, suggesting that dune dimensions should scale with the total shear stress applied and its distribution over a dune. Depth may not be the control itself, but it is incorporated in the calculation of total shear stress ($\tau = \rho g h S$, where ρ is the density of water, g is gravitational acceleration, and S is the slope). The observation that low-angle dunes do not grow as high in the flow as shallow-channel dunes can also be related to depth since low-angle morphologies are often attributed to suspended sediment. The propensity for suspension depends on the ratio of shear velocity (u_*) to settling velocity (w_s), which includes flow depth since $u_* = \sqrt{ghS}$. Combined, these physically-based arguments suggest that transport stage (τ_*/τ_{*c}) may be an important control on dune dimensions because τ is included in the calculation of τ_*/τ_{*c}, and u_*/w_s is directly proportion to τ_*/τ_{*c}, for a given grain size. Yalin (1964) acknowledged a

transport stage control in his original work, which was further supported in later data compilations by Yalin (1972) and Yalin & Karahan (1979). The underlying data confirm that dune steepness (*H/L)* increases and then decreases with τ_*/τ_{*c}.

The variability about depth-scaling relations in the compiled data set appears to derive from two sources: the transport stage control and natural variability within dune fields. In recognition of this, the data used to derive Equations 5.1, 5.2, and 5.3 were used to create uncertainty estimates that encapsulate both sources of variability. The uncertainty ranges offer a method to add error estimates to predictions of dune dimensions from flow depth or estimates of flow depth from dune dimensions. However, the two sources of uncertainly are combined in the estimate and cannot be separated within the data compilation. This required new experiments reported in Chapter 3.

5.2. Depth and transport stage controls on dune dimensions and variability

Flume experiments presented in Chapter 3 were used to better understand the role of depth and transport stage in controlling dune dimensions and variability. Three different flow depths (15, 20, 25 cm) were tested. Each flow depth had a series of runs with different transport stages. The transport stages allowed observations ranging from just above the threshold for sediment motion to near complete dune washout. The bed was mapped continuously during a 10-hour equilibrium period to develop dune dimension time series. Continual bed mapping provided observations that were used to derive true underlying mean values for each observation period. Mean values allow for an examination of dune-dimension controls while the distributions of data about the true means provide insight into the variability. While natural variability and transport stage controls were combined as sources of uncertainty in Chapter 2, the experimental design allowed for the controls on dune dimensions and variability to be separated.

Dune-depth scaling suggests that dune dimensions under the same flow depth should be the same regardless of the applied flow. The results showed that true mean dune sizes are larger in deeper flows, because there is more room in the flow for bedforms to grow. However, depth scaling is not consistent because it is affected by transport stage. Mean dune heights at moderate transport stages (e.g., BDLD, LMIX, UMIX) were larger than predicted by the scaling relation in Equation 5.1, and mean

lengths were longer than predicted with Equation 5.3 at higher transport stages. The range of observed depth-scaling relations indicates that dimensions are controlled by transport stage, in addition to the size of the flow, characterized by flow depth. Dune steepness increased and then decreased with transport stage, confirming previous observations (Yalin, 1972; Yalin & Karahan, 1979; Venditti et al., 2016; Chapter 2). However, the results quantitatively showed that this pattern occurs because *H* increases with transport stage until u_*/w_s ~ 0.96 and τ_*/τ_{*C} ~ 18, when *H* begins to decrease. Length remains relatively constant until u_*/w_s ~ 0.72 and τ_*/τ_{*C} ~ 8.5, when dunes begin to get longer.

There are physically-based reasons that explain the non-linear response of dune dimensions to transport stage. Dune height has been shown to decrease when large volumes of bed-material are moved through suspension. As suspension increases, less sediment is readily supplied to dune crests and slip faces, causing a decrease in dune height. Dune height was observed to decrease when u_*/w_s ~ 0.96, which is near the threshold value of 1, when significant suspension has been shown to occur (Bagnold, 1966; Nino et al., 2003). Smaller dune heights were also observed at the lowest transport stage (e.g., THLD), in the absence of suspension. Dunes during the lowest transport stage displayed shallower troughs, which resulted in lower heights. Trough scour may have been limited at the lowest transport stage by a reduction in turbulence associated with lower mean flow velocity. However, detailed measurements of coupled flow and sediment dynamics are needed to confirm this reasoning. It is unclear what promotes the lengthening of dunes at higher transport stages, but it may be related to increased particle excursion lengths.

The continual mapping of the bed allowed for an examination of how variability in bedform dimensions responded to flow depth and transport stage. The experiments showed that variability increases with flow depth since a larger range of *H* and *L* was possible at deeper flows. The increased variability with depth can be attributed to increased flow volume, allowing a wider range bedform dimensions within a bedform field. The results also show that variability in *H* and *L* increases with transport stage, indicating that transport stage is an additional source of variability.

5.3. Physically-based scaling relations that include uncertainty

The number of experimental observations in Chapter 3, allowed for the development of new parabolic transport stage scaling relations, using true mean values. The transport stage scaling relations have the following form:

$$\frac{H}{h} = a_{H/h} * \left(x - b_{H/h}\right)^2 + c_{H/h} \quad \text{(Eq. 5.5)}$$

$$\frac{L}{h} = a_{L/h} * \left(x - b_{L/h}\right)^2 + c_{L/h} \quad \text{(Eq. 5.6)}$$

where *x* is transport stage (defined as either u_*/w_s or τ_*/τ_{*c}), the coefficient *a* is the shape of the parabolic function, and *b* and *c* are the horizontal and vertical position of the curve inflection point, respectively. Coefficient values for Equations 5.5 and 5.6 derived from the true mean using τ_*/τ_{*c} are $a_{H/h}$ = -0.0010, $b_{H/h}$ = 17.69, $c_{H/h}$ = 0.4169, $a_{L/h}$ = 0.0192, $b_{L/h}$ = 8.459, and $c_{L/h}$ = 6.226. Values for *a*, *b* and *c* derived using u_*/w_s are available in Table 3.4.

The relations in Equations 5.5 and 5.6 reflect the observation that *H* and *L* respond non-linearly to transport stage. The horizontal inflection point, b, represents an important change in the scaling of dunes. The transport stage at *b* in Equation 5.5 indicates when *H* begins to decrease, rather than increase, with transport stage. Dune height relative to depth increases until τ_*/τ_{*c} = 18 (u_*/w_s = 0.96), suggesting the point when *H* begins to decrease is coincident with the threshold for substantial suspension. The value of *b* in Equation 5.6 shows the transport stage when *L* begins to increase with transport stage. Length scaling decreases slightly or remains constant until τ_*/τ_{*c} = 9 (u_*/w_s = 0.72) when lengthening occurs. Equations 5.5 and 5.6 represent a significant advancement from simple depth-scaling relations because they more realistically capture the physical controls on dune dimensions.

The regression analysis results based on the true mean values (Table 3.4) cannot be used with Equations 5.5 and 5.6 to add measures of uncertainty to predictions. However, it is useful to include the inherent variability in dune dimensions in circumstances when only single transects of a dune field are available or when

observations of cross-strata are made in sedimentary rock outcrop or cores. The coefficients in Equations 5.5 and 5.6 can be defined using the median values (Supplementary Table E2) rather than the true mean values, which allows for envelopes of variability about the median relations. Equations 5.5 and 5.6 should be used if grain size, slope, and flow depth can be measured or estimated because transport stage can be calculated using $\tau_* = \frac{\rho_w h S}{(\rho_s - \rho_w) D}$ and τ_{*c} from Shields' type diagrams (e.g., Brownlie, 1981). Alternatively, the suspension threshold can used by calculating $u_* = \sqrt{ghS}$ and w_s using either Dietrich (1982) or Ferguson and Church (2004). If the measures necessary to compute transport stage cannot be obtained, the depth-scaling relations (Equations 5.1 to 5.4) proposed in Chapter 2 are useful because they require only one variable. However, the uncertainty estimates used with the depth-scaling relations in Equations 5.1 to 5.4 include both the effects of transport stage and natural variability on dimensions. Equations 5.5 and 5.6 explicitly remove some uncertainty by including metrics of transport stage that more realistically reflect the control on dune dimensions.

Equations 5.5 and 5.6 require further testing with field data. It is likely that the relations can be readily applied in small channels, where the conditions are similar to the experiments in Chapter 3. However, it is unclear how well these relations will describe dunes in flows > 2.5 m since low-angle dunes do not grow as relatively high in the flow. Further testing in larger channels may result in some refinement of the coefficients in Equations 5.5 and 5.6, but the parabolic form should hold since it is consistent with the data compilation presented in Chapter 2. Unfortunately, it is difficult to compare Equations 5.5 and 5.6 to most previously published data since single measurements from a flume run or a transect of a natural dune field do not reveal true mean equilibrium dimensions.

5.4. Dune growth from a flat bed

The observation that transport stage is important for setting equilibrium dune dimensions lead to the investigation in Chapter 4 of how transport stage affects dune growth. Dune growth curves exhibit three different behaviours: 1) exponential growth, 2) punctuated growth, when a period of initially linear growth is abruptly interrupted by exponential growth and 3) instantaneous growth, when bed evolution happens so quickly that measurements of the phenomenon were impossible with the experimental design.

The growth behaviour was dependent on the applied transport stage, not flow depth. At low transport stages, growth curves are exponential, and the bed initially evolved through coalescence of smaller features, and then through a slow stretching process. At the moderate transport stages, when punctuated growth was observed, small bed features initially appeared and grew linearly with time until they had heights ~2 cm. At this height, a thick transport layer formed due to intense trough scour, and growth became exponential. Instantaneous growth was observed at the highest transport stage, as the bed rapidly evolved. These different forms of growth from a flattened bed have not been previously shown, likely because most experiments were limited to low transport stages.

Some previous work proposed that bedform growth curves follow power laws. Power laws can only be used when bedforms are growing and require a different function to detect when equilibrium dimensions are reached. The domains of the two functions are difficult to establish without knowing when the statistical steady state is reached. The identification of the statistical steady state is difficult due to natural variability in dune fields. Exponential functions better describe bedform growth to an equilibrium condition, and can be used to objectively define the period when the statistically steady state of bedform dimensions occurs.

5.5. A method for predicting dune growth

Predicting bedform growth requires knowledge of: 1) equilibrium dimensions for a given flow, 2) the form of the underlying growth relation, and 3) the time required to reach equilibrium. Equilibrium dimensions can be predicted using Equations 5.5 and 5.6. Exponential functions that can describe bedform dimensions during growth have the following form:

$$\frac{H}{H_e} = 1 - e^{\left(-b_H * \frac{t}{t_{eH}}\right)} \quad \text{(Eq. 5.7)}$$

$$\frac{L}{L_e} = 1 - e^{\left(-b_L * \frac{t}{t_{eL}}\right)} \quad \text{(Eq. 5.8)}$$

where t is time, b_H and b_L are height and length growth constants. The results showed that values for b_H and b_L do not vary in the experiments, suggesting they may be a

universal constant equal to 4.59. Comparison to other data sets (Iseya, 1984; Venditti et al., 2005) reinforce this idea.

Transport stage was shown to affect the time required for the height (t_{eH}) and length (t_{eL}) of dunes to reach equilibrium. Both t_{eH} and t_{eL} decreased non-linearly with τ_*/τ_{*c}, but there appears to be depth control on t_{eH} and t_{eL}. The depth effect occurs because larger scale dunes in deeper flows take longer to achieve equilibrium dimensions than smaller scale dunes as more bed material must be mobilized to alter their size. To address this scale dependence on t_{eH} and t_{eL}, the relations for t_{eH} and t_{eL} were made non-dimensional with h and mean velocity ($\overline{U}$) to give

$$t_{eH}\left(\frac{\overline{U}}{h}\right) = 270\frac{\tau_*}{\tau_{*c}}^{-1.24} \quad \text{(Eq. 5.9)}$$

$$t_{eL}\left(\frac{\overline{U}}{h}\right) = 112\frac{\tau_*}{\tau_{*c}}^{-0.837}. \quad \text{(Eq. 5.10)}$$

The exponential relations given by Equations 5.9 and 5.10 are powerful tools for predicting dune response to imposed flows.

The widespread application of Equations 5.9 and 5.10, in combination with Equations 5.5 to 5.8, requires consideration of a few caveats. The equations can likely be applied in their current state to small channels with beds consisting of similar grain size sediment to that used in these experiments (550 μm). It is probable that the relations can be applied in all channels, but the coefficients will need to be adjusted for deep rivers. Equations 5.9 and 5.10, in particular, require testing over a wide range of flows and sediment grain sizes to ensure the non-dimensional form of t_e is correct. Furthermore, low-angle morphologies may not respond to flows exactly as asymmetrical dunes, because a degree of freedom is provided by lee slope adjustment. Spatially-resolved observations of dune development during flood flows will provide the data necessary to test the proposed empirical relations. Once these data are collected, the proposed series of relations can be tested and refined to accurately predict equilibrium dune dimensions and growth as they respond to flows.

References

Adams, M.M., Bhattacharya, J.P., 2005. No change in fluvial style across a sequence boundary, Cretaceous Blackhawk and Castlegate Formations of central Utah, USA. Journal of Sedimentary Research, 75(6), 1038-1051.

Adriaanse, M., 1986. De ruwheid van de Bergsche Maas bij hoge afvoeren. Nota 86.19, Rijkswaterstaat, RIZA, Arnhem, The Nertherlands

Allen, J.R.L.,1968. Current Ripples. Elsevier, New York, NY.

Allen, J.R.L., 1970. A quantitative model of climbing ripples and their cross-laminated deposits. Sedimentology 14, 5–26.

Allen, J.R.L., 1973. Features of cross-stratified units due to random and other changes in bed forms. Sedimentology, 20(2), 189-202.

Allen, J.R.L., 1974. Reaction, relaxation and lag in natural sedimentary systems: general principles, examples and lessons. Earth Science Reviews 10, 263–342.

Allen, J.R.L., 1976. Computational methods for dune time-lag: Calculations using Stein's rule for dune height. Sedimentary Geol. 20(3), 165–216.

Allen, J.R.L., 1982. Sedimentary Structures: Their Character and Physical Basis. Elsevier, New York, NY.

Amsler, M. L., & Schreider, M. I., 1999. Dune height prediction at floods in the Paraná River, Argentina. River sedimentation: Theory and applications, 615-620.

Anderson, A.G., 1953. The characteristics of sediment waves formed on open channels. Proceedings of the Third Mid-Western Conference on Fluid Mechanics. University of Missouri, Missoula, pp. 397–395.

Andreotti, B., Fourrière, A., Ould-Kaddour, F., Murray, B., Claudin, P., 2009. Giant aeolian dune size determined by the average depth of the atmospheric boundary layer. Nature 457, 1120-1123.

Baas, J.H., 1994. A flume study on the development and equilibrium morphology of current ripples in very fine sand. Sedimentology, 41(2), 185-209.

Baas, J.H., 1999. An empirical model for the development and equilibrium morphology of current ripples in fine sand. Sedimentology 46, 123–138.

Baas, J.H., Oost, A.P., Sztano, O.K., Boer, P.L., & Postma, G., 1993. Time as an independent variable for current ripples developing towards linguoid equilibrium morphology. Terra Nova, 5(1), 29-35.

Baas, J.H., Best, J.L., Peakall, J., 2016. Predicting bedforms and primary current stratification in cohesive mixtures of mud and sand. Journal of the Geological Society 173(1), 12-45.

Bagnold, R.A, 1966. An approach to the sediment transport problem from general physics. Geol. Survey Prof. Paper 422-I, U.S. Government Printing Office, Washington, DC.

Barenblatt, G.I., 2003. Scaling. Cambridge University Press, Cambridge, UK.

Bartholdy, J., Flemming, B.W., Bartholomä, A., Ernstsen, V.B., 2005. Flow and grain size control of depth-independent simple subaqueous dunes. J Geophys Research 110:F04S16. doi:10.1029/2004JF000183

Bartholdy, J., Flemming, B.W., Ernstsen, V.B., Winter, C., 2010, Hydraulic roughness over simple subaqueous dunes. Geo-Marine Letters 30(1), 63-76.

Bartholdy, J., Ernstsen, V.B., Flemming, B.W., Winter, C., Bartholomä, A., Kroon, A., 2015. On the formation of current ripples. Scientific Reports 5, 11390. doi:10.1038/srep11390

Barton, J.R., Lin, P.N., 1955. A Study of the Sediment Transport in Alluvial Channels. Report No. 55Jrb2, Civil Engineering Department, Colorado A&M College, Fort Collins Colorado.

Bendat, J. S., & Piersol, A. G., 1966. Measurement and Analysis of Random Data, pp. 337–344, John Wiley, New York.

Bennett, S.J., Best, J.L., 1996. Mean flow and turbulence structure over fixed ripples and the ripple–dune transition. In: Ashworth, P.J., Bennett, S.J., Best, J.L., McLelland, S.J. (Eds.), Coherent Flow Structures in Open Channels. Wiley, Hoboken, NJ, 281–304.

Best, J.L., 1992. On the entrainment of sediment and initiation of bed defects: insights from recent developments within turbulent boundary layer research. Sedimentology 39, 797–811.

Best, J.L., 2005. The fluid dynamics of river dunes: a review and some future research directions. Journal of Geophysical Research, 110. F04S02. doi:10.1029/ 2004JF000218.

Best, J., & Kostaschuk, R., 2002. An experimental study of turbulent flow over a low-angle dune. Journal of Geophysical Research: Oceans, 107(C9).

Blom, A., Ribberink, J.S., de Vriend, H. J., 2003. Vertical sorting in bed forms: Flume experiments with a natural and a trimodal sediment mixture. Water Resources Research 39(2), 1025, doi:10.1029/2001WR001088.

Bradley, R.W., Venditti, J.G., Kostaschuk, R.A., Church, M., Hendershot, M., Allison, M.A., 2013. Flow and sediment suspension events over low-angle dunes: Fraser Estuary, Canada. Journal of Geophysical Research: Earth Surface 118, 1693–1709, doi:10.1002/jgrf.20118.

Bradley, R.W., & Venditti, J.G., 2017. Reevaluating dune scaling relations. Earth-Science Reviews, 165, 356-376.

Bridge, J.S., 1997. Thickness of sets of cross strata and planar strata as a function of formative bed-wave geometry and migration, and aggradation rate. Geology, 25, 971–974.

Bridge, J.S., 2003. Rivers and floodplains: forms, processes, and sedimentary record. Malden, Massachusetts, John Wiley & Sons, 491 p.

Bennett, S.J., Best, J.L., 1996. Mean flow and turbulence structure over fixed ripples and the ripple–dune transition. In: Ashworth, P.J., Bennett, S.J., Best, J.L., McLelland, S.J. (Eds.), Coherent Flow Structures in Open Channels. Wiley, Hoboken, NJ, 281–304.

Bridge, J.S., Best, J.L., 1997. Preservation of planar laminae due to migration of low-relief bad waves over aggrading upper-stage plane beds: comparison of experimental data with theory. Sedimentology 44, 253–262.

Bridge, J.S., Tye, R.S., 2000. Interpreting the dimensions of ancient fluvial channel bars, channels, and channel belts from wireline-logs and cores. AAPG Bulletin, v. 84/8, 1205-1228.

Brilhuis, R. 1988. Enkele hydraulische en morphologische parameter van de Nederlandse Rijntakken. Nota 88.003, Rijkswaterstaat, DBW/RIZA, Arnhem, The Netherlands

Brownlie, W. R., 1981. Prediction of flow depth and sediment discharge in open channel. Report No. KH-R-43A, W. M. Keck Laboratory of Hydraulics and Water Resources, California Institute of Technology, Pasadena, California, USA.

Carling, P.A., 1999. Subaqueous gravel dunes. Journal of Sedimentary Research 69, 534–545.

Carling, P.A., Golz, E., Orr, H.G., Radecki-Pawlik, A., 2000. The morphodynamics of fluvial sand dunes in the River Rhine near Mainz, Germany, Part I: Sedimentology and morphology. Sedimentology 47, 227–252.

Cartigny, M. J., Ventra, D., Postma, G., Den Berg, J. H., 2014. Morphodynamics and sedimentary structures of bedforms under supercritical-flow conditions: New insights from flume experiments. Sedimentology 61(3), 712-748.

Coleman, S.E., Melville, B.W., 1994. Bed-form Development. Journal of Hydraulic Engineering 120, 544–560.

Coleman, S.E., Zhang, M.H., Clunie, T.M., 2005. Sediment-wave development in subcritical water flow. Journal of Hydraulic Engineering 131, 106–111.

Colombini, M., 2004. Revisiting the linear theory of sand dune formation. J. Fluid Mech. 502, 1–16.

Colombini, M., & Stocchino, A., 2008. Finite-amplitude river dunes. Journal of Fluid Mechanics, 611, 283-306.

Church, M., 2006. Bed material transport and the morphology of alluvial river channels. Annual Reviews of Earth and Planetary Science 34, 325–354.

Damen, J. M., van Dijk, T. A. G. P., & Hulscher, S. J., 2018. Spatially varying environmental properties controlling observed sand wave morphology. Journal of Geophysical Research: Earth Surface.

Delft Hydraulics, 1979. Verification of Flume Tests and Accuracy of Flow Parameters. Note R 657-VI, The Netherlands.

Dietrich, W.E., 1982. Settling velocity of natural particles. Water Resources Research 18(6), 1615-1626.

Dietrich, W.E., & Smith, J.D., 1984. Bed load transport in river meander. Water Resources Research, 20, 1355–1380. doi:10.1029/WR020i010p01355.

Ditchfield, R., Best, J.L., 1990. Development of bed features: discussion. Journal of Hydraulic Engineering116, 647–650.

Einstein, H.A., & N.L. Barbarossa, 1952. River channel roughness, Trans. Am. Soc. Civ. Eng., 117(1), 1121–1132.

Engel, P., Lau, Y.L., 1980. Computation of bed load using bathymetric data. Journal of Hydraulic Division 106, 369–380.

Engelund, F., 1970. Instability in erodible channels. Journal of Fluid Mechanics 42, 225–244.

Engelund, F., Hansen, E., 1967. A Monograph on Sediment Transport in Alluvial Streams. Denmark Technical University, Copenhagen.

Flemming, B.W., 1988. Zur Klassifikation subaquatischer, strömungstransversaler Transportkörper. Bochumer Geologische und Geotechnische Arbeiten, 29: 93-97.

Flemming, B.W., 2000. The role of grain size, water depth and flow velocity as scaling factors controlling the size of subaqueous dunes. Proceedings of Marine Sandwave Dynamics, 23–24 March, Lille, France. 55–60.

Folk, R.L., 1980. Petrology of Sedimentary Rocks. Hemphill Publ. Co., Austin. 182 pp.

Franzetti. M., Le Roy, P., Delacourt, C., Garlan, T., Cancouet, R., Sukhovich, A., Deschamps, A., 2013. Giant dune morphologies and dynamics in a deep continental shelf environment: Example of the banc du four (Western Brittany, France). Marine Geology 346, 17-30.

Fredsøe J., 1974. On the development of dunes in erodible channels. Journal of Fluid Mechanics 64: 1–16.

Fredsøe J., 1979. Unsteady flow in straight alluvial streams: modification of individual dunes. Journal of Fluid Mechanics 91(3): 497–512.

Fredsøe, J., 1982. Shape and dimensions of stationary dunes in rivers. Journal of Hydraulic Division 108, 932–947.

Gabel , S.L., 1993. Geometry and kinematics of dunes during steady and unsteady flows in the Calamus River, Nebraska, USA. Sedimentology 40, 237-269.

Galeazzi, C.P., Almeida, R.P., Mazoca, C.E., Best, J.L., Freitas, B.T., Ianniruberto, M., Cisneros, J., & Tamura, L.N., 2018. The significance of superimposed dunes in the Amazon River: Implications for how large rivers are identified in the rock record. Sedimentology. doi:10.1111/sed.12471

Ganti, V., Paola, C., & Foufoula-Georgiou, E., 2013. Kinematic controls on the geometry of the preserved cross sets. Journal of Geophysical Research: Earth Surface 118(3), 1296-1307.

Garcia, M.H., 2008. Sedimentation Engineering, Processes, Measurements, Modeling, and Practice. ASCE Manuals and Reports on Engineering Practice No. 110. ASCE, New York, NY.

Gill, M.A., 1968. Rationalization of Lacey's regime flow equations. Journal of the Hydraulics Division 94(4), 983-996.

Gill, M.A., 1971. Height of sand dunes in open channel flows. Journal of the Hydraulics Division, 97(12), 2067-2074.

Giri, S., & Shimizu, Y., 2006. Numerical computation of sand dune migration with free surface flow. Water Resources Research, 42(10).

Grass, A.J., 1970. Initial instability of fine bed sand, J. Hydraul. Eng., 96(3), 619-632.

Guy, H.P., Simons, D.B., Richardson, E.V. 1966. Summary of alluvial channel data from flume experiments 1956-61. US Geol. Surv. Prof. Pap. 462-I. Washington, DC: US Geol. Surv.

Gyr, A., Schmidt, A., 1989. The different ripple formation mechanism. Journal of Hydraulic Research 27, 61–74.

Hendershot, M.L., Venditti, J.G., Bradley, R.W., Kostaschuk, R.A., Church, M., Allison, M.A., 2016. Response of low-angle dunes to variable flow. Sedimentology 63, 743–760. doi: 10.1111/sed.12236

Hendershot, M. L., Venditti, J. G., Church, M. , Bradley, R. , Kostaschuk, R. A., & Allison, M. A., 2018. Crestline bifurcation and dynamics in fluvially-dominated, tidally-influenced flow. Sedimentology. doi:10.1111/sed.12480

Holmes Jr, R.R., Garcia, M.H., 2008. Flow over bedforms in a large sand-bed river: A field investigation. Journal of Hydraulic Research 46(3), 322-333.

Hu, H., Wei, T., Yang, Z., Hackney, C. R., & Parsons, D. R. (2018). Low-angle dunes in the Changjiang (Yangtze) Estuary: Flow and sediment dynamics under tidal influence. Estuarine, Coastal and Shelf Science, 205, 110-122.

Huthoff, F., 2012. Theory for flow resistance caused by submerged roughness elements. J. Hydraul. Res. 50(1), 10–17.

Jackson, R.G., 1975. Hierarchical attributes and a unifying model of bed forms composed of cohesionless material and produced by shearing flow. GSA Bulletin 86, 1523-1533.

Jackson, R.G., 1976. Sedimentological and fluid-dynamic implications of the turbulence bursting phenomenon in geophysical flows. Journal of Fluid Mechanics, 77, 531–560.

Jerolmack, D. J., Mohrig, D., 2005. Frozen dynamics of migrating bedforms. Geology 33(1), 57-60.

Julien, P.Y., 1992. Study of bedform geometry in large rivers. Rep. Q1386, Delft Hydraulics, Emmeloord, The Netherlands.

Julien, P.Y., Klaassen, G.J., 1995. Sand–dune geometry of large rivers during floods. Journal of Hydraulic Engineering 121, 657–663.

Julien, P.Y., Klaassen, G.J., Ten Brinke, W.B.M., Wilbers, A.W.E., 2002. Case study: bed resistance of Rhine River during the 1998 flood. J. Hydraul. Eng., 128, 1042–1050.

Kamphuis, H., 1990. Sediment-transportmetigen rijntakken. Nota 90.075, Rijkswaterstaat, DBW/RIZA, Arnhem, The Netherlands.

Karim, F., 1995. Bed configuration and hydraulic resistance in alluvial channel flows Journal of Hydraulic Engineering. 121(1), 15–25.

Karim, F., 1999. Bed-form geometry in sand-bed flows. Journal of Hydraulic Engineering, 125(12), 1253-1261.

Kostaschuk, R.A., Church, M.A., 1993, Macroturbulence generated by dunes: Fraser River, Canada, Sedimentary Geology 85, 25–37.

Kostaschuk, R.A., Ilersich, S.A., 1995. Dune geometry and sediment transport. River Geomorphology, (ed Hickin, E.J.) 19–36 (John Wiley & Sons).

Kostaschuk, R.A., Villard, P.V., 1996. Flow and sediment transport over large subaqueous dunes: Fraser River, Canada. Sedimentology 43, 849–863.

Kostaschuk, R.A., Shugar, D., Best, J., Parsons, D., Lane, S., Hardy, R., Orfeo, O., 2009. Suspended sediment transport and deposition over a dune: Rio Parana, Argentina. Earth Surface Processes and Landforms 34, 1605–1611.

Kwoll, E., J.G. Venditti, R.W. Bradley, Winter, C., 2016. Flow structure and resistance over subaquaeous high- and low-angle dunes. J. Geophys. Res. Earth Surf. 121, 545–564 doi:10.1002/2015JF003637.

Lane, E.W., Eden, E.W., 1940. Sand waves in the Lower Mississippi River. J West Soc Eng 45(6), 281.

Leclair, S.F., 2002. Preservation of cross-strata due to migration of subaqueous dunes: an experimental investigation. Sedimentology 49, 1157–1180.

Leclair, S.F., 2011. Interpreting fluvial hydromorphology from the rock record: Large-river peak flows leave no clear signature. From river to rock record: The preservation of fluvial sediments and their subsequent interpretation: SEPM Special Publication, 97, 113-123.

Leclair, S.F., Bridge, J.S., Wang, F., 1997. Preservation of cross-strata due to migration of subaqueous dunes over aggrading and non-aggrading beds: comparison of experimental data with theory. Geoscience Canada 24, 55–66.

Leclair, S.F., Bridge, J.S., 2001. Quantitative interpretation of sedimentary structures formed by river dunes. Journal of Sedimentary Research 71, 713–716.

Leeder, M. R., 1983. On the Interactions between Turbulent Flow, Sediment Transport and Bedform Mechanics in Channelized Flows, in Modern and Ancient Fluvial Systems (eds J. D. Collinson and J. Lewin), Blackwell Publishing Ltd., Oxford, UK. doi: 10.1002/9781444303773.

Liu, H.K., 1957. Mechanics of sediment-ripple formation. Journal of Hydraulic Division, ASCE 83(HY2), 1–23.

Lunt, I.A., Smith, G.H.S., Best, J.L., Ashworth, P.J., Lane, S.N., Simpson, C.J., 2013. Deposits of the sandy braided South Saskatchewan River: Implications for the use of modern analogs in reconstructing channel dimensions in reservoir characterization. AAPG bulletin 97(4), 553-576.

Lynds, R. M., Mohrig, D., Hajek, E. A., & Heller, P. L., 2014. Paleoslope reconstruction in sandy suspended-load-dominant rivers. Journal of Sedimentary Research, 84(10), 825-836.

Ma, H., Nittrouer, J. A., Naito, K., Fu, X., Zhang, Y., Moodie, A. J., Wang, Y., Wu, B., & Parker, G., 2017. The exceptional sediment load of fine-grained dispersal systems: Example of the Yellow River, China. Science advances, 3(5), e1603114.

McElroy, B.J., 2009. Expressions and Implications of Sediment Transport Variability in Sandy Rivers. Ph.D. dissertation, University of Texas at Austin, Austin, TX.

McElroy, B., Mohrig, D., 2009. Nature of deformation of sandy bed forms. Journal of Geophysical Research 114, F00A04.http://dx.doi.org/10.1029/2008JF001220.

McLean, S.R., 1990. The stability of ripples and dunes. Earth Science Reviews 29, 131–144.

McLean, S. R., Nelson, J. M., & Wolfe, S. R., 1994. Turbulence structure over two-dimensional bed forms: implications for sediment transport. Journal of Geophysical Research: Oceans, 99(C6), 12729-12747.

Miller, D.M., 1984. Reducing transform bias in curve fitting. Am. Stat., 34, 124–126.

Mohrig, D., Smith, J.D., 1996. Predicting the migration rates of subaqueous dunes. Water Resources Research 32(10), 3207-3217.

Naqshband, S., Ribberink, J.S., Hurther, D., Hulscher, S.J.M.H., 2014a. Bed load and suspended load contributions to migrating sand dunes in equilibrium. J. Geophys. Res. Earth Surface 119, 1043–1063, doi:10.1002/2013JF003043.

Naqshband, S., Ribberink, J., Hulscher, S., 2014b. Using Both Free Surface Effect and Sediment Transport Mode Parameters in Defining the Morphology of River Dunes and Their Evolution to Upper Stage Plane Beds. J. Hydraul. Eng.,

Naqshband, S., Hoitink, A.J.F., McElroy, B., Hurther, D., & Hulscher, S.J.M.H., 2017a. A sharp view on river dune transition to upper stage plane bed. Geophysical Research Letters, 44, 11,437–11,444. https://doi.org/10.1002/ 2017GL075906

Naqshband, S., B. McElroy, & Mahon, R. C., 2017b. Validating a universal model of particle transport lengths with laboratory measurements of suspended grain motions, Water Resources Research., 53, 4106–4123, doi:10.1002/2016WR020024. 10.1061/(ASCE)HY.1943-7900.0000873, 06014010.

Nelson, J.M., McLean, S.R., Wolfe, S.R., 1993. Mean flow and turbulence over two-dimensional bedforms. Water Resources Research 29, 3935–3953.

Nelson, J.M., Logan, B.L., Kinzel, P.J., Shimizu, Y., Giri, S., Shreve, R.L., & McLean, S.R., 2011. Bedform response to flow variability. Earth Surface Processes and Landforms, 36(14), 1938-1947.

Nezu, I., Nakagawa, H., 1993. Turbulence in Open-Channel Flows. A.A. Balkema, Rotterdam.

Nino, Y., Lopez, F., & Garcia, M., 2003. Threshold for particle entrainment into suspension. Sedimentology, 50(2), 247-263.

Nikora, V.I., Hicks, D.M., 1997. Scaling relationships for sand wave development in unidirectional flow. J. Hyd. Engrg., ASCE, 123(12), 1152-1156.

Nittrouer, J. A., Mohrig, D., Allison, M.A., 2011. Punctuated sand transport in the lowermost Mississippi River. Journal of Geophysical Research, 116, 1914-1934. doi:10.1029/2011JF002026

Nowell, A.R.M., Church, M., 1979. Turbulent flow in a depth-limited boundary layer. Journal of Geophysical Research 84, 4816-4824.

Oke, T. R., 1978. Boundary layer climates, Methuen and Co., London.

Ohata, K., Naruse, H., Yokokawa, M., & Viparelli, E., 2017. New Bedform Phase Diagrams and Discriminant Functions for Formative Conditions of Bedforms in Open-Channel Flows. Journal of Geophysical Research: Earth Surface, 122(11), 2139-2158.

Paarlberg, A.J., Dohmen-Janssen, C.M., Hulscher, S.J.M.H., Termes, P., Schielen, R., 2010. Modelling the effect of time-dependent river dune evolution on bed roughness and stage. Earth Surf. Processes Landforms 35(15), 1854–1866.

Parsons, D. R., Best, J. L., Orfeo, O., Hardy, R. J., Kostaschuk, R., & Lane, S. N., 2005. Morphology and flow fields of three-dimensional dunes, Rio Paraná, Argentina: Results from simultaneous multibeam echo sounding and acoustic Doppler current profiling. Journal of Geophysical Research: Earth Surface, 110(F4).

Paola, C., Borgman, L., 1991. Reconstructing random topography from preserved stratification. Sedimentology 38(4), 553-565.

Peters, J.J., 1978. Discharge and sand transport in the braided zone of the Zaire estuary. Netherlands Journal of Sea Research 12(3), 273-292.

Ponten, A., Plink-Bjorklund, P., 2007. Depositional environments in an extensive tide-influenced delta plain, Middle Devonian Gauja Formation, Devonian Baltic Basin. Sedimentology 54(5), 969-1006.

Prent, M.T.H., Hickin, E.J, 2001. Annual regime of bedforms, roughness and flow resistance, Lillooet River, British Columbia, BC. Geomorphology 41, 369–390.

Pretious, E.S., Blench, T, 1951. Final report on special observations on bed movement in the lower Fraser River at Ladner Reach during the 1950 freshet. National Research Council of Canada, Fraser River Model Project.

Ranga Raju, K.G., Soni, J.P., 1976. Geometry of ripples and dunes in alluvial channels. Journal of Hydraulic Research 14(3), 241-249.

Robert, A., Uhlman, W, 2001. An experimental study on the ripple-dune transition. Earth Surface Processes and Landforms 26, 615–629.

Roden, J.E, 1998. The sedimentology and dynamics of mega-dunes, Jamuna River, Bangladesh. PhD thesis, Department of Earth Sciences and School of Geography, University of Leeds, Leeds, U.K.

Rood, K.M., Hickin, E.J., 1989. Suspended-sediment concentration and calibre in relation to surface-flow structure in Squamish River estuary, southwestern British Columbia. Canadian Journal of Earth Sciences 26(10), 2172-2176.

Rouse, H., 1939. Experiments on the mechanics of sediment suspension. In: Proceedings 5th International Congress on Applied Mechanics, pp. 550–554. Wiley, New York.

Rubin, D. M., Hunter, R.E., 1982. Bedform climbing in theory and nature. Sedimentology 29, 121–138.

Rudkivi, A., Witte, H.H., 1990. Development of bed features. J. Hyd. Engrg., ASCE, 116(9), 1063-1079.

Schindler, R.J., Robert, A., 2005. Flow and turbulence structure across the ripple–dune transition: an experiment under mobile bed conditions. Sedimentology, 52. http://dx.doi.org/10.1111/j.1365-3091.2005.00706x

Shen, H.W., Harrison, A.S., Mellema, W.J., 1978. Temperature and Missouri river stages near Omaha. Journal of the Hydraulics Division 104(1), 1-20.

Shields, A., 1936. Anwendung der Ahnlichkeitmechanik and turbulenzforschung auf die geschiebebewegung, Preussischen Versuchanstalt für Wasserbau und Schiffbau, No.26. Berlin, 1936

Shimizu, Y., Giri, S., Yamaguchi, S., & Nelson, J., 2009. Numerical simulation of dune–flat bed transition and stage-discharge relationship with hysteresis effect. Water Resources Research, 45(4).

Shinohara, K., Tsubaki, T., 1959. On the characteristics of sand waves formed upon the beds of the open channels and rivers. Research Institute for Applied Mechanics, Kyushu University.

Simons, D. B., Richardson, E.V., 1961. Forms of bed roughness in alluvial channels. Transactions of the ASCE 128, 284–302.

Simons, D.B., Richardson, E.V., Nordin, C.F., 1965. Bedload equation for ripples and dunes. US Geological Survey Professional Paper No. 462-H, 1–9.

Simons, D.B., Richardson, E.V., 1966. Resistance to flow in alluvial channels. US Geological Survey Professional Paper No. 422-J, pp. 1–61.

Singh, B., 1960. Transport of bed-load in channels with special reference to gradient and form. PhD Thesis, University of London, London.

Smith, J.D., 1970. Stability of a sand bed subjected to a shear flow of low Froude Number. Journal of Geophysical Research 75, 5928–5940.

Smith, J.D., McLean, S R., 1977. Spatially averaged flow over a wavy surface. Journal of Geophysical Research 82, 1735–1746.

Southard, J. B., 1991. Experimental determination of bed-form stability. Annual Review of Earth and Planetary Sciences, 19(1), 423-455.

Southard, J.B., Boguchwal, L.A., 1990. Bed configurations in steady unidirectional water flow part 2. Synthesis of flume data. Journal of Sedimentary Petrology 60, 658–679.

Stein, R.A. 1965. Laboratory studies of total load and apparent bed load. Journal of Geophysical Research 70(8), 1831-1842.

Stuckrath, F., 1969. Die Bewegung von Grossriffleln an der Sohle des Rio Parana, Mitteilungen. Franzius Institut Heft 32, Hannover, West Germany.

Sukhodolov, A.N., Fedele, J.J., Rhoads, B.L., 2006. Structure of flow over alluvial bed forms: An experiment on linking field and laboratory methods. Earth Surfurce Processes Landforms, 31, 1292–1310.

Southard, J.B., Boguchwal, L.A., 1990. Bed configurations in steady unidirectional water flow part 2. Synthesis of flume data. Journal of Sedimentary Petrology 60, 658–679.

Swanson, T., Mohrig, D., Kocurek, G., Perillo, M., & Venditti, J., 2018. Bedform spurs: A result of a trailing helical vortex wake. Sedimentology, 65(1), 191-208.

Terwindt, J.H.J., Brouwer, M.J.N., 1986. The behaviour of intertidal sandwaves during neap-spring tide cycles and the relevance to paleoflow reconstructions. Sedimentology, 33, 1–31.

Tjerry, S., J. Fredsøe, 2005. Calculation of dune morphology. J. Geophys. Res. 110, F04013, doi:10.1029/2004JF000171.

Tsubaki, T., Kawasumi, T., Yasutomi, T., 1953. On the influence of sand ripples upon the sediment transport in open channels. Rep Res Inst Appl Mech, 2, 241-256.

Tuijnder, A.P., Ribberink, J.S., Hulscher, S.J.M.H., 2009. An experimental study into the geometry of supply-limited dunes. Sedimentology 56, 1713–1727.

van den Berg, Jan H., 1987. Bedform migration and bed-load transport in some rivers and tidal environments. Sedimentology 34(4), 681-698.

van den Berg, J.H., van Gelder, A., 1998. Discussion of flow and sediment transport over large subaqueous dunes: Fraser River, Canada, by Kostaschuk R.A., Villard, P. Sedimentology 45, 217–219.

Van der Mark, C. F., Blom, A., & Hulscher, S. J., 2008. Quantification of variability in bedform geometry. Journal of Geophysical Research: Earth Surface, 113(F3).

van Rijn, L.C., 1984. Sediment transport III: bedforms and alluvial roughness. Journal of Hydraulic Engineering 110, 1733–1754.

van Rijn, L.C., 1993. Principles of Sediment Transport in Rivers, Estuaries and Coastal Seas. Aqua, Amsterdam.

van Urk, Al, Klaassen, G.L. 1982. Relationship for Bed Forms and Hydraulic Roughness. Report 61.000.04, Directorate Upper Rivers, Rijkswaterstaat, Arnhem, Netherlands.

Vanoni, V.A., Brooks N.H., 1957. Laboratory studies of the roughness and suspended load of alluvial streams, Report No E-68. Sedimentation Laboratory, California Institute of Technology: Passadena, CA, 120.

Venditti, J.G., 2007. Turbulent flow and drag over fixed two-and three-dimensional dunes. Journal of Geophysical Research: Earth Surface, 112(F4).

Venditti, J.G., 2013. Bedforms in sand-bedded rivers. Treatise on Geomorphology 9, 137-162, Shroder, J. (Editor in Chief), Wohl, E.(Ed.), Academic Press, San Diego, CA.

Venditti, J.G., Bennett, S.J., 2000. Spectral analysis of turbulent flow and suspended sediment transport over fixed dunes. Journal of Geophysical Research 105, 22035–22047.

Venditti, J.G., Bauer, B.O., 2005. Turbulent flow over a dune: Green River, Colorado. Earth Surface Processes and Landforms 30, 289-304, doi: 10.1002/esp.1142.

Venditti, J. G., Church, M., Bennett, S.J., 2005a. Morphodynamics of small-scale superimposed sand waves over migrating dune bed forms. Water Resour. Res. 41, W10423, doi:10.1029/2004WR003461.

Venditti, J.G., Church, M., Bennett, S.J., 2005b. On the transition between 2D and 3D dunes. Sedimentology 52 (6), 1343–1359.

Venditti, J.G., Church, M., Bennett, S.J., 2006. On interfacial instability as a cause of transverse subcritical bed forms. Water Resources Research 42, W07423. doi:10.1029/2005WR004346.

Venditti, J.G., Lin, C.Y.M., Kazemi, M., 2016. Variability in bedform morphology and kinematics with transport stage. Sedimentology 63, 1017–1040, doi: 10.1111/sed.12247.

Villard, P.V., Church, M., 2003. Dunes and associated sand transport in a tidally influenced sand-bed channel: Fraser River, British Columbia. Canadian Journal of Earth Sciences 40, 115–130.

Wan, Z., 1982. Bed-material movement in hyperconcentrated flow, Ser. Pap. 31, pp 79, Inst. of Hydrodyn. and Hydraul. Eng., Tech. Univ. Of Den., Lyngby.

Wan, Z., Wang, Z., 1994. Hyperconcentrated Flow. pp 290, A. A. Balkema, Brookfield, Vt.

Wijbenga, J.H.A., 1991. Analyse protoype-metingen (niet-) permanente ruwheid. Verslag onderzoek, Q1302, Delft Hydraulics, Emmeloord, The Netherlands.

Wilbers, A.W.E, 2004. Prediction of bedform characteristics and bedform roughness in large rivers. PhD thesis, Utrecht University.

Williams, G. P., 1970. Flume width and water depth effects in sediment-transport experiments. U.S. Geol. Surv. Prof. Pap., 562-H, 1–37.

Yalin, M.S., 1964. Geometrical properties of sand waves. Journal of the Hydraulics Division 90(5), 105-119.

Yalin, M.S., 1972. Mechanics of Sediment Transport. Pergamon, Oxford.

Yalin, M.S., 1985. On the determination of ripple geometry. Journal of Hydraulic Engineering 111, 1148–1155.

Yalin, M.S., Karahan, E., 1979. Steepness of sedimentary dunes. Journal of Hydraulic Division, ASCE 105(HY4), 318–392.

Znamenskaya, N. S., 1963. Experimental study of the dune movement of sediment. Soviet Hydrology: Selected Papers, pp. *253–275*, AGU*,* Washington, D. C.

Appendix A. Data Source References

Abdel-Fattah, S., Amin, A., & Van Rijn, L.C., 2004. Sand transport in Nile River, Egypt: Journal of Hydraulic Engineering, v. 130(6), p. 488-500.

Amsler, M.L., Prendes, H.H., Montagnini, M.D., Szupiany, R., & Garcia, M.H., 2003. Prediction of dune height in sand-bed rivers: The case of the Paraná River, Argentina, in Proceedings, 3rd IAHR Symposium on River, Coastal and Estuarine Morphodynamics, p. 1104-1113.

Bishop, C.T., 1977. On the time-growth of dunes. Master's thesis, Queen's University, Kingston, Canada.

Blom, A., Ribberink, J.S., & de Vriend, H.J., 2003. Vertical sorting in bed forms: Flume experiments with a natural and a trimodal sediment mixture: Water Resources Research, v. 39(2), 1025, doi:10.1029/2001WR001088.

Bridge, J.S., & Best, J.L., 1988. Flow, sediment transport and bedform dynamics over the transition from dunes to upper-stage plane beds: implications for the formation of planar laminae: Sedimentology, v. 35(5), p. 753-763.

Carling, P.A., 1999. Subaqueous gravel dunes. Journal of Sedimentary Research, 69(3).

Coleman, S.E., & Melville, B.W., 1996. Initiation of bed forms on a flat sand bed: Journal of Hydraulic Engineering, v. 122(6), p. 301-310.

Coleman, S., Zhang, M., & Clunie, T., 2005. Sediment-Wave Development in Subcritical Water Flow: Journal of Hydraulic. Engineering, v. 131(2), p. 106–111.

Culbertson, J.K., Scott, C.H., & Bennett, J.P., 1972. Summary of alluvial-channel data from Rio Grande conveyance channel, New Mexico, 1965-69: U.S. Geological Survey Professional Paper (Vol. 562), 49 p.

Gabel, S.L., 1993. Geometry and kinematics of dunes during steady and unsteady flows in the Calamus River, Nebraska, USA: Sedimentology, v. 40(2), p. 237-269.

Guala, M., Singh, A., BadHeartBull, N., & Foufoula-Georgiou, E., 2014. Spectral description of migrating bed forms and sediment transport: Journal of Geophysical Research Earth Surface, v. 119, doi:10.1002/2013JF002759.

Guy, H.P., Simons, D.B. & Richardson, E.V., 1966. Summary of alluvial channel data from flume experiments, 1956-61: U.S. Geological Survey Professional Paper (Vol. 462-I), 96 p.

Holmes Jr, R.R., & Garcia, M.H., 2008. Flow over bedforms in a large sand-bed river: A field investigation: Journal of Hydraulic Research, v. 46(3), p. 322-333.

Iseya, F., 1984. An Experimental Study of Dune Development and its Effect on Sediment Suspension: Environmental Research Center Papers no. 5. Environmental Research Center, The University of Tsukuba, Ibaraki, Japan, 46 p.

Jordan, G. F., 1962. Large submarine sand waves: Science, v. 136, p. 839-848.

Julien, P.Y, 1992. Study of bedform geometry in large rivers: Rep. No. Q 1386, Delft Hydraulics, Delft, The Netherlands, 79 p.

Korchokha, Y.M., 1968. Investigation of the dune movement of sediments on the Polomet River: Soviet Hydrology Selected Papers, v. 6, p. 541–559.

Kuhnle, R. A., & Wren, D.G., 2009. Size of suspended sediment over dunes: Journal of Geophysical Resources, v. 114 , F02020, doi:10.1029/2008JF001200.

Leclair, S.F., 2002. Preservation of cross-strata due to the migration of subaqueous dunes: an experimental investigation: Sedimentology, v. 49(6), p. 1157-1180.

Naqshband, S., Ribberink, J.S., Hurther, D., & Hulscher, S.J.M.H., 2014. Bed load and suspended load contributions to migrating sand dunes in equilibrium: Journal of Geophysical Research Earth Surfuce, v. 119, p. 1043–1063, doi:10.1002/2013JF003043.

Neill, C.R., 1968. Bed forms in the lower Red Deer River, Alberta: Journal of Hydrology, v. 7(1), p. 58-85.

Nordin, J.R., 1971. Statistical properties of dune profiles: U.S. Geological Survey Professional Paper (Vol. 562-F), 41 p.

Ramirez, M.T., & Allison, M.A., 2013. Suspension of bed material over sand bars in the Lower Mississippi River and its implications for Mississippi delta environmental restoration: Journal of Geophysical Research: Earth Surface, v. 118(2), p. 1085-1104.

Schindler, R.J., & Robert, A., 2005. Flow and turbulence structure across the ripple–dune transition: an experiment under mobile bed conditions: Sedimentology, v. 52(3), p. 627-649.

Shinohara, K., & Tsubaki, T., 1959. On the characteristics of sand waves formed upon the beds of the open channels and rivers: Research Institute for Applied Mechanics, Kyushu University, Reports, v. 7(25), p. 15-45.

Simons, D.B., Richardson, E.V. & Alebertson M.L., 1961. Flume Studies Using Medium Sand (0.45 mm): U.S. Geological Survey Professional Paper, v. 562-F , 76 p.

Simons, D.B., Richardson, E.V. & Haushild, W.L., 1963. Some effects of fine sediment on flow phenomena, U.S. Geological Survey Professional Paper, v. 1489-G, 47 p.

Southard, J. B., 1991. Experimental determination of bed-form stability. Annual Review of Earth and Planetary Sciences, 19(1), 423-455.

Strasser, M.A., Vinzon, S.B., & Kosuth, P., 2002. Bottom structures geometry of the Amazon River in International Conference on Fluvial Hydraulics, Louvain-la-Neuve, p. 1185-1193.

Stein, R.A., 1965. Laboratory studies of total load and apparent bed load: Journal of Geophysical Resources, v. 70, p. 1831–1842, doi:10. 1029/JZ070i008p01831.

Sukhodolov, A. N., Fedele, J. J., & Rhoads, B. L., 2006. Structure of flow over alluvial bedforms: an experiment on linking field and laboratory methods. Earth Surface Processes and Landforms, 31(10), 1292-1310.

Szupiany, R.N., Amsler, M.L., Hernandez, J., Parsons, D.R., Best, J.L., Fornari, E., & Trento, A., 2012. Flow fields, bed shear stresses, and suspended bed sediment dynamics in bifurcations of a large river: Water Resources Research, v. 48(11).

Toniolo, H., 2013. Bed Forms and Sediment Characteristics along the Thalweg on the Tanana River near Nenana, Alaska, USA: Natural Resources, v. 4, p. 20-30.

Tuijnder, A.P., Ribberink, J.S., & Hulscher, S.J., 2009. An experimental study into the geometry of supply-limited dunes: Sedimentology, v. 56(6), p. 1713-1727.

Van der Mark, C.F., Blom, A., & Hulscher, S.J.M.H., 2008. Quantification of variability in bedform geometry: Journal of Geophysical Research: Earth Surface, v. 113(F3).

Venditti, J.G., & Bauer, B.O., 2005. Turbulent flow over a dune: Green River, Colorado: Earth Surface Processes and Landforms, v. 30(3), p. 289-304.

Venditti, J.G., Church, M., & Bennett, S.J., 2005. On the transition between 2D and 3D dunes: Sedimentology, v. 52(6), p. 1343-1359.

Venditti, J.G., Lin, M.C.Y., & Kazemi, M (2016), Variability in bedform morphology and kinematics with transport stage: Sedimentology, doi: 10.1111/sed.12247.

Wijbenga, J.H.A., & Klaassen, G.J., 1983. Changes in Bedform Dimensions under Unsteady Flow Conditions in a Straight Flume, in Collinson, J.D. and Lewin, J. eds., Modern and Ancient Fluvial Systems: Blackwell Publishing Ltd., Oxford, UK, p 35-48.

Wilbers, A., 2004. The development and hydraulic roughness of subaqueous dunes [Ph.D thesis]: Netherlands, Utrecht University, 227 p.

Williams, G.P., 1967. Flume experiments on the transport of a coarse sand U.S. Geological Survey Professional Paper, v. 562-B, p. 1–31.

Wren, D. G., Kuhnle, R.A., & Wilson, C.G., 2007. Measurements of the relationship between turbulence and sediment in suspension over mobile sand dunes in a laboratory flume, Journal of Geophysical Resources, v. 112, F03009, doi:10.1029/2006JF000683.

Appendix B. Chapter 2 Supplementary Data File

Description:

The accompanying Excel spreadsheet includes all the data compiled and analyzed in Chapter 2 from the sources in Appendix A. The spreadsheet has two tabs; one for Flume Data and one for Field Data. Data are from the original authors except for Mean Flow Velocity values in italics, Shear Stress, and Sidewall Corrected Shear Stress. Mean Flow Velocity values in italics were calculated from the depth, channel width and discharge values reported by the author. Shear Stress values were calculated using $\tau = \rho_w g h S$ and sidewall corrections were made to the flume data using the Williams (1970) method (Eq. 2.21). 10°C water was assumed in the shear stress calculation (ρ_w= 999.7 kg/m3).

Filename:

Chapter2_Data.xlsx

Appendix C. Detailed Seatek Data Filtering Method

The following steps were performed to remove noise from the Seatak data used in Chapters 3 and 4:

1. Data points (*i*) in along stream profiles were removed where the next upstream point (*i*+1) and the previous downstream point (*i*-1) had a vertical elevation change (*dz*) > or < 1 cm (slope ~ +/- 0.77) (Supplementary Figure C1).

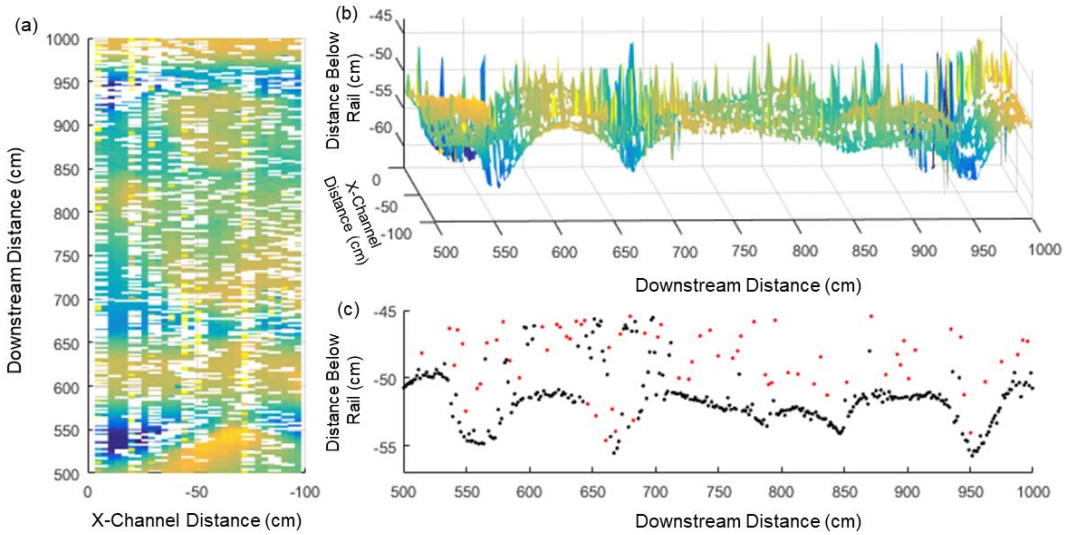

Supplementary Figure C1. (a) Top and (b) 3D view of bed once noise has been removed. (c) data along center profile. Red points are removed data during this step.

2. A moving average was calculated using 4 points in the upstream direction (*i*+4) and 4 points in the downstream direction (*i*-4) for each *i*. Data points (*i*) in a profile were removed when:

   a. *dz* between *i* and *i*+1 was < -1 cm and > or < 0.5 cm from the moving average

   b. *dz* between *i* and *i*-1 was > 1 cm and > or < 0.5 cm from the moving average

At high flow conditions (UMIX and SSPN), up to 5 sensors were too sensitive and failed to return a useable signal (Sensors #9, 18, 23, 26, 31). These profiles were removed if they if 35% of the data points in an along stream profile had been removed through the previous steps (Supplementary Figure C2).

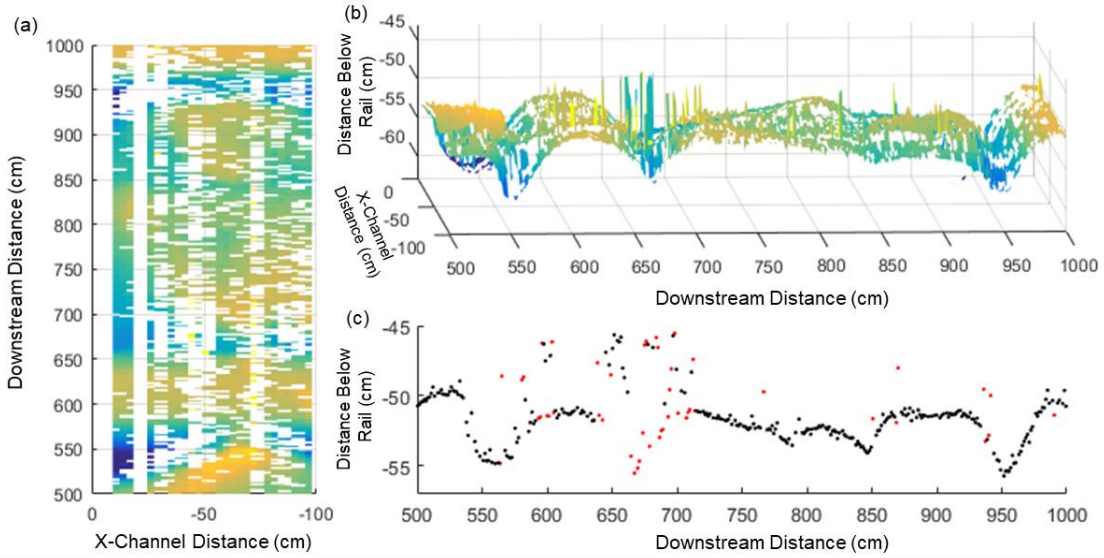

Supplementary Figure C2. (a) Top and (b) 3D view of bed once noise has been removed. (c) data along center profile. Red points are removed data during this step.

3. Data removed in along stream profiles were replaced with linear interpolation. If a profile was completely removed it was replaced using the mean of the two nearest sensors in the cross-stream direction (Supplementary Figure C3).

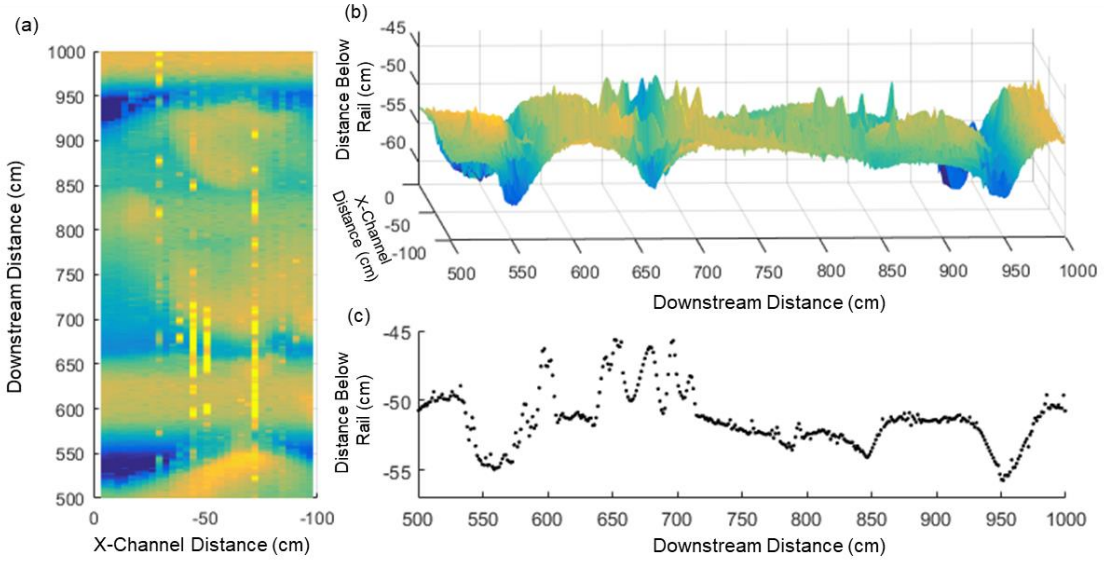

Supplementary Figure C3. (a) Top and (b) 3D view of bed once noise has been removed. (c) data along center profile.

4. A cross stream filter then removed any remaining noise or artificial spike by the linear interpolation. If a point was > 1.2 cm from the mean value of two adjacent data points in the cross stream, it was removed and replaced with the mean value of the two points (Supplementary Figure C4).

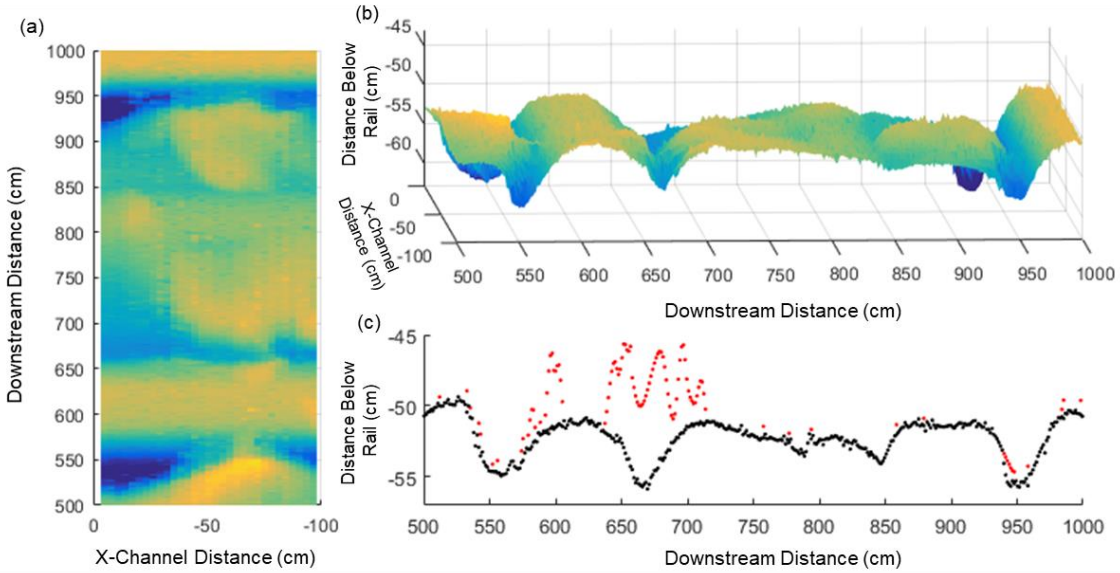

Supplementary Figure C4. (a) Top and (b) 3D view of bed once noise has been removed. (c) data along center profile. Red points are removed data during this step.

5. A final smooth was applied by using a moving window of 4 points ((*i*-2:*i*-1) and (*i* +1:*i*+2)) calculated about *i* in the downstream profiles. If *i* was greater than 0.50 cm from moving average, it was replaced with the average value (Supplementary Figure C5).

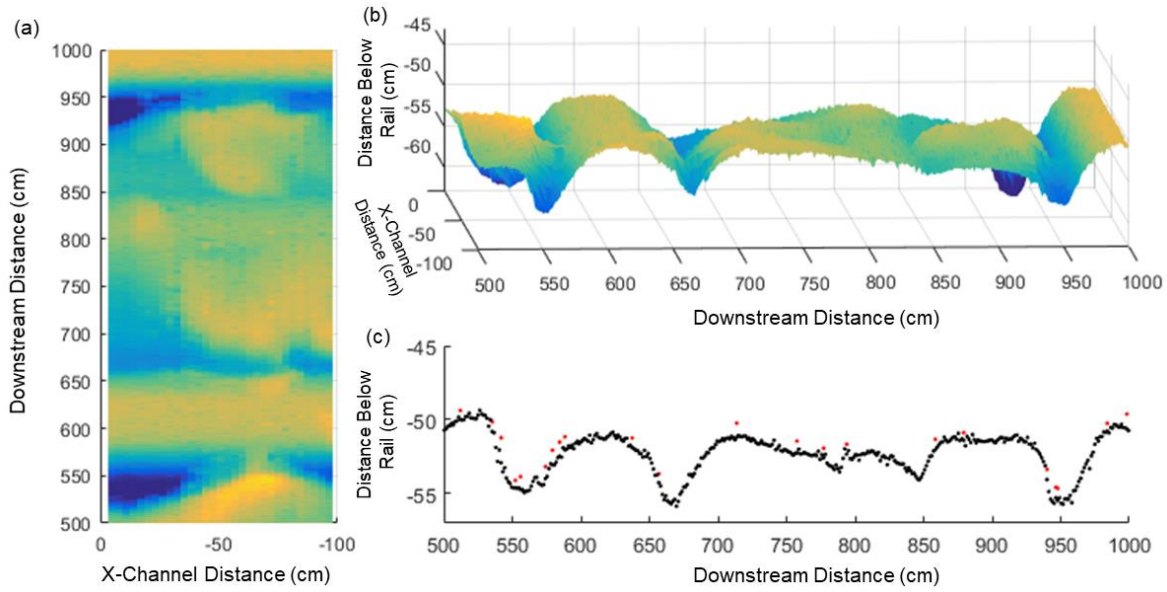

Supplementary Figure 5. (a) Top and (b) 3D view of bed once noise has been removed. (c) data along center profile. Red points are removed data during this step.

Appendix D. Chapter 3 Supplementary Figures

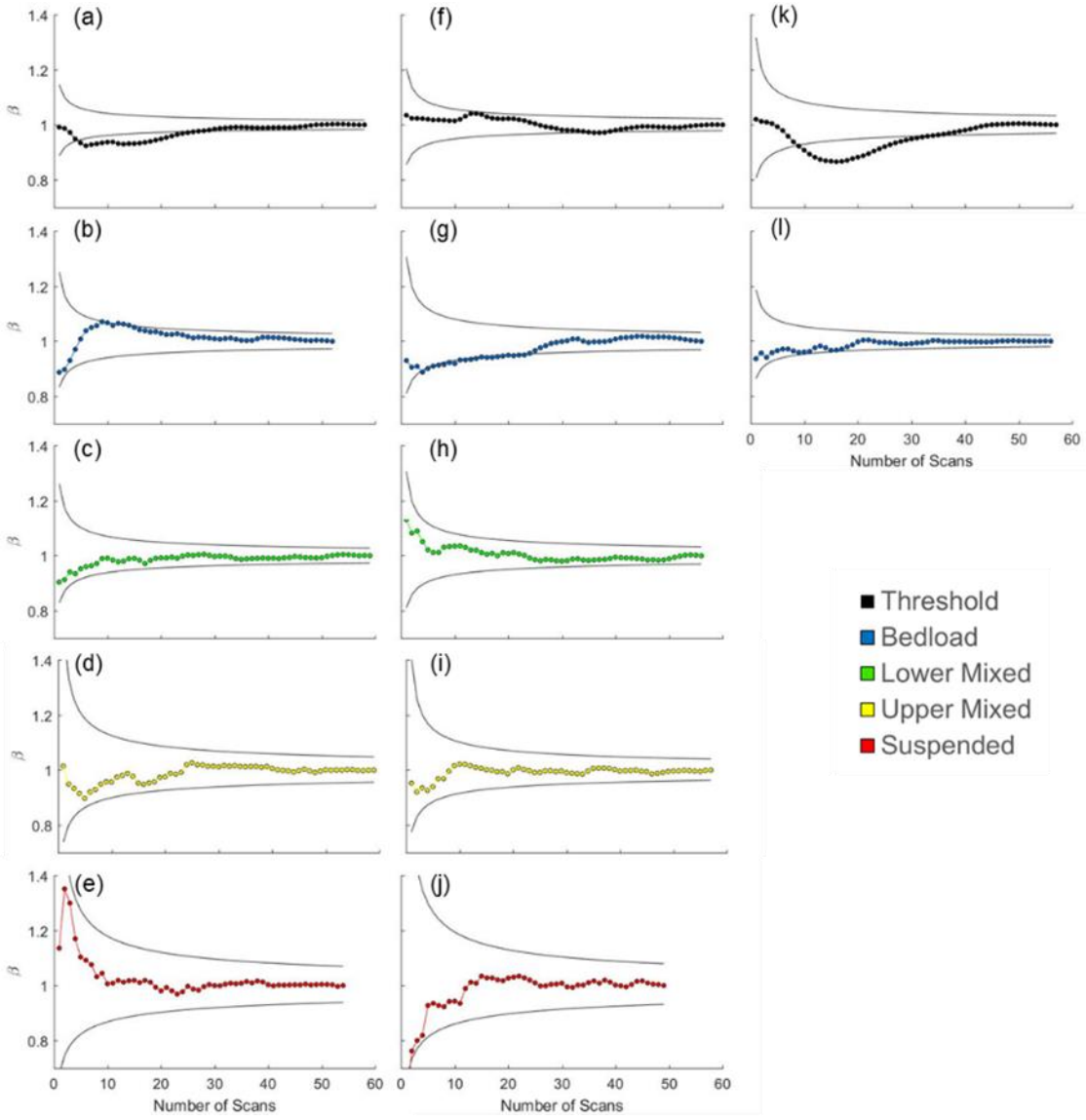

Supplementary Figure D1. Nonstationary incremental mean height β_H values for the (a-e) 15 cm conditions, (f-j) 20 cm conditions and (k-l) 25 conditions. The black line indicates the 95% confidence intervals for the mean values.

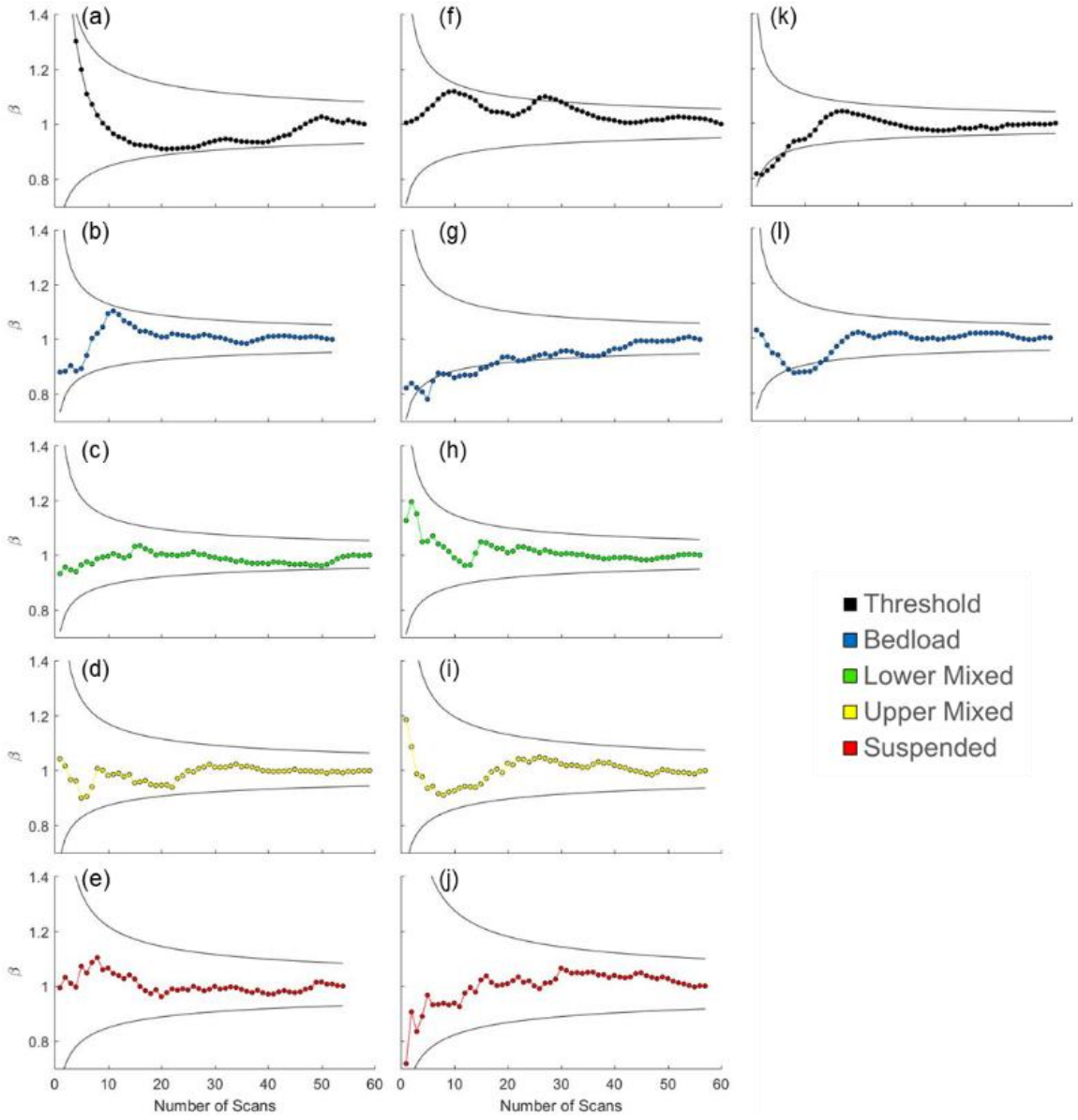

Supplementary Figure D2. Nonstationary incremental mean length β_L values for the (a-e) 15 cm conditions, (f-j) 20 cm conditions and (k-l) 25 conditions. The black line indicates the 95% confidence intervals for the mean values.

Appendix E. Chapter 3 Supplementary Tables

Supplementary Table E1. Transport stage and sediment transport fluxes measured and corrected for saltation.

			Helley-Smith		Syphon		Corrected Fluxes		
Condition	u_*/w_s	τ_*/τ_{*c}	n	Mean ($g\ s^{-1}\ m^{-1}$)	n	Mean ($g\ s^{-1}\ m^{-1}$)	q_{bl} ($g\ s^{-1}\ m^{-1}$)	q_{ss} ($g\ s^{-1}\ m^{-1}$)	q_s ($g\ s^{-1}\ m^{-1}$)
15-THLD	0.511	4.392	30	8.43	20	0.325	8.43	0	8.43
15-BDLD	0.882	13.26	28	20.8	19	3.79	14.81	0	14.81
15-LMIX	0.948	15.85	28	77.3	19	25.4	21.27	70.8	92.1
15-UMIX	1.04	19.03	26	196	19	47.5	59.62	161	220
15-SPSN	1.15	23.51	26	329	20	70.5	113.2	242	355
20-THLD	0.553	5.494	30	11.1	20	1.01	11.1	0	11.1
20-BDLD	0.779	10.69	30	32.0	20	4.12	21.93	0	33.6
20-LMIX	0.935	15.69	26	106	20	24.7	30.9	89.9	121
20-UMIX	1.10	21.22	28	176	19	60.4	56.3	158	214
20-SPSN	1.21	26.45	28	315	19	76.2	113	251	364
25-THLD	0.721	8.992	30	8.94	18	1.61	8.94	0	8.94
25-BDLD	0.891	13.51	29	32.5	17	10.3	35.48	0	35.48

Supplementary Table E2. Results of regression analysis using median values, 50% and 90% bounds and Equation 3.10.

			Median Relations			50% Upper Bound			50% Lower Bound			90% Upper Bound			90% Lower Bound		
Fig	*y*	*X*	*a*	*b*	*c*	*a*	*b*	*c*	*a*	*b*	*c*	*a*	*b*	*c*	*a*	*b*	*c*
16a	$\frac{H}{L}$	$\frac{u_*}{w_s}$	-0.2543	0.8411	0.0619	-0.2640	0.8393	0.0686	-0.2480	0.8404	0.0543	-0.2291	0.8490	0.0449	-0.3233	0.8572	0.0820
16b	$\frac{H}{h}$	$\frac{u_*}{w_s}$	-0.9111	0.9592	0.3997	-0.8738	0.9415	0.3716	-0.8614	1.000	0.4382	-0.9645	0.9132	0.3352	-0.7808	1.085	0.5066
16c	$\frac{L}{h}$	$\frac{u_*}{w_s}$	28.79	0.7339	5.351	42.11	0.7515	6.027	21.16	0.7336	4.902	12.34	0.7191	4.437	58.99	0.7641	7.229
16d	$\frac{H}{L}$	$\frac{\tau_*}{\tau_{*c}}$	-0.0314 x 10^{-2}	13.14	0.0614	-0.0325 x 10^{-2}	13.08	0.0681	-0.0305 x 10^{-2}	13.11	0.0537	-0.0290 x 10^{-2}	13.37	0.0448	-0.0405 x 10^{-2}	13.59	0.0818
16e	$\frac{H}{h}$	$\frac{\tau_*}{\tau_{*c}}$	-0.0014	15.95	0.4119	-0.0013	15.58	0.3820	-.00014	16.80	0.4505	-0.0015	14.94	0.3461	-0.0013	18.40	0.5161
16f	$\frac{L}{h}$	$\frac{\tau_*}{\tau_{*c}}$	0.0309	9.555	5.646	0.0466	10.24	6.417	0.0227	9.547	5.118	0.0124	8.742	4.575	-0.0004	10.61	0.0818

Appendix F. Chapter 3 Supplementary Videos

Description:

These videos show (a) bed maps, (b) 2D center line profiles, (c) height and (d) length time series for all individual scans from each run over the 10-hr equilibrium period.

Filename:

Supplementary Video F1: Equilibrium 15 cm Threshold (etd10769-15-thldeq.mp4)
Supplementary Video F2: Equilibrium 15 cm Bedload (etd10769-15-bdldeq.mp4)
Supplementary Video F3: Equilibrium 15 cm Lower Mixed (etd10769-15-lmixeq.mp4)
Supplementary Video F4: Equilibrium 15 cm Upper Mixed (etd10769-15-umixeq.mp4)
Supplementary Video F5: Equilibrium 15 cm Suspension (etd10769-15-spsneq.mp4)
Supplementary Video F6: Equilibrium 20 cm Threshold (etd10769-20-thldeq.mp4)
Supplementary Video F7: Equilibrium 20 cm Bedload (etd10769-20-bdldeq.mp4)
Supplementary Video F8: Equilibrium 20 cm Lower Mixed (etd10769-20-lmixeq.mp4)
Supplementary Video F9: Equilibrium 20 cm Upper Mixed (etd10769-20-umixeq.mp4)
Supplementary Video F10: Equilibrium 20 cm Suspension (etd10769-20-spsneq.mp4)
Supplementary Video F11: Equilibrium 25 cm Threshold (etd10769-25-thldeq.mp4)
Supplementary Video F12: Equilibrium 25 cm Bedload (etd10769-25-bdldeq.mp4)

Appendix G. Chapter 4 Supplementary Figures

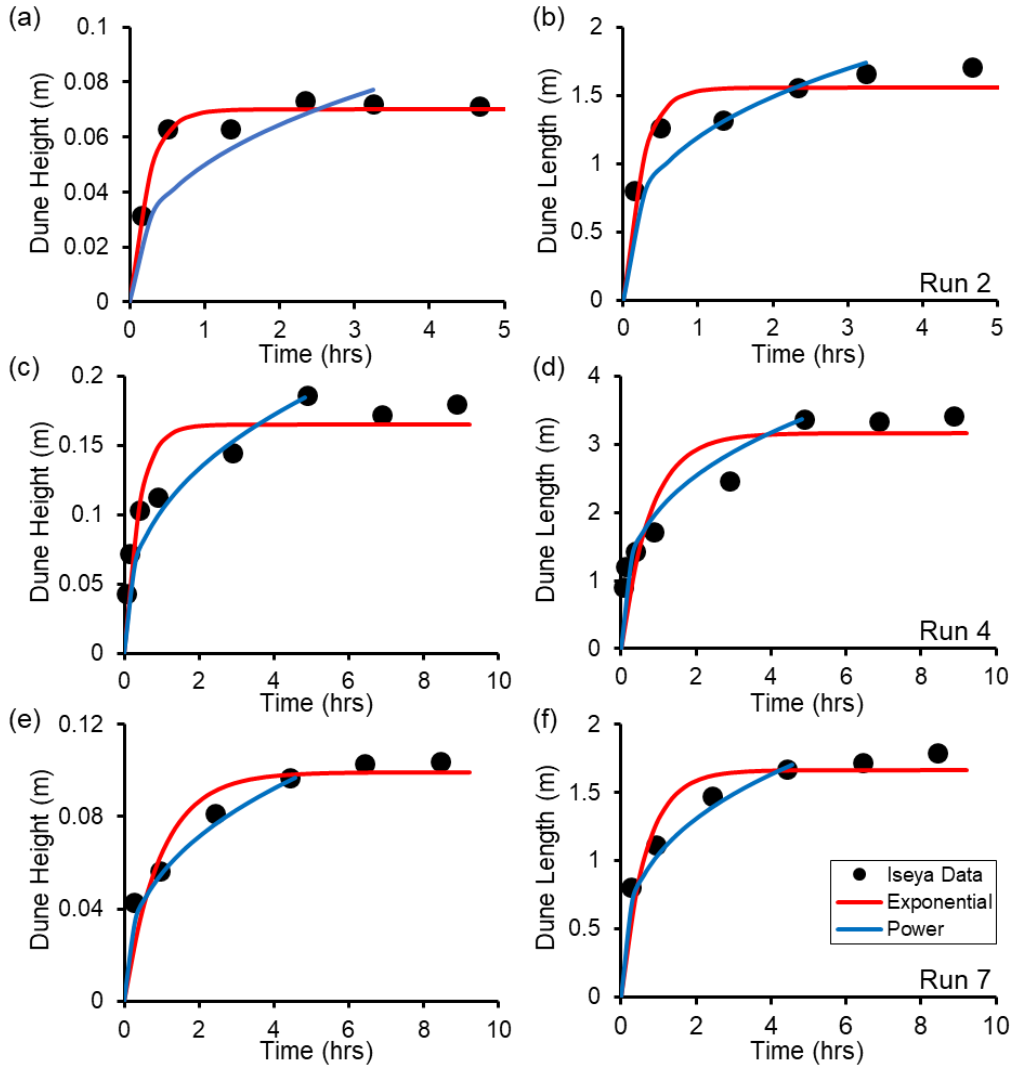

Supplementary Figure G1. Bedform height and length data from Iseya's (1984) (a,b) Run 2, (c,d) Run 4 and (e,f) Run 7.

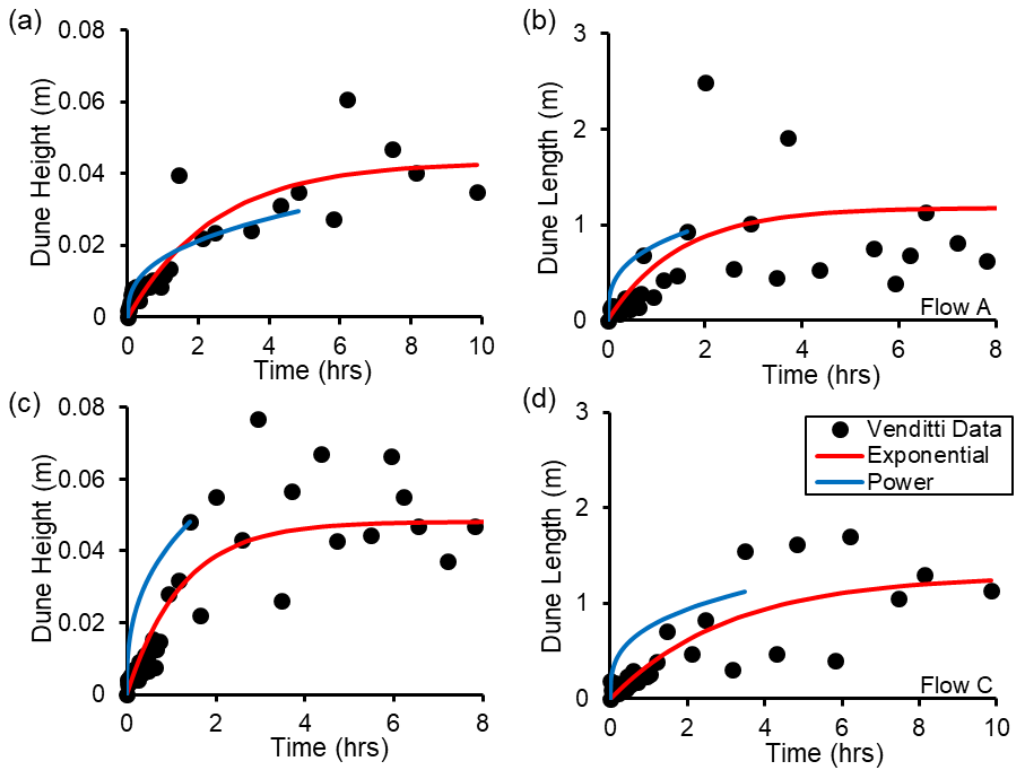

Supplementary Figure G2. Bedform height and length data from Venditti et al.'s (2005a) (a,b) Flow A, and (c,d) Flow C.

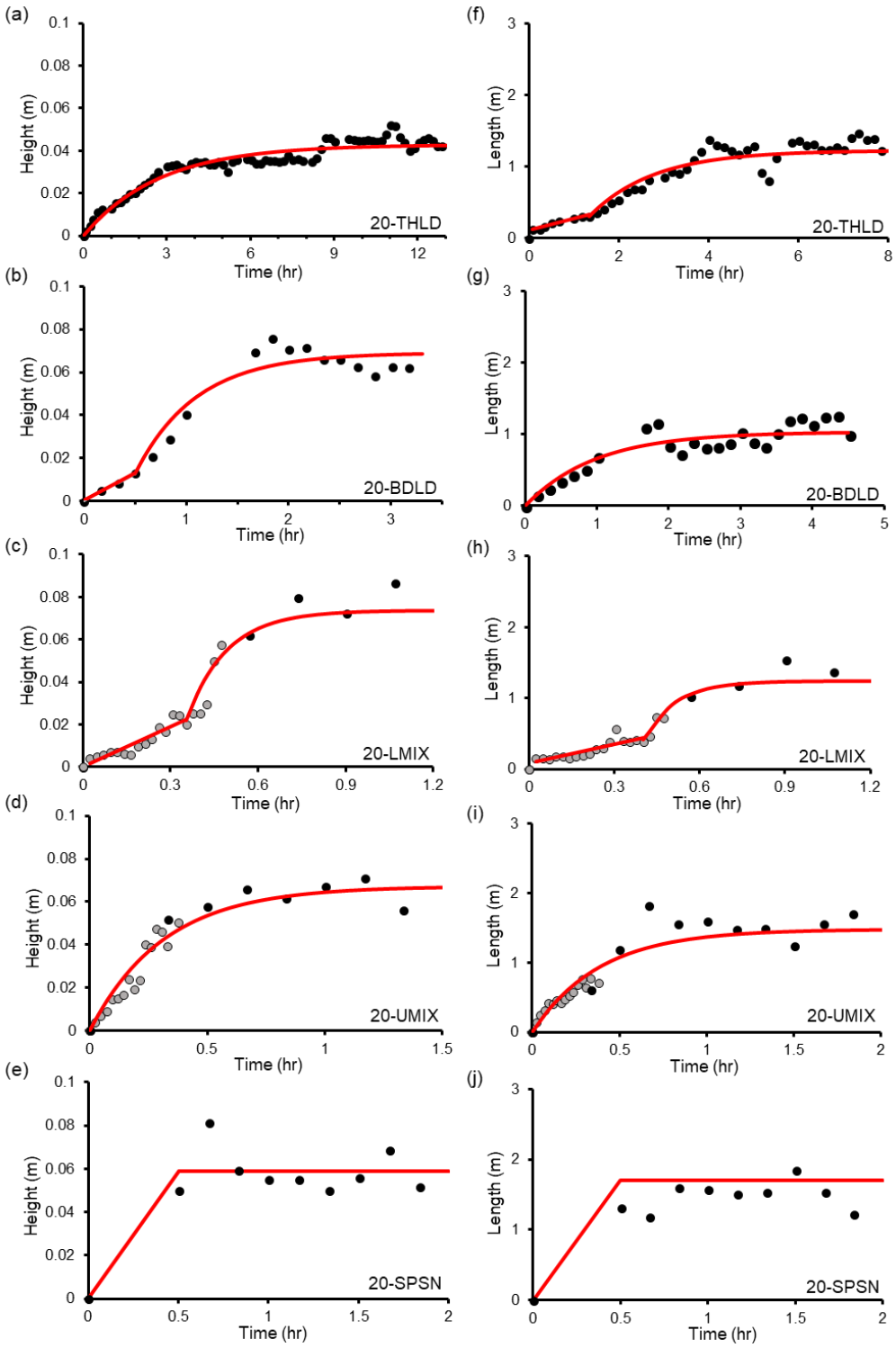

Supplementary Figure G3. Curve fits to the height (a-e) and length (f-j) time series data for the transport stage condition under the initial depth of 20 cm until equilibrium is achieved.

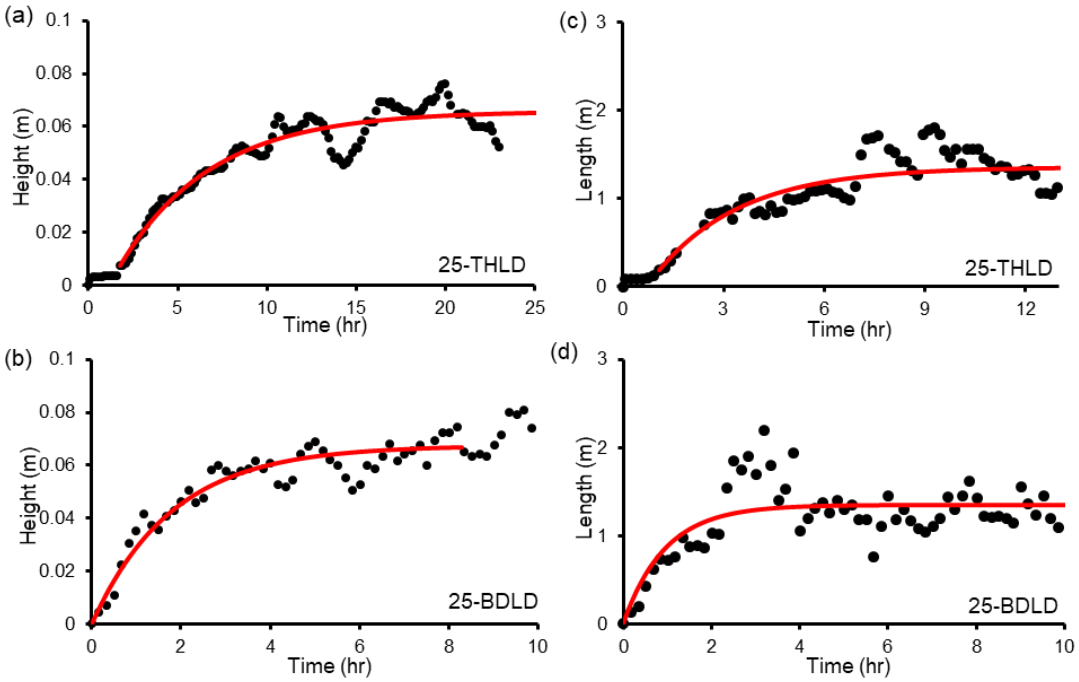

Supplementary Figure G4. Curve fits to the height (a-b) and length (c-d) time series data for the transport stage condition under the initial depth of 25 cm until equilibrium is achieved.

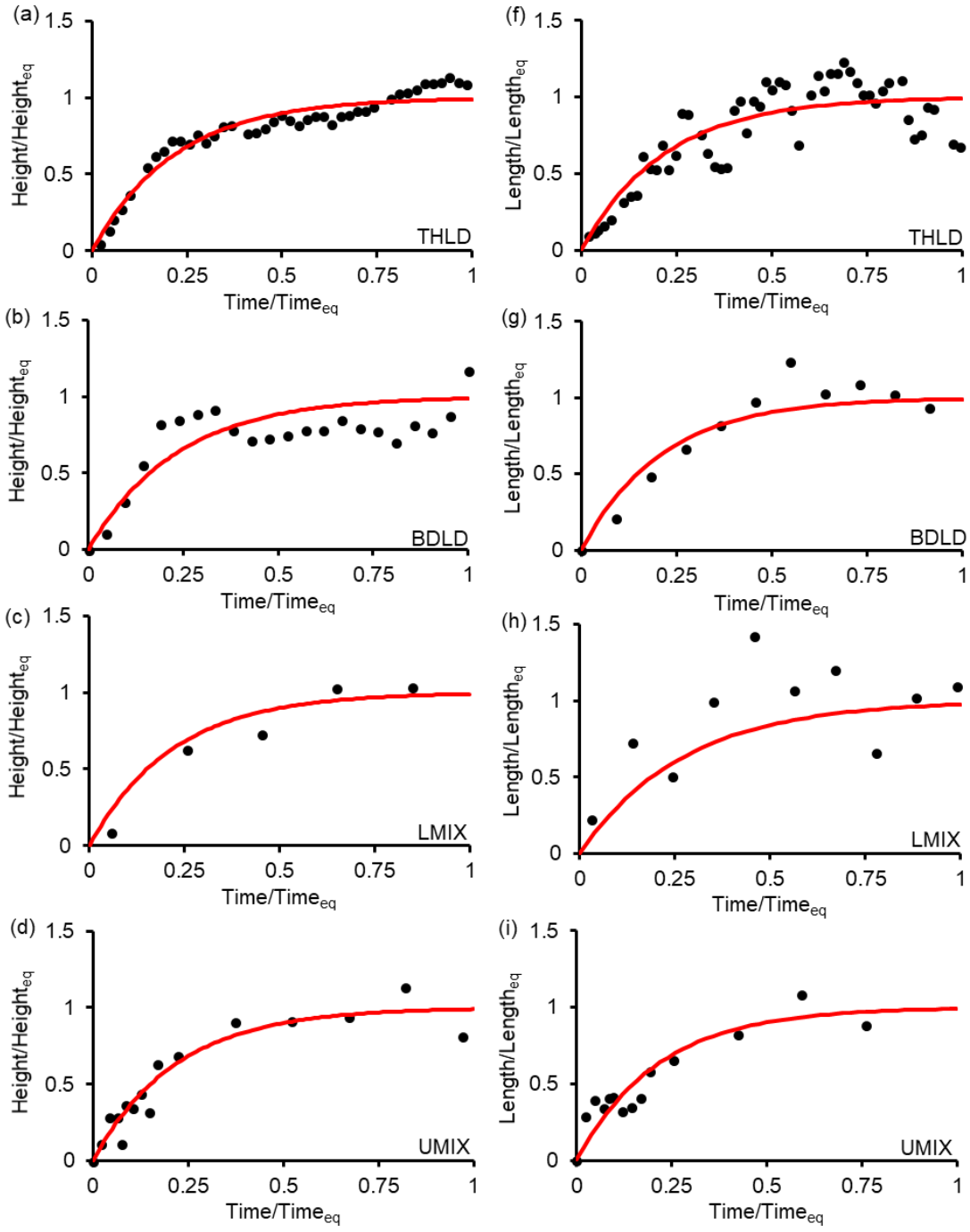

Supplementary Figure G5. Exponential fits (Equation 4.4) for the 15 cm runs.

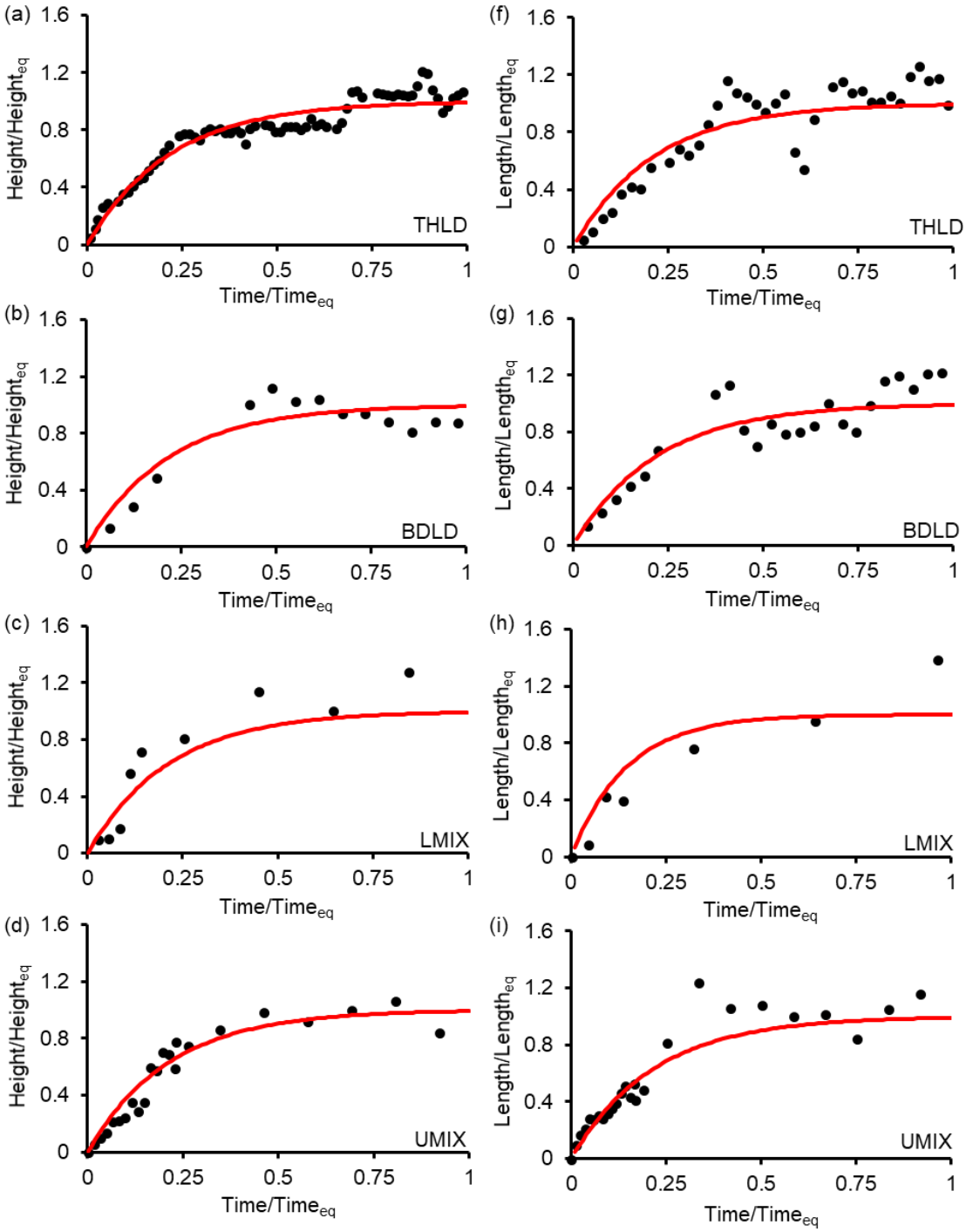

Supplementary Figure G6. Exponential fits (Equation 4.4) for the 20 cm runs.

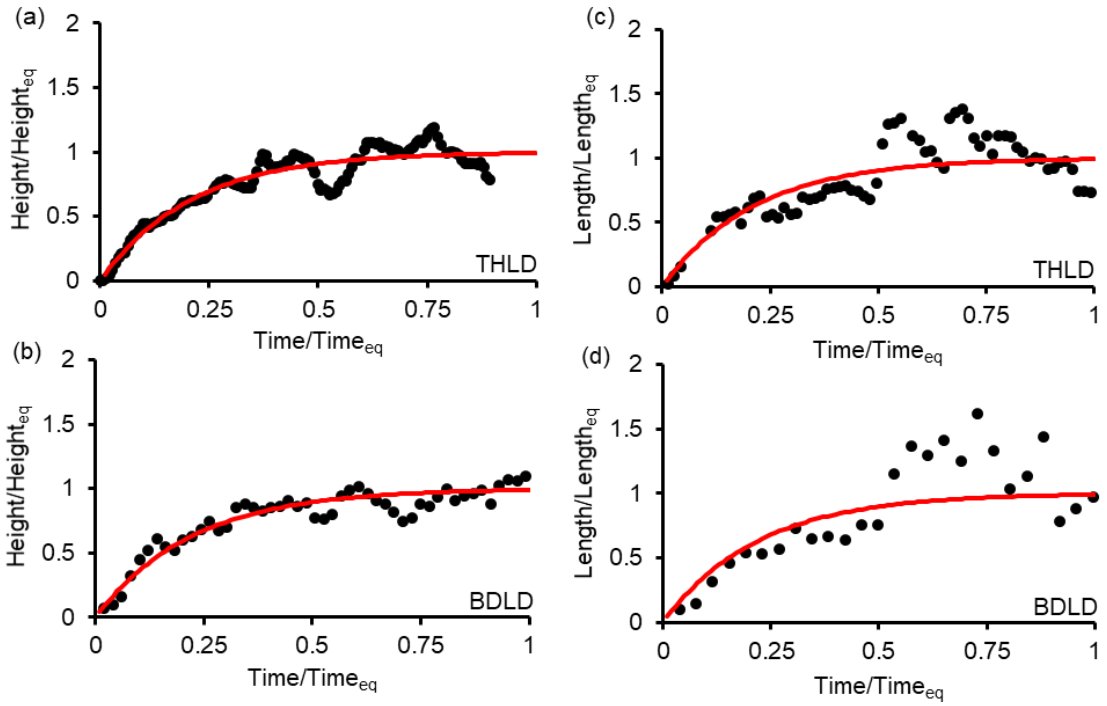

Supplementary Figure G7. Exponential fits (Equations 4.4) for the 25 cm runs.

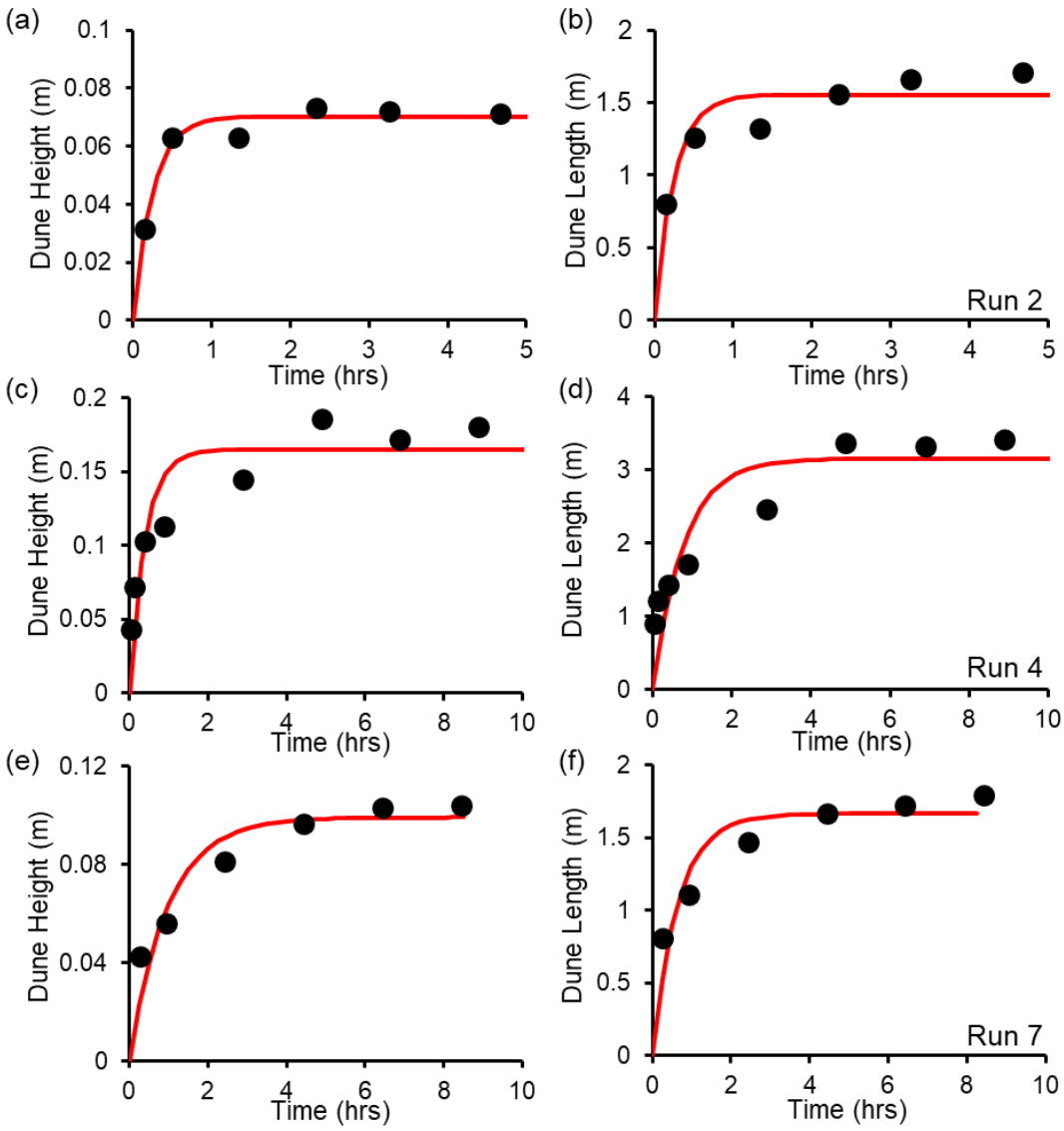

Supplementary Figure G8. Exponential fits (Equation 4.4) to the height and length time series from Iseya (1984).

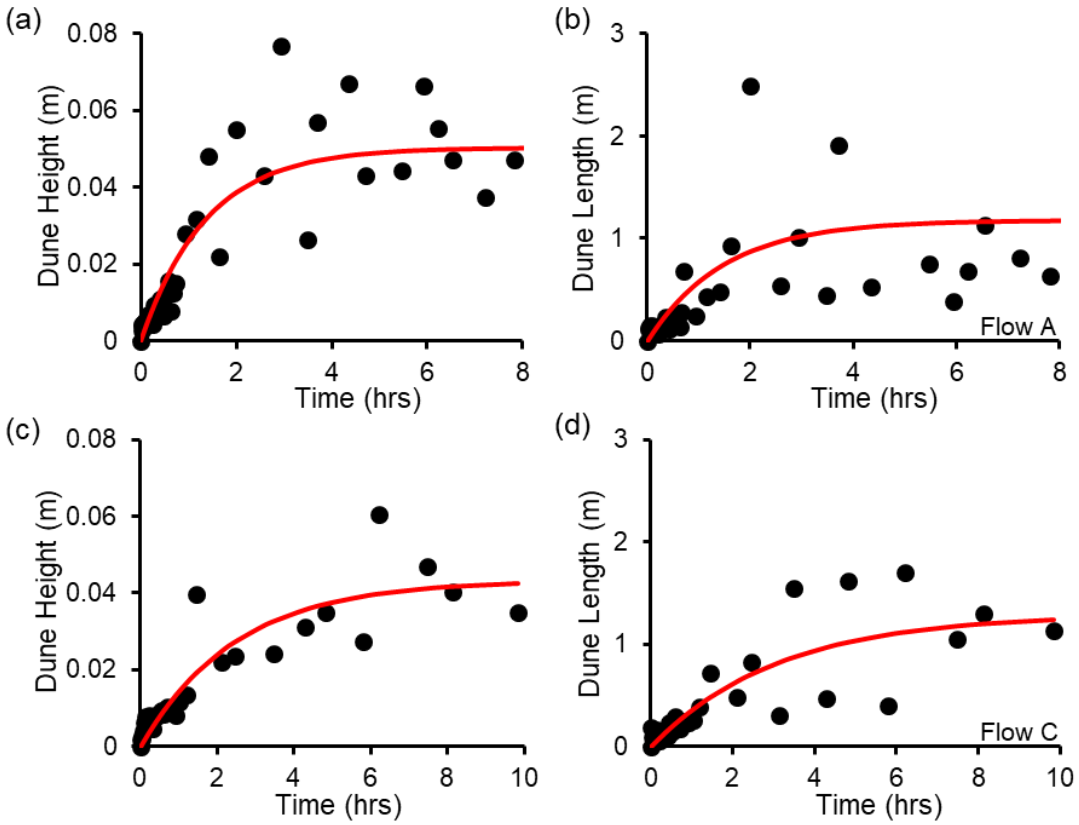

Supplementary Figure G9. Exponential fits (Equation 4.4) to the height and length time series from Venditti et al. (2005a).

Appendix H. Chapter 4 Supplementary Videos

Description:

These videos show (a) bed maps, (b) 2D center line profiles, (c) height and (d) length time series for all individual scans from each run. Scans are presented as the bed evolves from a flat bed for 10-hrs or until equilibrium is achieved. Lower case b in the figure name and file name are the redundant short scans.

Filename:

Supplementary Video H1: Growth 15 cm Threshold (etd10769-15-thld.mp4)
Supplementary Video H2: Growth 15 cm Bedload (etd10769-15-bdld.mp4)
Supplementary Video H3: Growth 15 cm Lower Mixed (etd10769-15-lmix.mp4)
Supplementary Video H3b: Short Growth 15 cm Low Mix (etd10769-15-lmix-short.mp4)
Supplementary Video H4: Growth 15 cm Upper Mixed (etd10769-15-umix.mp4)
Supplementary Video H4b: Short Growth 15 cm Up Mix (etd10769-15-umix-short.mp4)
Supplementary Video H5: Growth 15 cm Suspension (etd10769-15-spsn.mp4)
Supplementary Video H6: Growth 20 cm Threshold (etd10769-20-thld.mp4)
Supplementary Video H7: Growth 20 cm Bedload (etd10769-20-bdld.mp4)
Supplementary Video H8: Growth 20 cm Lower Mixed (etd10769-20-lmix.mp4)
Supplementary Video H8b: Short Growth 15 cm Low Mix (etd10769-20-lmix-short.mp4)
Supplementary Video H9: Growth 20 cm Upper Mixed (etd10769-20-umix.mp4)
Supplementary Video H9b: Short Growth 15 cm Up Mix (etd10769-20-umix-short.mp4)
Supplementary Video H10: Growth 20 cm Suspension (etd10769-20-spsn.mp4)
Supplementary Video H11: Growth 25 cm Threshold (etd10769-25-thld.mp4)
Supplementary Video H12: Growth 25 cm Bedload (etd10769-25-bdld.mp4)